DOCTOR OF PHILOSOPHY

The Human DNA damage sensor RAD9B affects CHK2-T68 Phosphorylation, p21 stability and cell survival in G1

Aljohani, Saad

Award date:
2016

Awarding institution:
Bangor University

THE HUMAN DNA DAMAGE SENSOR RAD9B AFFECTS CHK2-T68 PHOSPHORYLATION, p21 STABILITY AND CELL SURVIVAL IN G1

Saad Ali Aljohani
School of Biological Science
Bangor University

A thesis submitted for the degree of
Doctor of philosophy
Sep 2016

Declaration and Consent

Details of the Work

I hereby agree to deposit the following item in the digital repository maintained by Bangor University and/or in any other repository authorized for use by Bangor University.

Author Name: .....

Title: .....

Supervisor/Department: .....

Funding body (if any): .....

Qualification/Degree obtained: .....

This item is a product of my own research endeavours and is covered by the agreement below in which the item is referred to as "the Work". It is identical in content to that deposited in the Library, subject to point 4 below.

Non-exclusive Rights

Rights granted to the digital repository through this agreement are entirely non-exclusive. I am free to publish the Work in its present version or future versions elsewhere.

I agree that Bangor University may electronically store, copy or translate the Work to any approved medium or format for the purpose of future preservation and accessibility. Bangor University is not under any obligation to reproduce or display the Work in the same formats or resolutions in which it was originally deposited.

Bangor University Digital Repository

I understand that work deposited in the digital repository will be accessible to a wide variety of people and institutions, including automated agents and search engines via the World Wide Web.

I understand that once the Work is deposited, the item and its metadata may be incorporated into public access catalogues or services, national databases of electronic theses and dissertations such as the British Library's EThOS or any service provided by the National Library of Wales.

I understand that the Work may be made available via the National Library of Wales Online Electronic Theses Service under the declared terms and conditions of use (http://www.llgc.org.uk/index.php?id=4676). I agree that as part of this service the National Library of Wales may electronically store, copy or convert the Work to any approved medium or format for the purpose of future preservation and accessibility. The National Library of Wales is not under any obligation to reproduce or display the Work in the same formats or resolutions in which it was originally deposited.

Statement 1:
This work has not previously been accepted in substance for any degree and is not being concurrently submitted in candidature for any degree unless as agreed by the University for approved dual awards.

Signed …….. (candidate)
Date ……..

Statement 2:
This thesis is the result of my own investigations, except where otherwise stated. Where correction services have been used, the extent and nature of the correction is clearly marked in a footnote(s).
All other sources are acknowledged by footnotes and/or a bibliography.

Signed …… (candidate)
Date ……

Statement 3:
I hereby give consent for my thesis, if accepted, to be available for photocopying, for inter-library loan and for electronic storage (subject to any constraints as defined in statement 4), and for the title and summary to be made available to outside organisations.

Signed …… (candidate)
Date ……
NB: Candidates on whose behalf a bar on access has been approved by the Academic Registry should use the following version of Statement 3:

Statement 3 (bar):
I hereby give consent for my thesis, if accepted, to be available for photocopying, for inter-library loans and for electronic storage (subject to any constraints as defined in statement 4), after expiry of a bar on access.

Signed …… (candidate)
Date ……

Statement 4:
Choose one of the following options

a) I agree to deposit an electronic copy of my thesis (the Work) in the Bangor University (BU) Institutional Digital Repository, the British Library ETHOS system, and/or in any other repository authorized for use by Bangor University and where necessary have gained the required permissions for the use of third party material.	
b) I agree to deposit an electronic copy of my thesis (the Work) in the Bangor University (BU) Institutional Digital Repository, the British Library ETHOS system, and/or in any other repository authorized for use by Bangor University when the approved bar on access has been lifted.	
c) I agree to submit my thesis (the Work) electronically via Bangor University's e-submission system, however I opt-out of the electronic deposit to the Bangor University (BU) Institutional Digital Repository, the British Library ETHOS system, and/or in any other repository authorized for use by Bangor University, due to lack of permissions for use of third party material.	

Options B should only be used if a bar on access has been approved by the University.

In addition to the above I also agree to the following:

1. That I am the author or have the authority of the author(s) to make this agreement and do hereby give Bangor University the right to make available the Work in the way described above.

2. That the electronic copy of the Work deposited in the digital repository and covered by this agreement, is identical in content to the paper copy of the Work deposited in the Bangor University Library, subject to point 4 below.

3. That I have exercised reasonable care to ensure that the Work is original and, to the best of my knowledge, does not breach any laws – including those relating to defamation, libel and copyright.

4. That I have, in instances where the intellectual property of other authors or copyright holders is included in the Work, and where appropriate, gained explicit permission for the inclusion of that material in the Work, and in the electronic form of the Work as accessed through the open access digital repository, *or* that I have identified and removed that material for which adequate and appropriate permission has not been obtained and which will be inaccessible via the digital repository.

5. That Bangor University does not hold any obligation to take legal action on behalf of the Depositor, or other rights holders, in the event of a breach of intellectual property rights, or any other right, in the material deposited.

6. That I will indemnify and keep indemnified Bangor University and the National Library of Wales from and against any loss, liability, claim or damage, including without limitation any related legal fees and court costs (on a full indemnity bases), related to any breach by myself of any term of this agreement.

Signature: …… Date : ……

Dedication

To the memory of my father, Ali,
To my ever supportive, caring mother, Janet,
To my loving wife Asmaa, a constant source of inspiration and motivation to me,
To my brother Hassan, and my sisters Kellie, Ekram and Shadia,
I dedicate my work with wholehearted love and gratitude to you all,

Saad

Acknowledgments

I owe my deepest gratitude to my supervisor Dr. Thomas Caspari. Without his continuous optimism concerning this work, and his enthusiasm, guidance and support throughout the research and during the writing of this thesis, this study would probably have never been completed.

Special thanks are given to my research committee members, my internal examiner Dr. John Mulley and the Chairman Dr. Henk Braig, all of whom gave me kind and valuable comments and advice.

I am deeply grateful to my wife Asmaa Manjaf for her constant love and endless support, encouragement and patience.

Last but not least, it gives me great pleasure to acknowledge the help and support of my family. I am very grateful to my mother, brother and sisters for their unwavering belief in me and for supporting my dreams and my goals.

Without these people, I could never have completed this project. I really appreciate their help, most deeply and sincerely.

Thank you all.

Summary

The RAD9 protein assembles with RAD1 and HUS1 in the 9-1-1 DNA damage sensor complex (RAD9-HUS1-RAD1) which plays a crucial role in the activation of the DNA damage checkpoints by recruiting repair enzymes to DNA lesions and by initiating a cell cycle arrest. Why human cells express two RAD9 proteins, RAD9A and RAD9B, which share significant similarity is still very enigmatic. Moreover, both genes encode several splice variants with unknown function. While RAD9A is intensively studied, very little information is available about RAD9B. To get a deeper insight into the biology of RAD9B, two stable HEK293 cell lines were constructed which either over-express full-length human RAD9B-002 (417aa) or its N-terminally truncated splice variant RAD9B-001 (345aa) from an inducible promotor. These studies were complemented by the expression analysis of all five *RAD9B* splice variants at mRNA level in human tissues.

This study revealed for the first time specific activities of the two RAD9B variants. While both proteins target the CHK2-p21 signalling module, which regulates cell cycle progression from G1 into S phase and the response to DNA damage in G1/S, they do affect CHK2 kinase and the cell cycle regulator $p21^{WAF1/CIP1}$ in distinct ways. Elevated protein levels of full-length RAD9B initiate cell death in G1, cause the moderate hyperposphorylation of CHK2 and delay the degradation of p21 in the presence of oxidative stress. On the contrary, high levels of the N-terminally truncated variant RAD9B-001 only transiently block G1-S transition, cause a strong hyper-phosphosphorylation of CHK2 and delay p21 degradation in the response to UV irradiation. While the shorter variant may block p21 degradation in a PCNA-dependent manner in S phase, the full-length protein may act through the anaphase promoting complex (APC) when cells exit mitosis. The work provides also evidence that the hyper-phosphorylation of CHK2 is not dependent on the normal upstream kinase ATM, but on the mitotic regulator MPS1/TTK kinase.

Dissecting this novel regulatory network formed by the two splice variants of the human *RAD9B* gene may help to understand why RAD9B expression levels change in several human cancers including testicular cancer, myelogenous leukaemia, ovarian epithelial carcinoma and cervical carcinoma (HeLa) cells.

Abbreviations

°C	Degrees centigrade
2D	Two dimensions
3’	Three prime end of DNA
5’	Five prime end of DNA
APE1	Apurinic/apyrimidinic endonuclease 1
APS	Ammonium persulfate
ATM	Ataxia telangiectasia mutated
ATR	Ataxia telangiectasia and Rad3-related
Bad	Bcl-2 associated death promoter
Bax	Bcl-2 associated X protein
Bcl-2	B-cell lymphoma 2
Bcl-xl	Bcl lymphoma extra large
BER	Base excision repair
BH3	Bcl-2 homology 3
bp	Base pair
BRCA1	Breast cancer 1
BRCA2	Breast cancer 2
C	Cytoplasm
C-Abl	Abelson tyrosine kinase 1
cDNA	Complementary DNA
CDS	Coding DNA sequence
Chk1 Ser-345	Checkpoint kinase 1-phosph Serin 345
Chk1	Checkpoint kinase 1
Chk2 Thr-68	Checkpoint kinase 2-phosph threonine 68
Chk2	Checkpoint kinase 2
CMV	Cytomegalovirus
CPT	Camptothecin
C-terminal	Carboxy-terminal domain
DAPI	4′,6-Diamidino-2-phenylindole dihydrochloride
DEPC	Diethylpyrocarbonate
DMEM	Dulbecco's modified eagle's medium
DMP1	Dentin matrix acidic phosphoprotein 1
DMSO	Dimethyl sulfoxide
DMTF1	Myb-like transcription factor 1
DNA	Deoxyribonucleic acid
Dna2	DNA replication helicase nuclease 2
DSBs	Double strand breaks
E.coli	*Escherichia coli*
EDTA	Ethylenediamine tetraacetic acid
EGFP	Enhanced green fluorescent protein
ESE	Exonic splicing enhancer

ESS	Exonic splicing silencer
et al.	et alii (and others)
FBS	Fetal bovine serum
FRT	Flippase recognition target
G0	Quiescent phase of the cell cycle
G1	Gap-1 phase
G2	Gap-2 phase
GAPDH	Glyceraldehyde phosphate-dehydrogenase
GEM	Gemcitabine
GFP	Green fluorescent protein
GNL2	Guanine nucleotide-binding protein-like 2
H2AX	H2A histone family, member X
H_2O_2	Hydrogen peroxide
HEK293	Human embryonic kidney 293 cells
HeLa	Human cervix epithelioid carcinoma cells
hnRNPs	Heterogeneous nuclear ribonucleoproteins
HR	Homologous recombination
Hus1	Hydroxyurea sensitive
IF	Immunofluorescent staining
ISE	Intronic splicing enhancer
ISS	Intronic splicing silencer
KAP-1	Krab-associated protein 1
kD	Kilodalton
Kelly	Human neuroblastoma cells
L	Litter
LB	Luria Bertani
Ligl	DNA ligase 1
LP-BER	Long-patch base excision repair
M	Mitosis phase
MAPK	Map kinase
MC-F7	Human breast adenocarcinoma cell line
mg	Milligram
$MgCl_2$	Magnesium chloride
min	Minute
ml	Millilitre
mM	Millimolar
MMR	Mismatch Repair
MMS	Methyl methane sulfonate
MRN	Mre11-Rad50-Nbs1
mRNA	Messenger ribonucleic acid
NaCl	Sodium chloride
NCBI	National centre for biotechnology information
NEB	New England biolabs
NER	Nucleotide excision repair

NHEJ	Non homologous end joining
N-terminal	Amino-terminal domain
oligo-dT	Oligodeoxythymidylic acid
ORF	Open reading frame
p16INK4B	Inhibitor of cyclin-dependent kinase 4 and 6
p21WAF1/CIP1	Cyclin-dependent kinase inhibitor protein 1
p53	Tumour suppressor phosphoprotein p53
PAGE	Polyacrylamide gel electrophoresis
PBS	Phosphate-buffered saline
PCM	Pericentrioles matrix
PCNA	Proliferating cell nuclear antigen
PCR	Polymerase chain reaction
PLK	Polo like kinase
Pol β	DNA polymerase beta
PRKCD	Protein kinase C delta
PTM	Post-translational modification
PVDF	Polyvinylidene difluoride
Rad1	Radiation 1
Rad9	Radiation 9
RFP	Red fluorescent protein
RNA	Ribonucleic acid
ROS	Reactive oxygen species
rpm	Revolutions per minute
RT-PCR	Reverse-transcriptase polymerase chain reaction
S. cerevisiae	*Schizosaccharomyces cerevisiae*
S. pombe	*Schizosaccharomyces pombe*
SD	Standard deviation
SDS	Sodium dodecyl sulfate
SDS-PAGE	Sodium dodecyl sulfate-Polyacrylamide gel
shRNA	Short hairpin RNA or small hairpin RNA
SPB	Spindle pole body
SR-protein	RNA splicing protein
TAE	Tris-Acetate-EDTA
TCA	Trichloroacetic acid
TEMED	Tetramethylethylenediamine
Tet	Tetracycline
TopBP1	DNA topoisomerase 2-binding protein 1
UTR	Untranslated Region
UV	Ultraviolet
WB	Western blot
Wt	Wild type
ZTF-8	Zinc finger putative transcription factor
µg	Microgram
µl	Microliter

Contents

List of Figures

Chapter 1

Chapter 3

Chapter 4

Chapter 5

Chapter 6

List of Tables

Chapter 1

Chapter 2

Chapter 3

Chapter 6

Chapter 1: INTRODUCTION

1.1 Introduction

Why the human genome contains two closely related copies of the *RAD9* gene, *RAD9A* and *RAD9B*, is still unclear. RAD9A assembles with HUS1 and RAD1 in a ring complex, which is loaded at sites of DNA damage to generate a signal that arrests cell cycle progression, aids DNA repair or induces cell death (Parrilla-Castellar et al., 2004). Both, RAD9A and RAD9B can form the 9-1-1 ring complex (Perez-Castro & Freire, 2012). While *RAD9A* encodes three protein splice variants (391aa, 247aa, 10aa), *RAD9B* encodes five variants (429aa, 417aa, 345aa, 345aa, 341aa). None of these variants has been studied so far. This thesis presents evidence that the two RAD9B splice variants RAD9B-001 (345aa) and RAD9B-002 (417aa) regulate the phosphorylation status of CHK2, a kinase acting down-stream of the DNA damage sensor ATM (Tel1) kinase, in a manner which is independent of ATM. Elevated protein levels of RAD9B-002 strongly reduce cell proliferation, cause the accumulation of a sub G1 cell population and inhibit the phosphorylation of CHK2 in response to UV light and oxidative stress caused by H_2O_2. High levels of the shorter variant the N-terminally truncated splice variant RAD9B-001 (345aa), which misses the first 72 amino acids only transiently arrest cells in G1, cause an increase in the CHK2 phosphorylation in response to H_2O_2 and delay the degradation of the CDK inhibitor p21 in the response to UV light. Interestingly RAD9B-001 resembles the N-terminally truncated Rad9-M50 variant from *Schizosaccharomyces pombe* (*S. pombe*) (Appendix 7). The thesis also presents data showing that the yeast variant is recognised when expressed in human cells and contributes to the response to oxidative DNA damage.

1.2 Protein Variants

Many eukaryotic genes encode two or more protein isoforms (Rappsilber & Mann, 2002; Kelemen et al., 2013). Such isoforms show variation in length, share common exons, include variable exons, or possess different amino acids, as splicing events can alter the translational reading frame of the differentially spliced mRNAs (Ahmad et al., 2012).

Several mechanisms exist for generating the enormous diversity of proteins required to fulfil all the functions in a multicellular organism. These mechanisms include alternative splicing,

post-translational modifications (PTMs) and genetic variation (Ahmad et al., 2012). Protein variants can behave in radically different ways than the original proteins.

A good example is the Δ133p53β, a splice variant of the *TP53* gene. While *TP53* is considered a major tumour suppressor, Δ133p53β enhances cancer cell stemness in MCF-7 breast cancer cells indicating an opposite oncogene role (Arsic et al., 2015). Other important factors which are affected by protein variation include PTM, subcellular localisation, degradation and complex formation. Even subtle differences in the protein structure can result in these different behaviours. (Figure 1.1) (Hinkson & Elias, 2011; Lubec & Afjehi-Sadat, 2007; Godovac-Zimmermann et al., 2005). Furthermore, even the same isoform of a protein can reveal substantially different functions depending on its subcellular context, time of expression, or interaction partners (Ahmad et al., 2012).

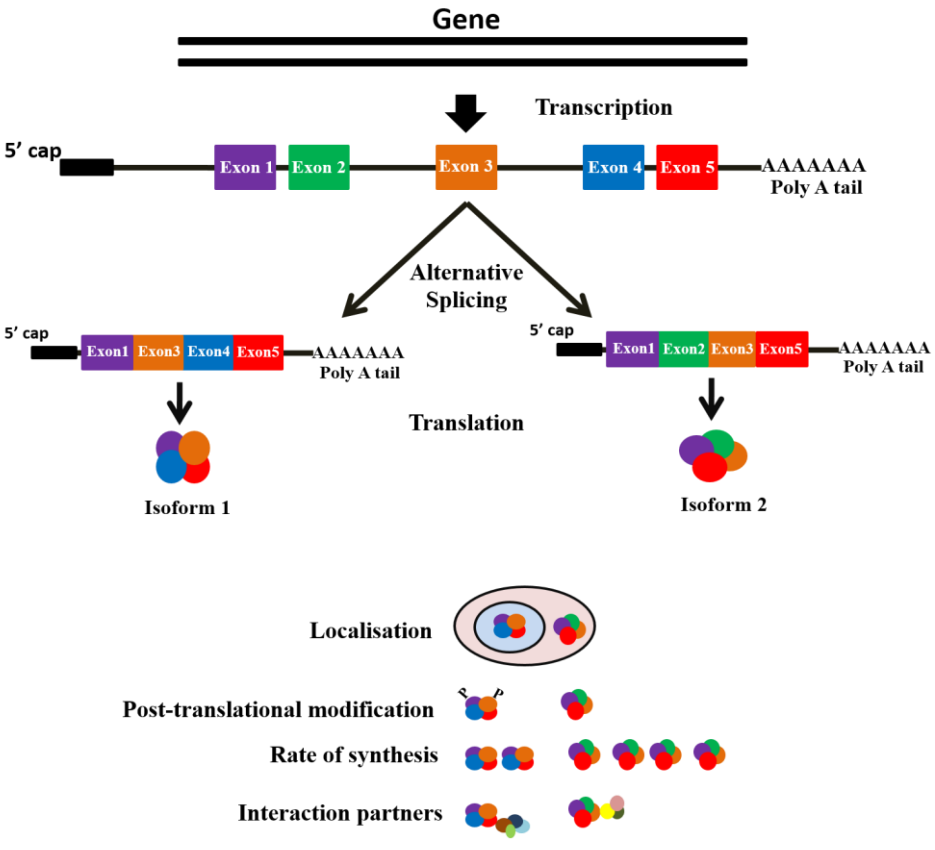

Figure 1.1 Protein variation results in different protein functional roles. Alternative splicing is one example of gene variation resulting in different transcripts of the gene with each containing different sequence regions of the original gene. This figure displays one type of alternative splicing (exon skipping) resulting in the removal of one exon from the original mRNA transcript. Different colours represent different exons and their protein products. Gene variation results in different protein isoforms leading to different roles as a result of their localisation, post-translational modification, rate of synthesis and interaction partners.

Gene duplication, a mechanism of which an extra copy of a gene is generated, may also be considered a form of protein variation. Duplicate proteins can share extensive sequence identity, yet minor alterations within the sequence can deliver novel effects (Ahmad et al., 2012). The outcomes of gene duplication can result in non-functional genes (degenerative mutations leading to a completely silenced gene), to subfunctional genes (both copies are affected by the accumulation of mutations where their functional capacity is reduced or becomes only partially compromised, as each copy partially retains a subset of its original function), or to neofunctional genes (one copy retains the original function while the other copy gains a preserved novel function) (Figure 1.2). Other outcomes of gene duplication may increase gene expression dosage or lead to differential regulation (both copies differ in the regulatory region allowing for enhanced expression or temporal functionality) (Ahmad et al., 2012; Ho et al., 2011; Louis, 2007; Lynch & Conery, 2000; Ohno, 1970)

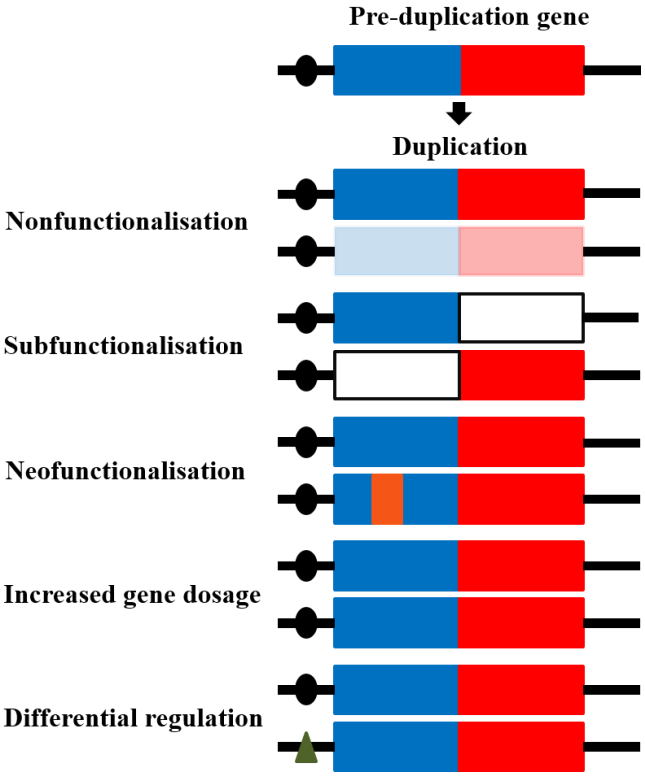

Figure 1.2 Different variation outcomes of gene duplication. Nonfunctionalisation results in the loss of one of the gene copies by degeneration or deletion. In subfunctionalisation, each copy partially functions in a complementary manner retaining the original function. Neofunctionalisation results in one gene copy having the original copy but the other copy has a novel function. Increased gene dosage results in identical copies of the original gene to fulfil the organism's requirements. In differential regulation, the two gene copies result in different regulator regions for enhanced expression.

The human *RAD9A* and *RAD9B* genes are a good example of gene duplication. While simple eukaryotic organisms like fission yeast (*S.pombe*) contain only one *Rad9* gene, complex eukaryotic organisms like mammals have two copies. The human *RAD9* genes share 36% identity and 48% identity (Dufault et al., 2003). Both RAD9 proteins assemble in the 9-1-1 ring (Figure 1.3), but due to their sequence diversity are expected to fulfil different functions. It should be also mentioned that RAD9A can also act outside of the 9-1-1 ring, for example in the context of androgen-regulated gene expression (Wang et al., 2004).

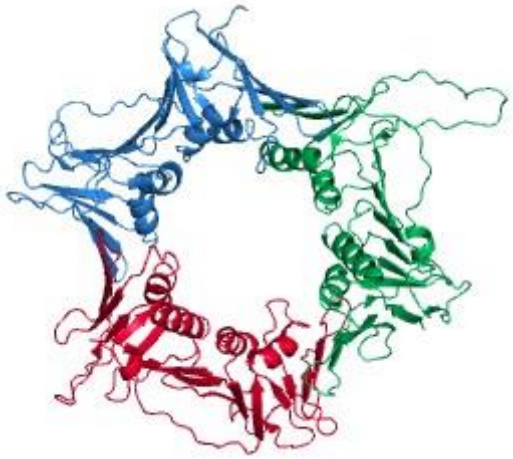

Figure 1.3 Structure of the human 9-1-1 ring. RAD9A (red), HUS1 (green), RAD1 (blue). The tail domain of RAD9A is missing, (structure ID: 3GGR, the image was produced with Polyview 3D) (Xu et al., 2009). The DNA would run through the central opening.

1.2.1 Alternative splicing

In the late 1970s, a comparison of adenovirus mRNA sequence with its corresponding nuclear sequence revealed a partial removal of the pre-mRNA sequence prior to its export to the cytosol where the remaining elements were joined together. Most mammalian transcripts undergo this process of alternative splicing (Kelemen et al., 2013; Berget, Moore & Sharp, 1977; Chow et al., 1977). Alternative splicing is catalysed by the spliceosome machinery consisting of five protein-RNA complexes (U1-U5) plus additional protein factors which bind to the pre-mRNA to excise the introns (Wahl et al., 2009). The combined exons form the mature mRNA which is exported into the cytoplasm whereas the remaining RNA regions of the pre-transcripts (e.g. introns) are degraded by nucleases or converted into small regulatory RNAs known as micro-RNAs (Kelemen et al., 2013; Sevignani et al., 2006; Sharp, 2005).

Alternative splicing allows for the combination of different protein-coding exons in the mature mRNA in different configurations resulting in diverse mature mRNA transcripts and, hence, different protein products (Kelemen et al., 2013). The mechanisms of alternative splicing include four basic modules: alternative 5' splice-site target, alternative 3' splice-site target, exon skipping and intron retention (Figure 1.4) (Nilsen & Graveley, 2010). An alternative splicing study on humans and mice revealed that exon skipping is the most common splice event (38.4% of all splice events), while 18.4% were due to alternative 3' splice events, 7.9% were 5' alternative splice sites and only 2.8% were due to intron retention. The remaining 32.4% were more complicated splice events (Sugnet et al., 2004).

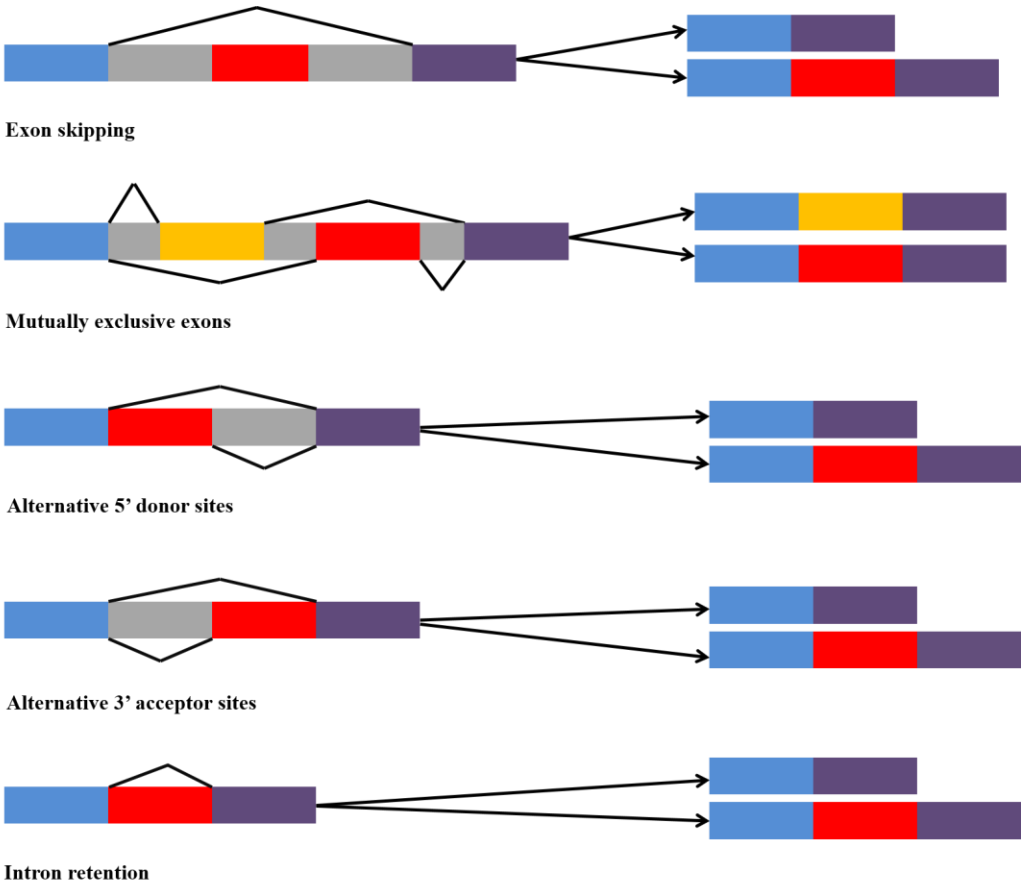

Figure 1.4 Basic mechanisms of alternative splicing in eukaryotic cells. Exon skipping: One exon is spliced out of the primary transcript and the other exons are rejoined together. This exon skipping mechanism is the most common of these mechanisms. Mutually exclusive exons: One of two exons are retained after splicing the primary mRNA transcript but not both. Alternative 3' and 5' sites: An alternative 5' or 3' splice site within one exon is a target for a spliceosome. Intron retention: An intron can be spliced out or retained within the mature mRNA transcript.

An exon-junction microarray study indicated that at least 74% of all human genes are alternatively spliced (Johnson et al., 2003). While this number may be surprising, perhaps even more notable is that 92–95% of all genes contain more than one coding exon (i.e., all genes that could theoretically be alternatively spliced) are indeed alternatively spliced (Pan et al., 2008; Wang et al., 2008). Alternative splicing is regulated at tissue level, at different developmental stages (Sánchez & Rodríguez, 2008), or during cell differentiation (Boutz et al., 2007; Makeyev et al., 2007). Some alternative splicing patterns occur in the response to external stimuli like neuronal activity (Xie & Black, 2001), in response to DNA damage (Shkreta & Chabot, 2015) (Figure 1.5) and in inhibition or activation of cell death (Mosley & Keri, 2006), or upon intracellular signalling (Lee et al., 2010; Lynch, 2007; Shin & Manley, 2004).

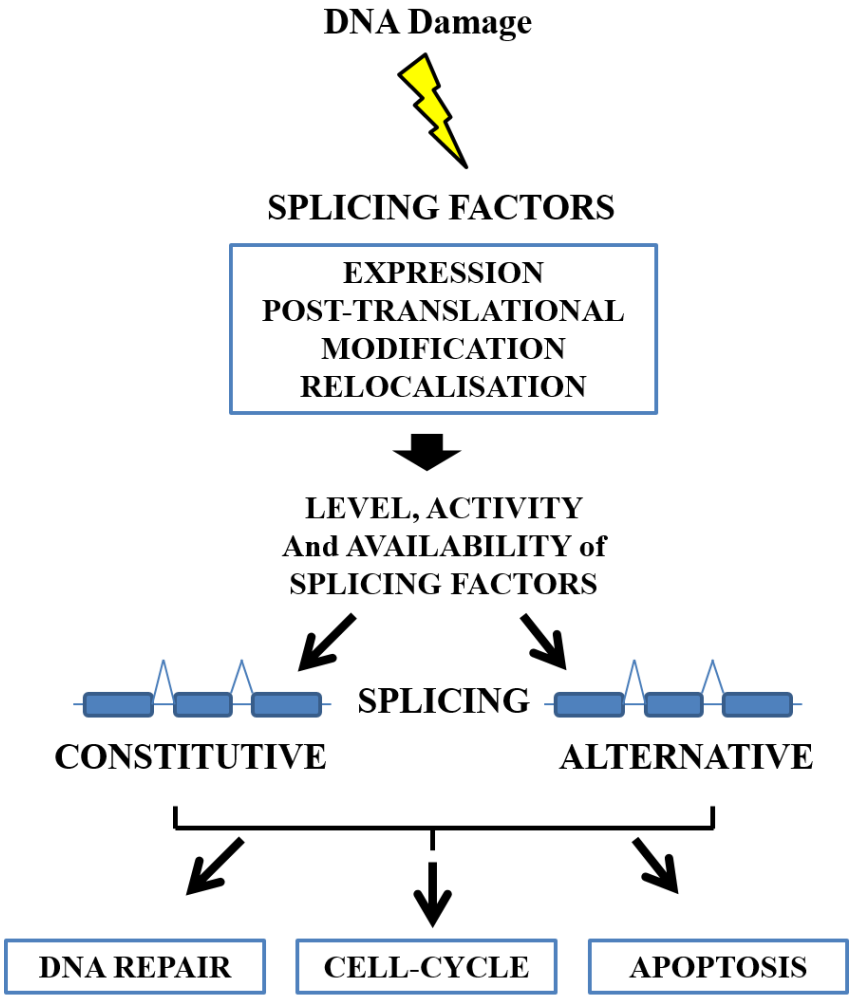

Figure 1.5 RNA splicing response to cellular stress. The activity of the splicing factors can alter in response to DNA damage, resulting in the production of different mRNAs which are used by cells to maintain genomic integrity. Image modified from Shkreta & Chabot (2015).

Moreover, alternative splicing has been linked with several diseases. A good example is the tumour-specific splice events affecting the *DMP1*/*DMTF1* gene which encodes a transcription factor that interacts with cyclin D and regulates G1/S transition. The *DMP1* gene encodes a tumour-suppressor variant DMP1α, and a tumour-promoting variant DMP1β. The ratio between both protein forms changes during the transformation of normal cells into malignant cells in the context of breast cancer (Tschan et al., 2003). Although more than 20,000 publications on alternative splicing exist, the functions of most of these splice variants are unknown, as most changes caused by alternative splicing are difficult to detect (Kelemen et al., 2013).

Regulators of alternative splicing fall into two main categories. The best studied of these regulators are the serine arginine protein (SR-protein) and heterogeneous nuclear ribonucleoproteins (hnRNPs) families. SR-proteins act by binding to enhancer elements in gene cassettes to recruit components of the splicing machinery. hnRNPs, in contrast, are RNA-binding proteins that bind silencer elements in gene cassettes to prevent the spliceosomal machinery from binding. These enhancers and silencers can be further divided into four groups depending on their location and function: exonic splicing enhancer (ESE), exonic splicing silencer (ESS), intronic splicing enhancer (ISE) and intronic splicing silencer (ISS) (Wang, Cao & Hannenhalli, 2015; Martinez-Contreras et al., 2008; Lin & Fu, 2007). In addition, the highly dynamic chromatin structure can influence the rate of transcription and, consequently, affect the pattern of transcription. In a study in which heterochromatin was induced by transfection with an interfering RNA, a reduction in the transcription elongation complex function was seen leading to changes in the alternative splicing pattern (Nilsen & Graveley, 2010; Alló et al., 2009). Moreover, DNA methylation has been shown to have a role in influencing splicing machinery, as nearly 20% of alternative splicing events occur under the regulation of DNA methylation (Yearim et al., 2015).

1.3 ATR-CHK1 and ATM-CHK2 pathways in response to DNA damage

The maintenance of genomic integrity is crucial for all organisms to ensure proper development and to protect their cells from tumorigenesis. Cells are constantly exposed to endogenous DNA lesions like base deamination or oxidation and DNA breaks that affect their genome integrity. Cells detect these DNA lesions through DNA-damage response pathways (DDRs) which are kinase cascades consisting of damage sensors, mediators and executioner proteins. The outputs of the DDR pathways include DNA repair, cell cycle arrests, induction of cell death and regulation of transcription (Manic et al., 2015; Giglia-Mari, Zotter & Vermeulen, 2011; Ciccia & Elledge, 2010) .

The two main DNA damage sensors are the ATM kinase (ataxia telangiectasia mutated serine/threonine kinase) and the ATR (ataxia telangiectasia mutated and Rad3-related serine/threonine kinase) kinase. While ATM recognises signals induced by DNA double strand breaks (DSBs) and signals to CHK2 (checkpoint kinase 2), ATR is activated by single stranded DNA (ssDNA) and translates the signal to CHK1 (checkpoint kinase 1). ATM phosphorylates CHK2 at Thr-68, whereas ATR modifies CHK1 at Ser-317 and Ser-345 (Smith et al., 2010). The structure of ATM kinase has been recently resolved. It shows that ATM forms a homodimer in its inactive state which is activated by autophosphorylation at Ser-1981 (Wang et al., 2016).

In addition to the CHK1 and CHK2 requirement for the activation of the DDR, both kinases play a crucial role in fundamental cellular processes such as DNA replication, chromatin structure, neuronal activities and development (Jackson & Bartek, 2009; Bartek & Lukas, 2003).

Recent work revealed a significant overlap between the ATM-CHK2 and ATR-CHK1 pathways. A good example of these overlapping roles is the p53, a main cell cycle regulator, functioning in DNA repair and apoptosis and also as a major tumour suppressor. Mutations in p53 are detected in approximately 50% of all human tumours, strongly reflecting its crucial role in defending against cancerous transformation (Hasanzadeh-Nazarabadi et al., 2012). In the presence of DNA damage, both ATM and CHK2 phosphorylate p53 at Ser-15 (ATM) and Ser-20 (CHK2) leading to its activation as a transcription factor to upregulate the cyclin dependent kinase inhibitor p21 thereby arresting the cell cycle in G1 (Ou et al., 2005;

Siliciano et al., 1997). ATR targets four phosphorylation sites in p53 under replication stress conditions (Ser-6, Ser-15, Ser-37, Ser-392) (Kulkarni & Das, 2008). CHK1 has also been shown to phosphorylate p53 at Ser-15 and Ser-20, the same sites as for CHK2 kinase, inhibiting p53 degradation by MDM2. This stabilizes p53 and allows it to act as transcription factor for p21 and a large number of other genes (Figure 1.6) (Ou et al., 2005; Shieh et al., 2000). The wider impact of these studies are a deeper insight into the molecular causes of cancer and the development of personalized medicine (Lu et al., 2014).

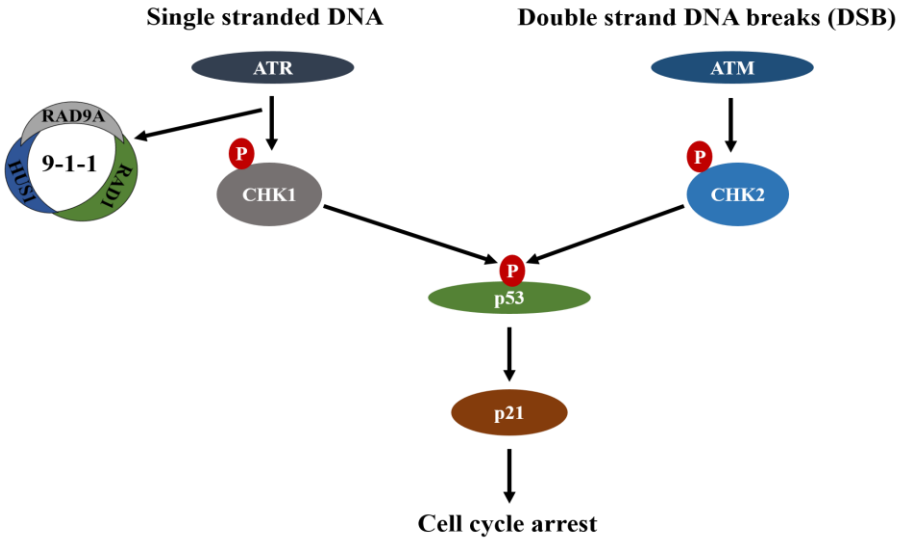

Figure 1.6 The two main checkpoint signalling pathways in response to genotoxic stress with an example of their overlapping functions. ATR kinase is mainly activated by single stranded DNA (ssDNA) which targets and phosphorylates CHK1 kinase at Ser-345 leading to its activation. This activation requires the 9-1-1 complex which is comprised of three proteins: RAD9, RAD1 and HUS1. The 9-1-1 complex facilitates ATR mediated phosphorylation and the activation of CHK1 kinase. In contrast, in response to double strand breaks, ATM kinase targets and phosphorylates CHK2 kinase at Thr-68. Both kinases, CHK1 and CHK2, have overlapping substrates among which is the tumour suppressor p53 which is phosphorylated by the two kinases at multiple sites Ser-15, Thr-18, Ser-20 and Ser-37. Activated p53 binds to the promoter region of p21 which recruits transcription factors leading to the accumulation of p21 protein levels and consequently blocks the cell cycle and allows for DNA repair.

1.3.1 The human 9-1-1 complex and paralogs of its component proteins

Many genotoxic stresses (e.g. UV, IR and replication stress) which result in a junction between single-stranded and double-stranded DNA trigger the loading of the 9-1-1 complex by RAD17. The 9-1-1 complex plays a role in the initiation of the DNA-damage checkpoint which results in a G1/S or G2/M arrest in addition to the onset of DNA-repair and apoptosis. The 9-1-1 complex acts as a DNA clamp to provide a stable basis for the assembly of DNA damage repair complexes. Significant homology exists with the PCNA sliding clamp, a clamp

that binds the DNA replication polymerases (e.g., POL δ) to the replication machinery. The PCNA clamp and the 9-1-1 complex are both loaded onto DNA by two clamp loaders: the Replication factor C (RFC) loads PCNA, whereas the RAD17-RFC complex loads the 9-1-1 ring. Both loading complexes share the four small subunits RFC (p36, p37, p38 and p40) which interact with a larger subunit (pl40) to form an ATPase. In the 9-1-1 clamp loader, the larger subunit (p140) is replaced with the RAD917 protein which interacts with the same small subunits (p36, p37, p38 and p40) as the PCNA clamp loader (Figure 1.7) (Parrilla-Castellar et al., 2004).

The 9-1-1 complex acts in ATR-CHK1 kinase signalling process when single-stranded DNA is exposed at stalled DNA replication forks or processed DNA breaks. ATR phosphorylates CHK1 at serine-345 in a chromatin complex that contains 9-1-1, Claspin and TOPBP1 (Tuul et al, 2013). In addition to its role in checkpoint activation, 9-1-1 also recruits DNA repair proteins such as DNA ligase I (LIGl), DNA polymerase β (POL β), the endonucleases FEN1 and APE1, and the base excision repair (BER) protein hMYH. The 9-1-1 complex stimulates the function of POL β and APE1 after a physical interaction, resulting in the efficient cleavage of the damaged sites and the promotion of the long patch BER (LP-BER) pathway. In addition, translesion DNA polymerase and FEN1 proteins interact with 9-1-1 and the PCNA clamp which also stimulates LP-BER. Why both clamps are needed for DNA repair remains unclear (Kai, 2013; Balakrishnan et al., 2009). One possibility is that PCNA provides a moving platform for these proteins during ongoing DNA replication whereas 9-1-1 is a stationary platform at damaged sites. The 9-1-1 complex also enhances the cleavage of damaged DNA by directly stimulating the activity of DNA2 and EXO1 nucleases to resect DNA. The DNA replication clamp PCNA similarly showed a role in stimulating EXO1 but not DNA2 nucleases (Ngo et al., 2014) .

The 9-1-1 complex also plays a role in the homologous repair of DSBs. A knockdown of human RAD9 showed strong cell sensitivity to ionizing radiation. However, RAD9-depleted cells did not show any effect on CHK2 phosphorylation in the response to DSBs indicating that the 9-1-1 complex does not initiate the ATM-CHK2 kinase pathway as it does for the ATR-CHK1 pathway (Kai, 2013; Roos-Mattjus et al., 2003).

The 9-1-1 complex also contributes also to mismatch repair (MMR). The mismatch recognition dimers MSH2-MSH3 (MUTSβ) and MSH2-MSH6 (MUTSα) interact with the

9-1-1 complex. The binding activity of MUTSα to DNA was stimulated by each subunit of the 9-1-1 complex. Following treatment in RAD9 knockdown cells with N-methyl-N'-nitro-N-nitrosoguanidine, a DNA-methylating agent, the MSH6 complex failed to locate to nuclei with abnormal nuclear morphologies. This strongly suports a role of the 9-1-1 ring in these MMR pathways (Bai et al., 2010).

In a recent study, the 9-1-1 complex in the *C. elegans* germline was found to interact with the ZTF-8 protein which plays an important role in the DNA repair of both mitotic and meiotic DSBs, as well as in the checkpoint activation in meiotic cells. In the presence of DSBs, the ZTF-8 protein co-localised to the damaged site where it interacted with the Rad1 subunit of the 9-1-1 complex. The ZTF-8 protein may act through the 9-1-1 complex pathway to repair stalled replication forks and DSBs (Kim & Colaiácovo, 2014).

While most of the literature focuses on Rad9 as part of the 9-1-1 complex, Rad9 has been shown to act outside the 9-1-1 ring. Some insights into Rad9 specific functions came from activities not shared by the other two subunits. The *S. pombe* Rad9 was found to have a role in the regulation of apoptosis after DNA damage by its interaction with proteins from the anti-apoptotic Bcl-2 family (mainly, Bcl-2 and Bcl-xl). However, Rad9 did not interact with pro-apoptotic proteins such as Bad and Bax. Moreover, over-expression of S. *pombe* Rad9 protein induced apoptosis in human cells suggesting that Rad9 can regulate cell death independently of the 9-1-1 complex (Komatsu et al., 2000). Indeed, during the onset of apoptosis in human cells, RAD9 is cleaved by caspase 3 and the N-terminal RAD9 section translocates to the cytoplasm where it interacts with the anti-apoptotic BCL-2 and BCL-XL proteins (Zhan et al., 2012; Lee et al., 2003). Another interaction partner of the human RAD9 protein is protein kinase C delta (PRKCD), a serine/threonine protein. PRKCD also appears to have contrasting roles in DNA damage-induced apoptosis. This protein has been noted to have an anti-apoptotic role during cytokine receptor-initiated cell death. Following UV irradiation, PRKCD initiates the G2/M DNA-damage checkpoint, whereas in the presence of extended DNA damage, it plays a role in the activation of p53 leading to cell death. In addition, PRKCD localizes to different sub-cellular sites (Golgi, mitochondria, nucleus, endoplasmic reticulum) which affects its pro- and anti-apoptotic functions (LaGory, Sitailo & Denning, 2010; Gomel et al., 2007). PRKCD interacts with and phosphorylates human RAD9 after DNA damage. The activation of PRKCD is necessary for the formation of the 9-1-1 complex

and for the RAD9-BCL-2 interaction to induce apoptosis. Cells lacking PRKCD showed a significant reduction in Rad9-mediated apoptosis (Yoshida et al., 2003).

The Abelson (ABL) protein is a nonreceptor tyrosine kinase (in contrast with PRKCD). ABL is responsible for the phosphorylation and activation of proteins involved in cytoskeletal dynamics. It also regulates cell adhesion and motility molecules (Yogalingam & Pendergast, 2008; Sossey-Alaoui, Li & Cowell, 2007; Hu et al., 2005). When severe DNA damage is present, ABL activates cell death through interactions with RAD9 resulting in the phosphorylation of the N-terminal BH3 domain thereby promoting the interaction between RAD9 and BCL-XL. In contrast, this phosphorylation had no impact on the formation of the 9-1-1 complex. These results suggest that ABL and PRKCD are two crucial proteins that target RAD9 outside of the 9-1-1 ring to induce apoptosis via BCL-2/BCL-XL (Yoshida et al., 2003).

Another important activity of RAD9 outside of the 9-1-1 ring is the androgen-induced activation of genes. Human RAD9 interacts with the androgen receptor through its C-terminal tail domain thereby inactivating the transcription complex (Wang et al., 2004).

Little is known about the functions of Rad1 and Hus1 outside the 9-1-1 complex. Both, human RAD1 and HUS1 form a 9-1-1 related complex with the RAD9 paralog, RAD9B, as will be discussed next. In addition, HUS1B, a paralog of human HUS1, was also reported to interact with RAD9 and RAD1 replacing HUS1 in a related 9-1-1 complex (Hang et al., 2002). Recent studies have linked HUS1 to 9-1-1 independent functions. HUS1 had a strong correlation with the cyclin-dependent kinase inhibitor $p21^{Waf1/CIP1}$ (p21). Hus1-deficient mouse embryonic-fibroblast cells failed to proliferate but cells continued to grow when p21 was inactivated suggesting a functional relation between Hus1 and p21 (Zhao et al., 2015). The Hus1 role in proliferation was also observed in mouse testicular germ cells as the loss of *Hus1* resulted in meiotic defects (Lyndaker et al., 2013). Moreover, human HUS1 has been found to be linked with fragile sites as the protein regulates the abundance of FHIT/FRA3B which binds to fragile sites (Pichiorri et al., 2008).

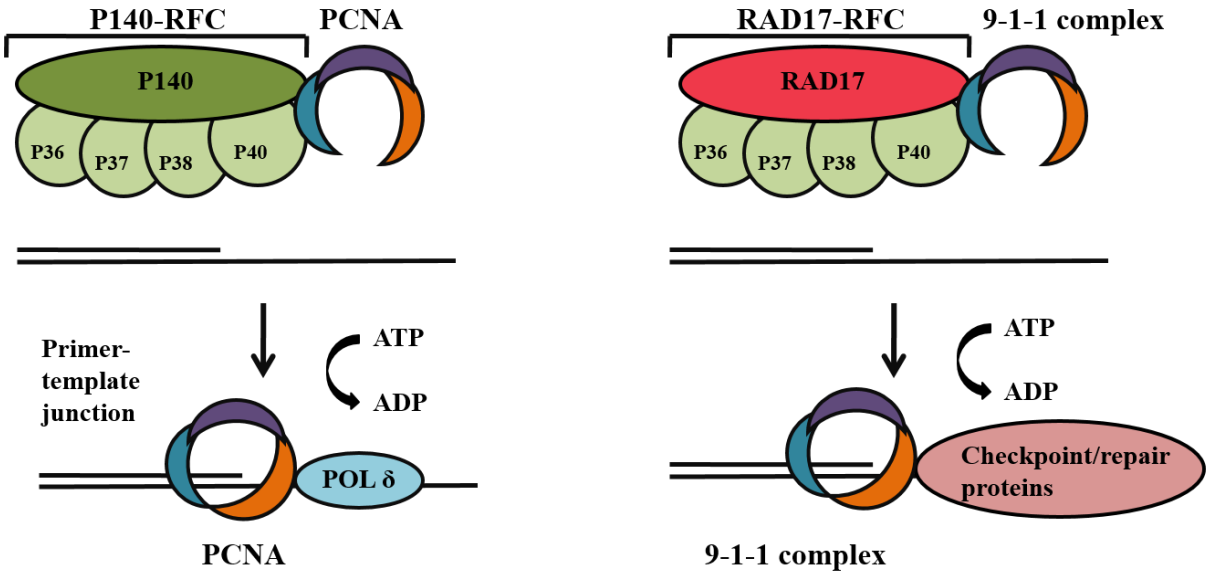

Figure 1.7 Similarity between PCNA and 9-1-1 clamps. The p140-RFC clamp loader loads the PCNA onto DNA replication sites. This clamp loader consists of four small subunits (p36, p37, p38 and p40) and one large subunit (p140). The RAD17-RFC clamp loader loads the 9-1-1 complex onto DNA damage sites similarly to PCNA. The two clamp loaders are similar, except that RAD17 replaced the p140 in the 9-1-1 clamp loader. Modified from Parrilla-Castellar et al. (2004).

1.3.1.1 RAD9B

As Given the importance of Rad9 for the activation of the ATR-Chk1 pathway, the gene is conserved in most eukaryotic cells and organisms. While single cell organisms like fission and budding yeast have only one *Rad9* gene, multicellular organisms have two closely related genes, *Rad9a* and *Rad9b*. Gene duplication is an important mechanism for creating genetic novelty and often new functions are acquired through genetic mobility caused by unequal crossing over during DNA recombination or retroposition (Magadum et al., 2013). At which stage the Rad9 gene underwent gene duplication is not known, but it is likely linked with the transition from unicellular to multicellular organisms. In line with gene duplication both human *RAD9* genes have 10 introns and 11 exons, which encode several protein coding splice variants. Three in the case of *RAD9A*, and five in the case of *RAD9B.* Rad9 and its role in radio-resistance was first discovered in the fission yeast *S. pombe* (Murray et al., 1991). Higher eukaryotic organisms may require more diverse functions of Rad9 which would explain the need for gene duplication. For instance, human RAD9 controls gene expression as it supresses the androgen receptor in prostate cells and also regulates cell death (Lieberman et al., 2011). The human *RAD9B* gene was identified in 2003 by a cDNA blast search revealing a short sequences on chromosome 12 with high similarity to *RAD9A* (Dufault et al., 2003). While *RAD9A* is found in most organisms, ranging from yeast to humans, *RAD9B* only exists in multicellular organisms (i.e. cow, horse, chimpanzee, mouse, platypus, human, dog, rhesus macaque, cat, carolina anole, wild boar, grey short-tailed opossum, red jungle fowl, western clawed frog, zebra fish, brown rat) (PANTHER Classification System, http://www.pantherdb.org. Accessed 31 January 2016). RAD9A seems to be more closely related to the yeast Rad9 protein since its expression partially complements the cell cycle checkpoint defects and restores radioresistance when expressed in the *S. pombe rad9* mutant and mouse ES *Rad9* deleted cells (Lieberman, 2006).

Human RAD9B has high homology with RAD9A in its N-terminal domain but much poorer homology in its C-terminal domain. It should be noted that the N-terminal portion of RAD9A is the domain that participates in the PCNA-like clamp complex. Therefore, RAD9B may also participate in a PCNA-like complex while providing complementation or different activities. Indeed, RAD9B was found to interact with HUS1, RAD1 and RAD17, indicating the formation of a 9-1-1-like complex. In addition, RAD9B interacted with the HUS1 paralog

Hus1B; however, the role of this interaction is still unclear (Perez-Castro & Freire, 2012 & Hopkins et al., 2003).

The predicted molecular mass of the RAD9A protein is around 42 kD. However, on a sodium dodecyl sulfate polyacrylamide gel electrophoresis (SDS-PAGE), RAD9A appeared larger with a molecular weight of 65 kD due to its rich C-terminal phosphorylation. When treated with phosphatase, RAD9A migrated faster and displayed its predicted molecular size. An analysis of RAD9B showed also many potential phosphorylation sites in its tail with 26 Ser and Thr residues. Unlike RAD9A, over-expressed RAD9B runs as a single band at its predicted size (46 kD) without a phosphorylation dependent shift. Treatment with phosphatase did not affect the migration of RAD9B, suggesting that RAD9B does not undergo extensive phosphorylation like RAD9A (Dufault et al., 2003).

In the latest study on RAD9B in human cells, RAD9B initiated a delay in G1/S transition in an ATR and JNK signalling-dependent manner (Perez-CastroFreire, 2012). Cells over-expressing RAD9B showed a G1 arrest 36 hr post-induction and this arrest was reversible as the cell entered G2 between 48 hr and 60 hr after induction. This arrest was specific to RAD9B as RAD9A over-expression failed to cause an arrest. The G1 arrest caused by RAD9B did not cause any checkpoint activation as no phosphorylation of CHK1, CHK2, p53, or p21 was observed. RAD9B was coimmunoprecipitated with RAD1, HUS1, RAD17 and the unphosphorylated form of RAD9A. However, unlike RAD9A, RAD9B did not interact with TOPBP1 and is therefore unlikely to contribute to the ATR-CHK1 signalling. RAD9B does respond to DNA damage since RAD9B localised to the nucleus under normal condition and re-localised to the nucleolus in the response to UV light in an ATR-JNK-dependent manner. In contrast, RAD9A remained outside the nucleolus after DNA damage (Perez-Castro & Freire, 2012). In another study, the cell cycle regulator p21 was reported to bind to intranucleolar bodies (INoBs), a structure in disturbed nucleoli (Abella et al., 2010). Interestingly, RAD9B and p21 proteins compartmentalised to these INoB structures after treatment with Adriamycin; induces reactive oxygen species (ROS), but they did not co-localise. RAD9B also physically interacted with the p21 protein under normal and stress conditions suggesting that RAD9B plays a role in checkpoint signalling or cell cycle arrest or DNA repair as p21 acts in all three pathways (Perez-Castro & Freire, 2012).

A northern blot analysis displayed the expression of *RAD9B* in only two tissues: intense expression in testis and lower expression in skeletal muscle. In addition, reverse transcription PCR (RT-PCR) analysis showed that *RAD9B* mRNA was expressed in human embryonic kidney (HEK293), myelogenous leukaemia (K562), ovarian epithelial carcinoma (OVCAR5) and cervical carcinoma (HeLa) cells. In a comparison between original mouse and human *Rad9b* expressed sequence tag (EST) sources, mouse *Rad9b* was derived from brain, liver and mammary gland tissues, whereas human *RAD9B* had one EST derived from fetal eye and five ESTs derived from testis tissue. This suggests that Rad9b is expressed in fewer tissues compared to Rad9a (Table 1.1) (Dufault et al., 2003).

Table 1.1 Human and mouse *Rad9b* expression tissues and possible function

Name	Tissue	Detection level	Function
Human RAD9B	Testis, skeletal muscle, fetal eye, embryonic kidney cells, myelogenous leukaemia, ovarian epithelial carcinoma, cervical carcinoma	mRNA	Unknown, (possibly in response to DNA damage)
Mouse Rad9b	Brain, liver, mammary gland, embryonic brain	mRNA	Stimulates growth and embryonic development

In a study investigating the functional role of Rad9b in mice, Rad9b revealed a different role from that observed in human cells. When *Rad9b* was partially deleted from embryonic stem cells (ES), embryos were completely resorbed in week 7.5 (E.7.5) while heterozygous embryos can live longer, up to E.12.5 or until a few days after birth. This suggests that Rad9b plays a role in the development of the embryo after E.7.5. Rad9b was also expressed in embryonic brain cells and the deletion of *Rad9b* in these tissues resulted in abnormal neural tube closure. In addition, the deletion of *Rad9b* in ES cells revealed a high sensitivity to mitomycin C and to gamma radiation compared to normal positive control cells although these cells showed a normal G2/M checkpoint and cell cycle arrest. These results suggest that

Rad9b plays an important role in embryonic development in addition to having a function in DNA-damage resistance (Leloup et al., 2010).

1.3.1.2 HUS1B

Human HUS1B shares 69% similarity to HUS1A and only 48% identity. HUS1B is thought to have a similar function to its paralog, HUS1A, as both are expressed in the same human tissues, with high expression of HUS1B in testis tissue. HUS1B was found to bind to Rad1, to which it is adjacent in the ring-like clamp complex. However, the two-hybrid system showed that HUS1B did not bind to RAD9A or HUS1. HUS1B co-immunoprecipitated however with both proteins suggesting weak interactions between HUS1B, RAD9 and HUS1 (Hang et al., 2002).

Interestingly, over-expression of HUS1B in HEK239 cells resulted in a strong increase in cell death with only 0.46% of the cells surviving, whereas over-expression of HUS1 showed 100% survival. These results suggest that HUS1B may have a role in cell death and may interact in different ways with RAD9 and RAD1 (Hang et al., 2002). A recent study linked the HUS1B function to fetal development and growth. The study focused on the analysis of DNA methylation of some genes linked with a low birth weight (LBW) among infants. DNA methylation play a crucial role in the control of gene expression, and aberrant methylation is responsible for various human diseases (Gapp et al., 2014; Heyn & Esteller, 2012). Analysis of the *HUS1B* gene in some placentas from LBW infants revealed that *HUS1B* was hypomethylated suggesting aberrant expression of the gene. In cell lines derived from trophoblastic cells, the *HUS1B* promotor was highly methylated, and an increase in gene expression was observed when the promotor was demethylated. These findings suggest that elevated HUS1B expression reduces fetal growth and that the effects of this dysregulation contributes to LBW. This is interesting since the function of RAD9B in mice was also linked to the growth and development of embryos. Hence, HUS1B may perform a specific role in embryos. Whether RAD9B is regulated in a similar manner is yet unclear and any role of human RAD9B in early development remains to be explored (Rumbajan et al., 2016).

1.3.1.3 Rad9-M50

The Rad9 protein is the conserved subunit of the 9-1-1 complex and found in higher and lower eukaryotic cells like fission yeast. Interestingly, fission yeast cells expresses a novel Rad9 variant that plays a role in the cellular response to heat stress. Elevated temperatures between 37–40°C result in the induction of Rad9-M50 as the mutation of the ATG codon 50 (M50) inhibited its expression. Thus, Rad9-M50 is an N-terminally truncated Rad9 protein which initiates from an internal translational start site at AUG-50 and may not substitute for Rad9A in the 9-1-1 complex. The expression of this variant under heat stress is independent of the mitogen-activated protein kinase (MAPK) which has a temperature-sensing role (Figure 1.8) (Janes et al., 2012).

Expression of Rad9-M50 correlates with the heat-induced dephosphorylation of Chk1 at Ser-345 in the presence of DNA damage. Later work by Rabiaa Oun in Caspari's group showed however that Chk1 dephosphorylation and Rad9-M50 inductions are parallel events which are not causatively linked (Oun & Caspari, unpublished). However, loss of Rad9-M50 shortens the heat-induced G2 arrest and regulates the MAP kinase Sty1/Spc1 (Janes et al., 2012; Oun & Caspari, unpublished). Interestingly, Rad9-M50 resembles the N-terminally truncated human RAD9B variants 001 (Appendix 7).

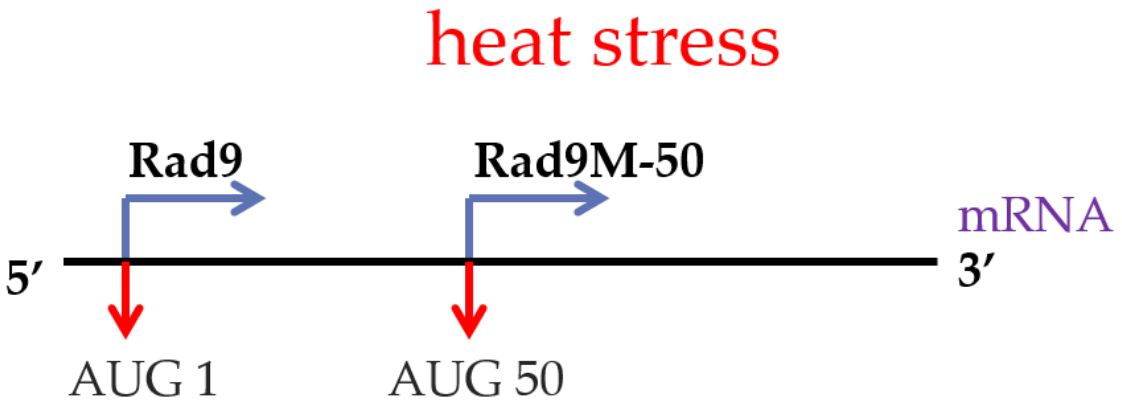

Figure 1.8 Heat inducible Rad9-M50. The yeast Rad9-M50 is induced by elevated temperatures through the alternative translation of a cryptic initiation codon at methionine-50 within the Rad9 transcript sequence.

1.3.2 CHK1 kinase

Checkpoint kinase 1 (CHK1) protein plays a major role in the DNA-damage response pathway, representing a connection between the master regulators of the cell cycle cyclin-dependent kinase and cyclins (CDK/cyclins), and the cell cycle major upstream sensors ATM and ATR serine/threonine proteins. CDC25A and CDC25C, two members of the CDC25 family, are a target for the CHK1 checkpoint regulator leading to the inhibition of cell cycle transition (Zhao et al., 2002; Mailand et al., 2000; Peng et al., 1997). CHK1 is a ~200 amino acid protein containing an N-terminal kinase domain and a C-terminal domain that share limited homology across species (Kosoy & O'Connell, 2008). CHK1 protein can respond to DNA DSBs but it mainly responds to DNA damage that causes single strand breaks, such as in UV light or replication stress, leading to its phosphorylation on the C-terminal residues Ser-317 and Ser-345 in an ATM-ATR-dependent manner. At the damage sites, replication protein A binds and directs the RAD17 RFC clamp loader complex to load the 9-1-1 complex on the 5' junction of the single stranded DNA. As a consequence of loading the 9-1-1 complex onto the damaged sites, the ATR activator topoisomerase-binding protein-1 (TOPBP1) is led to the damaged sites in an interaction among the C-terminus of the Rad9 protein and two C-terminal BRC1 (BRCT) motifs of the TOPBP1. The TOPBP1 then activates the ATR by a direct binding in an ATR interaction protein (ATR-ATRIP)-dependent manner leading to the phosphorylation and activation of its downstream checkpoint effector kinase, CHK1 (Figure 1.9) (Cimprich & Cortez, 2008; Jazayeri et al., 2006).

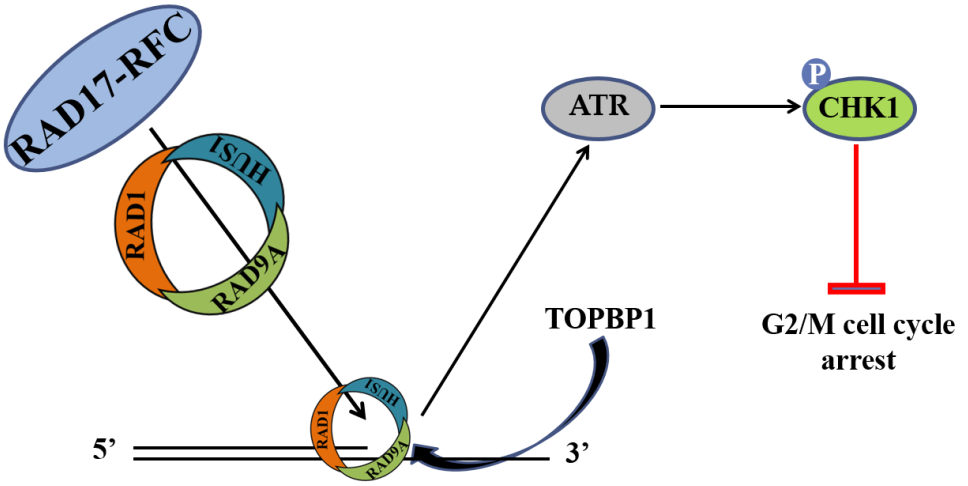

Figure 1.9 CHK1 activation in response to single stranded DNA (ssDNA). In response to single stranded DNA, the 9-1-1 complex is loaded onto the damaged sites by the clamp loader Rad17-RFC. The loading of the checkpoint clamp recruits the TOPBP1, which interacts with the clamp subunit RAD9 tail. The TOPBP1 then binds and activates the ATR protein in an ATRIP-ATR-dependent manner leading to the activation of CHK1 by ATR by direct phosphorylation at Ser-317 and Ser-345.

Human CHK1 has one alternative isoform: isoform 2. The CHK1 main isoform displayed a molecular weight of 56 kD on an SDS-PAGE gel whereas the smaller isoform 2 migrated faster revealing a size of 43 kD. CHK1 isoform 2 is an N-terminal truncated protein, termed CHK1 short (CHK1-S), containing 282 amino acids. CHK1-S was expressed at the mRNA level in multiple human tissues with high expression in fetal tissues. An immunoblot also detected CHK1-S in these fetal tissues. CHK1-S is an endogenous repressor of isoform 1, as isoform 2 interacts with and antagonizes isoform 1 at the N-terminal in a CHK1-dependent manner to block its kinase activity where they dissociate in response to DDRs. The interaction between the two isoforms is disrupted by ATR phosphorylation, which fits well with the activation of CHK1 isoform 1 partners by ATR. ATR is, therefore, able to disinhibit isoform 1 and allow the cell to enter into arrest when sufficient DNA damage is present (Pabla, Bhatt & Dong, 2012).

CHK1-S is also found in higher-than-normal levels in various cancers, suggesting that CHK1-S may accelerate the cell cycle and enhance the proliferation of the cells under these conditions. However, the overexpression of CHK1-S in the cancer cell lines resulted in early mitotic entry and the reduction of cellular proliferation, suggesting that CHK1-S plays a role in cellular proliferation (Pabla, Bhatt & Dong, 2012).

1.3.3 CHK2 kinase

DNA damage upregulates the checkpoint protein kinase 2 (CHK2), which itself plays a role in regulating cell cycle arrest, DNA repair, and apoptosis. The structure of CHK2 contains a SQ/TQ cluster domain (SCD) at the N-terminus composed of serine-glutamine and threonine-glutamine repeats. The SCD region is a phosphorylation target for the ATM protein after DNA damage. The SCD N-terminal region is followed by a forkhead-associated (FHA) domain and a carboxyl-terminal kinase catalytic domain. The CHK2 FHA domain serves as a binding region for CHK2-phosphorylated substrates, including other CHK2 SCD-phosphorylated molecules (Buscemi et al., 2006; Li et al., 2002; Ahn et al., 2000).

In a different role than CHK1, CHK2 mainly responds to DSBs and arrests the cell cycle at G1/S or G2/M through various mechanisms. An inactive form of CHK2 is mainly present in the nucleus during cell growth. After DNA damage, CHK2 is phosphorylated by the ATM protein on the Thr-68 phosphorylation site in addition to other sites within the SCD. The activation of CHK2 causes to its dimerization through the binding of the FHA domain of one monomer with the SCD domain of another, leading to CHK2 autophosphorylation on its kinase domain, followed by dissociation of the dimers into fully active monomers (Figure 1.10) (Zannini, Delia & Buscemi, 2014; Ahn et al., 2002; Xu, Tsvetkov & Stern, 2002).

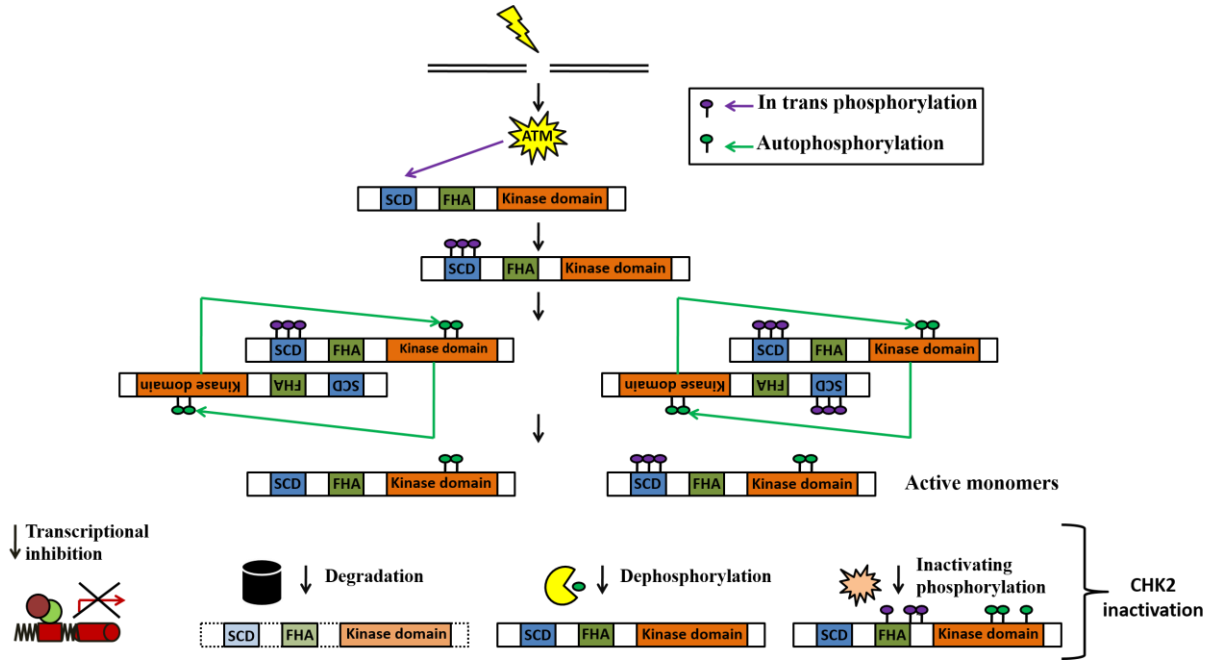

Figure 1.10 CHK2 activation and inactivation. In response to double stranded breaks (DSBs), the ATM protein phosphorylates and activates CHK2 at the rich SQ/TQ regions. The active CHK2 monomers associate with each other, leading to autophosphorylation at the kinase domain. The interacted monomers then successfully dissociate into single active monomers. CHK2 can be inactivated by being degraded or dephosphorylated or by inactivating phosphorylation. Modified from Zannini, Delia & Buscemi's study (2014).

Compared to members of the 9-1-1 complex and CHK1, a striking number of isoforms for CHK2 exist. The tumour suppressor CHK2 protein was revealed to have around 90 splice variants in breast cancer tissue. These splice variants were expressed in parallel with the main CHK2 transcript. In addition, normal tissues also expressed these various splice variants: however, the number was much less compared to breast cancer tissue. The majority of the CHK2 splice variants detected in breast cancer tissues were of four specific splice variants (Figure 1.11). These four CHK2 splice variants were selected and further analysed for their functional roles. The cellular localisation of the wild type (WT) CHK2 is linked to its biological function in the nucleus. When the four splice variants were integrated and overexpressed, they revealed a similar localisation to WT Chk2 in HCT116 and MCF-7 breast cancer cell lines. Two of these splice variants were enzymatically active while the other two were enzymatically inactive; however, all four splice variants had a significant impact on the WT CHK2 kinase activity through heterodimersation when there were overexpressed. Taken together, the functions of these isoforms are not clear; however, they do have a suppression role on WT CHK2 activity (Berge et al., 2010; Staalesen et al., 2004).

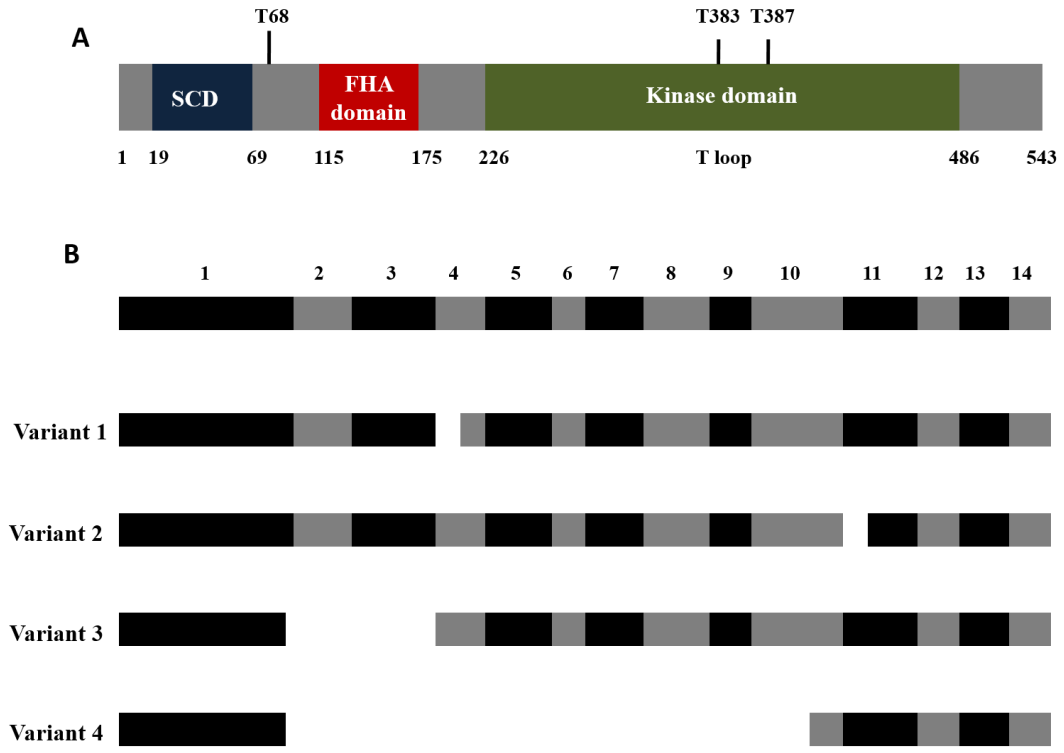

Figure 1.11 WT CHK2 and its splice variants. (A) CHK2 main structure representing the three domains (SCD, FHA and kinase domains). (B) Overview of CHK2 14 exons on the mature transcript and its four splice variants with the missing regions shown in gaps. Modified from Berge et al. (2010).

1.3.3.1 The p21^{Waf1} cyclin dependent kinase inhibitor, a major component of the ATM-CHK2-p53-p21 pathway

In the response to many stimuli, p21 promotes cell cycle arrest by directly interacting and inactivating the cyclin dependant kinases such as CDK1 and CDK2. The p21 protein can act as a sensor or as an effector of multiple anti-proliferative signals. Upon DNA damage, the ATM-CHK2 DDR pathway phosphorylates p53 at Ser-15 and Ser-20 which stabilizes the transcription factor resulting in the up-regulation of p21 and a G1 cell cycle arrest (Zannini, Delia & Buscemi, 2014; Bunz et al., 1998). The p21 protein also acts as an effector of multiple tumour suppressor pathways independently of p53 (Abbas & Dutta, 2009).

While the N-terminal domain of p21 serves as a binding site for its specific interaction with CDKs, its C-terminal domain associates with the co-factor of DNA polymerases, the PCNA ring complex, which is essential for DNA synthesis. This disrupts the PCNA interaction with the polymerases and stops DNA replication (Figure 1.12) (Abbas & Dutta, 2009; Soria et al., 2008; Moldovan, Pfander & Jentsch, 2007).

While the up-regulation of p21 by the p53 transcription factor is a specific and crucial cellular response to genotoxic stress which causes DNA breaks like gamma radiation, many studies have shown that a similar increase in p21 levels does not happen when DNA replication forks stall (Soria & Gottifredi, 2010). Treatment of cells with DNA replication stress agents such as HU, UV and MMS do not trigger an increase in the p21 expression levels. On the contrary, levels of p21 are down-regulated at both the mRNA and the protein level. The drop in p21 protein is initiated by the attachment of ubiquitin by the E3-ligase CRL4^{CDT2} complex leading to p21 proteolysis. This disrupts the p21-PCNA complex and allows PCNA to be mono-ubiquitinylated to initiate translesion DNA synthesis to bypass bulky nucleotides after UV irradiation or chemical treatment with MMS. During translesion synthesis the two standard DNA polymerases epsilon (leading strand) and delta (lagging strand) are replaced by special polymerases from the Y family on the PCNA complex (Zhao & Washington, 2017). Since the TLS process is not expected to occur outside of S phase, it is really interesting that PCNA and POL η from the Y family polymerases also form nuclear foci outside of the S phase in the response to UV irradiation. This indicates the existence of unknown functions of the Y family polymerases outside of the S phase (Soria & Gottifredi, 2010).

Depending on its expression levels, p21 has different impacts on the cell cycle and DNA replication. Very high levels of p21 impair PCNA-driven DNA replication, whereas basal expression of p21 during S phase selectively block the interaction of the PCNA ring with the TLS DNA polymerases without altering the loading and activity of the replicative polymerase δ (Figure 1.12-B). Therefore, p21 degradation is a crucial step for the success of TLS indicating that p21 plays a critical role in the control of the TLS polymerases under normal conditions preventing mutagenesis due to the poor proofreading activity of the TLS polymerases (Soria & Gottifredi, 2010; Abbas et al., 2008; Mattia et al., 2007).

In addition to its main activities related to the CDKs and the PCNA complex, p21 has other functions. p21 has been found to have both a positive and a negative impact on the expression of certain genes. For example, p21 has a positive impact on the induction of genes that regulate cellular senescence, and a negative impact on the transcription factor E2F1 which is important in G1-S transition. Moreover, p21 supresses the transcription of apoptotic genes in the response to DNA damage (Figure 1.12-C) (Kumari et al., 2015; Abbas & Dutta, 2009; Chang et al., 2000; Delavaine La & Thangue, 1999). In addition, p21 phosphorylation at Thr-145 by AKT Kinase results in its cytoplasmic localisation where it directly binds and inhibits the activity of pro-apoptotic proteins such as procaspase 3, caspase 8 and caspase 10 (Figure 1.11-D) (Roninson, 2002; Dotto, 2000). Contrary, p21 is believed to promote apoptosis and many other cellular functions through the large group of p21 activated kinases (PAK). Especially PAK2 is able to phosphorylate caspases after being activated by p21 binding (Suzuki et al., 2013). This may explain why the deletion of *p21* in mice fibroblast cells results in a significant reduction in apoptosis after treatment with multiple stimuli (Abbas & Dutta, 2009).

In malignant tissues, p21 is expressed at different levels depending on the type of cancer. Very low expression of p21 correlates with a poor prognosis in colorectal, small-cell lung, head and neck cancers because the low expression of p21 correlates with the absence of p53. A possible role of p21 as an oncogene was reported after the detection of elevated levels of p21 which correlated with aggressive growth of cervical, breast, prostate and ovarian cancers. A number of studies reported genetic variants in the *p21* gene that can increase cancer development in individuals. Polymorphisms in *p21* were reported to be linked with the increased risk of oesophageal, head and neck cancers. These polymorphisms in *p21* are

believed to influence the expression of p21 leading to a reduction of p21 protein levels in these cancers (Piccolo & Crispi, 2012; Wang et al., 2012; Yang et al., 2010).

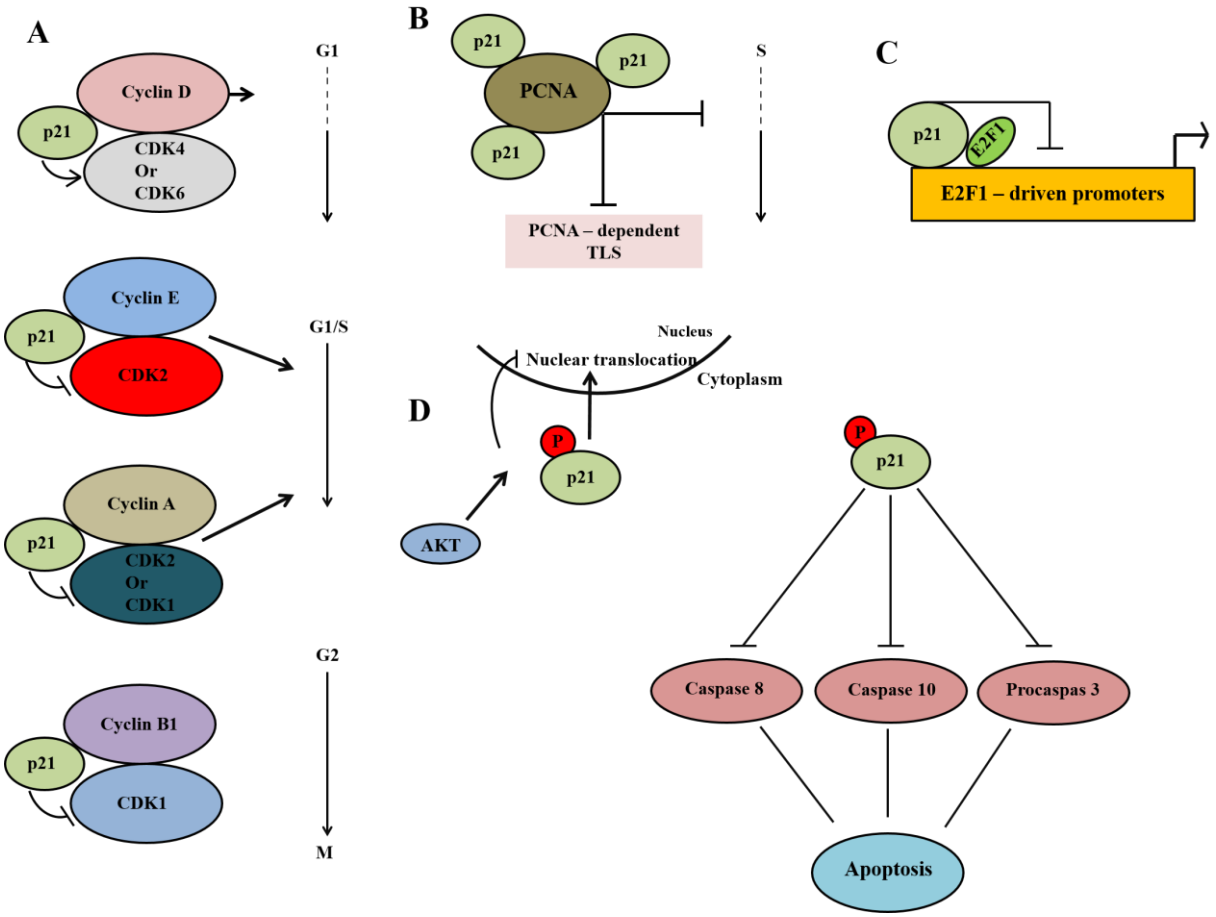

Figure 1.12 The different cytoplasmic and nuclear functions of the p21 protein. (A) p21 promotes cell progression through G1 by enhancing the kinase activity of cyclin dependent kinase 4 (CDK4) or CDK6 in a complex with cyclin D. During the G1 phase, p21 can block the kinase activity of CDK2-cyclin E or CDK2-cyclin A, an essential complex activity required for the progression into the S phase, thus causing G1/S arrest. p21 also inhibits the kinase activity of CDK1-cyclin A, required for cell progression through G2. Moreover, p21 inhibits the progression through G2 and G/M by inhibiting the kinase activity of CDK1-cyclin B1. (B) p21 interacts with the proliferative cell nuclear antigen (PCNA) through its C-terminal and inhibits DNA replication, allowing the cell to switch to PCNA-dependent DNA translesion synthesis. (C) p21 oncogenic activity acting as an anti-apoptotic through a direct binding and inhibition of the transcriptional activity of the transcription factor E2F1, whose transactivation activity is required for the transcription of apoptotic pathway genes. (D) The cytoplasmic p21 phosphorylation by AKT1 kinase prevents its translocation to the nucleus thus blocking its interaction with PCNA. The cytoplasmic p21 also shows an anti-apoptotic role by directly binding and inhibiting the activity of the pro-apoptotic proteins such as procaspase3, caspase 8 and caspase 10. Modified from Abbas & Dutta (2009).

1.3.3.2 The mitotic regulator monopolar spindle 1 (MPS1) and its relation to the CHK2 kinase

The kinase monopolar spindle 1 (MPS1) regulates centrosome duplication, chromosome segregation and the mitotic checkpoint. Centrosomes are microtubule organising centres consisting of two centrioles which are surrounded by pericentriolar material, a mass of protein responsible for the microtubule nucleation. G1 cells possess one centrosome which divides in S phase and moves to opposite poles in the cell in G2 to regulate the mitotic spindle in M phase (Figure 1.13). Because centrosomes regulate the mitotic spindle any misregulation or extra copies of centrosomes leads to abnormal chromosome segregation, a hallmark of cancer cells (Kasbek, Yang & Fisk, 2009; Fukasawa, 2007).

The activity of MPS1 kinase peaks at the G1-S transition initiating centrosome duplication in human cells. This was shown in HeLa cells where depletion of MPS1 is sufficient to prevent centrosome duplication. The oscillation of MPS1 kinase levels throughout the cell cycle are controlled by the E3 ligases APC-Cdc20 and APC-Cdh1 during mitosis and G1, respectively. The levels of MPS1 peak in mitosis before they gradually drop again when cells enter G1 (Cui et al., 2010; Kasbek et al., 2007). The prevention of MPS1 degradation or MPS1 over-expression can lead to centrosome re-duplication, a phenotype frequently observed in a number of human tumours, such as prostate and breast cancer. It also leads to chromosome segregation errors during mitosis and aneuploidy (Pihan et al., 2003; Lingle & Salisbury, 1999).

The mammalian spindle assembly checkpoint (SAC) consists of multiple proteins that sense the absence of an attached spindle at the kinetochore of the condensed chromosomes thereby delaying chromosome segregation and mitotic progression. This checkpoint is crucial to ensure the equal segregation of sister chromatids to maintain genomic stability (Yeh et al., 2014). Failure in the mitotic checkpoint results in chromosomal imbalance (aneuploidy) and causes chromosomal instability (von Schubert et al., 2015; Thompson, Bakhoum & Compton, 2010). This checkpoint is dependent on MPS1 kinase as the protein accumulates at the unattached kinetochores following its activation by polo-like kinase 1 (PLK1), a key regulator of mitotic entry, chromosome segregation and mitotic exit. Activated MPS1 leads to the activation and recruitment of the mitotic checkpoint components to kinetochores like KNL-1,

MAD1:C-MAD2 and BUB3:BUBR1 resulting in the activation of the spindle checkpoint and subsequent mitotic delay (Von Schubert et al., 2015; Liu, Davydenko & Lampson, 2012).

Recent studies revealed a close link between MPS1 and CHK2 kinase. CHK2 localises to centrosomes early in mitosis and to the midbody in late mitosis. A number of studies have now shown that PLK1 kinase targets and phosphorylates CHK2 at Thr-68 (Tsvetkov et al., 2003). In the presence of DNA damage, MPS1 phosphorylates CHK2 also at Thr-68 and activated CHK2 binds to and phosphorylates MPS1 on Thr-288. This suggests a feedback loop between the two kinases which may be regulated by PLK1. CHK2 is also required for the attachment of MPS1 to the kinetochores at the condensed chromosomes (Yeh et al., 2014; Yeh et al., 2009; Tsvetkov et al., 2003).

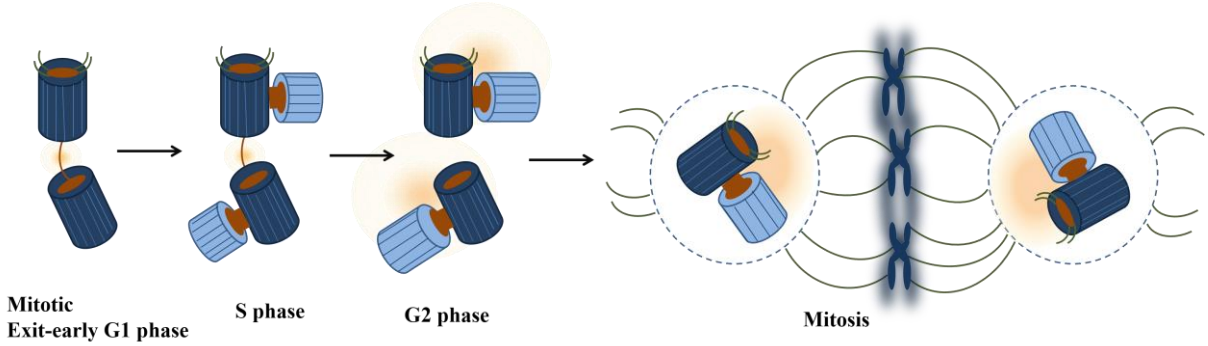

Figure 1.13 The centrosome duplication cycle. First, in the mitotic exit and the early G1 phase, the centrosome contains two centrioles associated by interconnecting fibres enclosed by the pericentrioles matrix (PCM; orange), which is essential for the nucleation and growth of the microtubules (Spindle fibres). Second, in the late G1/S, the centrioles start duplicating with the nucleation of daughter centrioles. During the late G2 phase, the procentrioles elongate and increase in size forming mature centrosomes and their PCM expands. Finally, at the G2/M transition, the centrosomes mature and separate orthogonally, oriented opposite each other and localised at opposite sides of the cell. The centrosomes then organise mitotic poles where they attach to the kinetochores of sister chromatids and evenly segregate into two cells. The mother and daughter centrioles disengage and the centrosomes duplication cycle is repeated again. Modified from Bettencourt-Dias & Glover (2007).

1.4 Cross talk between the DNA damage detection system and the mitotic regulators

It is increasingly apparent that the DDR communicates closely with the mitotic regulators. For instance, two main regulators of the mitotic phase, PLK1 and PLK3, are both regulated by DNA damage, and both are reported to interact with CHK2 kinase. In the response to ionising radiation, PLK3 interacts with and phosphorylates CHK2 kinase at Ser-62 and Ser-73, and this phosphorylation facilitates the subsequent phosphorylation of CHK2 on Thr-68 by ATM kinase leading to full checkpoint activation and cell cycle arrest (Bahassi et al., 2006; Tsvetkov et al., 2003).

The main regulators of the DDR, ATM, ATR, CHK1, CHK2 and p53, have all been reported to localise to the centrosome (Golan et al., 2010; van Vugt et al., 2010; Krämer et al., 2004; Tsvetkov et al., 2003). Mitosis is distinct from the remaining cell cycle phases as the DDR is inactivated during this stage (van Vugt et al., 2010). The question here is how mitotic cells manage to prevent the activation of the DNA damage response to allow cells to progress through mitosis. A good example of this relationship is 53BP1 which is a main regulator of the DDR and forms foci at DNA breaks together with γ-H2AX. During mitosis, and in the response to ionising radiation, mitotic kinases (CDK1 and PLK1) target and phosphorylate 53BP1 prevents 53BP1 from localising to the DNA lesions. PLK1 also phosphorylates CHK2 which inactivates the ATM-CHK2 signalling pathway. The involvement of mitotic kinases in silencing the DDR may explain their over-expression in many cancers (van Vugt et al., 2010; Sur et al., 2009; Gautschi et al., 2008; Strebhardt & Ullrich, 2006).

1.5 Aims of the project

Human cells contain two *RAD9* genes, *RAD9A* and *RAD9B,* which both encode highly related subunits of the RAD9-RAD1-HUS1 ring complex. The 9-1-1 ring is loaded at sites of DNA damage to aid DNA repair and to arrest cell cycle progression. Depletion of *Rad9a* in mice leads to skin cancer and human *RAD9A* promotes prostate cancer. While RAD9A is intensively, studied, very little is known about its paralog RAD9B. RAD9B assembles in the 9-1-1 ring and co-localises with the cell cycle regulator $p21^{Waf1}$ in the nucleolus after UV-induced DNA lesions. The human *RAD9B* gene encodes five protein splice variants of which one, RAD9B-001, resembles the N-terminally truncated Rad9 variant, Rad9-M50, found in

S. pombe cells. Rad9-M50 expression is induced by heat-stress and some forms of DNA damage from a cryptic translational start site within the *rad9* mRNA (Janes et al., 2012). While full-length Rad9 forms the 9-1-1 ring, Rad9-M50 regulates cell cycle progression at elevated temperatures in yeast.

To investigate the cellular roles of full-length RAD9B and its variant RAD9B-001, and to find out whether the yeast Rad9-M50 protein also functions in human cells, three stable HEK293 cell lines will be constructed in this project.

Induction with doxycycline will allow for the over-expression of the three Rad9 proteins. This system will be used to analyse the impact of elevated Rad9 protein levels on cell cycle progression, the response to heat and other environmental stresses, and to different types of DNA damage. The work will focus on the ATR-CHK1 and ATM-CHK2 kinase pathways. While ATR-CHK1 signalling is activated by single-stranded DNA, for example, at stalled DNA replication forks, ATM-Chk2 activity is stimulated by unprocessed DNA double-strand breaks.

These biochemical studies will be complemented by the analysis of the expression profiles of all five *RAD9B* splice variants at mRNA level in a panel of different human tissues. The outcomes of this project may help to understand the complex network of splice variants in healthy and malignant cells, and may provide an answer of why human cells express two close related *RAD9* genes.

Chapter 2: MATERIALS AND METHODS

2.1 Human cell lines

Table 2.1 Human cell lines used in this project

Cell Line Name	Genotype	Source
HeLa (human cervix epithelioid carcinoma cells)	-	Purchased from the Health Protection Agency (HPA) culture collection, cat.no 93021013
Kelly (human neuroblastoma cells)	-	Purchased from Sigma, cat.no. 9110411
Flp-In TREx HEK 293 (human embryonic kidney cells)	FRT integration site	A kind gift from Dr. Fumiko Isahsi, Oxford University
Flp-In TREx HEK 293-EGFP-RAD9B-001	*FRT::EGFP-RAD9B-001*	In current project
Flp-In TREx HEK 293-EGFP-RAD9B-002	*FRT::EGFP-RAD9B-002*	In current project
Flp-In TREx HEK 293-EGFP-Rad9-M50	*FRT::EGFP-Rad9-M50*	In current project
Flp-In TREx HEK 293-EGFP	*FRT::EGFP*	In current project

2.2 Plasmids

Table 2.2 Plasmids used in this project

Plasmid	Source
pcDNA5/FRT/To-EGFP	**Kind gift from Dr. Fumiko Isahsi, Oxford University**
pOG44	**Kind gift from Dr. Fumiko Isahsi, Oxford University**
phRAD9B-002 (MHS1010-202804714)	**Thermo Fisher Scientific**
pRFP-C-RS-shRNA-RAD9A (HT129859A)	**OriGene**
pRFP-C-RS-shRNA-RAD9A (HT129859B)	**OriGene**
pRFP-C-RS-shRNA-RAD9A (HT129859C)	**OriGene**
pRFP-C-RS-shRNA-RAD9A (HT129859D)	**OriGene**

2.3 Cell Line Growth and Maintenance

All cell lines in this project were grown in Dulbecco's modified Eagle's medium (DMEM) supplemented with 10% foetal bovine serum (FBS), 1% penicillin-streptomycin antibiotics, and with or without 200 mM L-glutamine solution in a humidified 37°C incubator. The medium was also supplemented with selective antibiotics depending on the growing cell line (Table 2.3). When the cells reached 80–90% confluency, they were passaged, as described in Section 2.3.3.

Table 2.3 Cell line growing media and conditions

Cell Line Name	CO_2	Media	Selective Antibiotic
Flp-In TrEx HEK293 (human embryonic kidney cells)	5%	DMEM, 10% FBS, 1% penicillin-streptomycin, 200 mM L-glutamine	100 µg/ml zeocin, 15 µg/ml blasticidin
HeLa (human cervix epithelioid carcinoma cells)	5%	DMEM, 10% FBS, 1% penicillin-streptomycin	-
Kelly (human neuroblastoma cells)	5%	DMEM, 10% FBS, 1% penicillin-streptomycin, 200 mM L-glutamine	-

2.3.1 Sources of cell line growth materials

Table 2.4 Sources of essential growth medium, reagents and antibiotics

Material	Source	Cat. No
DMEM	Lonza	BE12-614F
FBS	Sigma	F0804
Penicillin-streptomycin	Lonza	DE17-602E
L-Glutamine	Lonza	17-605C
Zeocin	Thermo Fisher Scientific	R25001
Blasticidin	Thermo Fisher Scientific	R21001
Doxycycline	Sigma	9891-5G
PBS	Lonza	BE02-017F
Trypsin	Lonza	CC-5012

2.3.2 Cell thawing

The vials of cells were removed from the liquid nitrogen container and placed immediately in a 37°C water bath until the last ice crystal was visible. Then the outside of the vials were decontaminated using 70% industrial methylated spirits and the cells were transferred to 10-cm plates containing 9 ml of DMEM free of antibiotics. The cells were allowed to attach and spread overnight in the 37°C incubator. The following day, the medium was aspirated off and replaced with fresh complete medium containing blasticidin and zeocin. Then the cells were incubated at 37°C and checked daily until the cells reached 80–90% confluency. The cells were then passaged as described next.

2.3.3 Cell passaging

The medium was removed from the plates when the cells were approximately 80–90% confluent. The cells were washed with 5 ml of 1x phosphate-buffered saline (PBS) to remove any medium or FBS residue (FBS inhibits trypsin). The PBS was removed and 1 ml of trypsin-ethylenediaminetetraacetic (trypsin-EDTA) was added directly to the cells and then the plates were placed in the incubator at 37°C for 5 min. After incubation, the plates were banged briefly to dislodge the remaining attached cells. The cells were then mixed by pipetting up and down to break up any clumps. The trypsinisation was inhibited by adding 9 ml of complete DMEM to the plates. Then 1 ml of the cell suspensions was transferred to new 10-cm plates containing 9 ml of complete DMED supplemented with blasticidin and zeocin (the dilution can be lowered if faster confluence is required). The plates were placed in a 37°C, humidified, CO_2 incubator until the cells reach 80–90% confluency at which point they were split again.

2.3.4 Cell freezing

Before starting, fresh freezing medium was prepared and then kept on ice (Table 2.5).

Table 2.5 Preparation of freezing medium

DMEM complete medium	0.9 ml
DMSO (dimethyl sulfoxide)	0.1 ml

The medium was removed from the plate once the cells reached approximately 80% confluency, and the cells were washed with 5 ml of 1x PBS. Trypsin (1 ml) was added directly to the cells and the plates were placed in a 37°C incubator for 5 min until the cells became unattached. Then the cells were pipetted up and down to break up any clumps. The trypsinisation was stopped by adding 9 ml of complete DMEM and the cells were counted (Section 2.3.5). All the cells were transferred to 15-ml tubes to be centrifuged for 5 min at 1,500 rpm at room temperature. A clear visible pellet was obtained, and the medium was aspirated off carefully. A density of 3 x 10^6 of cells was suspended in 1 ml of cold freezing medium (Table 2.5). The cell suspensions in freezing medium were transferred into labelled cryovials. All the cryovials were placed in the Mr. Frosty Freezing container and placed in the -80°C freezer overnight. The following day all cryovials were transferred to liquid nitrogen containers for long-term storage.

2.3.5 Cell counting

The medium was aspirated from the plates and the cells were washed with 1x PBS. The cells then were trypsinised and collected in 15-ml tubes, followed by centrifugation at 1,500 rpm for 5 min. The pellets were resuspended in 1 ml of 1x PBS, and 10 µl of the cell suspensions was mixed with 10 µl of 0.4% Trypan Blue solution (Sigma) by pipetting up and down. The mixtures were left for 2–3 min at room temperature. Then 10 µl of the mixtures was inserted into the outer opening of the counting slide chamber. The cell number count was obtained using the Bio-Rad TC20 Automated Cell Counter.

2.4 RNA Extraction

2.4.1 TRIzol RNA extraction

The cells were grown in their appropriate medium and at least 1 x 10^6 of cells were harvested. The medium was aspirated from the plate and the cells were washed twice with 1x PBS. 1 ml of TRIzol (Thermo Fisher Scientific) was added directly to the cells and then cells were removed gently from the plate using a cell scraper. The whole lysate was transferred to a 1.5 ml Eppendorf tube and the tube was left at room temperature for 5 min. Chloroform (250 µl) was added to the cell lysate and the tube was shaken vigorously for 15 s. The sample was allowed to sit at room temperature for 5 min, followed by centrifugation at 10,000 rpm for 5 min.

At this stage, three layers were obtained: clear aqueous (top layer), precipitated DNA (middle layer) and pink organic (bottom layer). The aqueous layer was carefully removed and placed in a new Eppendorf tube (approximately 1 mm of the aqueous layer was left to avoid DNA contamination). Isopropanol (550 ml) was added to the aqueous layer with gentle mixing and the tube was left at room temperature for 5 min. Then the sample was centrifuged at 4°C at full speed for 30 min. After centrifugation, the tube was placed on ice and the isopropanol was removed. The pellet was dissolved in 1 ml of 70% ethanol (ETOH) and 0.1% diethylpyrocarbonate (DEPC)-treated H_2O, followed by centrifugation at 9,000 rpm for 5 min. All the ETOH was removed from the tube and the pellet was allowed to air dry. The pellet then was resuspended in 30 µl of DEPC-treated H_2O. The concentration of the sample was measured using the NanoDrop ND-1000 (Thermo Fisher Scientific), and the RNA was stored at -80 °C until further use.

2.4.2 Column purification RNA extraction

Total RNA was isolated from the human cell lines using the RNeasy Mini Kit (Qiagen) according to the manufacturer's instructions. The RNA concentration and quality were obtained using the NanoDrop ND-1000. The RNA samples were stored at -80 °C until the day of use.

2.5 DNA extraction

DNA was extracted from at least 1 x 10^6 cells using the GenElute Mammalian Genomic DNA Miniprep (Sigma) according to the manufacturer's instructions. The extracted DNA concentration and quality were obtained using the NanoDrop ND-1000.

2.6 Polymerase Chain Reaction

2.6.1 Primers for expression detection

Table 2.6 Primers designed for the expression detection of *RAD9B* splice variants, *RAD9A*, *C12ORF32* and *ACTB*

Primer Name / detected variant	Primer Sequence	*Ta	Amplicon size
(L-001) *RAD9B-001*	**Forward** AAAGCCGTTTGGGAACTTGTGGA **Reverse** **ctacgatggaatctcgagTTAGAATATAGAGAAACTGC CAT	50°C	1363 bp
(L-001-002-005) *RAD9B-001, 002, 005*	**Forward** *atccgttacattatgcggccgcATGAGTGAAAATGAACTTG ACAC **Reverse** **ctacgatggaatctcgagTTAGAATATAGAGAAACTGC CAT	50°C	1038 bp
(L-002-005) *RAD9B-002, 005*	**Forward** *atccttacaatgcggccgcATGGCAGCCATGCTGAAGTG **Reverse** **atagttacgttctcgagTTAGAATATAGAGAAACTGCCA	52°C	1254 bp
(L-003-009) *RAD9B-003, 009*	**Forward** *atccttacaatgcggccgcATGGCAGCCATGCTGAAGTG **Reverse** **atagttacgttctcgagTTAGAATATAGAGAAACTGCCA	52°C	*003* (1290 bp) *009* (974 bp)
(S-001) *RAD9B-001*	**Forward** AAAGCCGTTTGGGAACTTGTG **Reverse** CGTGATAGAGCTTGAACTGC	50°C	215 bp
(S-001-002-005) *RAD9B-001, 002, 005*	**Forward** GTCAGCAACACAGAGGAAGTG **Reverse** TGCTTAATGATGGCTGAGCTGG	50 °C	196 bp
(S-003-009) *RAD9B-003, 009*	**Forward** GTCAGCAACACAGAGGAAGTG **Reverse** CATAGAACAGTATCCTCCACTG	50 °C	*003* (233 bp) *009* (123 bp)
RAD9A	**Forward** TCGCGGAGAGCTGGGCAG **Reverse** TCGCGGAGAGCTGGGCAG	52°C	196 bp
C12ORF32	**Forward** ATGCCTCCCAGAAAAAAACGCCGCC **Reverse** TCAGCTTTTCACAAGGAATTGGCTTC	55°C	717 bp
ACTB	**Forward** ACCAACTGGGACGACATGGAG **Reverse** TGCCAGTGGTACGGCCAGAG	52°C	223 bp

Ta: annealing temperature. S: short fragment. L: long fragment.

* indicates additional sequence contains *Not*1 recognition site designed in forward primer.

** indicates additional sequence contains *Xho*1 recognition site designed in reverse primer.

2.6.2 Two-step RT-PCR

2.6.2.1 cDNA synthesis

Total RNA was extracted from the cell lines using the RNeasy Plus Mini Kit, as mentioned in Section 2.4.2, or purchased from Clontech Laboratories (Human Total RNA Master Panel II). The quality and concentration of the RNA were obtained using the NanoDrop ND-1000. Then 1–2 µg of total RNA was converted to cDNA with the Tetro cDNA Synthesis Kit (Bioline) according to the manufacturer's instructions. Random and hexamer primers were used for the cDNA synthesis.

2.6.2.2 PCR reaction mixture and running program

The cDNA was used as a template for the amplification of the desired gene with BioMix Red (Bioline) as seen in Table 2.7.

Table 2.7 Two-step RT-PCR reaction mix

BioMix Red	25 µl
Forward primer	250 nM
Reverse primer	250 nM
cDNA	5 µl
DEPC-treated water	Up to 50 µl

The PCR reaction mixture was run using the standard PCR program seen in Table 2.8.

Table 2.8 Standard PCR program

Hot start	98°C	2 min
Denaturing	98°C	10 s
Annealing	Depends on primer pair	10 s
Extension	72°C	1 min/1 Kb
Final Extension	72°C	10 min
Number of cycles	35	-

The amplified PCR products were run on agarose gels as described in Section 2.7.

2.6.3 One-step RT-PCR

Total RNA samples extracted in the lab or the purchased from Clontech Laboratories (Human Total RNA Master Panel II) were used as a template in the one-step RT-PCR reaction using the MyTag One-Step RT-PCR Kit, (Bioline) using a concentration of 200 ng of total RNA per PCR. Specific primers for each gene and their expected size can be seen in (Table 2.6). The one-step RT-PCR reaction was set up as following:

Table 2.9 One-step RT-PCR reaction mix

MyTag One-Step mix (2x)	25 µl
Forward primer	250 nM
Reverse primer	250 nM
Total RNA	200 ng
Reverse transcriptase	0.5 µl
RiboSafe RNase Inhibitor 10 U/µl	1 µl
DEPC-treated water	Up to 50 µl

The one-step RT-PCR reaction mixture was run using the PCR program shown in Table 2.10.

Table 2.10 One-step RT-PCR program

Stage	Temperature	Time	Cycles
Reverse transcription	45°C	30 min	1
Polymerase activation	95°C	1 min	1
Denaturing Annealing Extension	95°C 55°C 72°C	10 s 10 s 30 s	 40
Final Extension	72°C	10 min	1

The amplified PCR products were analysed on agarose gels as mentioned in Section 2.7.1.

2.6.4 Real-time quantitative reverse transcription (qRT)-PCR

Total RNA was extracted from subconfluent cells and 1–2 µg of total RNA was reverse transcribed into cDNA, as previously mentioned in Sections 2.4.2 and 2.6.2.

2.6.4.1 qRT-PCR primers

All primers for the qRT-PCR were purchased from Qiagen (Table 2.11). The primers were chosen to be intron-spanning and designed to avoid any DNA contamination. All amplicons were smaller than 160 bp. The *TBP* and *TuBA* primers were used as a qRT-PCR positive normalisation control for the qPCR results.

Table 2.11 qRT-PCR primers

Gene	Source	Cat. No	Amplicon size
RAD9B	Qiagen	QT00016471	131-160 bp
RAD9A	Qiagen	QT00216846	141 bp
HUS1	Qiagen	QT00025165	105 bp
RAD1	Qiagen	QT00091287	113 bp
TBP	Qiagen	QT00000721	132 bp
TUBA	Qiagen	QT00062720	116 bp

2.6.4.2 qRT-PCR plate setup

The GoTaq qPCR master mix (Promega) was used for the qPCR. In a 96-well plate, the qPCR was set up in triplicate. Each reaction was set up as seen in Table 2.12.

Table 2.12 qPCR reaction mix

SYBR Green master mix	10 µl
cDNA	5 µl
qPCR primer	2 µl
Nuclease-free H_2O	3 µl

For the negative control, the qPCR was set up as seen in Table 2.13.

Table 2.13 Negative qPCR control mix

SYBR Green master mix	10 µl
NTR cDNA (No Reverse Transcriptase)	5 µl
qPCR primer	2 µl
Nuclease free H_2O	3 µl

2.6.4.3 qRT-PCR program

The 96-well plate was placed in the Bio-Rad CFX machine and the qPCR program was run as seen in Table 2.14.

Table 2.14 qPCR amplification program

Pre-denature	95°C
Denature	95°C
Annealing	60°C
Extension	72°C
Number of cycles	40

The qPCR results were analysed using the Bio-Rad CFX Manager Software (Version 2.1).

2.7 Agarose Gel Electrophoresis

Gel electrophoresis was used for the analysis of RNA, DNA, PCR products, amplified and digested plasmids. Different percentages of agarose gels were used depending on the fragment size as seen in Table 2.15.

Table 2.15 Agarose gel concentration vs fragment size

Size (bp)	Percentage	Agarose (g)	*1x TEA Buffer
100–250	2%	3	150 ml
250–1000	1.5%	2.25	150 ml
1000–10000	0.8%	1.2	150 ml

*1x TEA Buffer: 40 mM Tris (pH = 8), 20 mM acetic acid, 1 mM EDTA

Note: These volumes are prepared for the midi tanks.

The appropriate concentration from the above table was prepared and mixed by swirling. The gel mixture was microwaved for 2–3 min with swirling every 45 s. The gel was allowed to cool to 50°C and then 0.5 µg/ml of ethidium bromide was added to the gel. Then the gel was poured into the Bio-Rad trays and combes were placed immediately. The gel was allowed to set for at least 30 min. The set gel was placed in the BIO-RAD tank and filled with 500 ml of 1X TEA (Tris-acetate-EDTA) buffer.

2.7.1 Sample preparation and loading

The DNA and RNA samples were mixed with 6x Blue/Orange Loading Dye (Promega) just before loading onto the agarose gel. The first lane of the gel was loaded with either the DNA 1 kb standard (Promega) or the 100 bp Standard (Promega) depending on the size of the fragments loaded onto the gel. The gels were run at 100 V for 1 hr. Analysis of the agarose gels was carried out using the Doc200 machine (Bio-Rad) and the Quantity One 1-D analysis software (Bio-Rad).

2.7.2 DNA purification

The whole PCR sample (50 µl) was run and separated on agarose gel electrophoresis. The band of interest was cut out of the gel under the UV light and placed in a new Eppendorf tube. The DNA purification was performed using the ISOLATE II PCR and Gel Kit (Bioline) according to the manufacturer's instructions.

2.8 Western Blot

2.8.1 Protein Extraction

2.8.1.1 Whole cell extract

When cells were approximately 80% confluent, the medium was removed and cells were washed with 5 ml of cold 1x PBS. The cells then were trypsinised, collected in complete medium, and counted as mentioned in Section 2.3.5. The cells were centrifuged at 1,500 rpm for 5 min and the cell pellet was washed with cold 1x PBS. The cells were spun down again at 1,500 rpm for 5 min and the pellet was resuspended in whole protein lysis buffer (50 mM Tris-HCl (pH = 7.4), 200 mM NaCl, 0.5% Triton X-100) at a ratio of 100 µl lysis buffer for each 1 x 10^6 of cells. The cell lysate was supplemented with 1x protease inhibitor cocktail III for mammalian cells (1 µl/100 µl of lysis buffer, Melford), 125 U/ml Benzonase (Merck Millipore) and 1.5 mM $MgCl_2$. The extracts were kept on ice for 1 hr with vortexing every 15 min. The extracts were then centrifuged at full speed for 10 min at 4°C. The supernatant was transferred to a new Eppendorf tube and stored at -20°C until further use.

2.8.1.2 Protein fractionation

Subconfluent cells were washed with 1x cold PBS, trypsinised, and collected in cold complete medium. Then the cells were centrifuged at 1,500 rpm for 5 min and counted as mentioned in Section 2.3.5. For the cytoplasmic fraction, the pellet was resuspended in hypotonic buffer (50 mM Tris-HCl pH = 7.4, 0. 1 M sucrose) combined with an equal volume of Buffer C (1% Triton-X100, 10 mM $MgCl_2$) in a ratio of 100 µl of both buffers for each 1 x 10^6 cells. The cell lysate was supplemented with 1 µl protease inhibitor per 100 µl of combined lysis buffer, mixed gently and left on ice for 30 min. Then the lysate was centrifuged at 6,000 x g for 2 min at 4°C and the supernatant (cytoplasmic fraction) was transferred to a new Eppendorf tube. The remaining pellet (nuclear fraction) was washed once with 1x PBS to

remove any cytoplasmic protein residue and the cell pellet was collected again by centrifugation at 6,000 x g for 2 min at 4°C. The pellet was resuspended in 100 µl of Buffer N (50 mM Tris-HCl pH = 7.4, 100 mM KAc) per 1 x 10^6 cells. The nuclear fraction was supplied with protease inhibitor (1 µl/ 100 µl), 125 U/ml Benzonase and 1.5 mM MgCl2. Both fractions were stored at -20 °C until analysed on an SDS-PAGE gel.

2.8.2 Protein concentration

Before the protein samples were run on an SDS-PAGE gel, the concentration of each protein sample was measured using the BCA Protein Assay Kit (Thermo Fisher Scientific) according to the supplier's instructions. For the normal SDS-PAGE, native protein electrophoresis and Phos-tag electrophoresis, 30 µg of protein was loaded onto the gel.

2.8.3 Normal SDS-PAGE

2.8.3.1 SDS-PAGE Concentration

The protein samples were run on different concentrations of SDS-PAGE gels according to their size. The four SDS-PAGE concentrations used are shown in Table 2.16.

Table 2.16 Preparation of lower separation gel

Concentration	8%	10%	12%	15%
Number of gels	4	4	4	4
1 M Tris-HCl pH = 8.8	7.5 ml	7.5 ml	7.5 ml	7.5 ml
40% Acrylamide/Bis 37.5:1	4 ml	5 ml	6 ml	7.5 ml
20% *SDS	150 µl	150 µl	150 µl	150 µl
H_2O	8.5 ml	7.5 ml	6.5 ml	5 ml
10% *APS	100 µl	100 µl	100 µl	100 µl
*TEMED	30 µl	30 µl	30 µl	30 µl
Total	20 ml	20 ml	20 ml	20 ml

*SDS: Sodium dodecyl persulfate.
*APS: Ammonium Persulfate.
*TEMED: Tetramethylethylenediamine.

The prepared gels were cast between the Bio-Rad Blotting System glass plates and the gels were overlaid with drops of isopropanol to remove any bubbles. The gels were allowed to set for 30 min at room temperature. Once the separation gels were set, the isopropanol layer was washed using dH_2O. The stacking gels were then prepared as seen in Table 2.17.

Table 2.17 Preparation of upper stacking gel

Concentration	4%
Number of gels	4
1 M Tris-HCl pH = 6.8	1.5 ml
40% Acrylamide/Bis 37.5:1	1 ml
20% SDS	50 µl
H_2O	7.5 ml
10% APS	100 µl
TEMED	10 µl
Total	20 ml

The stacking gels were placed on top of the separation gel layers and combs were inserted immediately. The gels were allowed to set for 15 min at room temperature.

2.8.3.2 Protein sample preparation

Just before loading the protein extracts onto the SDS-PAGE gel, the samples were mixed with 4x Laemmli buffer (40% glycerol, 240 mM Tris-HCl pH = 6.8, 8% SDS, 0.04% bromophenol blue and 5% B-mercaptoethanol). Then the samples were denatured by boiling at 95°C for 5 min.

2.8.3.3 Running samples on SDS-PAGE

The gels were placed in Bio-Rad protein electrophoresis tanks filled with 1x SDS buffer (28.8 g glycine, 6.04 g Tris base, 2 g SDS, up to 2 L dH_2O). The combs were removed and the protein standard ladder (Thermo Fisher Scientific) was loaded onto the gels in parallel with the protein extracts. The electrophoresis gels were run at 100 V for 1.45 hr. When the electrophoresis was finished, the gels were removed from the tanks and transferred onto blotting membranes (See Section 2.9).

2.8.4 2D isoelectric focusing

2.8.4.1 2D sample preparation

Expression was induced by adding doxycycline (1 µg/ml) and then incubating overnight. After incubation, the cells were washed with 1x PBS, trypsinised, and spun down at 1,500 rpm for 5 min. The cell pellet was resuspended in IEF (isoelectric focusing) Buffer (7 M urea, 2 M thiourea, bromophenol blue) supplemented with protease inhibitor cocktail (1 µl/ 100 µl),

125 U/ml Benzonase and 1.5 mM MgCl2 in a ratio of 100 µl of IEF buffer per 1 x 10^6 of cells.

2.8.4.2 Running samples on a 2D isoelectric focusing machine

The 2D sample lysate (15 µl) was further diluted in 110 µl of IEF buffer and the total 125 µl was loaded onto the 2D tray. The immobilized pH gradient (IPG) strips nonlinear (pH 3–10, Bio-Rad) were carefully lowered onto the protein solution, making sure the protein solution was in contact with both electrodes. The strips were then overlaid with 2 ml of mineral oil and the 2D program was set up as seen in Table 2.18.

Table 2.18 2D electrophoresis program

Running	Active dehydration at 50 V for 12 hr
Focusing	Rapid method, 10,000 V, hold to 500 V

Once the run was finished, the strips were placed in 2D normal trays with the gel facing up. The strips were incubated for 10 min in 2D solution I (6 M urea, 0.375 M Tris-HCl (pH = 8.8), 2% SDS, 20% glycerol, 2% (w/v) Dithiothreitol (DTT)) and then they were incubated for another 10 min in 2 ml of 2D solution II (Tris-HCl pH = 8.8, 2% SDS, 20% glycerol, 2.5% (w/v) iodoacetamide). Both incubations were performed on the rocking platform at room temperature.

2.8.4.3 Running 2D strips on SDS-PAGE

The 2D strips were run on a 10% normal SDS-PAGE gel (Table 2.16). The electrophoresis gels consisted of only the lower separation layer. The separation gels were cast right to the top of the glass plates, leaving approximately 5 mm space to apply the strip. The electrophoresis gels were run at 100 V for 1.5 hr and the transfer and staining were performed as mentioned in Sections 2.9 and 2.10.

2.8.5 Native protein electrophoresis

2.8.5.1 Preparation of native PAGE

The native PAGE consisted of one gel layer prepared as seen in Table 2.19.

Table 2.19 Native gel components

Component	Volume
Polyacrylamide	2.5 ml
1.5 M Tris-HCl pH = 8.8	2.5 ml
H_2O	5.5 ml
10% APS	50 µl
TEMED	10 µl

*These volumes are sufficient for two gels.

2.8.5.2 Native protein sample preparation

The protein extracts were mixed with 2x native sample buffer (0.187 M Tris-HCl pH = 6.8, 30% glycerol, 80 µg/ml bromophenol blue) just before loading onto the native SDS-PAGE gel. The native gels were placed in electrophoresis tanks filled with 1x native gel running buffer (28.8 g glycine, 6 g Tris base, up to 2 L H_2O, final pH = 8.3). The native samples were loaded onto gels without boiling. The gels were run at 150 V for 1 hr.

2.8.6 Phos-tag gels

The lower separation gels were prepared as seen below (Table 2.20). The Phos-tag prepared gels were cast between the Bio-Rad Blotting System glass plates and the gels were overlaid with drops of isopropanol to remove bubbles. The gels were allowed to set for 30 min at room temperature. Once the separation gel was set, the isopropanol layer was washed using dH_2O. The stacking gel was then prepared as previously shown in (Table 2.17).

Table 2.20 Phos-tag PAGE lower gel preparation

Component	Concentration
Acrylamide/Bis 29:1	1.4 ml
1 M Tris-HCl pH = 8	1.8 ml
5 mM Phos-tag	70 µl
10 mM $MnCl_2$	70 µl
20% SDS	27 µl
TEMED	15 µl
10% APS	70 µl

The gels were run normally, as described in Section 2.8.3.3. After electrophoresis, the gels were washed three times in 1x transfer buffer supplemented with 20 mM EDTA to remove the Mn++ ions, as they interfere with the transfer. The transfer was performed as mentioned in Section 2.9 overnight at 10 V.

2.9 Membrane Transfer

In a tray containing 1x transfer buffer (28.8 g glycine, 6.04 g Tris base, 200 ml methanol, up to 2 L H_2O), the transfer sandwich was set up in the following order: black cassette on the bottom, pre-wet sponge, filter paper, equilibrated gel, PVDF or nitrocellulose membrane, filter paper, pre-wet sponge and red cassette on top. The transfer sandwiches were placed in the transfer tank filled with 1x transfer buffer, and the transfer was run at 65 V for 2.5 hr or at 10 V overnight. The PVDF, nitrocellulose and filter paper purchased from GE Health Life Sciences.

2.10 Membrane Blocking, Antibody Staining and Developing

The membranes were incubated in 3% milk blocking buffer (3% milk powder in 1x PBS, 0.05% Tween 20) for 1 hr on the rocking platform. The corresponding primary antibodies were diluted (for antibody concentrations see section 2.11) in blocking buffer. The diluted primary antibodies were added to the membranes in sealed plastic bags and incubated overnight. The primary antibodies were removed and the membranes were washed three times with 1x washing buffer (1x PBS with 0.05% Tween 20). Each wash was for 10 min at room temperature. The membranes were then incubated with the diluted secondary antibodies (see 2.11) in blocking buffer in sealed plastic bags for 1 hr. The membranes were then washed three times in 1x washing buffer, with each wash for 10 min.

The white (0.5 ml) and brown (0.5 ml) Western lightening ECl-plus solutions (PerkinElmer) were added to the membranes, making sure the mixed solution covered the whole membrane. Then the membranes were placed in plastic wallets in X-ray film boxes. In the dark developing room, one X-ray film (Thermo Fisher Scientific) was placed on top of each membrane with the plastic sheet between. The X-ray film box was closed firmly and the film was exposed for a few min (depending on the antibody and protein concentrations). The film was then developed using the OptiMax X-ray Processor machine.

2.11 Antibodies

Table 2.21 list of primary antibodies used in this project

Name	Company	Dilution	Product number
Anti-Fibrillarin	Abcam	1:500	AB5821
ATM	Cell Signalling	1:1000	2837
ATR	Cell Signalling	1:1000	2790
BAK	Cell Signalling	1:1000	3814
Bcl-2	Cell Signalling	1:1000	15071
Chk1	Cell Signalling	1:1000	2360
Chk2	Cell Signalling	1:1000	3440
GAPDH	Cell Signalling	1:5000	2118
GFP	Thermo Fisher Scientific	1:1000	MA5-15256
GFP	Santa Cruz	1:1000	B-2
Histon H3	Abcam	1:5000	AB1791
Hus1	Abcam	1:10000	AB96297
Lamin B	Santa Cruz	1:2000	M-20
p21	Cell Signalling	1:1000	2947
p53	Cell Signalling	1:1000	9282
PARP	Cell Signalling	1:1000	9542
p-ATM (Ser-1981)	Cell Signalling	1:1000	5883
p-ATR (Ser-428)	Cell Signalling	1:1000	2853
p-Chk1 (Ser-345)	Cell Signalling	1:500	2341
p-Chk2 (Thr-68)	Cell Signalling	1:500	2661
PCNA	Abcam	1:2000	AB29
p-p53 (Ser-15)	Cell Signalling	1:1000	9284
Rad1	Abcam	1:1000	AB5363
Rad9A	Fisher Scientific	1:1000	PA5-212 75

Table 2.22 list of secondary antibodies used in this project

Name	Company	Dilution	Product number
Alexa Flour 488	Thermo Fisher Scientific	1:500	A11059
Alexa Flour 532	Thermo Fisher Scientific	1:500	AB5821
Anti-Goat	Abcam	1:10000	AB6741
Anti-Mouse	Millipore	1:10000	402335
Anti-Rabbit	Millipore	1:10000	401315

2.12 Immunofluorescence Microscopy

2.12.1 Cell growth

In the tissue culture hood, coverslips (Chemglass) were placed in 24-well plates with enough covers for the antibody conditions. The coverslips were exposed to UV light (5 J/m^2) for 30 s to make sure all the coverslips were sterilised before use. Then the cells were seeded onto the coverslips at a confluency of 40–50% (approximately 50,000 cells per well) in 1 ml medium, and the cells were allowed to grow and spread for 1 day.

2.12.2 Cell fixation

After 24 hr of seeding, the medium was carefully aspirated and the cells were washed with 1 ml of warm 1x PBS. The cells were fixed by adding 0.5 ml of fixing solution to the wells (4% paraformaldehyde in 1x PBS) and the plates were left in the hood for 10 min for the cells to be fixed. Then the fixing solution was aspirated and replaced with 0.5 ml of permeabilisation solution (0.2% Triton in 1x PBS) and the plates were left in the hood for 10 min. The cells were then washed three times in 1x PBS, with each wash for 10 min on the rocking platform. The cells were blocked by adding 0.5 ml of FBS blocking solution (5% FBS in 1x PBS) and the plates were left on the rocking platform at room temperature for 1 hr.

2.12.3 Immunostaining

The blocking solution was aspirated off and 0.5 ml of the primary antibodies diluted in blocking solution was added directly to the cells, with all the coverslips well immersed. The cells were incubated overnight on the rocking platform at 4°C. The following day, the primary antibodies were aspirated off and the cells were washed three times in 1x PBS, with each wash for 10 min. Then, in a dark hood, 0.5 ml of secondary antibody Alexa Fluor 488 (green) or Alexa Fluor 532 (red) (depending on the co-staining) diluted in blocking solution was added to the cells, making sure all coverslips are immersed well. For concentrations of the primary and secondary antibodies, please refer to the antibodies table (Table 2.21). The plates were covered with foil and left on the rocking platform for 2 hr at room temperature.

2.12.4 Microscope slides mounting

On glass microscope slides, 10 µl of 4',6-diamidino-2-phenylindole (DAPI) mounting solution (Vector Laboratories) was placed where the sample coverslips were fixed. The coverslips were removed from the plates and the excess fluid was removed before the coverslips were carefully inverted onto the mounting solution. The coverslips then were surrounded on the edges with clear nail varnish and the slides were kept at 4°C until the samples were analysed. The samples were analysed with a LSM 710 Confocal Microscope using the 40x objective. The images were analysed and processed by Zen lite software.

2.13 Cell Synchronisation

2.13.1 Serum starvation

HEK293 and HeLa cells were seeded at 40% confluency onto 15-cm plates containing complete DMEM and allowed to attach for a few hours at 37°C. The cells were washed twice with 1x PBS to remove any remaining serum residue, followed by incubating the cells in FBS-free medium at 37°C for 24 hr. The cells then were stimulated by releasing the cells into complete medium. Whole protein extract and fixed samples were taken before and 6 hours post-release.

2.13.2 Cell senescence

Oxidative stress was applied to HEK293 and HeLa cells to induce cellular senescence. The cells were plated in 15-cm plates at ~40% confluency and were allowed to attach to the plates for a few hours. The medium then was aspirated from the plates and the cells were washed twice with warm 1x PBS to remove any FBS residue, followed with adding 15 ml of FBS-free medium supplemented with 200 µM H_2O_2 to the plates. The cells were incubated at 37°C for 1 hr. The medium then was removed, the cells were washed twice with warm 1x PBS followed by incubation in complete medium at 37°C for 3 days. Images were taken using the CMEX-5000 Camera (Euromex) placed on an Eclipse TS100 Microscope (Nikon). Protein and RNA were extracted 24, 48 and 72 hr after the treatment.

2.14 *RAD9B* Expression in Subconfluent and Superconfluent Cells

Cells were plated at a density of 1 x 10^6 and they were allowed to grow at 37°C in their appropriate medium. On day 4, total RNA was extracted from the subconfluent cells, as described in Section 2.4.2. For the superconfluent samples, the cells were allowed to grow for approximately 7 days with changing the medium on day 4. Total RNA was extracted from the subconfluent cells, as described in Section 2.4.2. The extracted RNA (200 ng) was used as a template for the amplification of full-length transcripts using one-step RT-PCR. Then 1 µg of total RNA was reverse transcribed into cDNA, which was used as a template for the detection of *RAD9B* splice variants using short internal primers.

2.15 Preparation and Analysis of Flow Cytometry Samples

Cells were seeded at 40% confluency and allowed to attach for a few hours at 37°C. The cells then were treated with the experiment-corresponding treatment. The cells then were incubated at 37°C until their sample extraction time. At the time of extraction, the cells were centrifuged at 1,500 rpm for 5 min, followed by washing the pellets with 1x PBS. The pellets then were resuspended in 100 µl of 1x PBS and fixed dropwise with ice-cold 100% methanol while the samples were vortexed. Then the samples were kept at -20°C for at least 24 hr. Just before analysis on the CyFlow CUBE 8 flow cytometry machine (Sysmex), the cells were spun down at 1,500 rpm and washed twice with 1x PBS to remove any remaining methanol residue. The cells were resuspended in staining solution (100 µg/ml RNAse and 50 µl/ml propidium iodide resuspended in 1x PBS) and incubated at 37°C for 30 min. the cells then were run through the flow cytometer machine and the samples were analysed using the Flowing Software 2.

2.16 Construction of Stable Human N-Terminal EGFP-Tagged Cell Lines

2.16.1 Cassette amplification

All primers used for the cloning of *RAD9B-001*, *RAD9B-002* and *Rad9-M50* were designed to have an *Not*I restriction site at the 5’ end of the forward primer and an *Xho*I restriction site at the 3’ end of the reverse primer to create sticky ends for cloning.

2.16.1.1 *RAD9B-001* amplification

The *RAD9B-001* was amplified by amplifying each of its nine exons individually, followed by fusion of the nine amplified exons using fusion PCR. The primers were designed to have an overlapping extension sequence allowing for the fusion. Table 2.23 shows the primers used.

Table 2.23 *RAD9B-001* construction primers

Primer Region and orientation	Sequence
Exon 1 (F)	*atccgttacattatgcggccgcATGAGTGAAAATGAACTTGACAC
Exon 1 (R)	AGACATCTAAAGATGGGCAAAATTGACTTCATTCCCAATTTGCATTTTAAATGG
Exon 2 (F)	TTTAAAATGCAAATTGGGAATGAAGTCAATTTTGCCCATCTTTAGATGTCTG
Exon 2 (R)	CATATATTATGAGTTCTTTTAATACCATGTCTGTAGAAGAATTGAATAACTACC
Exon 3 (F)	AGTTATTCAATTCTTCTACAGACATGGTATTAAAAGAACTCATAATATATGT
Exon 3 (R)	AAAAGAACAATGGCATCAGCAAGCAATCTTGGTTGAATCATTAGCGTATTAGTT
Exon 4 (F)	TAATACGCTAATGATTCAACCAAGATTGCTTGCTGATGCCATTGTTCTTTTT
Exon 4 (R)	TCACTGTGTACAGCATTGCTCAAATCCATTGATTCCTCATTAGAACTCTTGAGG
Exon 5 (F)	CAAGAGTTCTAATGAGGAATCAATGGATTTGAGCAATGCTGTACACAGTGAG
Exon 5 (R)	GTAGCTTCTGAAAATGTCAGTATTCCCTTCAATTCTTTGAAACAAAATGTTATT
Exon 6 (F)	AACATTTTGTTTCAAAGAATTGAAGGGAATACTGACATTTTCAGAAGCTACA
Exon 6 (R)	ATATCATCAATACTCAAAGCCAGAGGTTTCCCAGGGAAATCAAAATAAATGGAA
Exon 7 (F)	CATTTATTTTGATTTCCCTGGGAAACCTCTGGCTTTGAGTATTGATGATATG
Exon 7 (R)	CCAGCCTTTTTTTCAATCAGATCTGACCTTTTTCGTTTCTGTGAAAGACACAGG
Exon 8 (F)	GTGTCTTTCACAGAAACGAAAAAGGTCAGATCTGATTGAAAAAAAGGCTGGC
Exon 8 (R)	ACTGCTCCAAAGAACATGCAAGAAAACTTTCTGAGACACAGAGACCCTGGCACC
Exon 9 (F)	GCCAGGGTCTCTGTGTCTCAGAAAGTTTTCTTGCATGTTCTTTGGAGCAGTT
Exon 9 (R)	**ctacgatggaatctcgagTTAGAATATAGAGAAACTGCCAT

(F): forward. (R): reverse.
*atccgttacattatgcggccgc: additional sequence contains *Not*1 recognition site designed in forward primer.**ctacgatggaatctcgag: additional sequence contains *Xho*1 recognition site designed in reverse primer.

RNA was extracted from HEK293, as described in Section 2.4.2, and then it was converted to cDNA, as described in Section 2.6.2.1. The nine exons of *RAD9B-001* were amplified using the nine primer pairs from (Table 2.24). The PCR was set up as following:

Table 2.24 amplification of *RAD9B* PCR reaction mix

Forward primer	250 nM
Reverse primer	250 nM
cDNA	5 µl
5x GC buffer	10 µl
2 mM dNTPs	5 µl
HF Phusion polymerase	1 µl
Nuclease-free H_2O	24 µl

All amplified exons were purified from the agarose gel, as mentioned in Section 2.7.2 and fused to one fragment, creating the *RAD9B-001* cDNA using the fusion PCR, as seen in Tables 2.25, 2.26, 2.27 and 2.28.

Table 2.25 First fusion PCR reaction

Forward primer *atccgttacattatgcggccgcATGAGTGAAAATGAACTTGACAC	250 nM
Reverse Primer **ctacgatggaatctcgagTTAGAATATAGAGAAACTGCCAT	250 nM
Amplified exon	3–5 µl
5x GC buffer	10 µl
2 mM dNTPs	5 µl
HF Phusion polymerase	1 µl
Nuclease-free H_2O	Up to 50 µl H_2O

*atccgttacattatgcggccgc: additional sequence contains *Not*1 recognition site designed in forward primer.**ctacgatggaatctcgag: additional sequence contains *Xho*1 recognition site designed in reverse primer.

The fusion PCR consisted of two stages as following:

Table 2.26 First stage of fusion PCR

Pre-denature	98 °C	2 min
Denature	98 °C	30 s
Anneal	55 °C	30 s
Extend	72 °C	1 min
Number of cycles	10	-

Once the first PCR reaction stopped, the second fusion reaction mix was added to the same PCR tube as following:

Table 2.27 Second fusion PCR reaction mix

Forward primer	500 nM
Reverse primer	500 nM
5x HF buffer	15 µl
2 mM dNTPs	10 µl
HF Phusion polymerase	1 µl
Nuclease-free H_2O	14 µl H_2O

The fusion PCR reaction was then run using the program shown in Table 2.28.

Table 2.28 Second stage of the fusion PCR

Pre-denature	98 °C	2 min
Denature	98 °C	30 s
Anneal	55 °C	30 s
Extend	72 °C	1 min
Final extension	72 °C	10 min
Number of cycles	30	-

The amplified *RAD9B-001* was analysed on agarose electrophoresis, purified, and sent for sequencing.

2.16.1.2 Amplification of *RAD9-002*

The *RAD9B-002* was amplified from the purchased plasmid (Thermo Fisher Scientific, MHS1010-202804714) as mentioned in 2.6.2.2 using the cloning primers seen in Table 2.29.

Table 2.29 *RAD9B* amplification primers

Primer	Sequence
Forward	atccttacaatgcggccgcATGGCAGCCATGCTGAAGTG
Reverse	atagttacgttctcgagTTAGAATATAGAGAAACTGCCAT

The amplified *RAD9B-002* was analysed on agarose electrophoresis, purified, and sent for sequencing.

2.16.1.3 Amplification of *Rad9-M50*

RNA extracted from yeast was used as a template to amplify Rad9-M50 as mentioned in section 2.6.2.2 using the cloning primers shown in Table 2.30.

Table 2.30 *Rad9-M50* amplification primers

Primer	Sequence
Forward	atccttacaatgcggccgcATGATTAAATCCGAGAACAGTC
Reverse	atagttacgttctcgagCTAACTCGAAGAATTGAGCTG

The amplified *Rad9-M50* was analysed on agarose electrophoresis, purified and was sent for sequencing.

2.16.2 PCR Fragment and vector digestion

The primers used to amplify the inserts were designed to contain a restriction site for *Not*I (**gcggccgc**) and *Xho*I (**ctcgag**). Both the pcDNA5/FRT/TO vector and the PCR product were purified from agarose and the digestion was carried out according to NEB (New England Biolabs' (NEB) basic protocol as seen in Table 2.31.

Table 2.31 Restriction digest reaction mix

Restriction Enzyme	5 units 0.5 µl	10 units 1 µl
DNA	0.5 µg	1 µg
10X NEB buffer	2.5 µl	5 µl
Nuclease-free water	Up to 25 µl	Up to 50 µl
Incubation time	1–1.5 hr	1–1.5 hr
Temperature	37°C	37°C

The digestion reaction was inactivated by loading the total reaction onto an agarose gel followed by gel purification. The 50 µl reaction was used for cloning purposes whereas the 25 µl reaction was used to confirm of the cloning.

2.16.3 Insert and vector ligation

The EGFP tag was inserted into the N-terminal of the pcDNA5/FRT/TO plasmid at the *Kbn*I site by Dr. Fumiko Isashi's research group (Oxford University). The *RAD9B-001*, *RAD9B-002* and *Rad9M-50* insert cDNAs were ligated into the pcDNA5/FRT/TO plasmids in a 3:1 ratio respectively. The ligation reactions were performed as shown in Table 2.32.

Table 2.32 Insert and vector ligation reaction

Component	Volume
Vector DNA	X µl
Insert DNA	X µl
T4 ligase buffer	2 µl
T4 ligase enzyme	1 µl
Nuclease-free water	Up to 20 µl

The ligation mixtures were mixed gently and left at 16°C overnight. The mixtures were then saved at -20°C until needed for transformation into *E. coli* cells.

2.16.4 Transformation

2.16.4.1 Transformation of ligated plasmid into *E. coli*-competent cells

The Alpha-Select Gold Efficiency Competent Cells (Bioline) were transfected with 5 µl of the ligated plasmid in a tube placed on ice. The tube was flicked gently without vortexing and incubated on ice for 30 min. The cells were then heat shocked at 42°C for 30 s, followed by placing the tube on ice for 5 min. Luria-Bertani (LB) medium (1 ml of 10 g Tryptone, 10 g NaCl, yeast extract 5 g, up to 1 L H_2O) was added to the cell mixture, mixed gently and placed on a 37°C shaker for 1 hr. Several 10-fold serial dilutions were prepared and 100 µl of each dilution was spread on LB ampicillin agar plates (10 g Tryptone, 10 g NaCl, yeast extract 5 g, 50 µg/ml ampicillin (Amp), up to 1 L H_2O). The plates were incubated at 37°C for 24 hr.

2.16.4.2 Plasmid extraction from *E. coli* cells

The plasmid DNA was extracted from *E. coli* cells with either the ISOLATE II Plasmid Mini Kit (Bioline) if a high concentration of plasmid DNA was not required or the GenElute Plasmid midiprep Kit (Sigma) if a high concentration of DNA plasmid was required. Both extraction types were done according to the manufacturer's instructions.

2.16.4.3 Insertion confirmation

The resulting plasmids described in Section 2.16.3 were digested with *Not*I and *Xho*I restriction enzymes, as described in Section 2.16.2 for the 25 µl reaction. Only 10 µl of the digestion reaction was loaded onto agarose gel and successful insertion was determined by corresponding band size.

2.16.5 RAD9B-001 repair

The sequenced form of the cloned *RAD9B-001* revealed a four-base pair deletion at the 3' end. This was corrected by designing primers containing the missing base pairs and binding a few base pairs before the deletion at the 5'end and a few base pairs before the deletion at the 3' end. The PCR was done by using the cloning forward primer with the reverse fixing primer and the forward fixing primer with the reverse cloning primer (Table 2.33). Both amplified fragments were purified from the agarose gel. The purified

fragments were then fused together and amplified using the fusion PCR as mentioned previously (Section 2.16.1.1). The fusion PCR product was then recloned into pcDNA5/FRT/TO-EGFP and sent for sequencing.

Table 2.33 Primers for the repair of *RAD9B-001*

Primer	Sequence
RAD9B-001 forward	**atccgttacattatgcggccgcATGAGTGAAAATGAACTTGACAC
Fixing primer reverse	GCCAGAGGTTTCCCAGGGAAATCAAAATAAATGGATATAGGAGCATGTGTAG
Fixing primer forward	GCTACACATGCTCCTATATCCATTTATTTTGATTTCCCTGGGAAACCTCTGGC
RAD9B-001 reverse	*atagttacgttctcgagTTAGAATATAGAGAAACTGCCAT

*atccgttacattatgcggccgc: additional sequence contains *Not*1 recognition site designed in forward primer.**ctacgatggaatctcgag: additional sequence contains *Xho*1 recognition site designed in reverse primer.

2.16.6 *Rad9-M50* repair

The cloned *Rad9M-50* displayed two substitution mutations within the sequence. These substitutions were corrected by designing primers in which the forward primer contained the change codon approximately 10 nucleotides from the 3' end of the primer to allow for correct binding. The reverse primer started at the 5' end with one base pair next to the beginning of the forward primer (Table 2.34). These substitutions were corrected using the Q5 Mutagenesis Kit (New England Biolabs) according to the manufacturer's instructions.

Table 2.34 Primers for the repair of *Rad9-M50*

Primer	Sequence
Rad9-M50 forward fixing primer 1	cttgcaactgTagttggatcagatg
Rad9-M50 reverse fixing primer 1	aatgaactgcgcttcaatttc
Rad9-M50 forward fixing primer 2	ggaaatagaTggcagcacagttc
Rad9-M50 reverse fixing primer 2	catcatagatgacacctcttg

-The sequences highlighted in red represent the substitution mutations.

2.16.7 Transfection of constructed plasmid into the Flp-In TREx HEK 293 cell line

The four plasmids pcDNA5/FRT/TO-EGFP-RAD9B-001, pcDNA5/FRT/TO-EGFP-RAD9B-002, pcDNA5/FRT/TO-EGFP-Rad9M-50 and the empty control pcDNA5/FRT/TO-EGFP were transfected into the Flp-In TrEx HEK293 cell line in parallel with the pOG44 plasmid in a 1:9 ratio, respectively. The transfection was established using the LyoVec transfection reagent (InvivoGen) according to the product's instructions. The transfected cells were allowed to grow in antibiotic-free medium for 24 hr. After 24 hr, the medium was removed and replaced with warm medium supplemented with 1 µg/ml hygromycin used as the transfection selective marker. Then the cells were left to grow for two weeks until single cell clones appeared. The medium containing the selective marker was replaced every 3–4 days.

2.16.8 Isolation of hygromycin-resistant colonies

Approximately 2 weeks post-transfection, single hygromycin-resistant colonies were isolated using cloning cylinders (Sigma). The medium was removed from the plates and the cells were washed once with 1x PBS. The cloning cylinder was then replaced gently over the colony, making sure the cylinder was attached firmly to the plate with no space between the cylinder and the plate. The cylinder was filled with 100 µl of trypsin and the plates were incubated for 5 min at 37°C. Individual colonies then were removed to 6-well plates and allowed to grow in hygromycin-supplemented medium until the cells were confluent. Once cells reached confluence, the cells were spilt into 10-cm plates where they were either checked for their integrations or frozen down.

2.16.9 Integration confirmation

Confirmation of the plasmid integration into the genome of the HEK293 cells was confirmed using three methods. First, the genomic DNA was extracted from each cell line as mentioned in 2.5 and PCRs were carried out with the extracted DNA using two sets of primers. The first set were the same flanking primers used for cloning the variant whereas the second set was a combination of the forward CMV promotor and the specific reverse variant primer (Table 2.35). Second, total protein was extracted (See 2.8.1.1) from either induced cells using doxycycline (1 µg/ml) or non-induced cells. The protein extracts were subjected to western blot (2.8.3) and immunoblotted with the GFP antibody. Third, induced and non-induced cells

were immunostained with the GFP antibody and analysed under the confocal microscope (2.12). Untransfected HEK293 were used as a second negative control.

Table 2.35 Primers to confirm integration

Gene	Primer sequence	Amplicon size (bp)
RAD9B-001	**Forward***atccgttacattatgcggccgcATGAGTGAAAATGAACTTGAC **Reverse****ctacgatggaatctcgagTTAGAATATAGAGAAACTGCCAT	1038 bp
CMV promotor-RAD9B-001	**Forward** CGCAAATGGGCGGTAGGCGTG **Reverse** ****ctacgatggaatctcgagTTAGAATATAGAGAAACTGCCAT	2081 bp
RAD9B-002	**Forward** *atccttacaatgcggccgcATGGCAGCCATGCTGAAGTG **Reverse** **atagttacgttctcgagTTAGAATATAGAGAAACTGCCAT	1254 bp
CMV promotor-RAD9B-002	**Forward** CGCAAATGGGCGGTAGGCGTG **Reverse** **atagttacgttctcgagTTAGAATATAGAGAAACTGCCAT	2297 bp
Rad9M-50	**Forward** *atccttacaatgcggccgcATGATTAAATCCGAGAACAGTC **Reverse** **atagttacgttctcgagCTAACTCGAAGAATTGAGCTG	1134 bp
CMV promotor-Rad9M-50	**Forward** CGCAAATGGGCGGTAGGCGTG **Reverse** **atagttacgttctcgagCTAACTCGAAGAATTGAGCTG	2177 bp

* indicates additional sequence contains *Not*1 recognition site designed in forward primer.
** indicates additional sequence contains *Xho*1 recognition site designed in reverse primer.

2.17 Time course induction of the FRT system

The EGFP-RAD9B-001 constructed cell line was seeded at 30% confluency and allowed to grow overnight. The following day, the cells were induced by adding doxycycline (1 µg/ml) to the same growing medium. Then either whole protein extraction (Section 2.8.1.1) or total RNA extraction (Section 2.4.2) was performed at 2, 4, 8, 12, 18, 24 and 48 hr post-induction. The protein extracts were analysed on normal SDS-PAGE gels (Section 2.8.3) and probed with the GFP antibody. Total protein was extracted from non-induced cells and used as a negative control. The *RAD9B-001* mRNA was amplified from the extracted RNA using one-step RT-PCR, as mentioned in Section 2.6.3. *ACTB* primers were used as a positive control.

2.18 Expression stability after the removal of the doxycycline inducer

The four constructed cell lines were plated at 20% confluency and incubated overnight. The growing medium was then injected with 1 µg/ml of doxycycline and the cell lines were further incubated for 18 hr. Whole protein extracts were prepared (Section 2.8.1.1) at this

point for the 0 hr sample. The medium was then removed from the plates and the cells were washed twice with 1x PBS for the removal of doxycycline residue. The cell were incubated in doxycycline-free medium until whole protein was extracted at 12, 24 and 48 hr after the inducer was removed. Protein extracts were run on normal SDS-PAGE gels (Section 2.8.3) and immunoblotted with the GFP antibody.

2.19 Cellular localisation of the EGFP-recombinant proteins

The cellular localisation of the EGFP-RAD9B-001, EGFP-RAD9B-002, EGFP-Rad9M-50 and the control EGFP was tested under normal and UV damage conditions. The localisation of the recombinant proteins was analysed by protein fractionation (Section 2.8.1.2) or by immunostaining (Section 2.12) using the GFP antibody. Other proteins were tested for their localisation in the constructed cell lines with their corresponding antibodies as indicated in the experiment.

2.20 Influence of overexpressed recombinant proteins on desired targets

The constructed cell lines were induced for different durations, as indicated in the experiment, reaching a maximum confluency of 90% on the day of harvesting. Other cells were left without induction as a control. At the desired induction time, either whole protein (Section 2.8.1.1) or total RNA (Section 2.4.2) was extracted from the cell lines. Either qPCR (Section 2.6.4), RT-PCR (Section 2.6.3), or western blotting (Section 2.8.3) was done to investigate the influence of the recombinant protein overexpression on the genes or proteins indicated in the experiment.

2.21 Effect of recombinant protein overexpression on cell cycle progression

EGFP-RAD9-001 and EGFP-RAD9-002 constructed cell lines were seeded at 30% confluency and the cell were allowed to attach for a couple of hours, followed by induction by adding 1 µg/ml of doxycycline to the medium. A plate from each cell line was left without induction as a control. Flow cytometry samples were extracted 24, 36 and 48 hr post-induction and analysed on the flow cytometry machine, as mentioned in Section 2.15.

2.22 HuSH shRNA Knockdown system

HuSH RAD9A knockdown plasmids were purchased from Origen. The four plasmids are listed in (Table 2.2).

2.22.1 Amplification of HuSH knockdown plasmids

All RAD9A-shRNA plasmids were amplified using the Alpha Select Gold Efficiency Component Cells growing on selective chloramphenicol plates (34 µg/ml). The transformation steps are the same as mentioned in Section 2.16.4.

2.22.2 Transfection of shRNA plasmids into HEK 239 cells

The shRNA-RAD9A vector was transfected into HEK293 cells using the Lipofectamine 2000 transfection reagent (Thermo Fisher Scientific). The Opti-MEM reduced serum medium (Thermo Fisher Scientific) was used to mediate the transfection as per the supplier's instructions. The cells were transfected with a single shRNA vector of the four supplied shRNAs or a mixture of the four shRNA vectors as a transient transfection. The transfected cells were grown in puromycin (3 µg/ml) selective medium for 72 hr, followed by either whole protein or total RNA extraction (Sections 2.4.2 and 2.8.1.1).

2.23 RAD9B-001 immunoprecipitation

The EGFP-Rad9B-001 cell line was either left without induction or induced overnight by adding doxycycline (1 µg/ml). The cell were washed with 1x PBS, trypsinised, and spun down at 1,500 rpm for 5 min. RAD9B-001 was immunoprecipitated from the cell pellet with the GFP nap agarose resin kit (allelebiotech) according to the manufacturer's instructions.

2.23.1 Immunoprecipitation buffers

1x Lysis buffer: 20 mM Tris-HCl pH = 7.5, 150 mM NaCl, 1 mM EDTA and 0.5% NP-40.
1x Binding buffer: 10 mM Tris-HCl pH = 7.5 and 150 mM NaCl.
1x Wash buffer: 10 mM Tris-HCl pH = 7.5 and 500 mM NaCl.
1x Elution buffer: 200 mM glycine pH = 2.5.
1x Neutralization buffer: 1 M Tris Base.

2.24 DNA-Damage Treatments

2.24.1 UV light treatment

Cells were grown in their appropriate medium until they reached 70-80% confluency. For the constructed cell lines, cells were induced using doxycycline (1 µg/ml) 18 hr before treatment. Just before the cells were exposed to UV light, the medium was removed from the plate and the cells were washed with 5 ml of warm 1x PBS. The removal of the medium is essential as the medium will reflect the UV light. The plates were placed in the UV radiation machine and the cells were treated at a dose of 40 J/m^2. The medium was added again to the plates, and the cells were left to recover in the incubator at 37°C. Protein or RNA was extracted (Sections 2.4.2 and 2.8.1.1) at different times post treatment, as indicated in the experiment.

2.24.2 Heat treatment

For the constructed cell lines, cells were induced for 18 hr by adding doxycycline (1 µg/ml) before starting the treatment. Subconfluent cells were placed in a 43°C incubator for 1 hr, followed by recovery at 37°C for different length of times. Whole protein or total RNA was extracted at indicated times in the experiment (Section 2.4.3, 2.8.1.1).

2.24.3 H_2O_2 treatment

Cell were grown in complete medium until cells reached 80% confluency. With the constructed cell lines, cells were induced for 18 hr by adding doxycycline (1 µg/ml) before treatment. The complete medium was replaced with FBS-free medium supplemented with 500 µM H_2O_2 and the plates were incubated at 37°C for 1 hr. The medium then was replaced with complete DMEM, and the cells were allowed to recover at 37°C for different lengths of time. Whole protein or total RNA was extracted at the indicated times in the experiment (Section 2.4.3, 2.8.1.1).

2.25 Apoptosis Induction

Protein expression was induced overnight with 1 µg/ml doxycycline. The following day, the induced and non-induced cells were exposed to two UV light doses (15 J/m^2 and 40 J/m^2), as mentioned in Section 2.24.1. The cells were further incubated and whole protein was

extracted at 12, 24 and 48 hr after UV treatment (See Section 2.8.1.1). Protein extracts were run on normal SDS-PAGE gels and immunoblotted with the indicated antibodies (See Section 2.8.3).

2.26 Cell viability post induction

The four constructed cell lines were plated at density of 3 x 10^5 and allowed to grow in either medium supplemented with 1 µg/ml doxycycline or medium free of the inducer. Every 24 hr, the induced and non-induced cells were washed, trypsinised, and collected for counting, as mention in Section 2.3.5.

2.27 MPS1 Inhibition

Cells were seeded at 10% confluence and allowed to grow for 24 hr. Medium containing 2 µM MPS1 inhibitor (Selleck Chemicals) was added directly to the cells, and the cells were further incubated for 72 hr with replacing the medium with warm fresh medium containing the MPS1 inhibitor every 24 hr. Whole protein was then extracted from the treated and normal cells. The protein extracts were analysed on normal SDS-PAGE gels (See Section 2.8.3).

Chapter 3: ANALYSIS OF THE HUMAN RAD9B SPLICE VARIANTS AT mRNA LEVEL IN VARIOUS HUMAN TISSUES

3.1 Introduction

Human cells contain two RAD9 genes: *RAD9A* and *RAD9B*, in addition to the RAD9-like locus *C12ORF32* (chromosome 12 open reading frame 32). While *RAD9A* has been extensively studied, little is known about *RAD9B* and *C12ORF32*. *RAD9B* and *C12ORF32* are both located on chromosome 12 while *RAD9A* is located on chromosome 11. RAD9B variants resemble the N-terminal truncated Rad9-M50 yeast protein. Interestingly, the C12ORF32 protein is shorter than the normal RAD9A protein, more closely resembling the yeast Rad9-M50 variant (Appendix 9). In contrast to *S. pombe*, all human isoforms are alternative splice variants rather than alternative translation products.

According to the National Centre for Biotechnology Information's (NCBI, http://www.ncbi.nlm.nih.gov. Accessed 26 September 2016) database, human *RAD9B* (RAD9 checkpoint clamp component B, also known as Rad9 homolog B (*S. pombe*)) has nine splice variants: *RAD9B-001*, *RAD9B-002*, *RAD9B-003*, *RAD9B-004*, *RAD9B-005*, *RAD9B-006*, *RAD9B-007*, *RAD9B-008* and *RAD9B-009*. Of these, only five protein isoforms are produced (Table 3.1).

The *RAD9B* transcripts differ from each other in a couple of points. The *RAD9B-001*, *RAD9B-002* and *RAD9B-005* transcripts have very long 3' UTR tails distinguishable from the other two variants *RAD9B-003* and *RAD9B-009*. The *RAD9B-003* isoform encodes the largest protein (429 aa) while *RAD9B-009* is the smallest (341 aa) of the isoforms. The long 3' UTR tails of *RAD9B-001*, *RAD9B-002* and *RAD9B-005* encompass nearly 50% of the length of the mRNA which could harbour an additional open reading frame (Figure 3.1). The *RAD9B-001* and *RAD9B-005* transcripts share an identical coding region with 72 aa missing from the *RAD9B-001* 5' end compared to the other isoform.

Table 3.1 Human RAD9B transcripts in the Ensemble database

Name	Number of exons	Transcript length (bp)	cDNA length (bp)	Protein	predicted Protein size (aa)
RAD9B-001	11	2794	1038	yes	345
RAD9B-002	11	2732	1254	yes	417
RAD9B-003	12	1846	1290	yes	429
RAD9B-004	12	2843	264	Nonsense	87
RAD9B-005	11	2727	1038	yes	345
RAD9B-006	5	463	-	No	-
RAD9B-007	5	506	-	No	-
RAD9B-008	6	556	-	No	-
RAD9B-009	9	1373	1026	yes	341

This table illustrates the nine splice variants of the *RAD9B* gene. Only the *RAD9B-001, 002, 003, 005* and *009* transcripts code for protein whereas *RAD9B-004* transcripts produce a nonsense-mediated decay protein. The information in this table was obtained from the Ensemble database (http://www.ensembl.org. Accessed 26 September 2016).

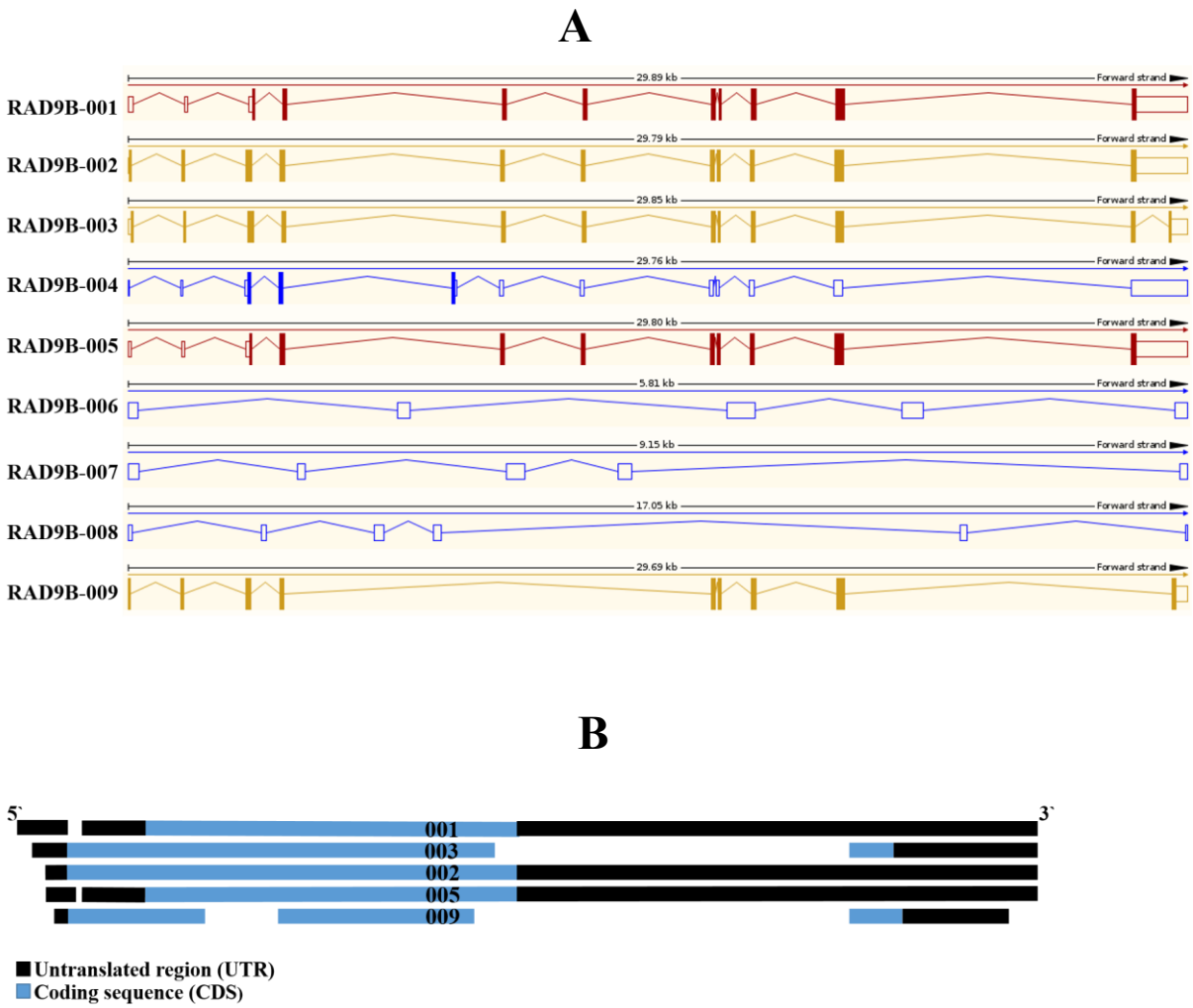

Figure 3.1 Structure analysis of *RAD9B* and its splice variants. (A) Diagram obtained from the Ensemble database, showing the structure and total number of exons of the *RAD9B* gene and its splice variants. The filled boxes indicate the coding exons while the blank boxes reflect the noncoding exons. The lines linking the boxes represent the introns. The name of the variant is shown to the left side. (B) The transcriptional sequence of the *RAD9B* variants. The black colour indicates the untranslated region of the transcript while the blue colour reflects the coding region of the transcript. All information was obtained from the Ensemble data base (http://www.ensembl.org. Accessed 26 September 2016).

Unlike *RAD9A*, *RAD9B* is only expressed in a few tissues with high expression in the testis and low expression in skeletal muscle at the mRNA level (Dufault et al., 2003). The Human Transcriptome Database for Alternative Splicing showed that *Rad9B* is only expressed in testis tissue (http://h-invitational.jp. Acssessed 26 Spetember 2016).

A report by Kim and colleagues (2010) detected very low expression of *C12ORF32* in normal human tissues except for the small intestine, testis, ovary, prostate and thymus. Interestingly, *C12ORF32* was highly expressed in 11 breast cancer cell lines with a remarkable difference at expression level when compared to normal tissues.

Knockdown of *C12ORF32* expression in two breast cancer cell lines showed an inhibition of G1/S transition and an increase in the sub-G1 population probably due to cell death. The C12ORF32 protein was found to be processed from a 35 kDa precursor to a 16 kDa protein which accumulated in breast cancer (Kim et al., 2010).

As mentioned in the introduction, alternative splicing could be specific to a certain cell phase or inducible by a certain treatment, such as UV light or heat stress. Splice variant expression was also reported to be elevated at the end of the cellular life span, a stage known as cellular senescence (Blanco et al., 2008). Cells continually experience exogenous and endogenous stress, and their response could lead to complete recovery; alternatively, in some cases, it could be fatal. Cells can also undertake a different response, a mechanism in which cells enter permanent, irreversible cell cycle arrest. These cells can remain in a nonproliferative viable state known as cellular senescence for months (Campisi, 2013; Campisidi & Fagagna, 2007; Ben-Porath & Weinberg, 2005). One of the main regulators of senescence is the p21 protein, which shows a significant up-regulation under these conditions and is a primary marker of stress-senescence induction. Since p21 was reported to share a role with RAD9B in response to DNA damage beside their reported physical interaction, in this chapter, cell senescence was induced in normal and carcinoma cells, and the expressions of *RAD9B* splice variants were investigated (Perez-Castro & Freire, 2012; Cmielova & Rezacova, 2011).

The latest study on RAD9B showed that the overexpression of RAD9B results in G1 cell cycle arrest (Perez-Castro & Freire, 2012). It is likely that RAD9B has a functional role in this phase of the cell cycle. Therefore, in this chapter, cell populations were collected in the desired cell cycle phase through cell synchronisation followed by the analysis of the mRNA levels in different *RAD9B* splice variants. This was designed to help to reveal changes in RAD9B expression throughout the cell cycle.

Although it has been reported in various databases that *RAD9B* is poorly or not expressed at all in most human tissues, except in the testis, and since the *RAD9B* splice variants have never been fully studied, the expression of the *RAD9B* splice variants were investigated in various human tissues in addition to different cell lines at the mRNA only since no validated antibody for the detection of RAD9B was available. Moreover, in addition to the aforementioned tested conditions for the expression levels of *RAD9B* such in senescence cells and cell cycle specificity, the expression of *RAD9B* was also investigated under other conditions such as cell

super confluency and heat stress, as *RAD9B* may be an inducible gene as in the case of the yeast *Rad9-M50*.

3.2 Results

3.2.1 Primer design to distinguish among the RAD9B splice variants

With the very high identity amongst *RAD9B-001*, *RAD9B-002*, *RAD9B-003*, *RAD9B-005* and *RAD9B-009* (Appendix 1) in mind, two sets of primers were designed to distinguish between them. The first set amplifies the full length transcript whereas the other set was designed to amplify short regions of the different *RAD9B* transcripts.

To amplify short regions of each splice variant (Figure 3.2-B), three pairs of primers were designed. The first pair (S-001-002-005) binds to *RAD9B-001*, *RAD9B-002* and *RAD9B-005* and amplifies the same 196 bp region. The second pair of primers (S-003-009) share the same forward primer of the first pair but utilize a different reverse primer that goes across a long gap present in *RAD9B-003* and *RAD9B-009* and binds to the 3' end of all the transcripts. This pair (S-003-009) binds to all five variants, amplifying short fragments for *RAD9B-003* (233 bp) and *RAD9B-009* (123 bp) and amplifying long regions (1172 bp) of *RAD9B-001*, *RAD9B-002* and *RAD9B-005*. The last pair (S-001) was unique for *RAD9B-001*, amplifying a short region (215 bp) of its 5' end.

The primers designed across long regions were unique for each splice variant, except for *RAD9B-002* and *RAD9B-005* (Figure 3.2-A). The first pair of primers (L-001) amplifies the *RAD9B-001* coding sequence (CDS) and part of the 5' untranslated region (UTR) with a size of 1363 bp.

The other pair (L-001-002-005) detects three variants (*RAD9B-001*, *RAD9B-002* and *RAD9B-005*) at the same size (1038 bp), amplifying the whole *RAD9B-001* CDS and only a part of the CDS for *RAD9B-002* and *RAD9B-005*. This pair of primers was used to amplify the full-length (CDS) sequence of the *RAD9B-001* for the construction of the stable cell lines (Chapter 4). In addition, another pair of primers (L-002-005) were designed for the construction of the RAD9B-002 stable cell line, amplifying the CDS of both *RAD9B-002* and *RAD9B-005* nearly at the same size (~1254 bp) as the amplified *RAD9B-005* is only seven bp shorter than the

RAD9B-002. The last pair of primers (L-003-009) was designed to detect the full-length expression of *RAD9B-003* and *RAD9B-009* by amplifying 1290 bp and 974 bp sized fragments, respectively. All primers designed across long regions can specifically amplify all *RAD9B* splice variants with the exception of *RAD9B-002* and *RAD9B-005*. The primers sequence table can be seen in Table 2.6.

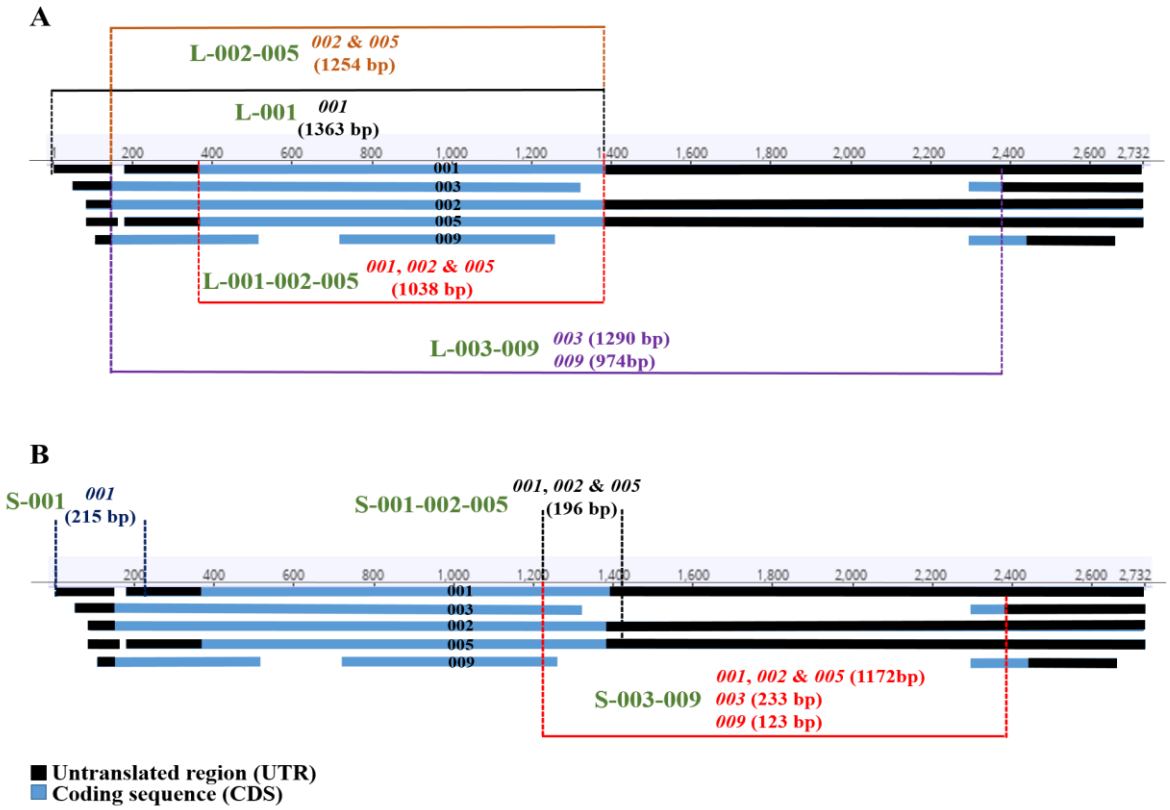

Figure 3.2 Primer design to amplify *RAD9B* and its splice variants. (A) Sites of primer binding across *RAD9B* splice variants and amplifying full length transcripts. (B) Sites of primer binding across *RAD9B* splice variants and amplifying short regions. The colours (brown, black, red, blue and purpule) indicate the amplified splice variants and their expected size (bp). The letters and numbers in green indicate the name of primers, L (long), S (short).

3.2.2 Expression levels of the *RAD9B* splice variants

The expression levels of the *RAD9B* splice variants was investigated in three human cell lines: HEK293 (non-malignant embryonic kidney cell line), HeLa (cervical cancer) and Kelly (neuroblastoma cell line). All five variants of *RAD9B* were tested using intron-spanning primers to amplify long and short regions. RNA at two concentrations was reverse transcribed into cDNA and different concentrations of cDNA were used as the RT-PCR template. The *ACTB* (Beta Actin) gene expression was used as a control for the cDNA quality and to compare *Rad9B* variant expression levels.

The set of primers (S-001-002-005 & L-001-002-005), (Figure 3.2-A & B), amplifying long and short identical regions of the *RAD9B-001*, *RAD9B-002* and *RAD9B-005* variants showed evidence of some or all these three variants in all cell lines whereas no amplification was obtained for the full length mRNA of *RAD9B-003* and *RAD9B-009* (Figure 3.3). However, using the primers (S-003-009), (Figure 3.2-A & B), amplifying the short regions of the variants showed the expression of the *RAD9B-009* variant but not of *RAD9B-003* in all the three cell lines. The primers used for the long regions seemed to have less amplification copy efficiency than the primers for the short regions. The HEK293 cells had the highest expression of all variants while very low expression was obtained in the brain carcinoma cells. Having expression in all three cell lines, they were used in most of this project's experiments. DNA sequencing confirmed the identity of the identical short and long region of the *RAD9B-001*/*002*/*005* and the specific region of *RAD9B-009*.

The increased concentration of the template cDNA enhanced the amplification of the *RAD9B* variants indicating that they are expressed at low levels. The increase in the template concentration correlated directly with the amplification of the variants, especially when amplifying the small regions. This proportion was observed among all three cell lines (Figure 3.3).

The cDNA dilution factor is usually from 1:5 to 1:10 in most RT-PCR protocols. The results obtained here show that the cDNA dilution factor plays an important role in the detection of the variants, and apparently this might have been the reason for the negative RT-PCR results obtained in the early stages of the project. The best intensity was observed when the 2 µg reverse transcribed RNA was used and only two-fold diluted.

Higher dilutions than two-fold resulted in either negative PCRs in some cell lines or weak signals in other cell lines. Conversely, the expression of *ACTB*, as seen in (Figure 3.3-B), can be detected up to a dilution factor of 100-fold. This implies that the expression levels of the *RAD9B* splice variants are at least 50 times lower compared to *ACTB*. Taking together, the detection or amplification efficiency of low expressed genes such in the case of the *RAD9B* splice variants can be enhanced by controlling the templated concentration.

A

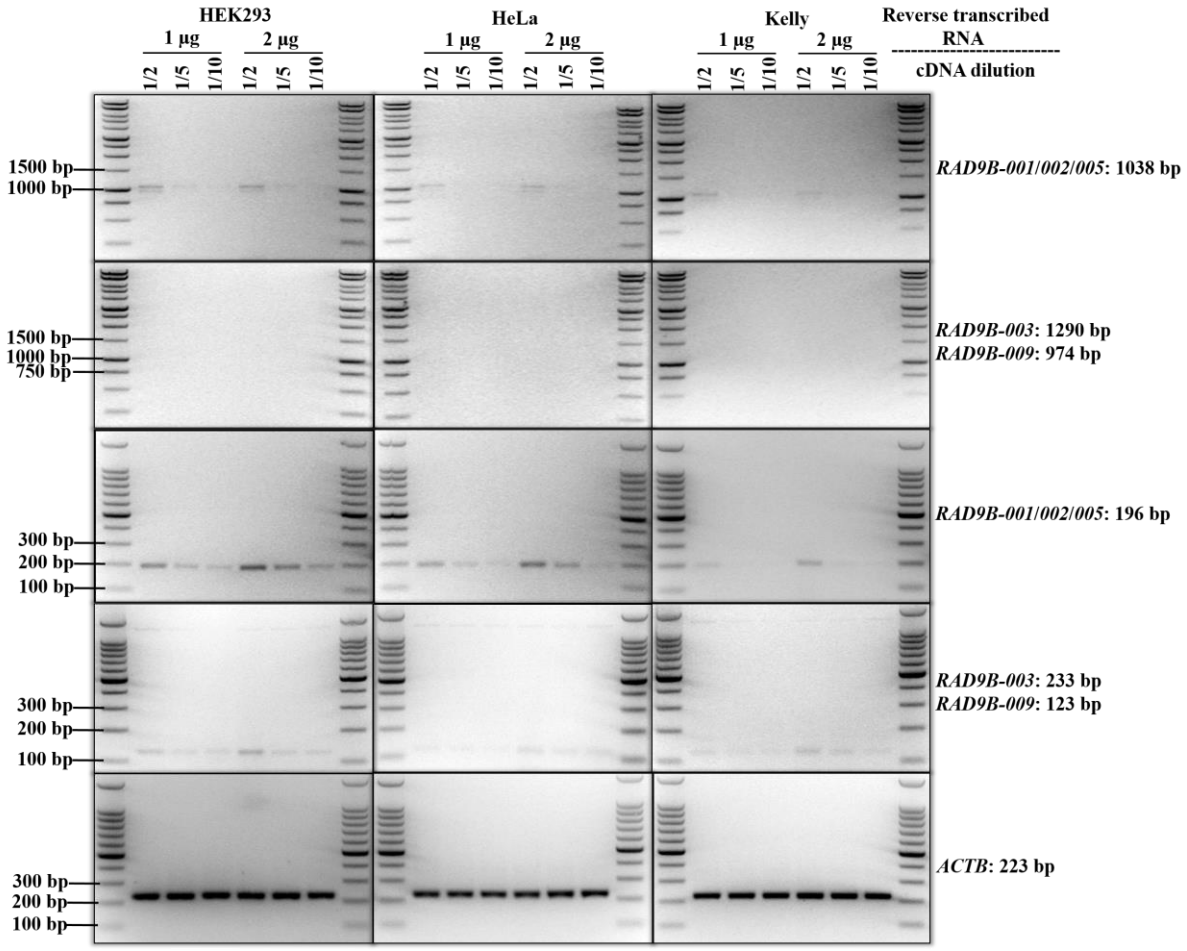
HEK293
HeLa
Kelly
1 µg
2 µg
1/2
1/5
1/10
Reverse transcribed RNA
cDNA dilution
1500 bp
1000 bp
750 bp
300 bp
200 bp
100 bp
RAD9B-001/002/005: 1038 bp
RAD9B-003: 1290 bp
RAD9B-009: 974 bp
RAD9B-001/002/005: 196 bp
RAD9B-003: 233 bp
RAD9B-009: 123 bp
ACTB: 223 bp

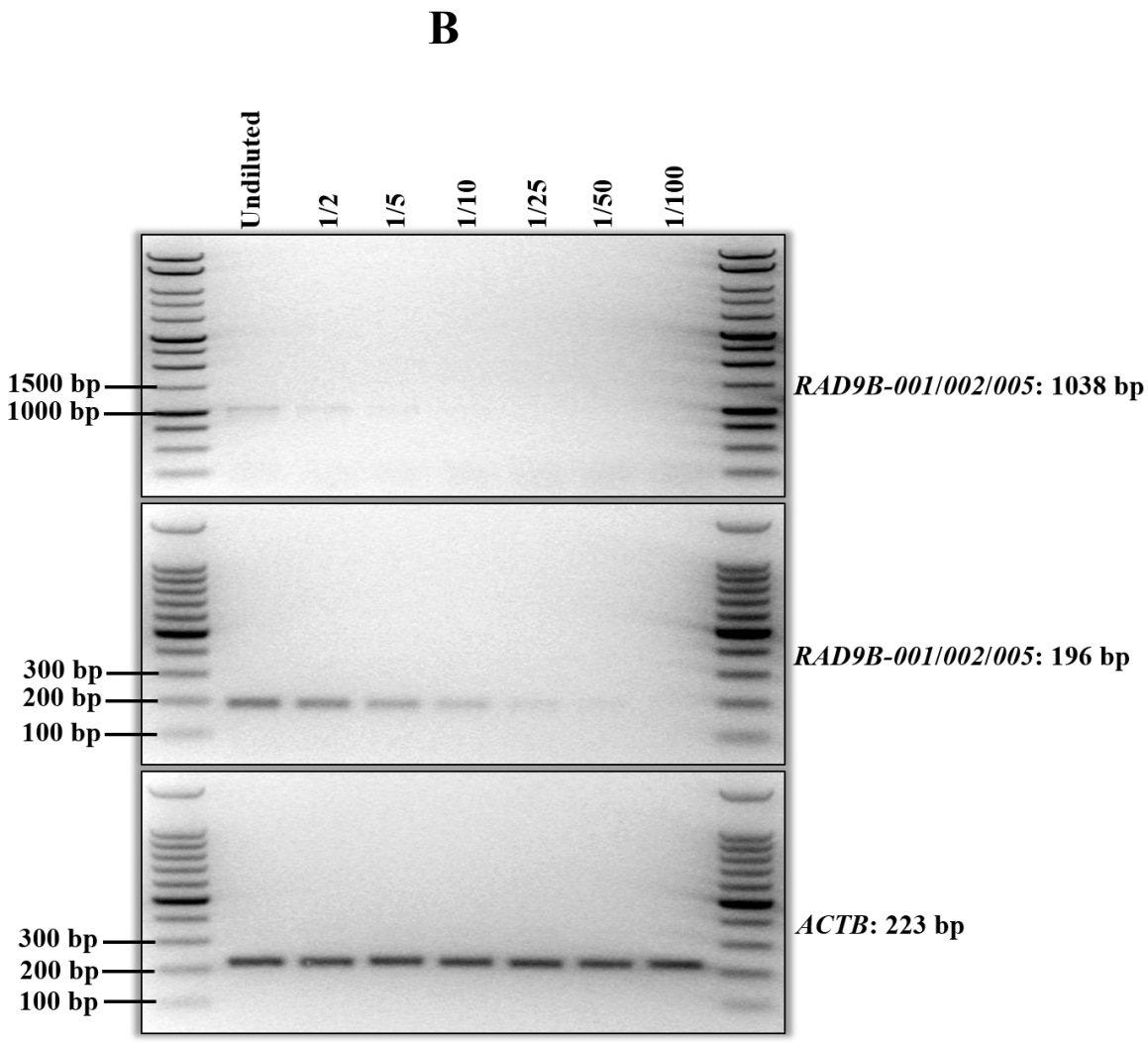

Figure 3.3 Analysis of *RAD9B* splice variants amplification using different template concentrations. (A) RT-PCRs of the *RAD9B* variants in three different cell lines (HEK293, HeLa and Kelly) using different RT-PCR template concentrations. Reversed transcribed RNA concentration and cDNA dilution factor is seen above the figure. The amplified variant and its expected size (bp) are shown on the right side. A volume of 10 µl of the RT-PCR was loaded on agarose gel for all the *RAD9B* variants and *ACTB*. (B) 1 µl of RNA extracted from HEK293 cells was reverse transcribed into cDNA, followed by a series of dilutions. RT-PCRs of *RAD9B-001*, *002* and *005* in HEK293 cells with primers to amplify short and long regions with varying RT-PCR template concentrations (up to 100-fold dilution). *ACTB* was used for cDNA quality and as a high expression control gene. RT-PCRs amplifying long regions for *RAD9B-001*, *002*, *005*, *003* and *009* were run on 0.8% agarose gels. RT-PCRs amplifying short regions for *RAD9B-001*, *002*, *005*, *003* and *ACTB* were run on 1.5% agarose gels. RT-PCR amplifying short regions for *RAD9B-009* was run on a 2% agarose gel. For the RT-PCRs, 10 µl was loaded on the agarose gel for all the *RAD9B* variants and only 5 µl for the *ACTB*.

3.2.3 Column vs. TRIzol RNA extraction

Since the expression of *RAD9B* is extremely low as observed using the two-step RT-PCR, two RNA extraction methods were compared to enhance the detection of *RAD9B* variants. Both the column and the TRIzol method resulted in high-quality RNA (Figure 3.4); however, the TRIzol method resulted in DNA contamination, even without disturbing the interphase containing the genomic DNA. Several attempts to remove the DNA from the RNA samples with DNase resulted in either failure or RNA quality loss. Using genomic DNA contaminated RNA for RT-PCR, and especially for qPCR, can be a problem, even when using intron-spanning primers. These primers cannot guarantee accurate RNA quantification, as it might result in a false positive. Therefore, all future RNA samples will be extracted using the column method.

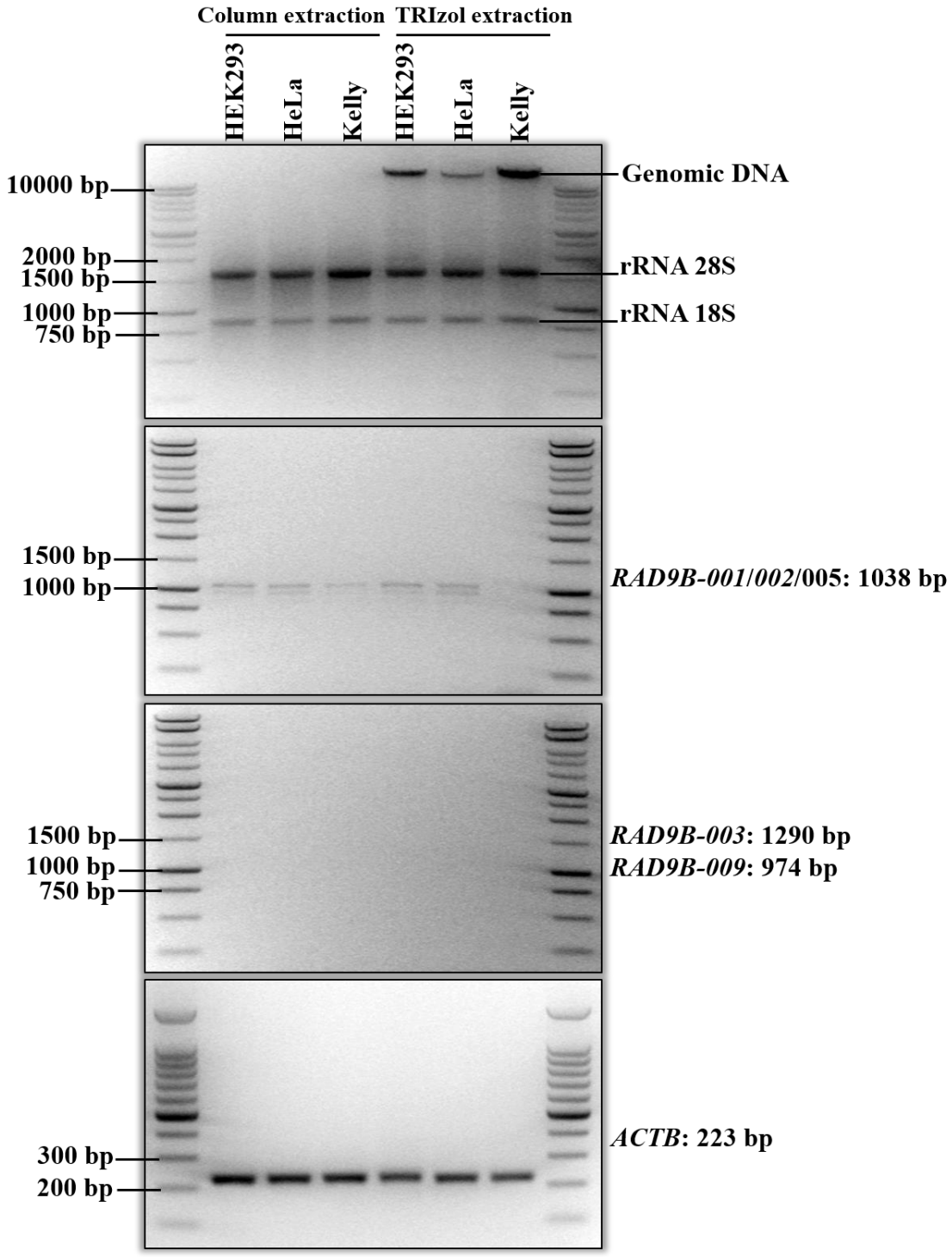

Figure 3.4 Comparison of column and TRIzol RNA extractions. Agarose gel analysis of RNA extracted from HEK293, HeLa and Kelly cell lines by either column or TRIzol extraction. The RNA extracted by both methods show high quality RNA represented in the ribosomal RNA (rRNA) 18S and 28S. DNA contamination is observed within all RNA extracted from the three cell lines with the TRIzol method. RNA extracted by both methods were reverse transcribed into cDNA. The cDNA was used for the amplification of *RAD9B* splice variants using flanking primers. Both methods resulted in very weak amplification of the *RAD9B* splice variants. *ACTB* was used as a positive control. Name of the amplified splice variant and its expected size can be seen on the right side.

3.2.4 One-step and two-step RT-PCR

Due to the insufficient amplification results of *RAD9B* obtained from the RT-PCR experiments, the amplification of the *RAD9B* splice variants was investigated using two different amplification methods to search for the best amplification conditions. Here two kits (the one-step RT-PCR method and the previously used two-step RT-PCR method) were compared for their amplification efficiency using the HEK293, HeLa and Kelly cell lines. The first method (one step), was performed including both the reverse transcriptase step of the RNA template and the PCR reaction in the same tube. However, the second method (two-step) involved creating the reverse transcription step separately, and then the cDNA template was added to the PCR reaction. Interestingly, almost all samples were positive for the *RAD9B* variants when using the one-step RT-PCR method. The exception was the *RAD9B-009* variant, which was not expressed in any of the cell lines. In comparison, only the primer pair (L-001-002-005) (Figure 3.2-A), amplifying *RAD9B-001/002/005*, gave a weak positive PCR-amplification signal in the HEK293 and HeLa cell lines when using the two-step RT-PCR method, and no positive reaction was obtained for the other primer pair detecting *RAD9B-002/005* or the primers detecting *RAD9B-003* and *RAD9B-009*. The one-step RT-PCR method confirmed the expression of RAD9B variants in both HEK293 and HeLa cells but at a much lower level in the neuroblastoma cells (Figure 3.5). The identities of the *RAD9B* fragments were confirmed by DNA sequencing.

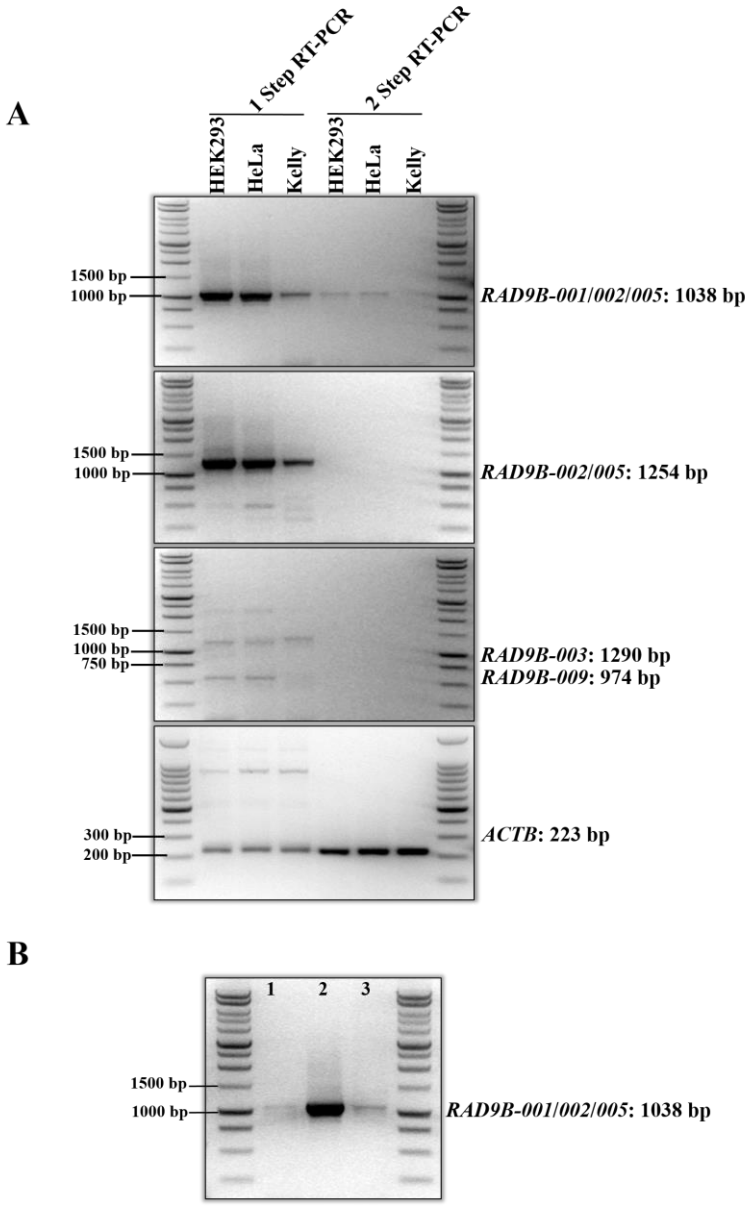

Figure 3.5 Analysis of *RAD9B* variants amplification following RNA extraction via one-step RT-PCR and two-step RT-PCR methods. (A) For lanes 1, 2 and 3, 200 ng of total human RNA extracted from three different cell lines were reverse transcribed and amplified by the Bioline One-Step RT-PCR Kit using specific primers for the *RAD9B* variants. For lanes 4, 5 and 6, 1 µg of total RNA extracted from three different cell lines were reverse transcribed by the Bioline cDNA synthesis kit, followed by amplification using Bioline Red Mix polymerase in two separate steps. *ACTB* was used as a positive control for cDNA quality. (B) For lane 1, 1 µg of total RNA extracted from HEK293 cells was reversed transcribed by the Bioline cDNA synthesis kit, followed by *RAD9B* amplification with Bioline Red Mix polymerase in two separate steps. Lane 2, 200 ng of total human RNA extracted from HEK293 cell were transcribed and amplified by Bioline One-Step RT-PCR kit using specific primers for *RAD9B-001*. For lane 3, 1 µg of total RNA extracted from HEK293 cell was transcribed by the Bioline cDNA synthesis kit, followed by *RAD9B* amplification using the Bioline One-Step polymerase in two separate steps. All *RAD9B* variants were run on a 0.8% agarose gel. The *ACTB* control was run one a 1.5% agarose gel. The size of each amplified variant is shown to the right side.

3.2.5 A possible novel *RAD9B* splice variant expressed in HEK293 and HeLa cell lines

The (L-003-009) primers (Figure 3.2-A) designed to amplify *RAD9B-003* (1290 bp) also bind to *RAD9B-009* but amplify a shorter fragment (974 bp). This pair of primers also binds to *RAD9B-001*, *RAD9B-002* and *RAD9B-005*, resulting in a larger amplicon of ~ 2220 bp. However, no other fragment can be amplified when aligning the pair of primers to all nine *RAD9B* splice variants. Interestingly, RT-PCR experiments using the (L-003-009) primers revealed a novel, shorter *RAD9B* splice variant with a size of 540 bp (Figure 3.6). This short fragment was sequenced a number of times using the same forward and reverse primers. This revealed an identical region (500 bp) to the *RAD9B-003* 5' region but with some alterations at the very end of the *RAD9B-S003* 3' end (40 bp) (Appendix 11). The new splice variant will be referred to as *RAD9B-S003*.

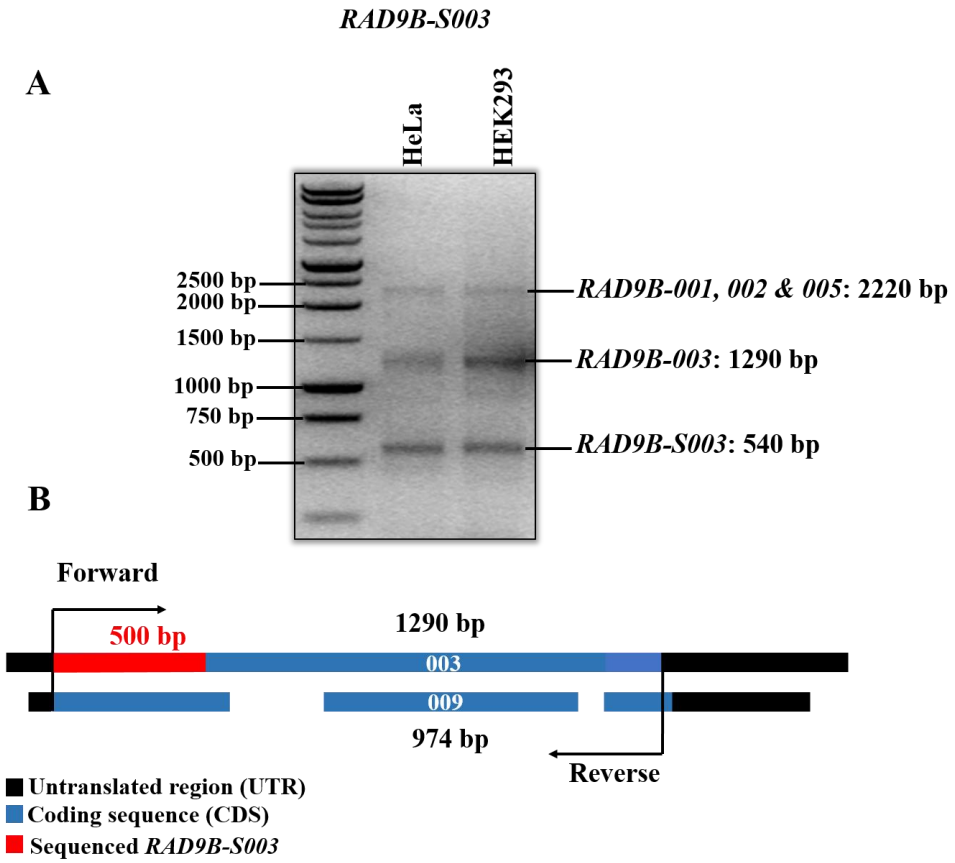

Figure 3.6 Expression of short *RAD9B-003* fragment in HEK293 and Hela cells. Total RNA was extracted from HEK293 and HeLa cells and 200 ng was used for the amplification of *RAD9B-003* using the One-Step RT-PCR Kit. The RT-PCR revealed a new short *RAD9B-003* (*RAD9B-S003*) with an approximate size of 540 bp. (B) Diagram showing the *RAD9B-S003* sequence seen in (Red), covering 500 bp of the *RAD9B-003* 5' end. No expression of *RAD9B-009* can be seen in the HEK293 or HeLa cell lines. The top band on the agarose gel represents *RAD9B-001*, *RAD9B-002* and *RAD9B-003*.

3.2.6 Expression of *RAD9B* variants in several human tissues

Having identified the right conditions to amplify the *RAD9B* splice variants, the differential expression of the *RAD9B* variants was validated among 20 different human tissues to discover any tissue specificity as indicated by the published data (Table 3.3), (Hopkins et al., 2003; Dufault et al. 2003). For this, the primers (S & L) were used (Figure 3.2). The first primers set (L) amplified the long regions of the *RAD9B* variants using the one-step RT-PCR and the other set (S) amplified small regions of the variants with the two-step RT-PCR protocol. The primers used are specific for each of the *RAD9B-001*, *RAD9B-003* and *RAD9B-009* variants, but *RAD9B-002* and *RAD9B-005* were amplified with an almost identical sequence and size (Figure 3.2-A).

The RT-PCR revealed the expression of *RAD9B-001* and *RAD9B-002*/*RAD9B-005* in most of the 20 tissues tested whereas *RAD9B-003* was detected only in few tissues (Figure 3.7). The primers designed for the *RAD9B-003* variant also detects the *RAD9B-009* variant (974 bp) and, as in the previous RT-PCRs across the HEK239, HeLa and Kelly cell lines, the full length *RAD9B-009* variant was not detected in any of the 20 tissues. Among all the tissues, all *RAD9B* splice variants were highly expressed in testis tissue relative to the other tissues. Surprisingly, testis tissue did not express the full-length *RAD9B-009* transcript.

The *RAD9B-001* variant was expressed in 19 of the 20 normal tissues, and the highest expression levels were detected in the testis and whole brain. No expression could be detected in the placenta tissue and only minor expression was seen in the bone marrow, adrenal gland, salivary gland, spleen and small intestine issues. The rest of the tissues had a moderate expression of this variant.

The expression of *RAD9B-002* or *RAD9B-005* was not seen in placenta tissue but was detected in the other tissues in a similar tissue-specificity to *RAD9B-001*. Interestingly *RAD9B-003* expression was detected in fetal brain and testis tissue, and it was almost undetectable in salivary gland, brain (whole) and lung tissue. The small inducible transcript (*RAD9B-S003*) of this variant was highly detected in testis and almost undetectable in the salivary gland, fetal brain, fetal liver and lung.

Since the expression of the *RAD9B-009* full-length transcript was not detected, primers detecting a small region at the 3' end of this variant were used (Figure 3.2-B). The two-step RT-PCR protocol gave interesting results as the *RAD9B-009* 3' end region was expressed in most tissues, with the highest expression levels detected in testis and colon tissues. The primers designed to amplify the *RAD9B-009* variant (123 bp) also amplifies a 233 bp sized fragment at the 3' end region of the *RAD9B-003* variant (Figure 3.2-B). Interestingly, It seems that both variants are jointly expressed in both colon and testis tissue. This 3' end region of the *RAD9B-003* variant was not amplified in any of the other tissues.

Table 3.3 Source of total RNA for the amplification of the *RAD9B* splice variants

TISSUE	SOURCE	AGE
Heart	Pooled from 3 male Caucasians	30, 30, 39
Adrenal gland	Pooled from 62 male/female Caucasians	15–61
Salivary gland	Pooled from 24 male/female Caucasians	16–60
Bone marrow	Pooled from 4 male/female Caucasians	58–76
Brain (whole)	Pooled from 4 male Asians	21–29
Foetal brain	Pooled from 21 spontaneously aborted male/female Caucasians	26–40
Foetal liver	Pooled from 3 male/female Asians	20–38
Kidney	40-year-old female Caucasians	-
Liver	Pooled from 3 male Asians	24–64
Lung	Pooled from 3 male/female Caucasians	32–61
Placenta	Pooled from 3 Caucasians	23–30
Prostate	Pooled from 12 male Caucasians	20–58
Skeletal muscle	20-year-old male Caucasians	-
Spleen	Pooled from 15 male/female Caucasians	22–69
Testis	Pooled from 7 Asians Caucasians	24–87
Thymus	Pooled from 2 male Caucasians	18–57
Uterus	Pooled from 8 Caucasians	23–63
Colon	Pooled from 3 male Asians	24–29
Small intestine	Pooled from 5 male/female Caucasians	20–61
Spinal cord	Pooled from 7 male Asian/Caucasians	20–59
Stomach	50-year-old male Caucasians	-

A

	Heart	Adrenal gland	Salivary gland	Bone marrow	Brain (whole)	Fetal brain	Fetal liver	kidney	Liver	Lung	Placenta	Prostate	Skeletal muscle	Spleen	Testis	Thymus	Uterus	Colon	Small intestine	Stomach
RAD9B-001	0.8	0.1	0.2	0.1	1.5	0.3	0.6	0.4	0.7	1	0	0.4	1.1	0.2	2	0.4	0.7	0.8	0.2	0.7
RAD9B-002/005	0.8	0.2	0.2	0.2	1.8	0.9	1.2	1.2	0.8	1.5	0.3	0.3	0.3	0.1	3	0.4	0.3	0.3	0.1	0.3
RAD9B-003	0	0	0.1	0	0.1	0.3	0	0	0	0.1	0	0	0	0	1.8	0	0	0	0	0
RAD9B-S003	0	0	0.1	0	0	0.1	0.1	0	0	0.1	0	0	0	0	1	0	0	0	0	0
RAD9B-009	0	0	0	0	0	0	0	0	0	0	0	0	0	0	0	0	0	0	0	0

B

	Heart	Adrenal gland	Salivary gland	Bone marrow	Brain (whole)	Fetal brain	Fetal liver	Kidney	Liver	Lung	Placenta	Prostate	Skeletal muscle	Spleen	Testis	Thymus	Uterus	Colon	Small intestine	Stomach
RAD9B-001/002/005	0.2	0	0	0.2	0.3	0.3	0.2	0.1	0.3	0.3	0.1	0.1	0.2	0.2	0.3	0.3	0.2	0.2	0.1	0.1
RAD9B-001	0.1	0	0	0	0.2	0.2	0.1	0.1	0	0.2	0	0	0.2	0	0.4	0.1	0.1	0	0	0
RAD9B-003	0	0	0	0	0	0	0	0	0	0	0	0	0	0	0.2	0	0	0.2	0	0
RAD9B-009	0.1	0.1	0.1	0.2	0.2	0.1	0.1	0.1	0.1	0.1	0	0	0	0	0.5	0	0	0.3	0	0

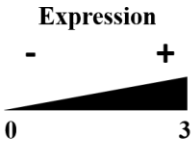

Figure 3.7 Expression of *RAD9B* splice variants in multiple human tissues. The diagram is based on the expression of *RAD9B* in several human tissues (Human Total RNA Master Panel II, Clontech Laboratories) was analysed using two amplification methods; the sensitive one-step RT-PCR method to amplify long transcripts and the less sensitive two-step RT-PCR method to amplify short regions of *RAD9B*. (A) The expressions of *RAD9B-001, 002/005, 003* and *009* across several normal human tissues based on the detection of the full length CDS of the *RAD9B* splice variants using the sensitive one-step RT-PCR method. (B) The expressions of *RAD9B* in the same tissues based on the detection of small internal regions of the *RAD9B* splice variants. The amplification was performed using the less sensitive two-step RT-PCR method. The values (0–3) represent the expression levels, where 0 signifies no expression and 3 indicates very high expression. The expression levels were based on the intensity of the amplified PCR fragments detected on agarose gel. The intensity of the bands was estimated using the ImageJ 2.0 software program. The full results of the agarose gel analysis can be seen in Appendix 1.

3.2.7 Expression of the Rad9-Rad1-Hus1-interacting nuclear orphan 1 (*C12ORF32*) in normal human tissues

The C12ORF32/RHINO protein co-localises with the 9-1-1 ring in human cells after UV treatment interacts physically with the ring and is required for the full phosphorylation of CHK1 at Ser-317 (Cotta-Ramusino et al., 2011). A previous study reported that *C12ORF32* expression is hardly detectable in 16 normal human tissues that were tested in their study (Kim et al., 2010). Since 13 of the 16 tested normal tissues were the same tissues used for the detection of the *RAD9B* variants (Figure 3.7), the expression of *C12ORF32* was further analysed in all the 20 human tissues used to test the expression of the *RAD9B* variants. This will help to further test the efficiency of the modified RT-PCR conditions used to amplify such weakly expressed genes, and also to compare the expression of these two genes searching for any tissue-dependent expression similarity.

Interestingly *C12ORF32* was expressed in 19 of the 20 normal human tissues. The expression was relatively good in some tissues (Brain (whole), fetal brain, fetal liver, kidney, prostate, testis, thymus and small intestine) and less so in others, contrary to the results of the 2010 study (Figure 3.8).

Similarly to *RAD9B-001* and *RAD9B-002/005,* elevated expression levels of *C12ORF32* were detected in both brain and testis. *C12ORF32* was also highly expressed in the thymus in contrast to the *RAD9B* variants, and liver was the only tissue not showing any expression of the *C12ORF32* gene. The rest of the tissues reflected moderate to weak expression of this gene. These outcomes show that *C12ORF32* and *RAD9B* expressions do not share tissue-dependent similarity, and that *C12ORF32* is expressed in non-malignant human tissues.

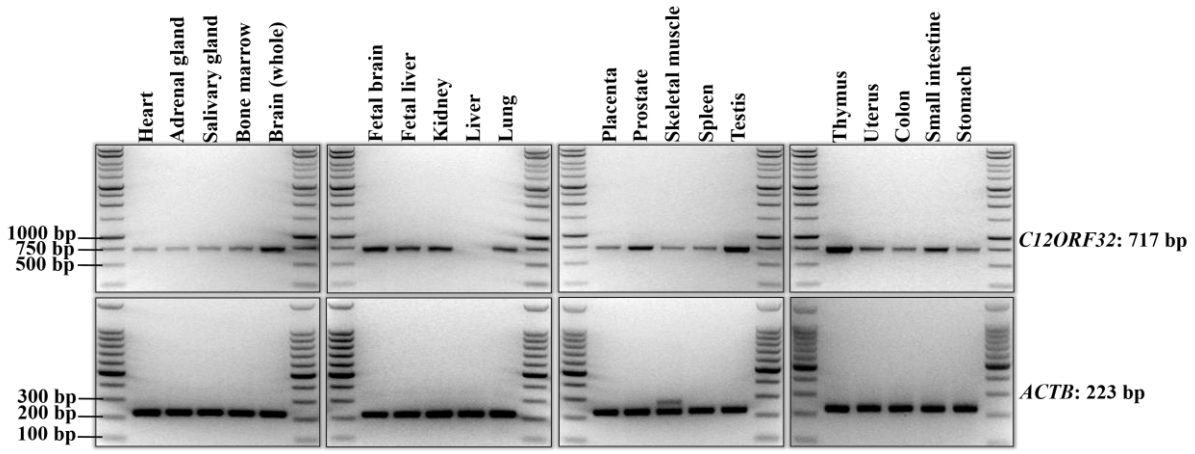

Figure 3.8 Expression analysis of human *C12ORF32* in various normal human tissues. Agarose gel shows the RT-PCR of the Rad9-Rad1-Hus1-interaction nuclear orphan across various human tissues. cDNA was reverse transcribed from the Human Total RNA Master Panel II (Clontech Laboratories). *ACTB* was used as a positive control for cDNA quality. The expected size (bp) of the amplified gene name is shown to the right.

3.2.8 *RAD9B-001* and *RAD9B-002* expression is downregulated in confluent HEK293 cells but not HeLa cells

In previous experiments, expression of the *RAD9B* variants was low in dividing cells of normal and cancer cell lines. Therefore, it was investigated whether their levels change once cells have ceased division and entered the confluent state. Normal HEK293 and cancer HeLa cell lines were used. To obtain confluent conditions, both cell lines were grown for seven days until the cells stopped dividing due to contact inhibition.

The one-step RT-PCR results for the confluent cells when compared to dividing cells revealed a confluence-dependent mRNA decrease for *RAD9B-001*. The expression of the *RAD9B-001* variant seemed negatively influenced by confluency in HEK293 cells, but not in HeLa cells (Figure 3.9-B). The *RAD9B-002/005* variants also seemed to have lower expression in post-confluent HEK293 cells. However, it is unknown which of the two variants is affected as the (L-002-005) primers (Figure 3.2-A) detects both variants nearly at the same length (1254 bp). The levels of *RAD9B-003* did not show any changes, neither did *RAD9B-S003* (Figure 3.9-B).

As in the previous experiments, full length *RAD9B-009* could not be detected. Two-step RT-PCR amplifying the short region of *RAD9B-009* revealed no changes under these cellular confluent conditions (Figure 3.9-C).

The *ACTB* expression did not change in the confluent cells confirming the accuracy of the low expression results obtained for *RAD9B-001* and *RAD9B-002/005*.

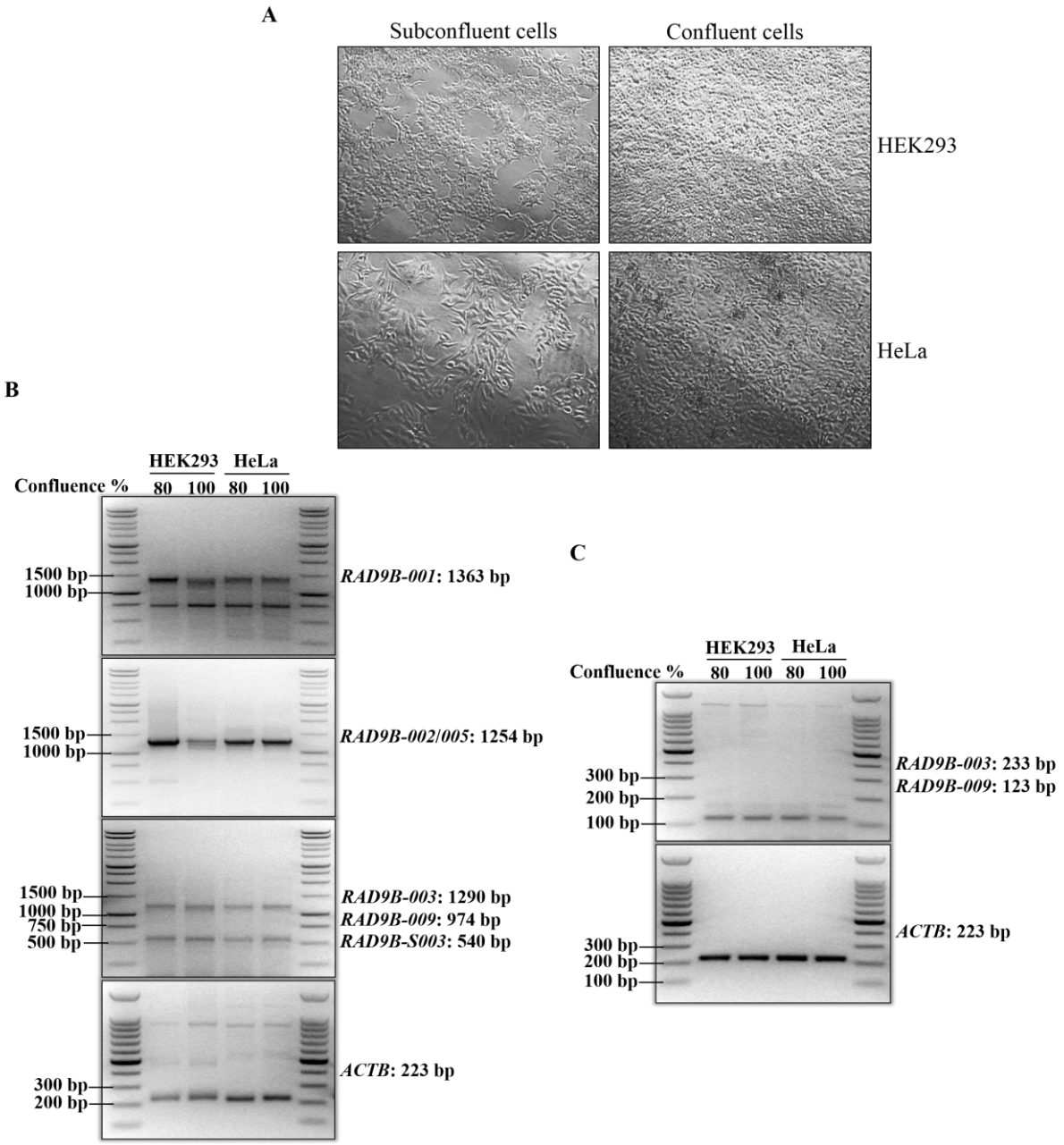

Figure 3.9 RT-PCR analysis of the *RAD9B* splice variants in subconfluent and confluent cells. (A) HEK293 and HeLa cell lines were plated and allowed to grow for 3–4 days until the subconfluent stage or for 7 days until the confluent stage. Images were taken with a CMEX-5000 Camera (Euromex) placed on an Eclipse TS100 Microscope (Nikon). (B) One-step RT-PCR analysis of *RAD9B* variants in HEK293 and HeLa subconfluent and confluent cells. Primers to amplify full-length variant transcripts were used. (C) Total RNA extracted from HEK293 and HeLa subconfluent and confluent cells was reverse transcribed, followed by PCR amplification of *RAD9B-009* variants. *ACTB* was used as a control for RNA and cDNA quality. Name of amplified gene and the expected size (bp) can be seen to the right.

3.2.9 Cellular senescence up-regulates *RAD9B-001* and *RAD9B-009* expression levels

To investigate whether cellular senescence influences the expression of the *RAD9B* variants, cellular senescence was triggered in the HEK293, HeLa and Kelly cell lines. Non-proliferating enlarged, vacuolated cells are two markers for cellular senescence. Therefore, the capability of oxidative stress to induce cellular senescence was examined in these cell lines by exposing them to a sublethal dose of hydrogen peroxide (200 µM H_2O_2, 1 hr). Out of the three cell lines, neuroblastoma Kelly cells were extremely sensitive to H_2O_2 with all cells dead at 24 hr after addition of hydrogen peroxide. The senescence markers were visibly induced in HEK293 and HeLa cells 48 hr after addition of the hydrogen peroxide (Figure 3.10-A).

In addition to these markers, the effect of oxidative stress was examined on the main regulatory proteins of cellular senescence: p21 and p16 (Campisi, 2013). Protein samples were extracted from both normal HEK293 and HeLa cell lines at 48 hr and 72 hr after treatment. Western blot analysis showed moderately elevated levels of p21 and p16 in HEK293 cells 48 hr after treatment. Contrarily, in HeLa cells under the same conditions, p21 expression was down-regulated 48 hr after treatment and levels were back to normal after 72 hr, but no changes were seen in p16 expression (Figure 3.10-B). Taken together, these findings indicate that cellular senescence was induced in HEK293 cells and possibly in HeLa by a different mechanism.

To investigate whether the *RAD9B* variants are up-regulated or down-regulated under senescent conditions, mRNA levels were analysed using one step and two step RT-PCR. The analysis revealed the up-regulation of *RAD9B-001* 48 hr after treatment in HEK293 and HeLa cells. The smaller band appearing on the agarose gel did not change under senescent conditions in HEK293 cells, but was down-regulated at the 72 hr time point in HeLa cells (Figure 3.10-C). However, the DNA sequence of the smaller band (~750bp) revealed that it was an unrelated ribosomal gene (*RPL3*). Expression of *RAD9B-002*/*005* and *RAD9B-003* did not change under senescence conditions, but the short splice variant *RAD9B-S003* increased 72 hr after treatment in HEK cells. In Hela cells, *RAD9B-002* was slightly down-regulated 48 hr post treatment, mimicking the p21 protein expression levels, as seen in Figure 3.10-C.

The full-length *RAD9B-009* variant was not expressed in either of the two cell lines under normal conditions nor under senescence. Two step RT-PCR amplifying the short region of *RAD9B-009* revealed an up-regulation in HEK293 cells with a possible new splice variant that could have a specific role for inducing cellular senescence (Figure 3.10-D).

A

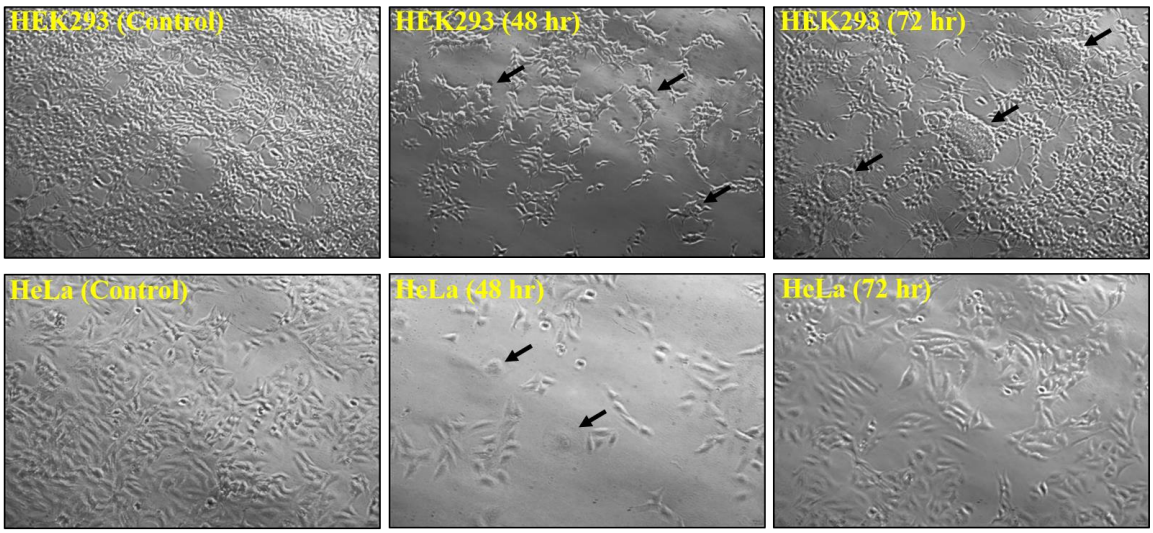

B

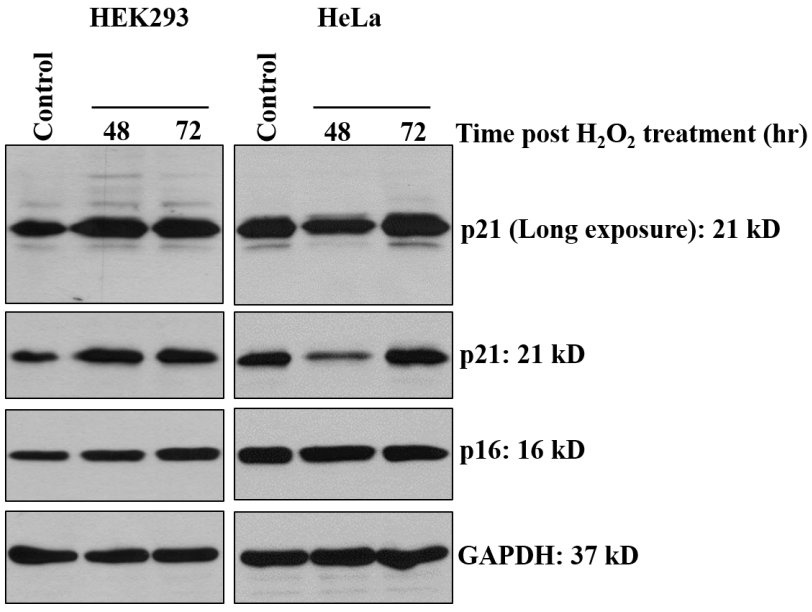

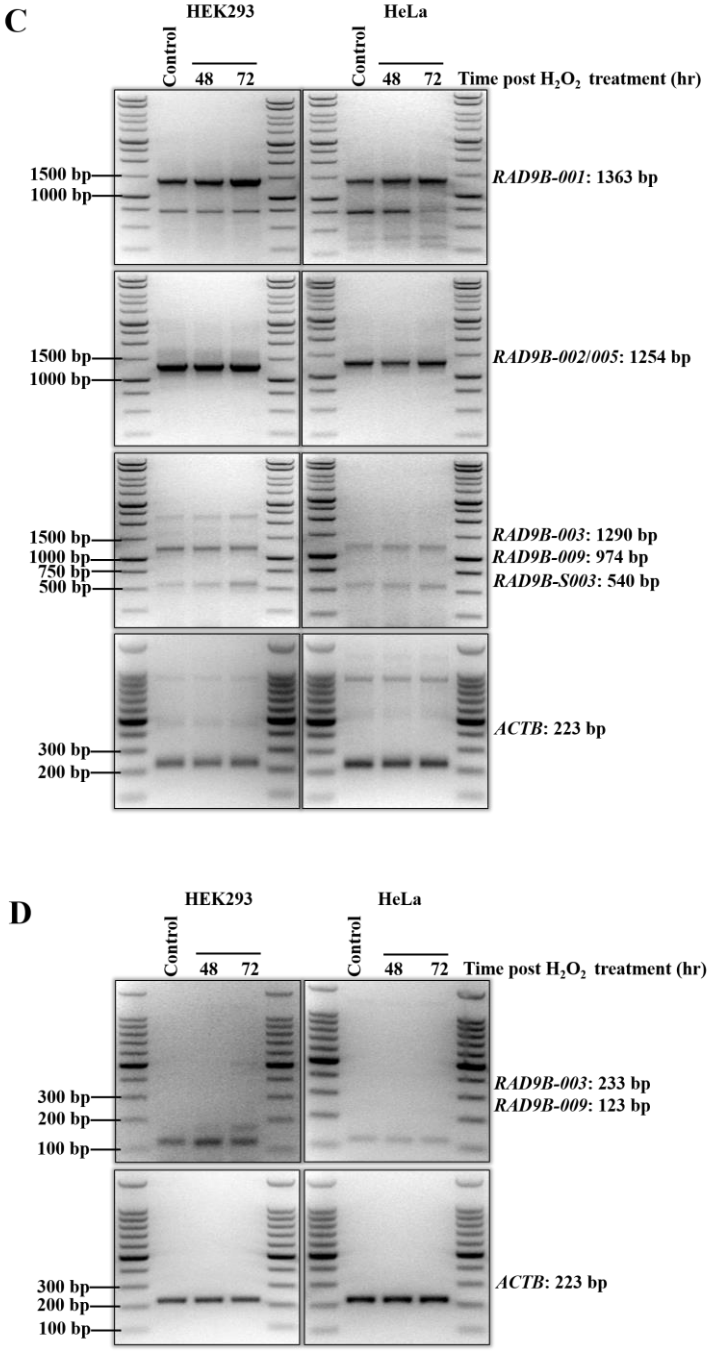

Figure 3.10 Upregulation of *RAD9B* variant in oxidative stress-induced senescent cells. Cellular senescence was induced in HEK293 and HeLa cells with 200 µM H_2O_2. Cells were treated for 1 hr and then allowed to recover for 48 and 72 hrs. (A) Cells were either grown under normal conditions for 72 hr (Control) or treated with H_2O_2 for 1 hr and proliferated for 48 and 72 hrs after treatment. Images were taken with a CMEX-5000 Camera (Euromex) placed on an Eclipse TS100 Microscope (Nikon). (B) Protein levels of p21 and p16 in HEK293 and HeLa senescent cells analysed by western blotting. (C) One-step RT-PCR analysis of *RAD9B* variants in HEK293 and HeLa normal and senescent cells. Primers to amplify the full length variant transcripts were used. (D) Total RNA extracted from HEK293 and HeLa normal and senescent cells was reverse transcribed, followed by PCR amplification of the *RAD9B* variants. Internal primers amplifying short regions of *RAD9B-003* and *RAD9B-009* were used. *ACTB* was used as a control for RNA and cDNA quality. Name of gene and the expected size (bp) can be seen to the right.

3.2.10 *RAD9B* splice variants are highly expressed in G1 phase

Overexpression of human *RAD9B* was found to cause a G1 cell arrest (Perez-Castro & Freire, 2012). To investigate whether the different *RAD9B* splice variants are specifically expressed in the G1 phase, both HEK293 and HeLa cells were synchronised in G1 by serum starvation. The two cell lines were plated and allowed to attach for a few hours. Then the cells were grown in FBS-free medium for 24 hr, followed by release in rich medium for 6 hr. The cells, including the control cells grown in complete medium, were fixed immediately after the 24 hr starvation period and 6 hr after release. Total RNA was extracted at these times as well.

The fixed cells were analysed by flow cytometry, revealing the success of G1 arrest in both HEK293 and HeLa cells, as the G1 DNA content increased after the 24 hr starvation period. However, HeLa cells showed a stronger increase compared to HEK293 cells (Figure 3.11).

The *RAD9B-001* expression levels increased slightly in G1-synchronised HEK293 cells though the expression returned to normal 6 hr after release. Based on the histogram, the cells started entering the normal cell cycle at this point. The signal for *RAD9B-002*/*RAD9B-005* also increased slightly in G1, but the expression dropped significantly when the cells entered the cell cycle. The *RAD9B-003* and *RAD9B-S003* expression increased in G1 and remained high when cells entered the cell cycle. No change in the expression of *RAD9B-009* was observed. These results indicate that especially expression of *RAD9B-002*/*005* may change throughout the cell cycle with an expression peak in the G1 phase.

Starved HeLa cells showed a similar change in *RAD9B-001* expression as HEK293 cells. Expression of *RAD9B-001* peaked in G1 enriched cells. Interestingly, expression of *RAD9B-002*/*005* strongly increased in serum starved HeLa cells and remained high 6 hr after release (Figure 3.12-A). *RAD9B-003* and *RAD9B-009* also showed an increase in their expression in G1 and after the release. These results strongly indicate a role of *RAD9B-001* and *RAD9B-002/005* in the G1 phase of the cell cycle in both HEK293 and Hela cells.

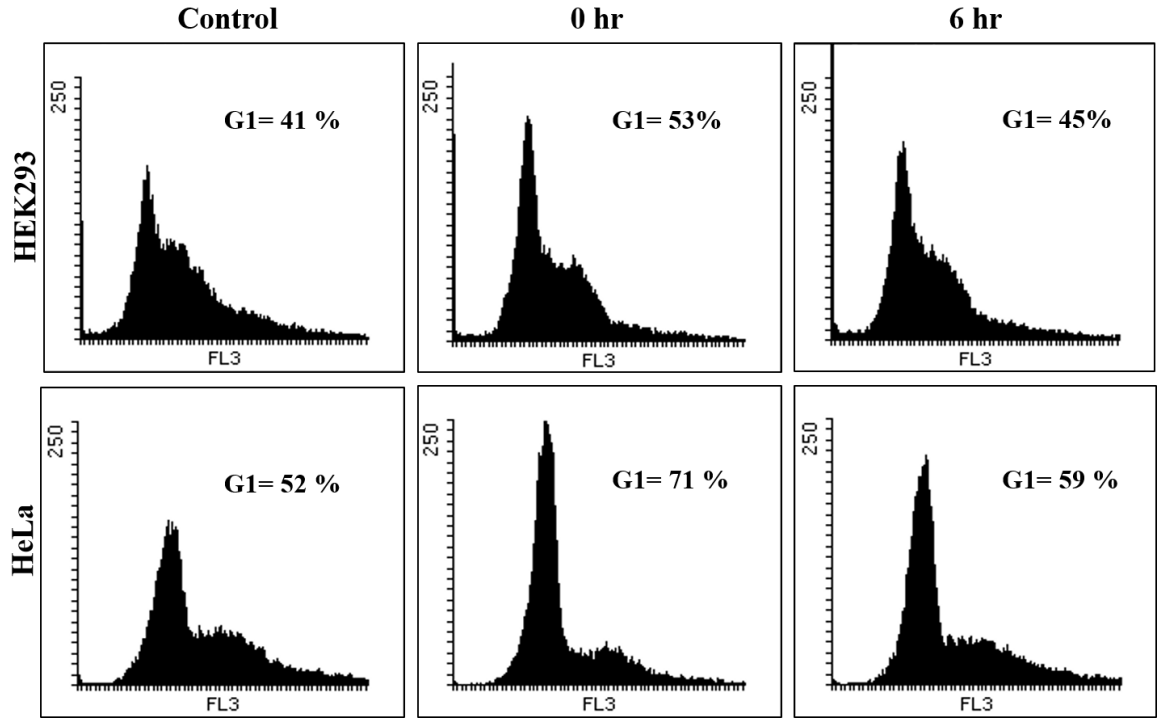

Figure 3.11 Serum starvation-induced G1 cell cycle arrest in HEK293 and HeLa cells. Cells were grown in FBS-free medium for 24 hr, followed by release into rich medium. Cells were fixed with methanol at 0 h and 6 hr after release in addition to normal control cells and analysed by the flow cytometry. G1 arrest can be seen clearly with the 0 hr sample immediately after the end of the serum-starvation period whereas cell started entering the normal cell cycle 6 hr after release. The histogram of the cell cycle phases was done after gating on propidium iodide-stained cells with the Flowing software 2.5.1.

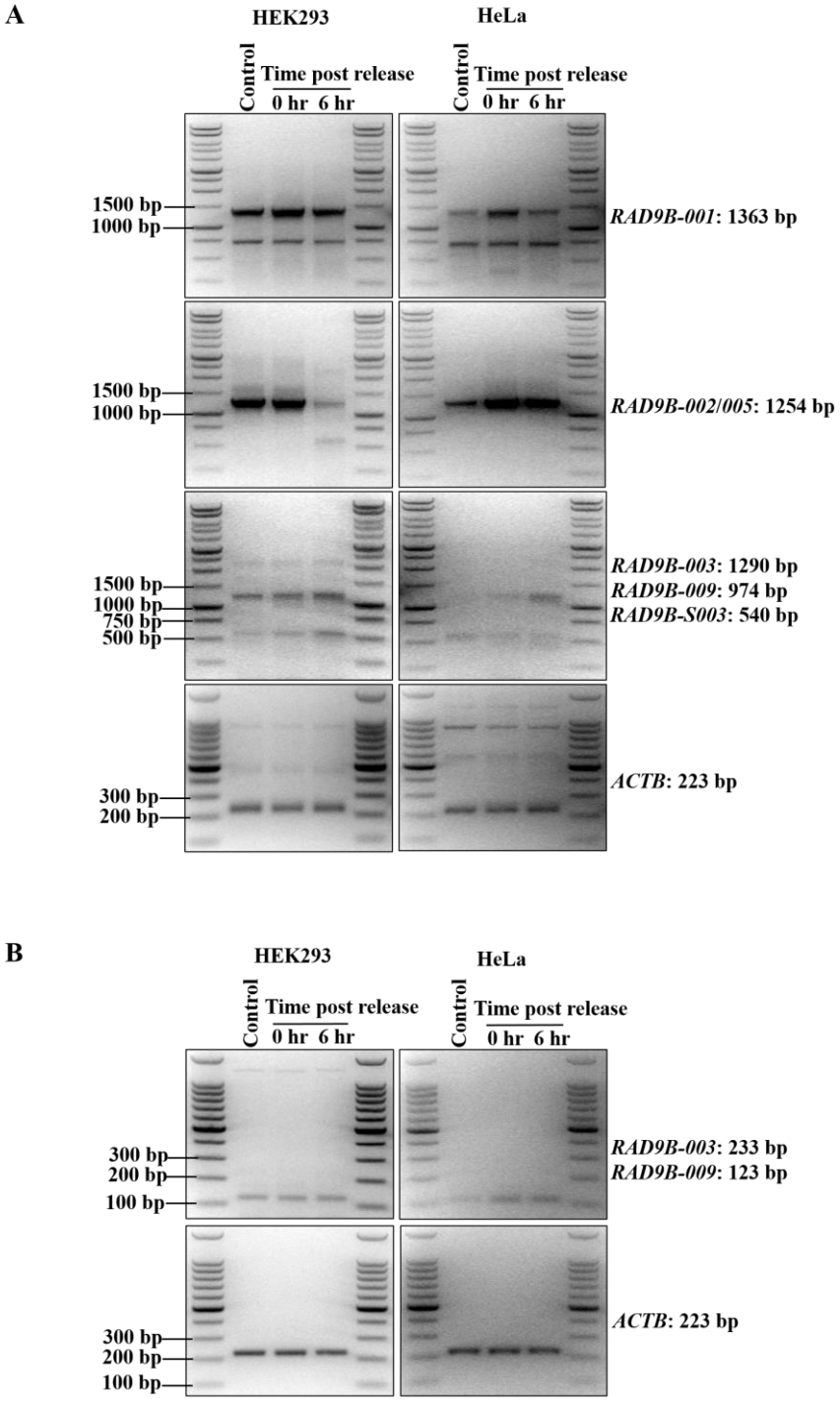

Figure 3.12 Up-regulation of *RAD9B* variant in G1-arrested cells by serum starvation. RT-PCR analysis of the of *RAD9B* splice variants in G1 cell cycle arrested cells. Total RNA was extracted from normal cells and G1-arrested cells immediately after the end of the arrest period and at 6 hr post release. (A) One-step RT-PCR analysis of *RAD9B* splice variants in HEK293 and HeLa normal and G1-arrested cells. Primers to amplify full-length variant transcripts were used. (B) Total RNA extracted from HEK293 and HeLa normal and G1-synchronised cells was reverse transcribed followed by PCR amplification. Internal primers amplifying short regions of *RAD9B-003* and *RAD9B-009* were used. *ACTB* was used as a control for RNA and cDNA quality. Name of gene and the expected size (bp) can be seen to the right.

3.3 Discussion

The key findings of this chapter are: (1) all five *RAD9B* are expressed at the mRNA level in HEK293 human embryonic kidney cells, HeLa cervical cancer cells and Kelly neuroblastoma cancer cells as well as in wide range of different human fetal and adult tissues. (2) The 5' end region of *RAD9B* encodes for a short novel splice variant (*RAD9B-S003*) which is only expressed in a limited number of tissues. (3) Unlike the reported specific expression of the RAD9-HUS1-RAD1 interacting nuclear orphan 1 (*C12ORF32*/*RHINO*) in breast cancer cell lines, here its expression is detected in almost all normal human tissues that have been tested. (4) *RAD9B-001* and *RAD9B-002*/*005* expression is down-regulated in non-dividing cells but not *RAD9B-003* or *RAD9B-009* indicating their role in the regulation of the ongoing cell cycle (5) The serum starvation response of *RAD9B* splice variants suggests a possible involvement in the regulation of G1 phase by *RAD9B* splice variants in HEK293 and HeLa cells. (6) Since *RAD9B* splice variants were up-regulated during senescence, and given their high expression in fetal tissues, this indicates a possible new role of *RAD9B* splice variants in the reported senescent stages during embryonic development.

Cloning of human *RAD9B* in 2003 revealed the existence of a second *RAD9* gene in the human genome which is closely related to *RAD9A*. The cloned *RAD9B* cDNA turned later out to be identical to *RAD9B-002* although the first three amino acids (MAA) are absent from the published sequence. In addition to the *RAD9B-002* transcript, the human *RAD9B* gene encodes four protein coding variants of which *RAD9B-001* has been studied here (Dufault et al., 2003) .

Table 3.4 Human *RAD9B* splice variants analysed in this study

hRad9B Variant	Specific Amplification	Amino Acids	Comment
RAD9B-001	yes	345	-
RAD9B-002	no (jointly with 005)	417	Full-length RAD9B
RAD9B-003	yes	429	-
RAD9B-005	no (jointly with 002)	345	ORF identical to 001
RAD9B-009	yes	341	-

The amplification of the *RAD9B* splice variants using the two RT-PCR techniques (one-step and two-step RT-PCR) showed the higher efficiency of using the one-step RT-PCR

in a situation where very low expressed genes were amplified. Among most databases of gene expression, at both the mRNA and protein levels, expression of *RAD9B* was reported in a very limited number of tissues. The results obtained at the beginning of this project were indeed consistent with these databases as *RAD9B* could not be amplified from a large number of the cell lines that were tested. However, several attempts at amplification of the low expressed *RAD9B* splice variants revealed possible alternative RT PCR conditions that could be used for the successful amplification of such low expressed genes. Therefore, it cannot be concluded that a certain gene is not expressed in a certain tissue, as shown in the results chapter regarding the amplification of the *RAD9B* splice variants and the amplification of the *C12ORF32*, as these showed that low expressed genes require special amplification conditions.

A significant difference in efficiency between the one-step and two-step RT PCRs was evident in the amplification of the *RAD9B* splice variants. The amplification of the full coding sequence of the splice variants was either negative or almost undetectable when amplified by the two-step RT-PCR, while in comparison, the one-step RT-PCR revealed a decent amplification signal for the *RAD9B* splice variants. This is a result of all the cDNA from the RT reaction being used in the PCR reaction providing sensitive detection. However, when applying the one-step method, the quality of the RNA must be taken into account. The extracted RNA must be free of any contaminants such as buffer salts and phenol that would affect the sensitivity of the RT reaction. In addition, the temperature of the primers should be taken into account when designing primers for the one-step PCR to avoid primer dimer formation during the PCR procedure as the primers are present during the RT reaction step at low temperatures.

The two-step RT PCR revealed less sensitivity for the amplification of low expressed genes than the one-step method. However, some alterations in the two-step RT-PCR can enhance the amplification of such genes. Generally, in the RT-PCR reaction, oligo dT primers or random hexamers are used. The oligo dT primers prime at the 3' tail of the mRNA, initiating reverse transcription until the reverse transcriptase enzyme efficiency drops, and are therefore not ideal for the amplification of long mRNA transcripts.

The random hexamer primers prime randomly along the mRNA, producing small, unequally amplified cDNA fragments. The choice of usage between the two primers depends on the specific primer binding regions on the mRNA transcript. The specific primers that were used for the detection of the *RAD9B* splice variants differ in their binding sites. Therefore, to ensure an efficient amplification of the *RAD9B* splice variants, a mixture of oligo dT and random hexamer primers were used for the RT reaction, which resulted in positive outcomes for the amplification of the *RAD9B* splice variants. Moreover, the dilution of the cDNA plays an important role in the amplification of low expressed genes. Minimising the cDNA dilution can contribute to the enhancement of the PCR detection of low expressed genes. Most published RT-PCR results use a cDNA dilution factor greater than 1:5. As a consequence, some genes can be reported to be expressed in only a few tissues, which is a false interpretation of the results due to the cDNA concentration that was used in the analyses. However, in this project, when a low dilution of 1:2 of cDNA was used, *RAD9B* and *C12ORF32* were detected in a large number of tissues.

The similarity between RAD9A and RAD9B is higher in their N-terminal sections, which both form the 9-1-1 ring, whereas their C-terminal tails are much more diverse. Interestingly, only one phosphorylation site of RAD9A, Ser-387, is conserved in RAD9B (Ser-409). Northern blot analysis showed three *RAD9B* transcripts (4.4, 3.0, and 2.2 kb) in testis and skeletal muscle, two transcripts in heart (4.4, 2.2 kb) and one larger transcript in brain (5.0 kb). *RAD9B* expression was also detected in K562, HeLa, OVCAR5, and HEK293 cell lines (Dufault et al., 2003). Using a more sensitive one-step RT PCR test with specific flanking primers, expression of *RAD9B* could be detected in more tissues as originally known (Figure 3.7).

While full-length *RAD9B-002*/*005* was expressed in all tested tissues with the exception of the placenta, the highest levels were detected in brain, kidney, lung and testis, fetal brain and liver (Figure 3.7). All variants except *RAD9B-009* were present in testis. The N-terminally truncated variant *RAD9B-001* was also present in most tissues with the exception of placenta. It highest levels were found in the brain and estis. The longest variant *RAD9B-003* was weakly expressed in the salivary gland, brain, fetal brain and lung. Taken together, the *RAD9B* variants do have a tissue specific expression pattern although the two variants analysed here, *RAD9B-001* and *RAD9B-002* are found in most tissues.

The *C12ORF32*/*RHINO* gene has previously been shown to be involved in mammary carcinogenesis. Very high expression was detected in 11 breast cancer cell lines by two-step RT-PCR and northern blot compared to extremely weak detected expression in only few normal tissues (Kim et al., 2010). Interestingly, depletion of *C12ORF32* significantly supressed the growth of breast cancer cell lines by cells accumulating in sub-G1 population indicating cell death. Despite reported weak expression of *C12ORF32* in normal tissues, here, its expression was detected in 19 out of 20 normal tissues that were tested. The inconsistency with the published results is due to using a high template concentration that has been shown to be effective in the case of low expressed genes (Figure 3.3). The expression of *C12ORF32* was highly abundant in brain (whole), fetal brain, fetal liver and testis similarly to the expression of *RAD9B* but also showed different expression specificity in other tissues. It is unclear from this RNA panel experiment whether an expression relation exist between *RAD9B* and *C12ORF32*, however, a possible role between the two may exist in the brain and fetal tissues.

The high expression levels of *RAD9B-001*, *RAD9B-002*/*005* and *RAD9B-003* in the devolving and mature brain are in line with a study by Leloup et al. who showed that mouse *RAD9B* plays an important role in brain development (Leloup et al., 2010). Interestingly, full length *RAD9B-003* was found only in the testis and the fetal brain, and it was barely detectable in the salivary gland, the whole brain and the lung. This suggests that this splice variant may play a role in brain development. However, when small internal primers were used for the detection of the *RAD9B-003* splice variant, it was found expressed only in testis and colon indicating that a new splice variants may exist in these tissues.

```
              10        20        30        40        50        60
RAD9B-003 MAAMLKCVMSGSQVKVFGKAVQALSRISDEFWLDPSKKGLALRCVNSSRSAYGCVLFSPV
          ::::::::::::::::::::::::::::::::::::::::::::::::::::::::::::
RAD9B-002 MAAMLKCVMSGSQVKVFGKAVQALSRISDEFWLDPSKKGLALRCVNSSRSAYGCVLFSPV
              10        20        30        40        50        60

              70        80        90       100       110       120
RAD9B-003 FFQHYQWSALVKMSENELDTTLHLKCKLGMKSILPIFRCLNSLERNIEKCRIFTRSDKCK
          ::::::::::::::::::::::::::::::::::::::::::::::::::::::::::::
RAD9B-002 FFQHYQWSALVKMSENELDTTLHLKCKLGMKSILPIFRCLNSLERNIEKCRIFTRSDKCK
              70        80        90       100       110       120

             130       140       150       160       170       180
RAD9B-003 VVIQFFYRHGIKRTHNICFQESQPLQVIFDKNVCTNTLMIQPRLLADAIVLFTSSQEEVT
          ::::::::::::::::::::::::::::::::::::::::::::::::::::::::::::
RAD9B-002 VVIQFFYRHGIKRTHNICFQESQPLQVIFDKNVCTNTLMIQPRLLADAIVLFTSSQEEVT
             130       140       150       160       170       180

             190       200       210       220       230       240
RAD9B-003 LAVTPLNFCLKSSNEESMDLSNAVHSEMFVGSDEFDFFQIGMDTEITFCFKELKGILTFS
          ::::::::::::::::::::::::::::::::::::::::::::::::::::::::::::
RAD9B-002 LAVTPLNFCLKSSNEESMDLSNAVHSEMFVGSDEFDFFQIGMDTEITFCFKELKGILTFS
             190       200       210       220       230       240

             250       260       270       280       290       300
RAD9B-003 EATHAPISIYFDFPGKPLALSIDDMLVEANFILATLADEQSRASSPQSLCLSQKRKRSDL
           ::::::::::::::::::::::::::::::::::::::::::::::::::::::::::::
RAD9B-002 EATHAPISIYFDFPGKPLALSIDDMLVEANFILATLADEQSRASSPQSLCLSQKRKRSDL
             250       260       270       280       290       300

             310       320       330       340       350       360
RAD9B-003 IEKKAGKNVTGQALECISKKAAPRRLYPKETLTNISALENCGSPAMKRVDGDVSEVSESS
           ::::::::::::::::::::::::::::::::::::::::::::::::::::::::::::
RAD9B-002 IEKKAGKNVTGQALECISKKAAPRRLYPKETLTNISALENCGSPAMKRVDGDVSEVSESS
             310       320       330       340       350       360

             370       380       390       400       410       420
RAD9B-003 VSNTEEVPGSLCLRKFSCMFFGAVSSDQQEHFNHPFDSLARASDSEEDMNNVCCRKEFNG
          ::::::::::::::::::::::::::::::::::::::::::::::::::        :
RAD9B-002 VSNTEEVPGSLCLRKFSCMFFGAVSSDQQEHFNHPFDSLARASDSEEDMNN--------G
             370       380       390       400       410


RAD9B-003 SDAKYFCII
          :    : :.
RAD9B-002 S----FSIF
```

Figure 3.14 Alignment of RAD9B-002 and RAD9B-003. The alignment was created using ALIGN tool (http://xylian.igh.cnrs.fr/bin/align-guess.cgi. Accessed 20 August 2016). The two splice variants differ only at the very end of the C-terminus.

It is worth noting that the variant RAD9B-003 differs only by 13 amino acids at its very end from the full-length RAD9B protein RAD9B-002 (Figure 3.14). This implies that the C-terminus, which is highly charged in the case of RAD9B-003, plays an important role in brain development.

The expression analysis reported here identified a shorter version of the *RAD9B-003* transcript, *RAD9B-S003*, in which its expression starts at the ATG start code of the ORF of *RAD9B-003* but terminates approximately half way through the full length sequence. This suggests that *RAD9B-S003* is a new *RAD9B* splice variant. The *RAD9B-S003* is highly expressed in testis tissue, moderately expressed in the HEK293 and HeLa cells, and hardly detectable in the salivary gland, fetal brain, fetal liver and lung tissues. Its size appears to be smaller in the fetal brain (Appendix 1) while its expression follows the expression of the full-length *RAD9B-003*, it is absent in adult brain (Figure 3.7). Being detected in the two and only fetal tissues in the RNA tissue array, this short *RAD9B* splice variant may play a similar role to the *RAD9B-003* that is involved in the early developmental stages. In recent studies, a large number of short open reading frames (sORF) of between 15 and 138 amino acids have been identified in human tissues. These small ORFs were reported to play a role in the cell signalling and DNA repair. *RAD9B-S003* may belong to this novel class of short peptides and proteins although it was not reported in these publications (Ma et al., 2014; Slavoff et al., 2013).

Since it was reported that over-expression of *RAD9B* results in a G1 cell cycle arrest (Perez-Castro & Freire, 2012), the possible involvement of *RAD9B* in a G1 arrest was tested in HEK293 and HeLa cells by serum starvation. The two cell lines revealed interesting differences regarding the expression of the *RAD9B* splice variants. In HEK293 (non-malignant cells) and HeLa (cervical cancer cells), *RAD9B-001*, *RAD9B-005*/*002* and *RAD9B-003* showed elevated expression levels when cells were starved (Figure 3.12-A). This indicates a role of these variants in G1 or in the response to starvation. HeLa cells were different from HEK293 cells in that they showed also elevated expression of *RAD9B-009* (Figure 3.12-B). The latter is interesting as full-length *RAD9B-009* was not detected in any tested tissue (Figure 3.7) suggesting a possible involvement in the regulation of the G1 phase.

The accurate transition of the cell cycle from the G1 to S phase is crucial for cell proliferation, and its misregulation can lead to oncogenesis (Bertoli, Skotheim & de Bruin, 2013). *RAD9B-*

002 levels may have a crucial impact on the G1-S transition in HEK293 cells. This was concluded after the reduction in *RAD9B-002/005* expression during this cell cycle transition in HEK293 cells (Figure 3.12-A). In contrast, *RAD9B-002/005* levels increased during G1 in malignant HeLa cells during the transition to the S phase suggesting that G1-S transition is independent of *RAD9B-002/005* in this cell line (Figure 3.12-A). In addition, analysis of *RAD9B-003* and *RAD9B-009* also revealed high expression levels during G1-S transition in the HeLa cells while *RAD9B-001* did not (Figure 3.11-A & B). Although cells grown to the confluent stage generally reveal a G1 cell cycle arrest (Hayes et al., 2005), the analysis of *RAD9B* splice variants in these contact inhibited cells revealed a different expression profile from that obtained in G1 cells arrested by serum starvation. Both splice variants *RAD9B-001* and *RAD9B-002/005* expression levels were reduced (Figure 3.9), suggesting a different role of RAD9B-001 and RAD9B-002/005 in the permanent G1 block as in contact inhibited cells.

As mentioned previously, mouse *Rad9b* is crucial for embryonic development and is mainly expressed in the embryonic tissues at week 7.5 and particularly in brain tissue at weeks 8.5 and 9.5, whereas depletion of mouse *Rad9b* in embryos results in their early death (Leloup et al., 2010). The analysis of the RNA tissue samples supports this finding as all human *RAD9B* splice variants were expressed in fetal brain tissue. Given that senescence plays an important role in embryogenesis in a p21 dependent manner independently of DNA damage (Muñoz-Espín et al., 2013; Storer et al., 2013), it is interesting that *RAD9B-001*, *RAD9B-009* and *RAD9B-S003* were upregulated at the mRNA level in senescent HEK293 cells (Figure 3.10-C). Also *RAD9B-009* revealed an additional band in senescent HEK293 cells indicating a possible new role of *RAD9B* splice variants during embryonic development (Figure 3.10-D). This conclusion is supported by the co-compartmentalisation of over-expressed RAD9B and p21 in nucleoli (Perez-Castro & Freire, 2012).

Chapter 4: CONSTRUCTION OF STABLE HUMAN CELL LINES EXPRESSING RAD9B-001, RAD9B-002 AND YEAST RAD9-M50

4.1 Introduction

S. pombe Rad9-M50 is a heat-inducible protein variant of the DNA damage checkpoint protein Rad9 which regulates a heat induced G2 arrest and is linked with the de-phosphorylation of Chk1 kinase at elevated temperature (Janes et al., 2012). So far, human RAD9B has not been found to have a similar role as a heat-inducible protein. However, the RAD9B variant 001 shares similar features with yeast Rad9-M50 as both proteins lack extended sections of the N-terminus (49 aa SpRad9-M50; 72 aa RAD9B-001). While RAD9B-001 is produced by alternative splicing, yeast Rad9-M50 is an alternative translation product initiated from the cryptic start site AUG-50.

The expression of the full-length *RAD9B-001* splice variant was highest in brain, heart, skeletal muscle and testis, and up-regulated in serum starved G1 cells (Figure 3.7 & Figure 3.11). The second RAD9B splice variant, RAD9B-002, resembles RAD9A. It is identical to RAD9B-001, except that it contains an additional 72 aa at the N-terminus. The corresponding mRNA follows a similar expression pattern as *RAD9B-001* but with higher expression levels in lung, liver and kidney (Figure 3.7). It is quite intriguing that the RAD9B-002 and RAD9B-001 proteins resemble the *S. pombe* full-length RAD9 and Rad9-M50 proteins as this implies a conserved requirement for a N-terminally shortened RAD9 variant. As shown in Figure 4.1, both shorter RAD9 proteins may adopt in a similar structure consisting of two domains.

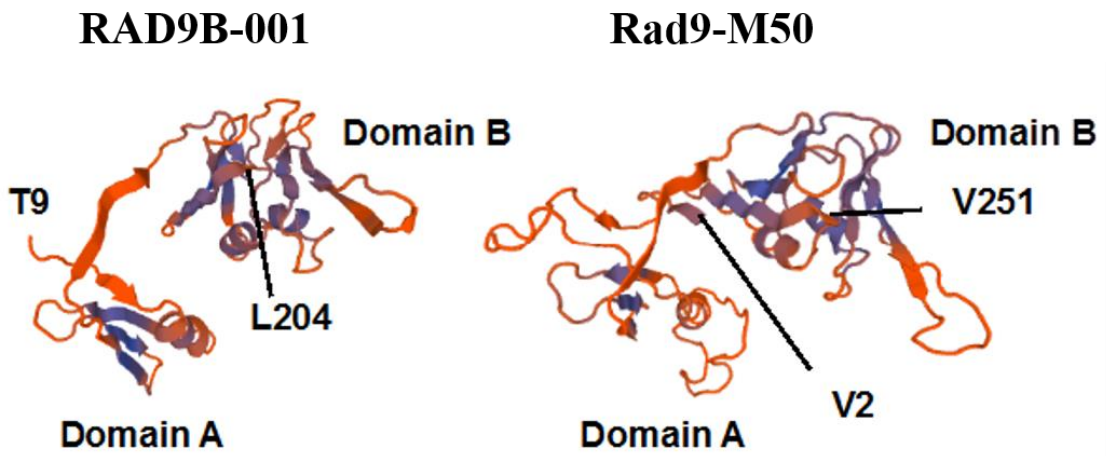

Figure 4.1 Models of human RAD9B-001 and *S. pombe* Rad9-M50. Both models were generated using the Swiss Model server (**https://swissmodel.expasy.org**. Accessed 30 August 2016). Both models are based on the crystal structure of human RAD9A (ID:3ggr.1), (Xu et al., 2009). The identity scores are 37.8% for human RAD9B-001 and 27.2% for yeast Rad9-M50. The first and last amino acids are indicated. The sequence coverage for RAD9B-001 is T9 - L204 and for Rad9-M50 V2-V251. Both proteins adopt a similar fold with two domains, domain A and domain B, linked by an extended beta-sheet. In the case of the yeast variant, the N-terminal part of the protein may make contact with domain B.

As mentioned before, the human RAD9B gene expresses 9 splice variants of which only 5 are protein coding (RAD9B-001, 002, 003, 005 and 009). These five splice variants were all analysed at the mRNA level in normal and carcinoma cell lines under different conditions (Chapter 3). Since the commercially available anti-RAD9B antibodies (antibodies-online (AA150-258), Abcam (ab72873)) failed to detect endogenous RAD9B proteins, it was decided not to order custom-made antibodies. This approach was also hampered by the high similarity of the different protein splice variants (Figure 3.1). Therefore, two RAD9B splice variants (RAD9B-001 and RAD9B-002) were studied at the protein level using an inducible protein expression system. Both variants were chosen because of their homology with RAD9A and the yeast Rad9M-50 protein, respectively. In addition, a third cell line, expressing the yeast Rad9-M50 protein, was constructed to investigate whether human cells would be able to utilise the yeast protein in comparison with the related human variant RAD9B-001. Moreover, human RAD9A and the yeast Rad9 full length were not included in the experiments due to time limitations of the project and also because concentrating on a small number of cell lines made it possible to investigate the roles of RAD9B in greater depth. To construct stable cell lines expressing RAD9B-002 (417 aa), RAD9B-001 (345 aa)

or *S. pombe* Rad9-M50 (377 aa), the HEK293 Flp-In integration system from Invitrogen was used.

The Flp-In system allows for the integration of any cDNA into the genome of the Flp-In T-REx HEK293 cell line, taking advantage of the DNA recombination system from *Saccharomyces cerevisiae* (*S. cerevisiae*) (Sauer, 1994; Craig, 1988). The Flp-In T-REx HEK293 cell line has been generated by the insertion of the pFRT/lacZeo vector into its genome, as this vector provides the recombination FRT target site for the recombinase enzyme expressed from the pOG44 plasmid into the host cell line. Successful integration results in a switch from zeocin resistance coming from the laz/Zeocin expression gene under the control of the SV40 promotor to hygromycin resistance which is on the integration plasmid pcDNA5/FRT/TO.

To insert RAD9B or yeast Rad9M-50 into the genome of the Flp-In T-REx HEK293 cell line, the corresponding cDNAs must first be cloned into the pcDNA5/FRT/TO plasmid. This vector contains two major components of the Flp-in system: one FRT site serving as a second target for the Flp recombinase enzyme and the hygromycin selective gene. Co-transfection of the recombinant pcDNA5/FRT/TO plasmid with the pOG44 plasmid expressing the Flp recombinase under the control of the CMV promotor (Buchholz et al., 1996) will allow the enzyme to initiate recombination between the two FRT sites (one in the genome and one on the recombinant plasmid) resulting in the stable integration. The recombinant cell line will then show resistance to hygromycin and sensitivity to zeocin. The Flp-In T-REx HEK293 cell line contains also the pcDNA6/TR plasmid which expresses high levels of the tetracycline suppressor that binds to the CMV promotor upstream of the recombinant cDNA resulting in its induction upon addition of doxycycline (Figure 4.2).

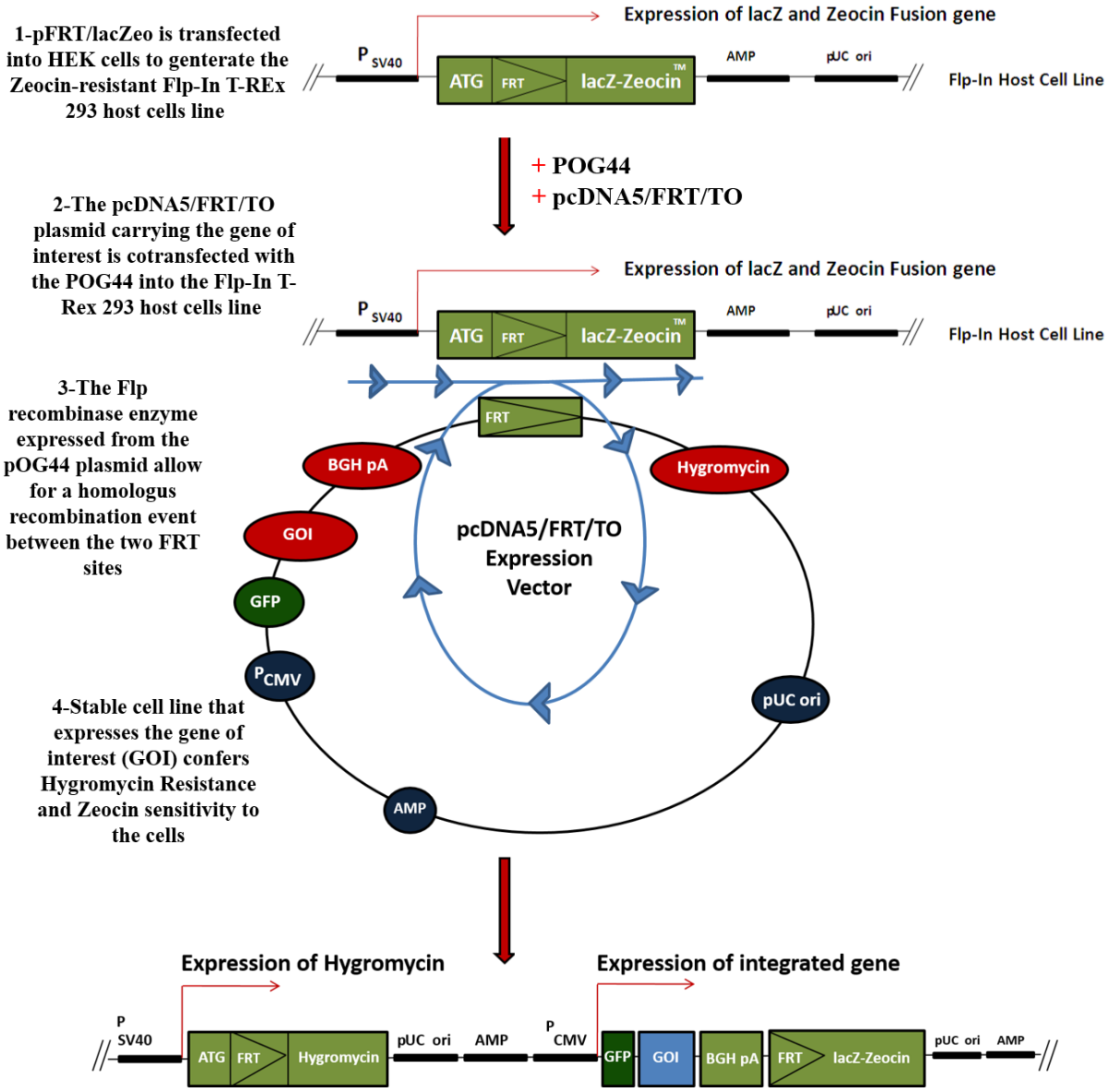

Figure 4.2 Integration of *RAD9B* and *Rad9M-50* into the Flp-In T-REx HEK293 cells. Co-transfecting the pcDNA5/FRT/To plasmid carrying *RAD9B-001*, *RAD9B-002* or *Rad9-M50* with the POG44 plasmid into the Flp-In TrEx HEK293 cells. The POG44 plasmid expresses the Flp enzyme, allowing for Flp recombination events between the two FRT sites in the pcDNA5/FRT/To plasmid and in the host HEK293 genome. The inserted genes are expressed under the control of the pCMV promotor following induction by doxycycline. The stable cell line confers sensitivity to zeocin and resistance to hygromycin.

4.2 Results

4.2.1 Construction and amplification of *RAD9B-001*, *RAD9B-002* and *SpRad9-M50.*

Since the initial attempts to clone the full-length *RAD9B-001* cDNA failed (this was before the RT-PCR conditions were optimised), overlapping primers were designed to construct the cDNA by fusion PCR. To this end, the nine coding exons of *RAD9B-001* with complementary sequence extension at either primer end were individually amplified and later fused using the flanking primers which also contained the restriction sites (Figure 4.3-A & B).

The fusion PCR displayed an amplified fragment with the expected size of this variant (1038 bp). Subsequent DNA sequencing confirmed the successful construction of the *RAD9B-001* cDNA. However, the DNA sequencing also revealed a four-nucleotide deletion in the 3' end region of the variant and this deletion was repaired by designing new fixing primers as summarised in the next section.

Since the *RAD9B-002* cDNA could also not be amplified at the beginning of the project, its cDNA was purchased and re-amplified from the acquired plasmid. The amplicon of *RAD9B-002* had the expected size (1254 bp, Figure 4.3-C). Subsequent sequencing confirmed that the amplicon is 100% identical to *RAD9B-002*. The *S. pombe* Rad9-M50 cDNA (1134 bp) was amplified from a yeast cDNA library and sequenced. As in the case of *RAD9B-001*, the sequence showed three mismatches in the 3' end section which were also repaired.

As a first step to construct the stable cell lines, the amplified and repaired cDNAs were cloned into the plasmid pcDNA5/FRT/TO. The primers for the amplification of the inserts were designed to have an additional sequence motif for the restriction enzymes *Xho*I at the 5' end and *Not*I at the 3' end. All three genes were cloned into the pcDNA5/FRT/TO vector restricted with *Xho*I and *Not*I. Figure 4.4 shows the successful cloning of the cDNAs.

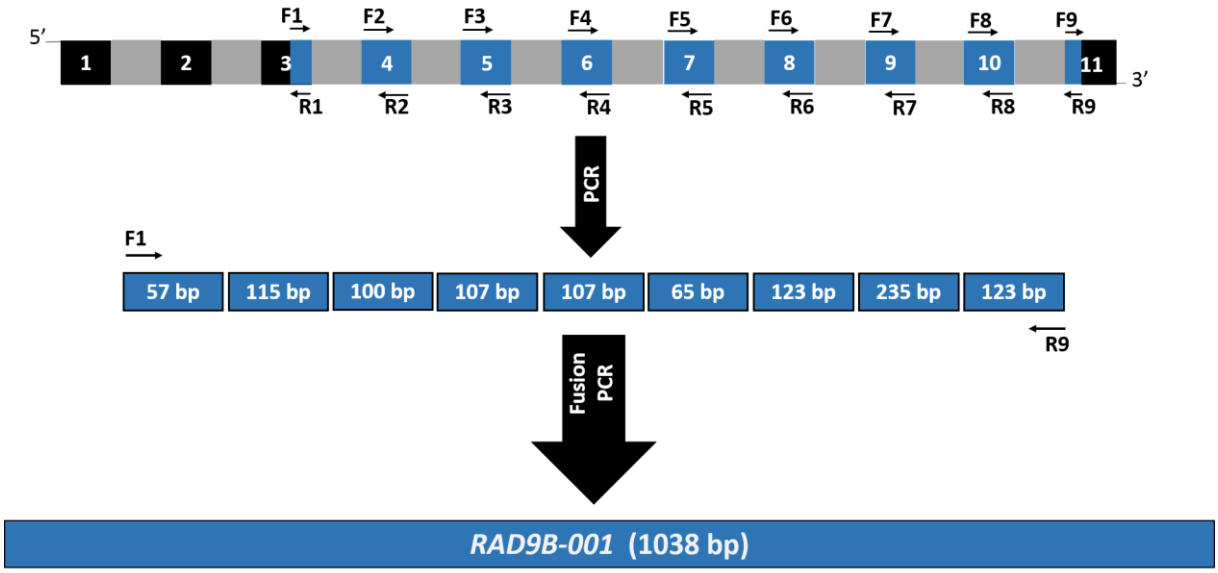
5′
F1
F2
F3
F4
F5
F6
F7
F8
F9
1
2
3
4
5
6
7
8
9
10
11
3′
R1
R2
R3
R4
R5
R6
R7
R8
R9
PCR
F1
57 bp
115 bp
100 bp
107 bp
107 bp
65 bp
123 bp
235 bp
123 bp
R9
Fusion PCR
RAD9B-001 (1038 bp)

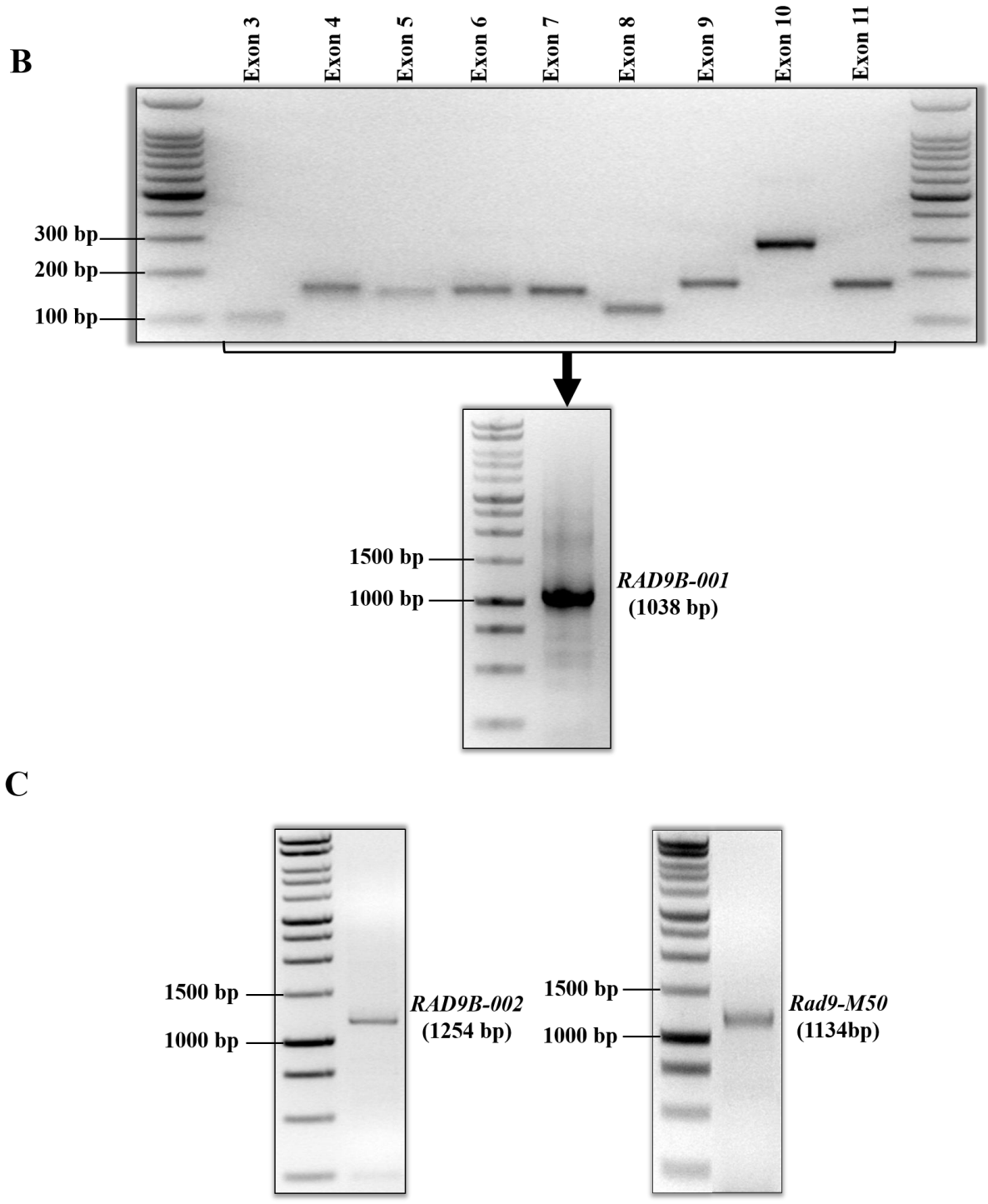

Figure 4.3 Construction of *RAD9B-001* and the amplification of *RAD9B-002* and yeast *Rad9-M50*. (A) Diagram showing the primers designed to amplify the 9 exons of *RAD9B-001* from the HEK293 cell genome. (B) Agarose gel showing the 9 amplified coding exons of the *RAD9B-001* and the successful fusion of these exons by fusion PCR. (C) PCRs for the amplification of *RAD9B-002* and yeast *RAD9-M50* were subjected to agarose gel revealing their corresponding transcript sizes (1254 bp and 1134 bp, respectively).

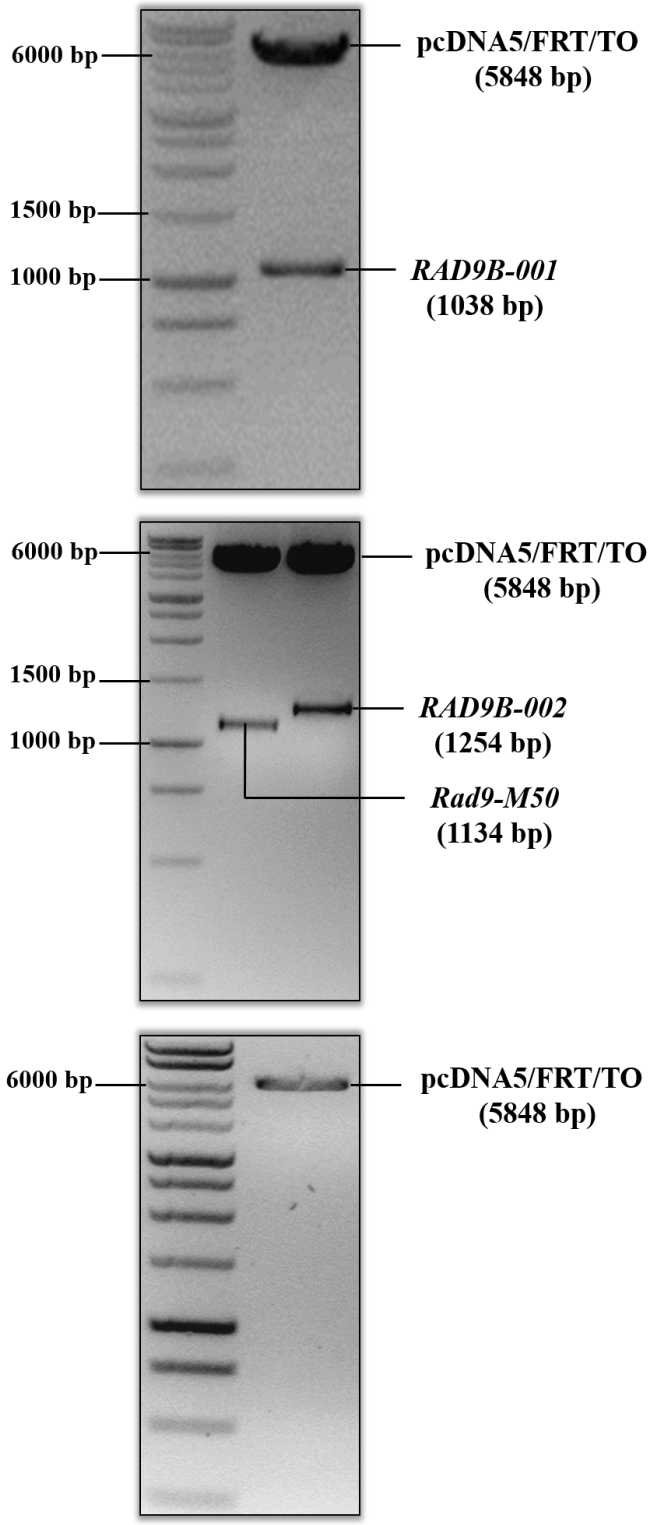

Figure 4.4 Confirmation of successfully cloning inserts into the pcDNA5/FRT/TO vector. The *RAD9B-001*, *RAD9B-002* and *Rad9-M50* inserts were cloned into the pcDNA5/FRT/TO plasmid. The plasmid was digested with *Xho*I and *Not*I restriction enzymes to confirm the cloning. The cut plasmid appears on the top of the agarose gel with a size of 6514 bp (pcDNA5/FRT/To 5800 bp and GFP 714 bp). The bottom bands represent the inserts *RAD9B-001* (1038 bp), *RAD9B-002* (1254 bp) and *Rad9-M50* (1134 bp). The empty pcDNA5/FRT/To plasmid was also digested with the same enzyme as a negative control.

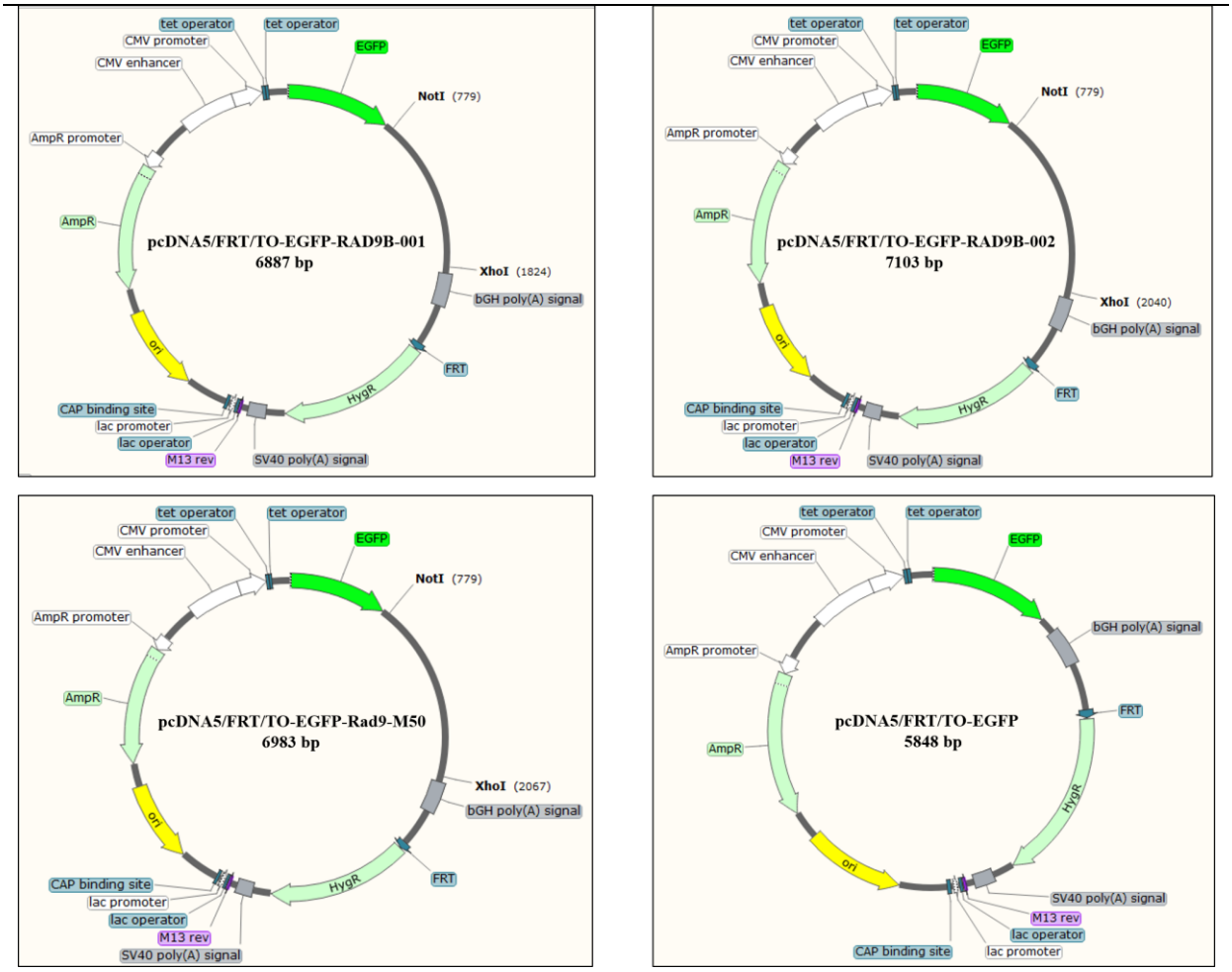

Figure 4.5 Diagram of the empty pcDNA5/FRT/TO plasmid and the plasmid after insertion of *RAD9B-001*, *RAD9B-002* and *Rad9-M50*. An overview of the pcDNA5/FRT/TO plasmid inserted with *RAD9B-001*, *RAD9B-002* or *Rad9-M50* between the *Not*I and *Xho*I restriction sites or left without insertion as a control. All plasmids contain an identical EGFP tag, except for the EGFP tag in the empty pcDNA5/FRT/TO, which is extended by a 28 aa until the first stop codon.

4.2.2 Repair of RAD9B-001 and Rad9-M50

As shown in Figure 4.6, the *RAD9B-001* cDNA contained a four-base-pair deletion close to the 3' end which was the binding site of the forward primer number 6 used for the construction of the cDNA. The four-base-pair deletion was corrected by designing new primers with complementary extensions overlapping the opposite strand. These primers bind a few base pairs at either site of the deletion resulting in two fused overlapping fragments amplified by PCR (Figure 4.6). The sequence of the repaired *RAD9B-001* was 100% identical to the sequence curated at the NCBI data base.

The sequence for the cloned yeast *Rad9-M50* cDNA revealed three mismatches in the 3' end region. One of the mismatches was silent while the other two resulted in an amino acid substitution (alanine with valine, and arginine with tryptophan). The mismatches were corrected with the Q5 Mutagenesis Kit (New England Biolabs), which allows for the replacement of one or multiple base pairs in a sequence. Two pairs of primers were designed to repair the two mismatches. The forward primer contained the altered codon approximately 10 nucleotides away from the 3' end of the primer to allow for the correct binding. The reverse primer started at the 5' end with one base pair next to the beginning of the forward primer. This allowed for the correction of the first mismatch. The plasmid having the corrected first mismatch was used as a template to correct the second mismatch in the same way (Figure 4.7). The DNA sequence of *Rad9-M50* revealed a successful repair.

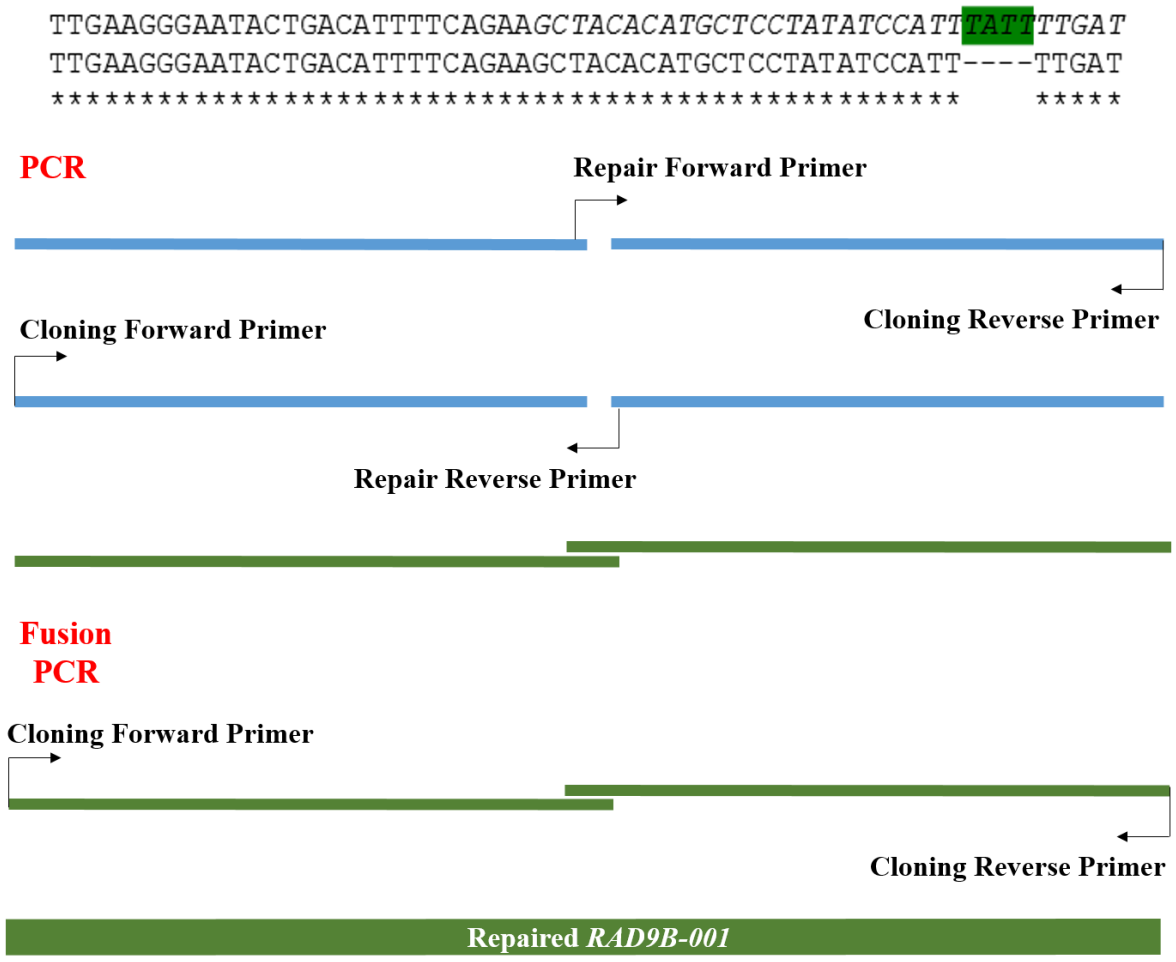

Figure 4.6 Repair of *RAD9B-001* by fusion PCR. The four missing base pairs in the *RAD9B-001* sequence are shown in green at the top of the figure. The deletion was fixed by using primers that bind to a few base pairs before the deletion (forward repair primer) with the original reverse primer, and bind to a few base pairs after the deletion (reverse repair primer) with the original forward primer. Both fixing primers have an extension of the opposite strand's complementary sequence. The amplified fixed fragments were fused together and re-amplified with fusion PCR. The fusion PCR revealed the correct full sequence of *RAD9B-001*.

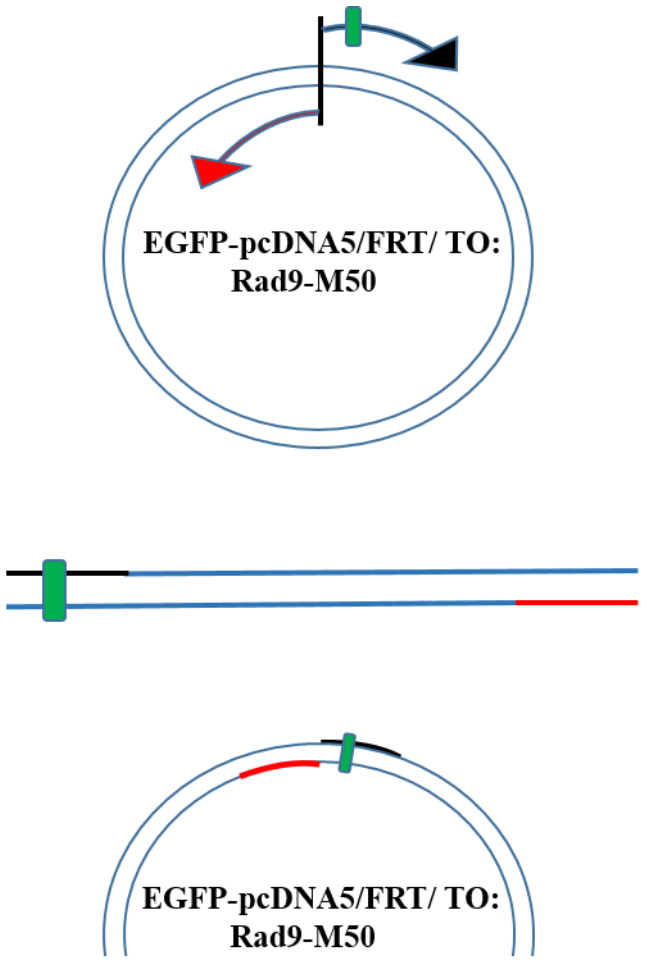

Figure 4.7 Repair of *Rad9-M50* substitutions with the Q5 Mutagenesis Kit. Two mismatches within the sequence of *Rad9-M50* were fixed using the Q5 Mutagenesis Kit (New England Biolabs). The forward primer (black) contains the correct altered base pair (green). The reverse primer (red) binds to the base pair next to the start binding region of the forward primer, allowing for the amplification of *Rad9-M50* with the corrected mismatch. The same corrected plasmid was used as a template for the correction of the second substitution using new designed primers containing the right sequence.

4.2.3 Construction of stable RAD9B and SpRad9-M50 cell lines

The stable cell lines expressing the two human RAD9B splice variants or the yeast Rad9-M50 were established by transfecting the EGFP-pcDNA5/FRT/TO plasmid carrying either *RAD9B-001*, *RAD9B-002*, *SpRad9-M50* gene or the empty plasmid (negative control) into human Flp-in T-REx HEK293 cells. The plasmids were co-transfected with the pOG44 plasmid to mediate the homologous recombination event between the two FRT sites, allowing the integration of RAD9B or Rad9-M50 into a specific genomic FRT site. It is important to emphasise that all engineered cell lines still express the endogenous RAD9A and RAD9B proteins. Due to time restriction, the endogenous RAD9 genes were no deleted.

Following the transfection, the cells were allowed to grow for two days. Then the cell-growing medium was supplemented with hygromycin instead of the zeocin to select for integrants.

4.2.4 Confirmation of integrants into the Flb-In T-REx HEK293 cell line

The successful integration of the two *RAD9B* splice variants and the yeast *Rad9-M50* into the Flp-in T-REx HEK293 cell genome was investigated by three methods. First, the whole genomic DNA was extracted from the transfected cells. The primers used to analyse the integrants were the same primers used for the cloning of the variants (L-001-002-005, L002-005 and Rad9-M50 primers, Figure 3.2). In an additional test, a forward primer designed to bind at the CMV promotor upstream of the EGFP-Rad9 genes was used in combination with the reverse cloning primer. The PCR analysis confirmed the integration of all cDNAs (Figure 4.8-A).

The second method used to confirm the integration was performed at the protein level. Whole protein was extracted from the recombinant cell lines in the presence and absence of the inductor doxycycline (tetracycline family). All induced cells displayed a positive signal as detected with an anti-GFP antibody. The GFP signal in the EGFP-Control cell line appeared larger in size, 30 kD instead of 27 kD. This difference in size is a result of the EGFP tag in the EGFP-pcDNA5/FRT/TO plasmid. The plasmid does not contain a stop codon as it was designed for the integration of cDNAs down-stream of the EGFP tag resulting in an extra 28 amino acids in the empty plasmid.

The non-induced cells showed no GFP signals on the western blot (Figure 4.8-B) Both results of the PCRs and western blots confirmed the successful integration of the three cDNAs and the empty control plasmid into the genome of the Flp-in TREx HEK293 cells.

Confocal microscopy analysis was the third method used for the confirmation of stable cell lines. The cells were induced overnight, followed by fixation with paraformaldehyde, and then stained with the anti-GFP antibody. The results were consistent with those obtained from the PCRs and western blots (Figure 4.9). Untransfected HEK293 cells were used as a negative control and no GFP signal was obtained. Interestingly all EGFP-Rad9 proteins localised predominantly to the cytoplasm in untreated but induced cells.

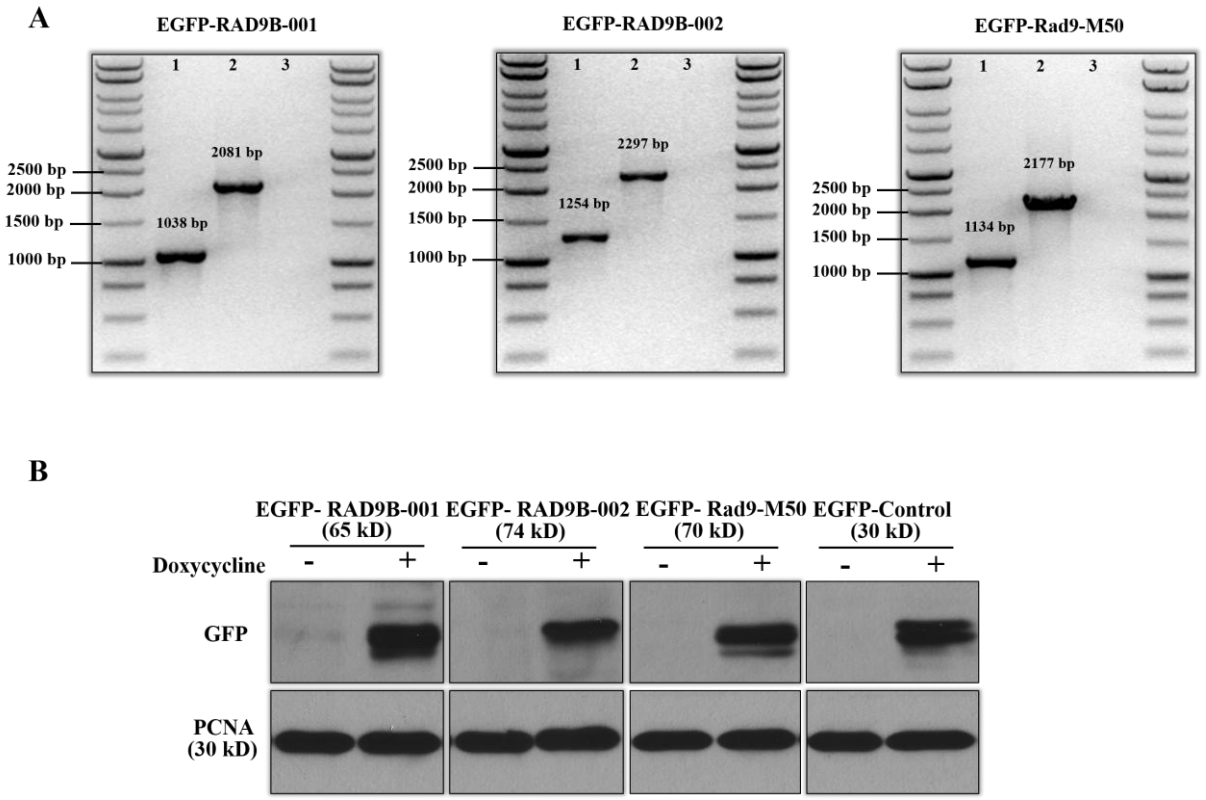

Figure 4.8 Confirmation of the integration of EGFP-RAD9B-001, EGFP-RAD9B-002, Rad9-M50 and EGFP-Control into the cell lines. (A) Genomic DNA was extracted from the integrated cell lines and successful integration was confirmed by PCR. Lane 1: Using the forward and reverse specific primers of the integrant. Lane 2: Using a forward primer that binds to the CMV promoter in combination with the reverse specific primer of the integrants. Lane 3: Using the forward and reverse specific primers for the integrant on genomic DNA extracted from the EGFP-Control cell line. Amplicon sizes (bp) are indicated on top of the bands. (B) Western blot analysis of the EGFP-recombinant proteins. Cell lines were either induced with doxycycline or left without induction as a negative control. PCNA protein was used as a positive control.

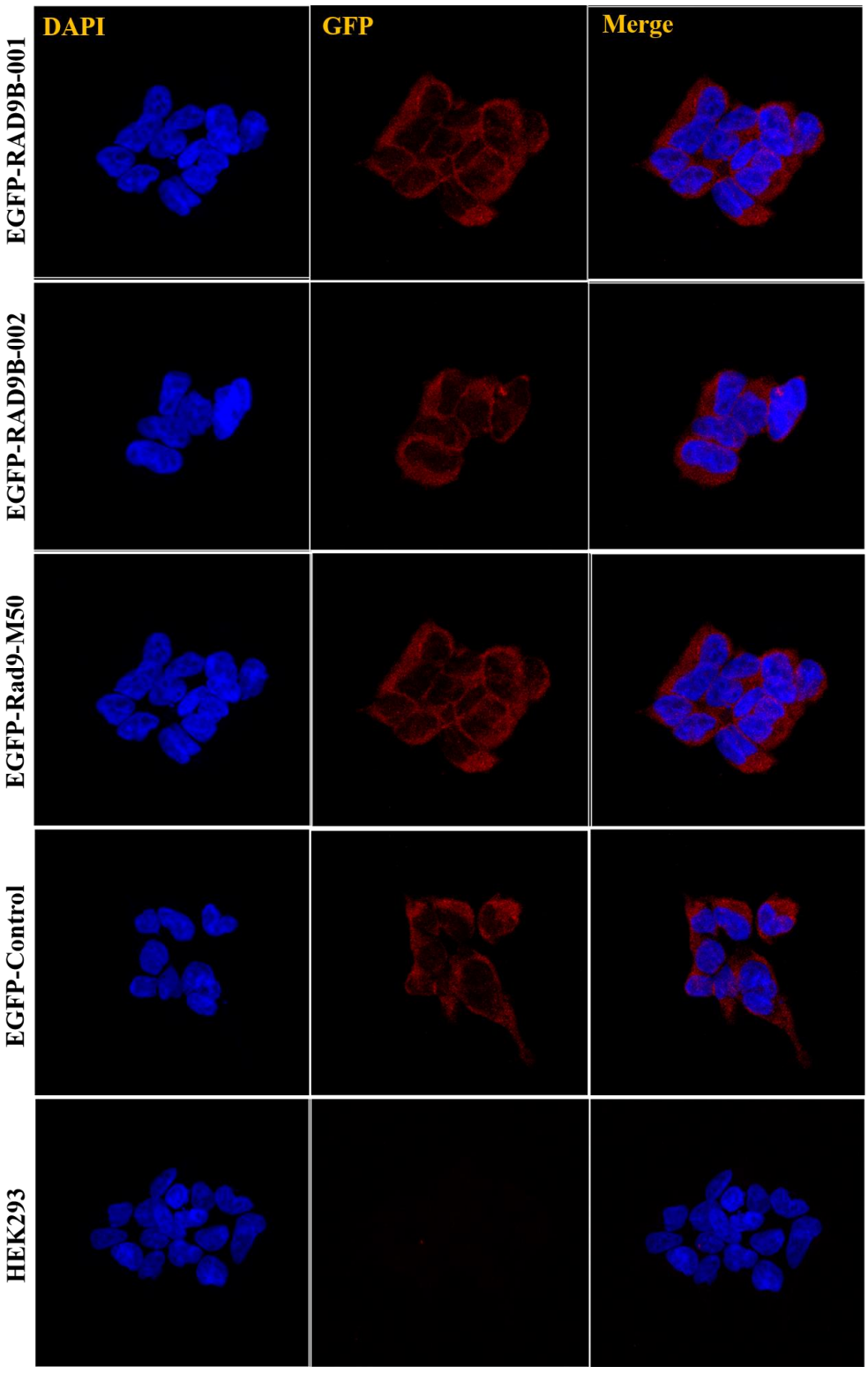

Figure 4.9 Immunostaining of the overexpressed EGFP tagged proteins. The cells were grown overnight on coverslips in medium containing doxycycline, followed by fixation with 4% paraformaldehyde. Then the cells were stained with GFP antibody in combination with the secondary Alexa Fluor 568 antibody (red). Images were taken using the LSM710 confocal microscope. Images were taken with the 40x objective and processed using the Zen lite software. The HEK293 cell line was used as a negative control.

4.2.5 Induction kinetics of the Flp-FRT system

As the integrated proteins were artificially expressed, it was important to test the induction conditions before starting the experiments. The time of induction after the addition of doxycycline was tested to obtain the optimal time with the highest levels of the expressed protein. The EGFP-RAD9B-001 cell line was induced with doxycycline and RNA as well as protein were extracted at different times after induction. As shown in Figure 4.10, expression of the *EGFP-RAD9B-001* mRNA was induced within 2 hr and expression was highest 12 hr post induction. The corresponding protein was weakly expressed at the 2 hr time point and continued to accumulate reaching its highest level 18 hr post-induction.

To investigate the stability of the integrated protein after the removal of doxycycline, all the cell lines were induced for 18 hr, followed by the removal of doxycycline. Proteins were extracted at different times up to 72 hr after the removal of the inducer. Surprisingly, the experiment revealed the presence of all recombinant proteins up to 72 hr in the absence of the inducer. This result indicates a high stability of the expressed proteins in untreated HEK293 cells (Figure 4.11).

Another feature of this system worth noting is that it has a low basal activity in the absence of doxycycline. As can be seen in Figure 4.11, Rad9-M50 was expressed in the absence of doxycycline (Non-induced cells) at a quite high level, while lower levels of EGFP-RAD9B-001 were detected. This background activity may arise from antibiotics in the fetal bovine serum. It is however interesting that the levels of the yeast Rad9 variant are so high compared to the other constructs.

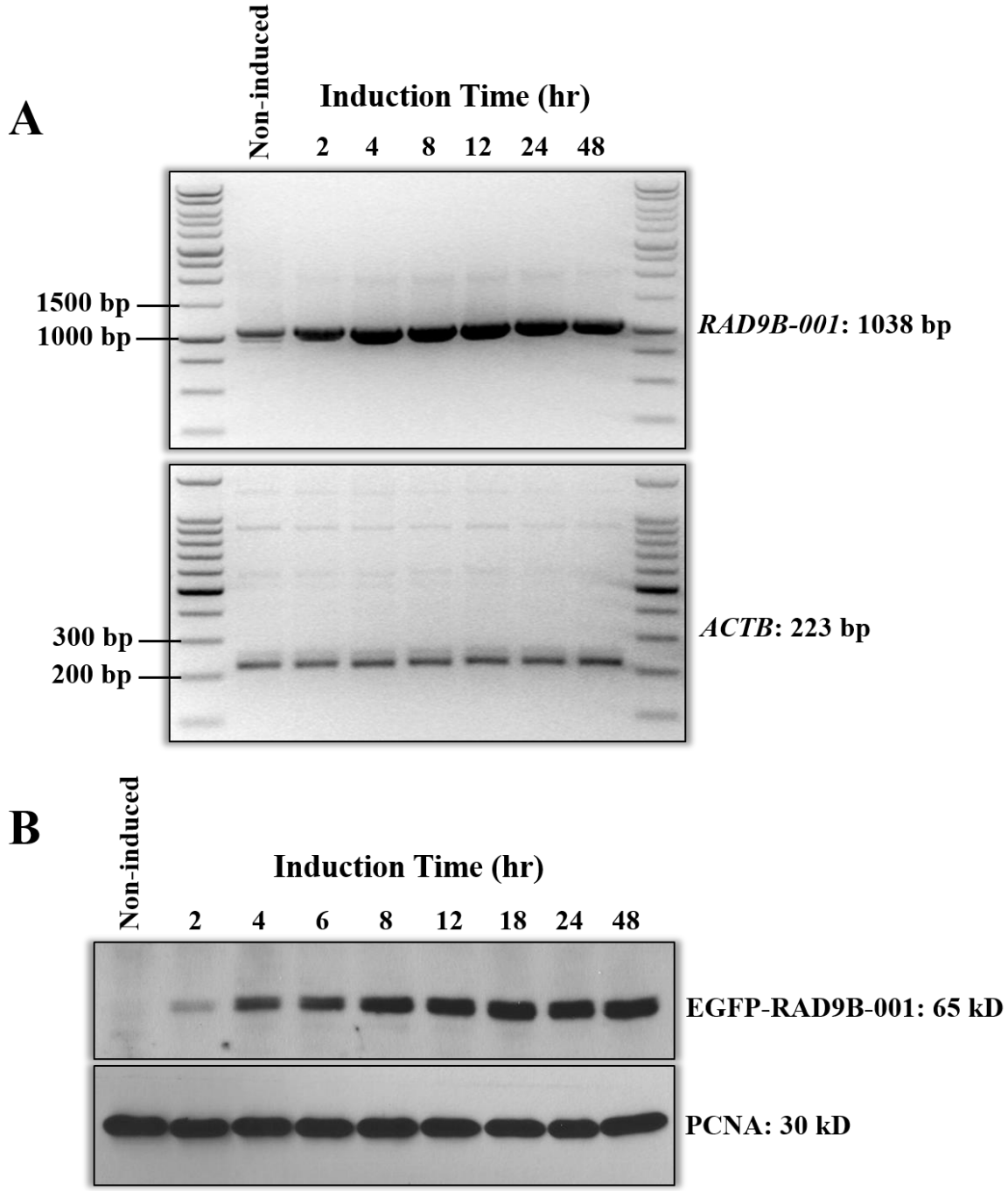

Figure 4.10 Time course induction of the Flp-FRT system. The EGFP-RAD9B-001 cells were either treated with doxycycline (1 μg/ml) or left without induction (control). (A) RT-PCR analysis of the control and induced *RAD9B-001*. Samples were extracted at different points post induction, as indicated at the top of the figure. *ACTB* was used as a positive control. Amplicon size is indicated on the right side. (B) SDS-PAGE of EGFP-RAD9B-001 in samples prepared from either non-induced cells or induced cells for different times post induction, as indicated in numbers at the top of the figure. PCNA protein was used as a positive control. Protein sizes are shown in kD to the right.

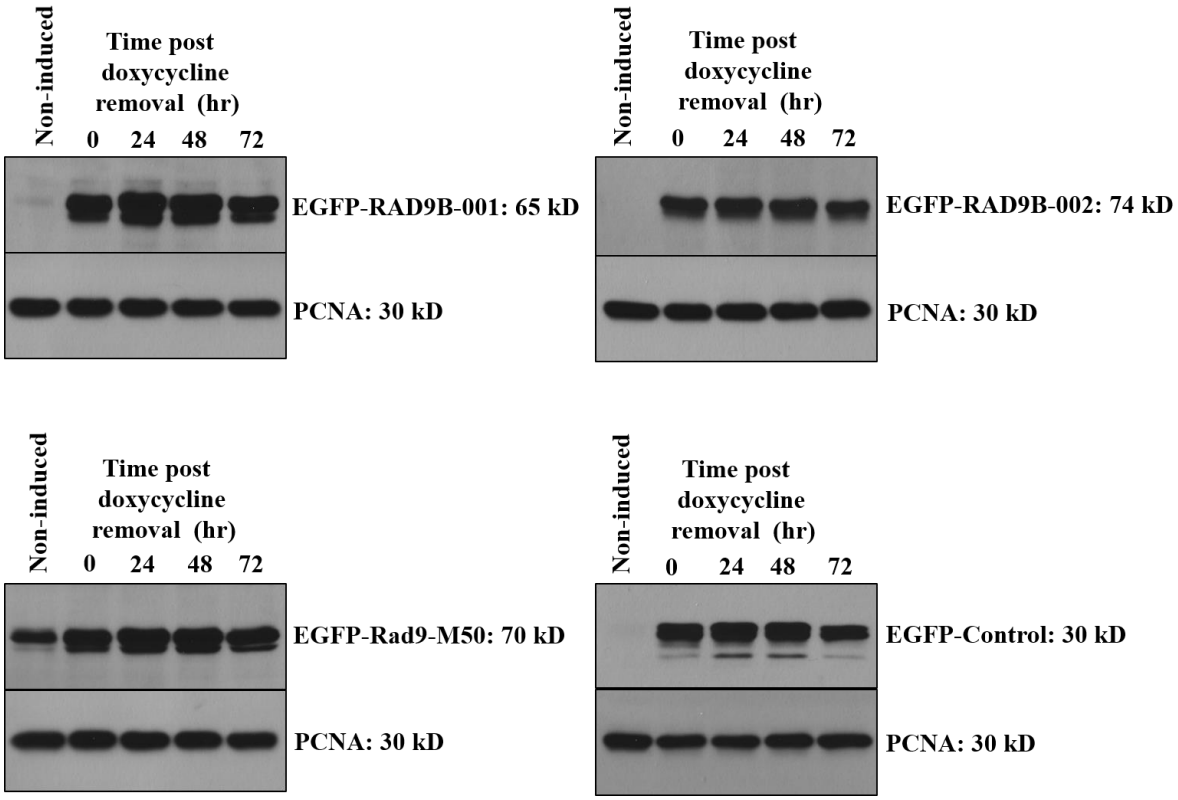

Figure 4.11 Induced protein stability following removal of doxycycline. The transfected cell lines were induced with doxycycline (1 μg/ml) for 18 hr, followed by the removal of the inducer. Protein was extracted from the four constructed cell lines (EGFP-RAD9B-001, EGFP-RAD9B-002, EGFP-Rad9-M50 and EGFP-Control) at the indicated times. Samples were analysed on SDS-PAGE and immunoblotted with the GFP antibody. Protein extracts were also probed with PCNA antibody used as appositive control.

4.2.6 A possible cleavage event affects the RAD9B-002 protein

While conducting the induction experiments, cleavage of the recombinant RAD9B-002 protein was detected. This cleavage was observed in all RAD9B-002 lysates. The cleavage event produced two small forms with molecular weights of 40 kD and 27 kD, suggesting a cleavage site with the N-terminal of RAD9B-002, as the EGFP tag which is used for the detection of RAD9B-002 on western blot is designed on the N-terminal of RAD9B-002 (Figure 4.12-A).

Interestingly, a second cleavage event was also detected which produced a fragment similar in size to EGFP-RAD9B-001. No cleavage was detected when RAD9B-001 or Rad9-M50 were over-expressed (Figure 4.12-A). The cleavage happened regardless of the cells' passage number, being detected in both low and high passage numbers. A possible explanation for this cleavage is that expression of the full-length EGFP-hRAD9B-002 protein has a negative impact on the host cell and that the cleavage reduces this. As mentioned in section 4.2.7, the over-expression of EGFP-RAD9B-002 leads to an accumulation in the sub G1 cell population, strongly indicating that this variant induces apoptosis that may force cells to cleave this variant to prevent cell death. It is also worth mentioning that a complete loss of the integrated EGFP-hRad9B-002 gene was observed, making it possible that the cells somehow removed this recombinant gene from their genome.

To investigate the induced *RAD9B-002* at the mRNA level, RNA was extracted from the induced and non-induced EGFP-RAD9B-002 and from the cleaved EGFP-Rad9B-002 cells. RT-PCR revealed the presence of *RAD9B-002* mRNA from the cleaved cell line but at a lower level than in the intact EGFP-RAD9B-002 cell line. Hence, affected cells may also reduce the transcription of the recombinant gene or cells which have lost the recombinant gene accumulate in the culture.

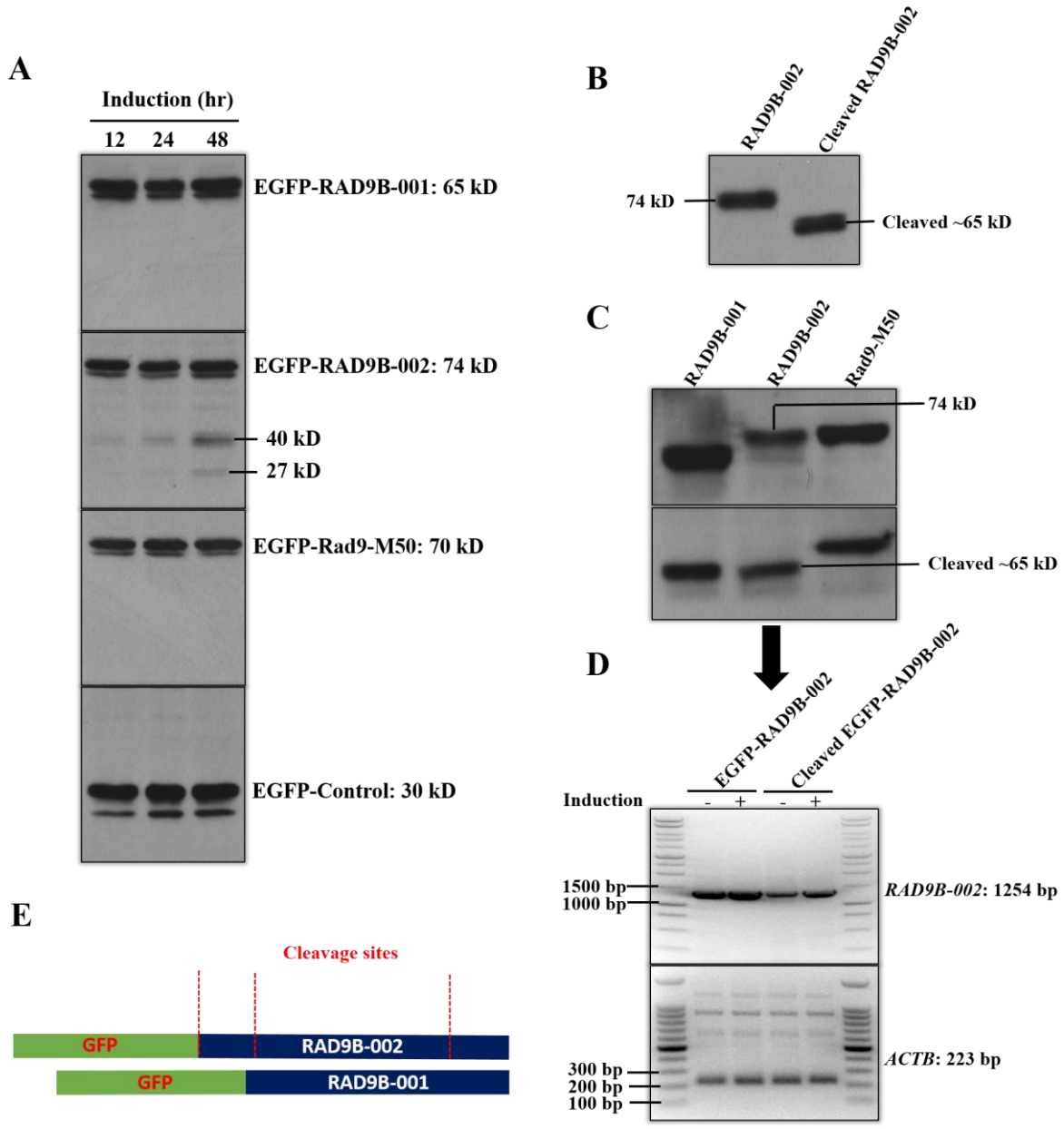

Figure 4.12 Cleavage of RAD9B-002 protein. (A) Western blot analysis of overexpressed EGFP-RAD9B-001, EGFP-RAD9B-002, EGFP-Rad9-M50 and EGFP-Control cell lines. The cell lines were induced with doxycycline (1 µg/ml) and the protein was extracted at the indicated times. In comparison to other cell lines, EGFP-RAD9B-002 revealed two cleaved bands on SDS-PAGE with size of 27 and 40 kD. (B) Cleavage of RAD9B-002 revealing a band of 65 kD compared to the full-length size of 74 kD. (C) The RAD9B-002 protein before and after cleavage in comparison to the size of RAD9B-001 and Rad9-M50. (D) Total RNA was extracted from non-induced and induced EGFP-RAD9B-002 cell lines (Normal and cleaved), followed by amplification of *RAD9B-002* with the One-step RT-PCR Kit in which *ACTB* was used as a positive PCR control. (E) Diagram showing the possible cleavage sites within the RAD9B-002 protein.

4.2.7 Analysis of the cell cycle progression in over-expressing cell lines

The over-expression of RAD9B forces the cells to accumulate in the G1 phase (Perez-Castro & Freire, 2012). It should be pointed out here that it is unclear which full-length RAD9B variant was used in this experiment. It was therefore investigated whether RAD9B-001 or RAD9B-002 proteins have a similar impact on the cell cycle. Both cell lines were induced with doxycycline and the cell cycle was analysed by flow cytometry. The cell cycle progression was analysed at different times after induction. As shown in Figure 4.13, the over-expression of RAD9B-001 increased slightly the amount of G1 cells 24 hr post-induction from 55% to 62%. However, this transient arrest only lasted for a short period of time as the percentage of G1 cells returned to normal after 36 hr. These results suggest that RAD9B-001 might be the splice variant used in the Perez-Castro & Freire's (2012) study.

The FACS analysis for RAD9B-002 expressing cells was very different. Its up-regulation resulted in the accumulation of a sub-G1 population, which was also observed at a lower level in non-induced cells as a result of the low background expression of RAD9B-002. Nearly 12% of the cell population were in the sub-G1 phase 24 hr after induction and this number increased a further to 23% after 48hr. The sub-G1 peak suggests that over-expression of RAD9B-002 may drive cells into apoptosis. However, this apoptotic induction was specific to this splice variant and was not observed for RAD9B-001. The over-expression of these two RAD9B splice variants have therefore different outcomes on the cell cycle, suggesting different roles for the two variants.

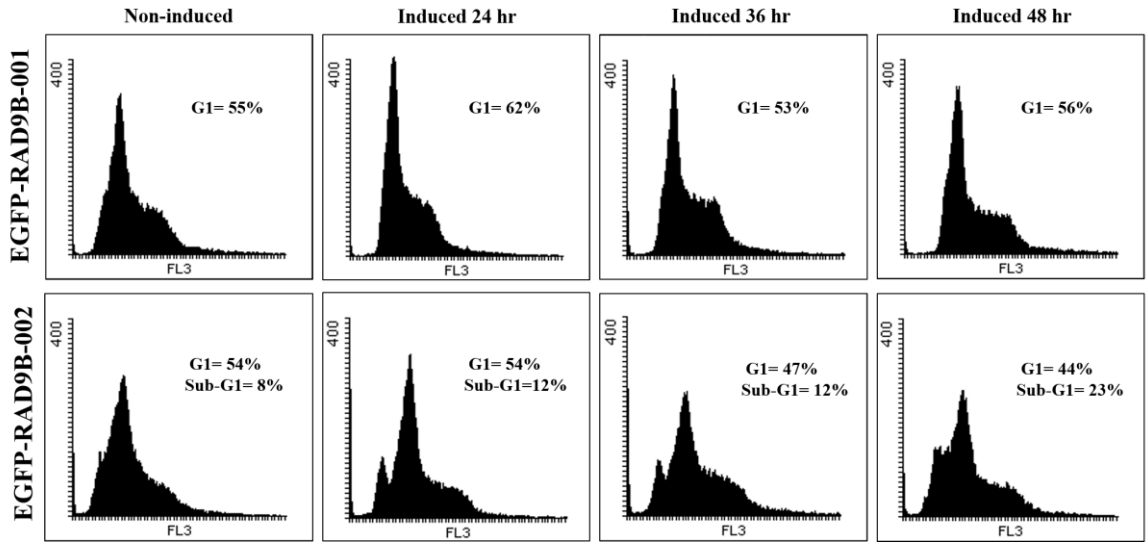

Figure 4.13 Different patterns of cell cycle progression caused by the overexpression of the two RAD9B splice variants HEK293 cells. Histograms of flow cytometry showing DNA content in overexpressed EGFP-RAD9B-001 and EGFP-RAD9B-002 cell lines. The two cell lines were induced with 1 µg/ml doxycycline, and cells were fixed with ice-cold 100% methanol after different induction points. The histogram of the cell cycle phases was obtained after gating on propidium iodide-stained cells using the Flowing software 2.5.1.

4.2.8 Overexpression of RAD9B-001 and RAD9B-002 has a negative impact on cell proliferation

The flow cytometry indicated that cells over-expressing RAD9B-001 or RAD9B-002 arrest in G1 and sub G1, respectively. Therefore, the effect of their expression on cell proliferation was analysed by measuring the cell count of induced and non-induced cells at different times after seeding.

The results were consistent with the flow cytometry findings. Both the EGFP-RAD9B-001 and EGFP-RAD9B-002 cell lines showed significant inhibition of cell proliferation compared to the EGFP-Control cell line. (Figure 4.14). The EGFP-Rad9-M50 and the EGFP-Control cell lines showed a similar growth rate in the presence and absence of doxycycline. However, over-expression of EGFP-RAD9B-002 had a very strong negative impact on cell growth consistent with the accumulation of sub-G1 cells. The cell proliferation experiment results were also consistent with the transient G1 arrest of EGFP-RAD9B-001 expressing cells from the flow cytometry analysis, as growth of the induced cell population was retarded although not to the same extend at in the case of EGFP-RAD9B-002. Both cell lines grew also more slowly in the absence of doxycycline which is due to the low basal expression level of the variants.

Expression of the yeast protein had no impact on cell growth. This answered the question regarding the possible impact of adding the doxycycline on cell growth, as it seems that it had no influence on cell proliferation for at least the 4 days of incubation.

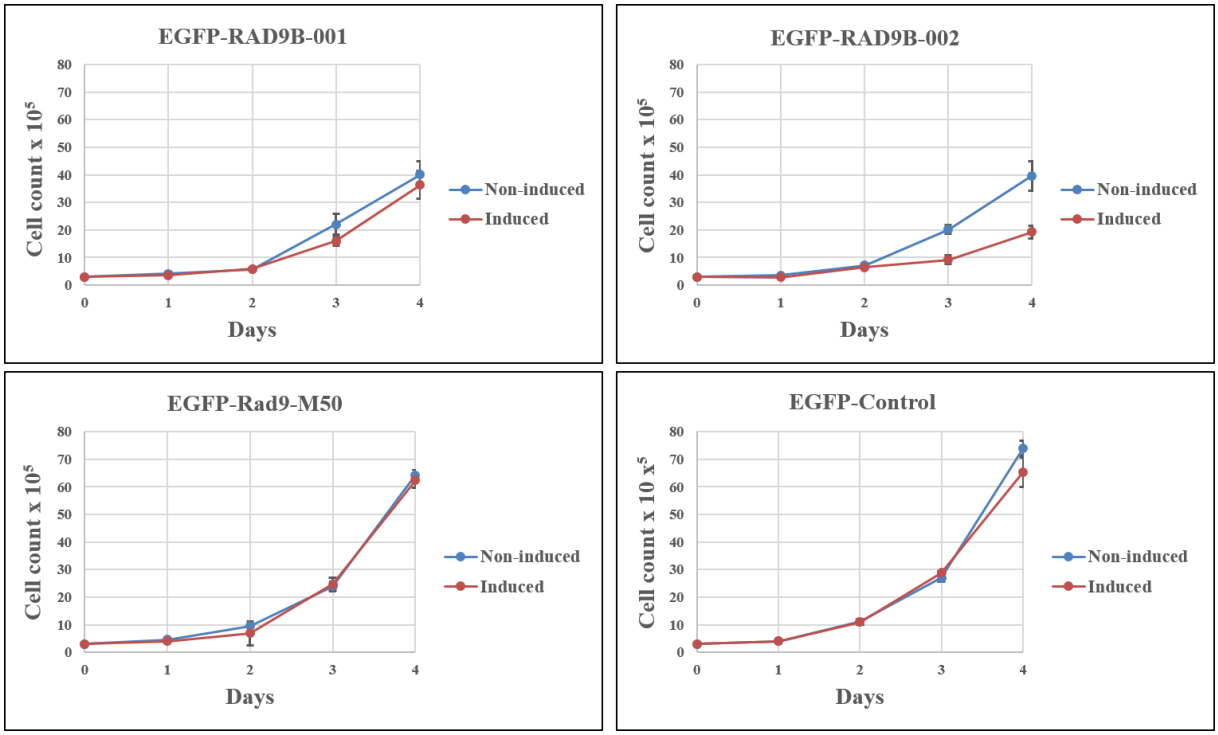

Figure 4.14 Cell growth graph showing the impact of RAD9B-001 and RAD9B-002 overexpression on cellular proliferation. Proliferation of either induced or non-induced RAD9B-001, RAD9B-002, Rad9-M50 and control cell lines. Cells were plated at 3 x 10^5 density in medium with and without doxycycline, and they were collected and counted every 24 hr for 4 days using the Bio-Rad TC20 Automated Cell Counter. Graphs were created using Excel 2013 software. The (I) symbol on the growth curve indicates the standard deviation of three repeats.

4.2.9 Analysis of apoptosis-related protein markers in the overexpressing EGFP-RAD9B-002 cell line

To further investigate the possible role of RAD9B-002 in inducing apoptosis, proteins involved in the activation of the apoptotic pathway were analysed in the over-expressing EGFP-RAD9B-002 cell line. The apoptotic proteins analysed in this experiment are known apoptotic markers, showing in the case of apoptosis a decrease in the expression of BCL-2, an increase in the expression of BAK and p53, and a cleavage of the PARP by caspase 3 (Wu et al., 2015; Wang et al., 2013).

The EGFP-RAD9B-002 cell line was induced for 8, 12, 24 and 48 hr and whole protein was extracted at these times. All extracts were subjected to western blot and immunoblotted for the apoptotic marker proteins. As mentioned in Section 4.2.6, RAD9B-002 is cleaved resulting in two forms (27 kD and 40 kD). This cleavage happened in an induction time-dependent matter. The amount of the cleaved forms were barely detectable after 8 hr of induction but cleavage increased significantly 24 and 48 hr post-induction (Figure 4.15).

Interestingly, as a result of RAD9B-002 over-expression, the cleaved PARP product increased slightly compared to the non-induced control cells. This cleavage reached its highest peak at 24 hr of RAD9B-002 induction. To test whether RAD9B-002 is a cleavage target for caspase 3 like the PARP protein, the protease sites within RAD9B-002 were analysed using the Peptide Cutter-ExPASy tool. RAD9B-002 contained multiple possible target sites for many proteases; however, it did not have any target sites for Caspase 3 or any of the other caspases involved in the apoptotic pathway, suggesting a different cleavage role than that of the apoptotic PARP protein. No expression alterations were observed amongst the other apoptotic markers, indicating that over-expression of RAD9B-002 induces apoptosis in a p53-independent manner.

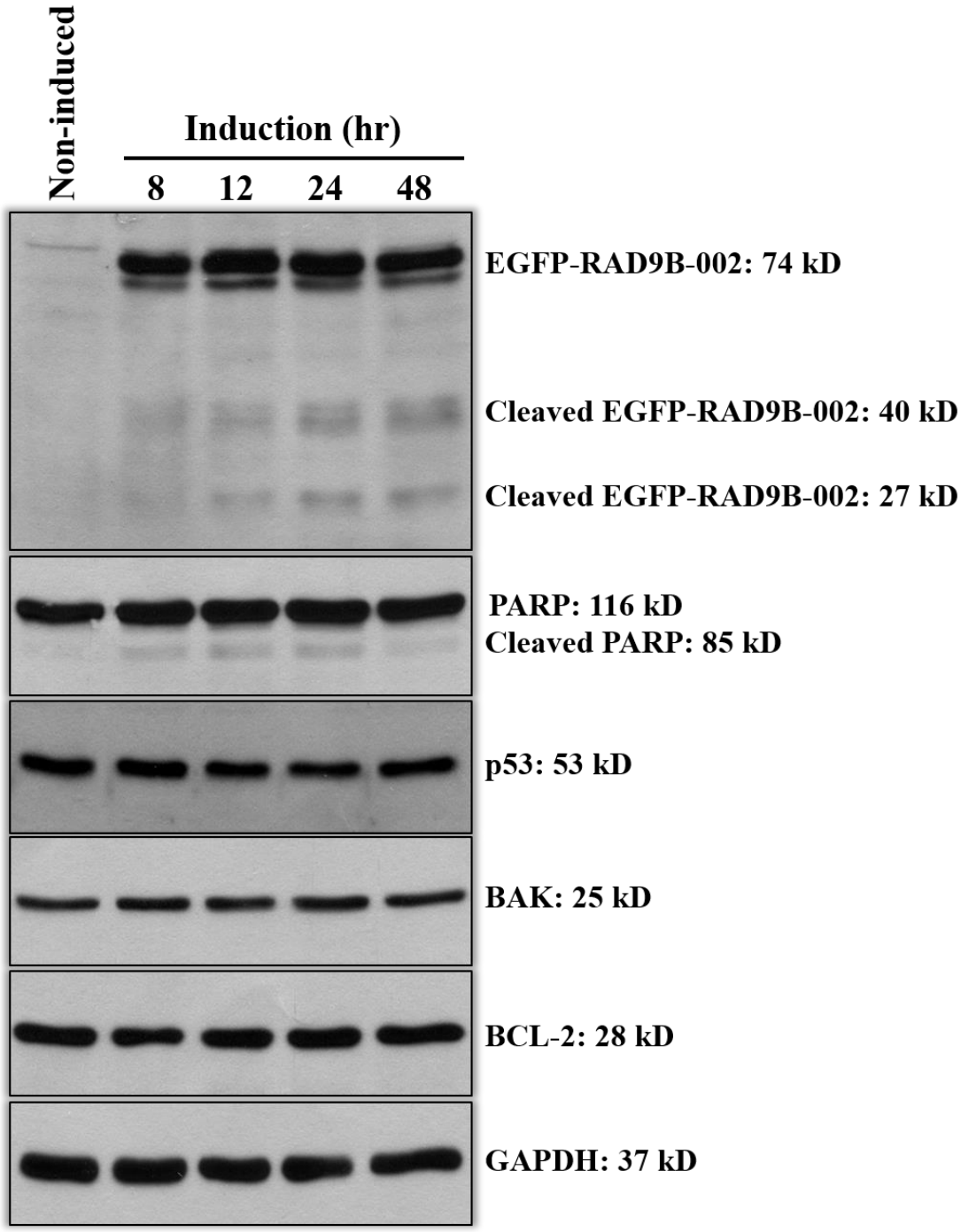

Figure 4.15 Overexpression of RAD9B-002 does not show a major influence on the apoptosis pathway. The human RAD9B-002 variant was overexpressed in the HEK293 cell line for different lengths of time (hr), as indicated at the top of the figure. Whole protein was extracted at the indicated time points, subjected to SDS-PAGE and immunoblotted with GFP antibody for the detection of EGFP-RAD9B-002, in addition to different antibodies against apoptotic proteins (PARP, p53, BAK and BCL-2). The GAPDH was used as a loading control.

4.2.10 Investigating the post-translational modification of human RAD9B and yeast Rad9-M50

RAD9B-001, RAD9B-002 and Rad9-M50 have multiple phosphorylation sites in their protein sequences. Here, the post-translational modification of the recombinant proteins was analysed using two methods. Isoelectric focusing (2D electrophoresis) and phos-tag SDS page (Caspari & Hilditch, 2015). To test whether any post-translational modifications would affect the EGFP domain of the fusion proteins, EGFP expression was induced in the control cell line. Although isoelectric focusing indicated the presence of between 3 and 4 forms of the Rad9 fusion proteins in undamaged cells, the EGFP-Control cell line revealed a similar pattern of three isoforms of the EGFP protein alone (Figure 4.16). This shows that the post-translational modifications are not specific to the Rad9 moiety of the fusion proteins but to the EGFP domain. It is therefore very likely that EGFP, either alone or fused to Rad9 becomes modified in HEK293 cells.

When the same cell lines were analysed by phos-tag electrophoresis to determine their phosphorylation status; phosphorylated proteins migrate more slowly in this assay, only EGFP-RAD9B-002 and the yeast EGFP-Rad9-M50 protein displayed slower migrating bands indicative of phosphorylation (Figure 4.16-C). Interestingly, EGFP-Control did not display any additional bands which indicates that the modifications detected by isoelectric focusing, which detects any modification that changes the overall charge of the protein, are not phosphorylation events. Taken together this implies that EGFP-RAD9B-002 and the yeast Rad9-M50 protein are phosphorylated in undamaged HEK293 cells.

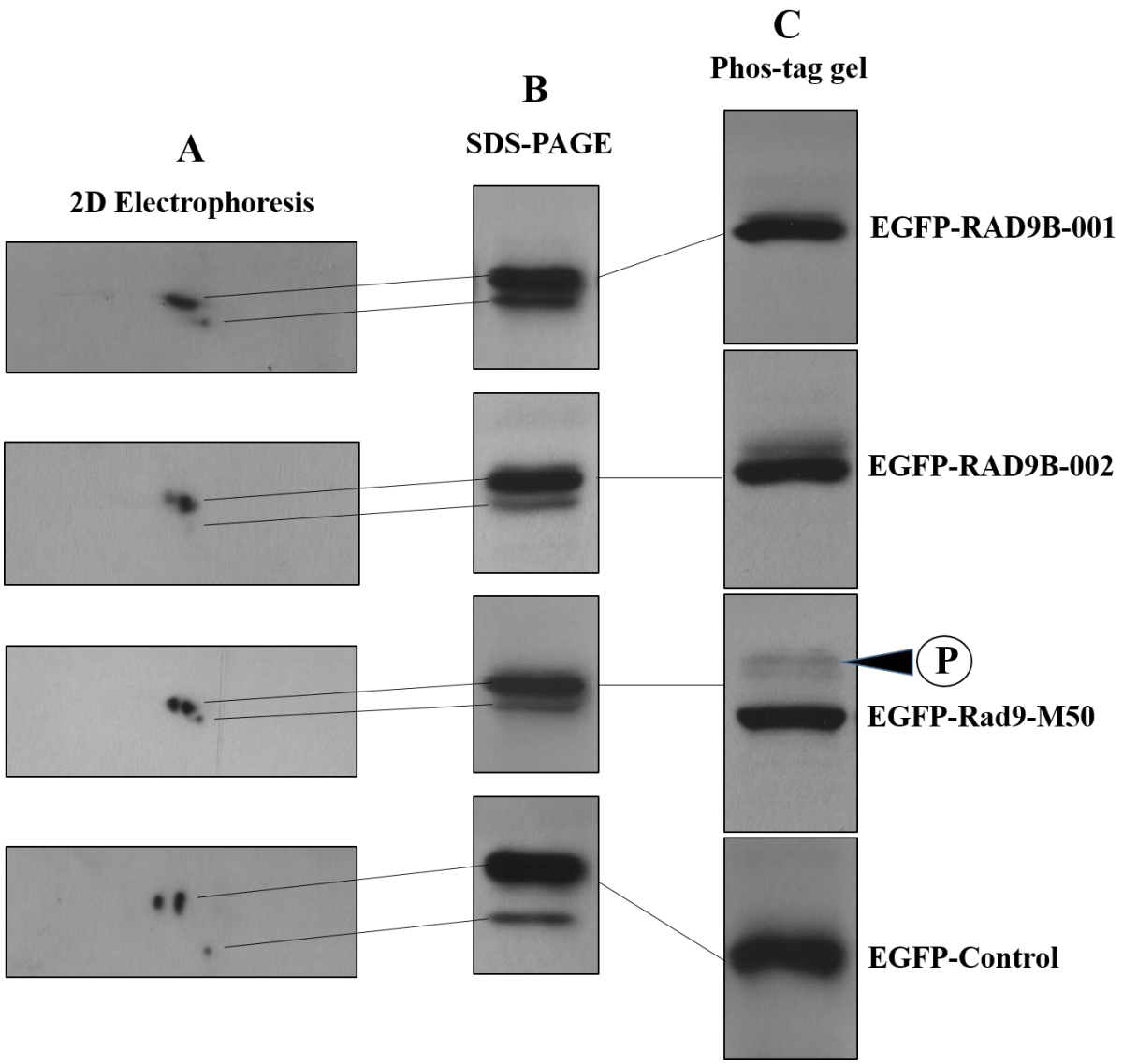

Figure 4.16 Analysis of post-translational modification of recombinant proteins. (A) 2D isoelectric focusing of the EGFP-RAD9B-001, EGFP-RAD9B-002, EGFP-Rad9-M50 and EGFP-Control induced proteins. Approximately 20 μg of protein was loaded on a nonlinear 7-cm strip (pH 3–10) and focused using the 2D isoelectric focusing machine followed by SDS-PAGE analysis. All membranes were immunoblotted with GFP antibody. (B) Whole protein extracted from the induced constructed cell lines were run on normal SDS-PAGE and immunoblotted with GFP antibody. (C) Whole protein extracted from the induced constructed cell lines were run on phos-tag gels and immunoblotted with GFP antibody.

4.2.11 Heat stress does not regulate the expression of *RAD9B*

According to the Human Protein Atlas database (http://www.proteinatlas.org. Accessed 15 June 2016) RAD9B was only expressed at the protein level in two tissues: skeletal muscle and testis. Therefore, a number of commercial RAD9B antibodies were not efficient in detecting RAD9B splice variants in cell lines, such as HEK293, HeLa, MCF7 (breast cancer) and Kelly as no expression was detected on western blot even with as high as 50 µg of whole protein. This might be due to low protein expression, as was shown with the splice variants mRNA expression (Chapter 3). However, at late stages of this project, we kindly received a RAD9B antibody created in Perez-Castro & Freire's (2012) study. This antibody was validated by the detection of the over-expressed recombinant EGFP-RAD9B-002 protein (Figure 4.17).

The Perez-Castro & Freire's RAD9B antibody was used to test whether the expression of RAD9B is elevated similarly to Rad-M50 in response to heat stress. HEK293 cells were heat treated for 1 hr and the cells were allowed to recover up to 2 hr after treatment, the time in which checkpoint pathways are activated.

The immunoblot results showed elevated phosphorylation of the CHK1 protein, reflecting the activation of the ATR-CHK1 checkpoint as a result of the heat-stress treatment. The expression of RAD9B was not detected with the commercial antibody in normal cells or heat-stressed cells. In addition, the RAD9B antibody from Perez-Castro & Freire's group appeared to detect a protein with a ~ 46 kD molecular weight corresponding to the size of RAD9B-002 and RAD9B-003 with no expression changes to RAD9B under heat stress. However, other smaller bands (22 kD, 26 kD and 32 kD) were also detected in both normal and treated samples (Figure 4.17). The smallest band could reflect *RAD9B-S003* described in Section 3.5.2 as the size of the PCR fragment corresponds to the size of the band on the SDS-PAGE gel. However, this small band did not show any changes in response to heat stress. Taking these results together, *RAD9B* is not heat inducible as in the case of the yeast *Rad9M-50*.

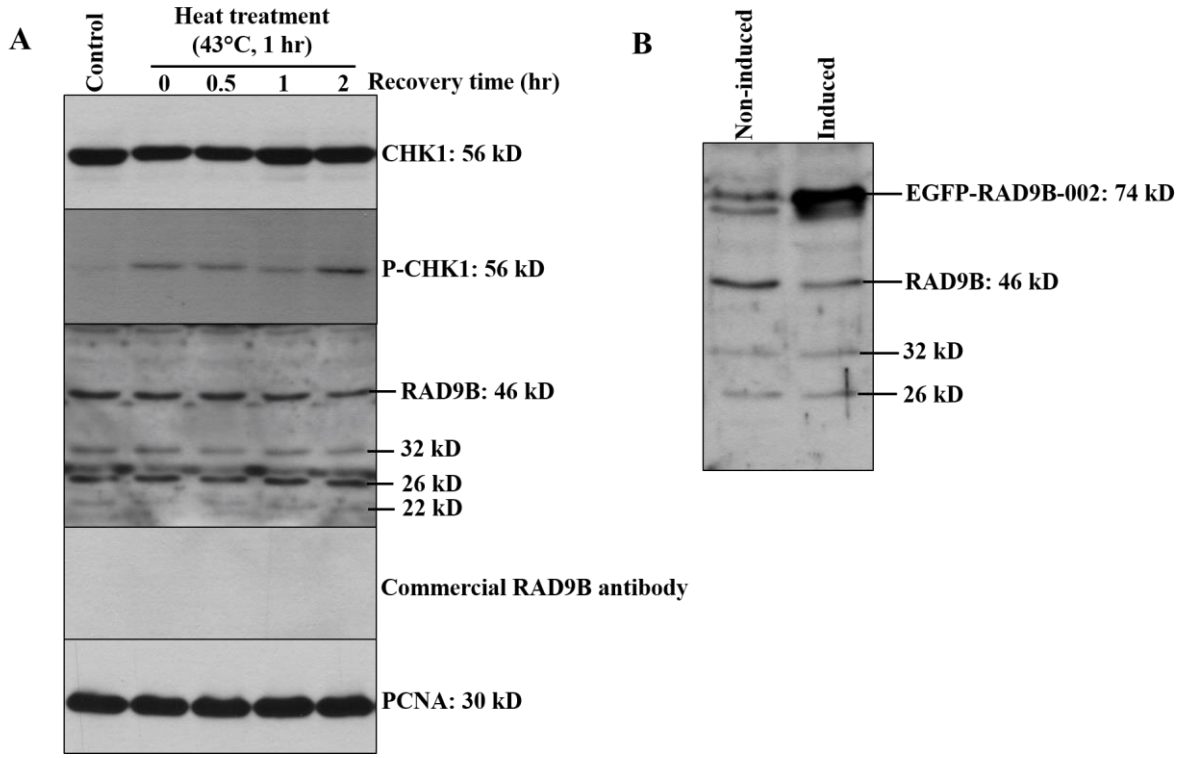

Figure 4.17 Analysis of RAD9B response to heat stress. (A) HEK293 cells were heat treated at 43°C for 1 hr and then the cells were allowed to recover for up to 2 hr after treatment. Whole protein was extracted from normal and heat-treated cells at the indicated times. Protein samples were analysed by western blotting with two different antibodies against RAD9B. Only one antibody revealed the expression of RAD9B at 46 kD and three smaller bands at 32 kD, 26 kD and 22 kD. The CHK1 phosphorylation confirmed the success of the heat treatment. RAD9B expression was normalised to the expression of the control PCNA protein . (B) Validation of RAD9B antibody from Perez-Castro & Freire's study. Whole protein was extracted from a constructed cell line expressing the RAD9B-002 tagged with GFP (27 kD) before and after induction. The engineered RAD9B-002 was displayed with a size of 74 kD indicating the validation of the RAD9B antibody.

4.2.12 RAD9B-001, RAD9B-002 and Rad9M-50 do not influence the phosphorylation of CHK1 in HEK293 cells under heat stress

The 2012 study by Janes et al. showed that the yeast Rad9 variant Rad9M-50 can reprogram the DNA damage response in *S. pombe* cells at elevated temperatures. The study also showed that Chk1 becomes dephosphorylated at Ser-345 when *S. pombe* cells are shifted to 40°C, which correlates with the induction of the variant (Janes et al., 2012). In human cells, CHK1 is rapidly phosphorylated at Ser-345 by ATR kinase at elevated temperatures (Turner & Caspari, 2014). Moreover, recent work by our group (unpublished data) showed that while the induction of Rad9M-50 and the dephosphorylation of Chk1 are two correlative events they are not causatively linked.

To test whether the presence of RAD9B splice variants or the yeast Rad9-M50 variant has any effect on the human cell response under heat stress conditions, the EGFP-RAD9B-001, EGFP-RAD9B-002 and EGFP-Rad9-M50 cell lines were shifted to the elevated temperature of 43°C for 1 hour and the cells were allowed to recover at 37°C for various durations, followed by protein extraction. First, the phosphorylation status of CHK1 was investigated by normal SDS-PAGE using a phospho-specific antibody against the CHK1 Ser-345 site. Consistent with published work (Tuul et al., 2013), CHK1 was highly phosphorylated at Ser-435 in response to heat stress. This phosphorylation was detected immediately after the heat shock treatment and increased rapidly for up to 4 hours in recovery at 37°C. As seen in Figure 4.18, over-expression of RAD9B splice variants or of the yeast Rad9 does not correlate with a decrease in CHK1 phosphorylation at S345, as was found in *S. pombe*, indicating a different mechanism for human cells in response to heat stress.

Other proteins that are activated by heat stress, such as ATM, ATR and CHK2, were also analysed in constructed cell lines under heat stress. No changes in the protein expression levels or in their phosphorylation statuses were observed as a consequence of the over-expression of either RAD9B or yeast Rad9-M50 (Figure 4.19).

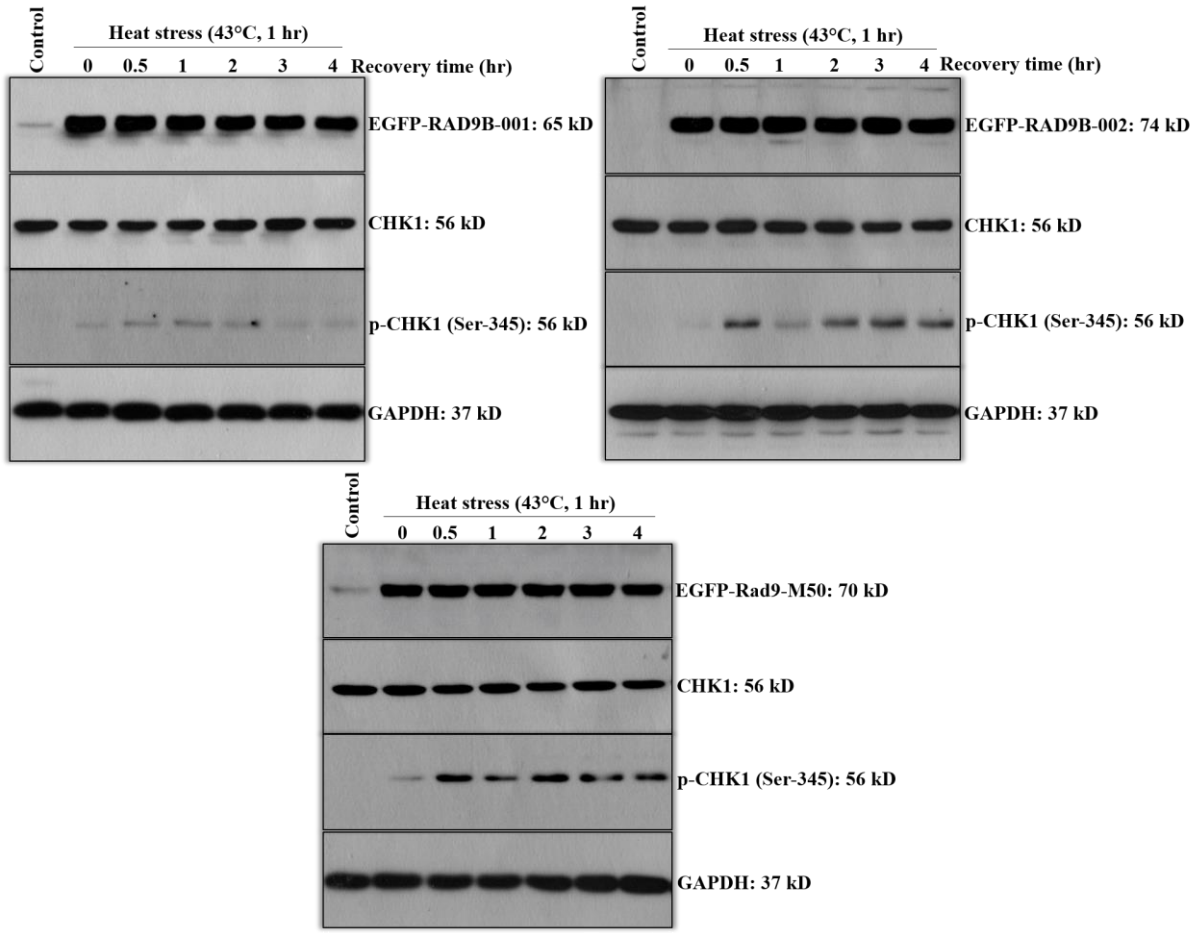

Figure 4.18 Analysis of CHK1 phosphorylation under heat stress in the constructed cell lines. RAD9B-001, RAD9B-002 and Rad9M-50 cell lines were heat shocked at 43°C for 1 hr. The cells were allowed to recover and then whole protein was extracted from the recovered cells at the indicated times. The extracts were subjected to SDS-PAGE and immunoblotted with CHK1, p-CHK1 (Ser-345), GFP and GAPDH antibodies.

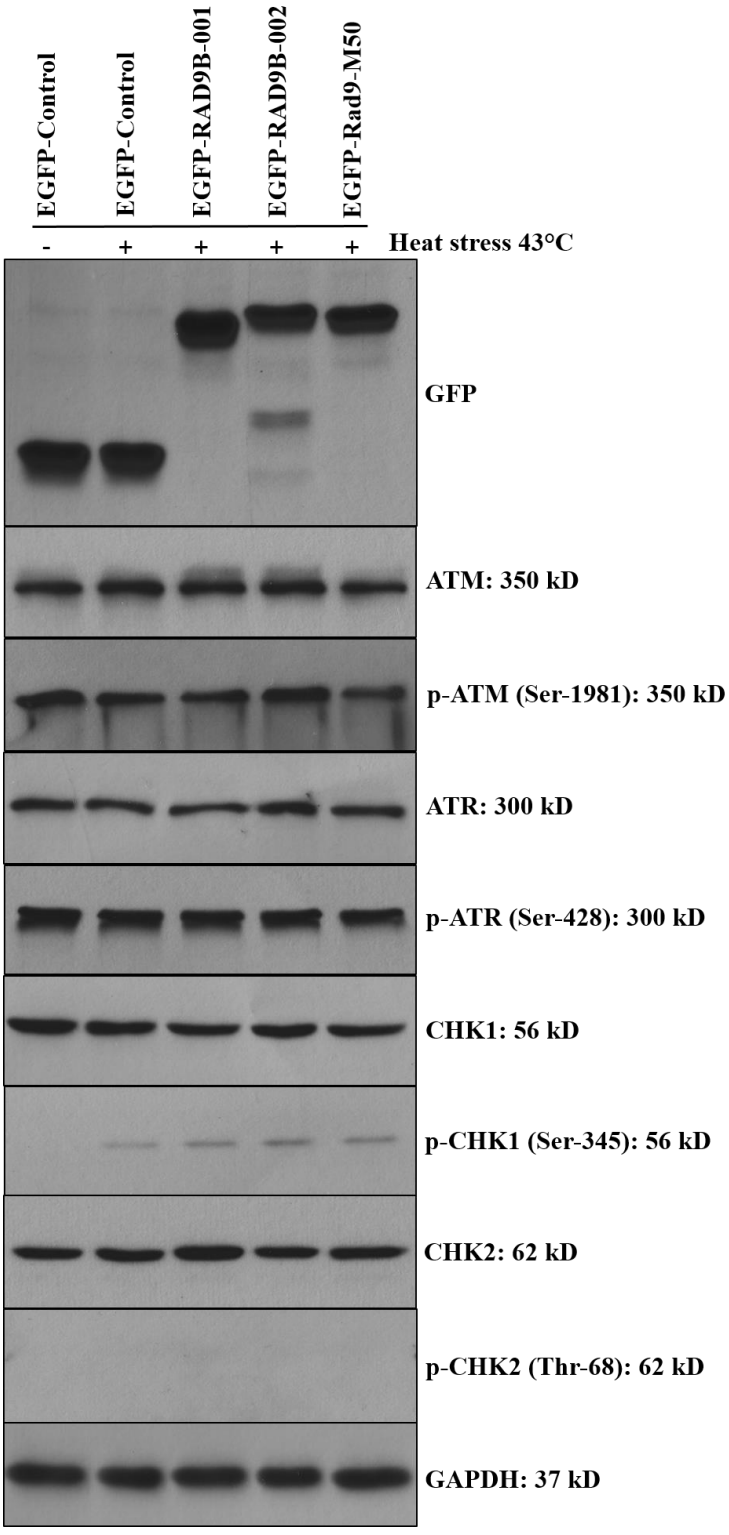

Figure 4.19 Analysis of major checkpoint proteins under heat stress in the constructed cell lines. The constructed cell lines were heat shocked at 43°C for 1 hr. The cells were allowed to recover and then whole protein was extracted from normal and treated cells 1 hr post treatment. The extracts were subjected to SDS-PAGE and immunoblotted with the indicated antibodies. The expression of the analysed proteins was normalised to the expression of GAPDH.

4.2.13 Effects of RAD9B-001 and RAD9B-002 over-expression on the cell cycle regulator p21$^{Cip1/WAF1}$

The CDK regulator and DNA repair factor p21$^{Cip1/WAF1}$ (p21) interacts with a large number of kinases including the cyclin-dependent kinases and CHK1 as well as with DNA repair proteins like PARP. The protein contains multiple phosphorylation sites and over-expression studies suggest the possibility that p21 interacts with RAD9B (Perez-Castro & Freire, 2012; Child & Mann, 2006). To determine the relation between these two proteins and whether the over-expression of RAD9B has an impact on p21, the protein levels of p21 were analysed in cells with elevated levels of RAD9B. A time course of RAD9B-001 and RAD9B-002 induction revealed no impact on the expression of p21, as its levels remained stable up to 24 hr post induction. However, when extracts from the same time points were run on phos-tag SDS page, p21 became highly phosphorylated in both cell lines resulting in an additional p21 band at approximately 30 kD. This phosphorylation was induced from 2 hr onwards after the induction of RAD9B and lasted for at least 24 hr (Figure 4.20). However, RAD9B-001 seemed to have a slightly higher impact on p21 phosphorylation than RAD9B-002. Although PCNA is a target of p21, PCNA expression remained stable through the time course of both RAD9B splice variants.

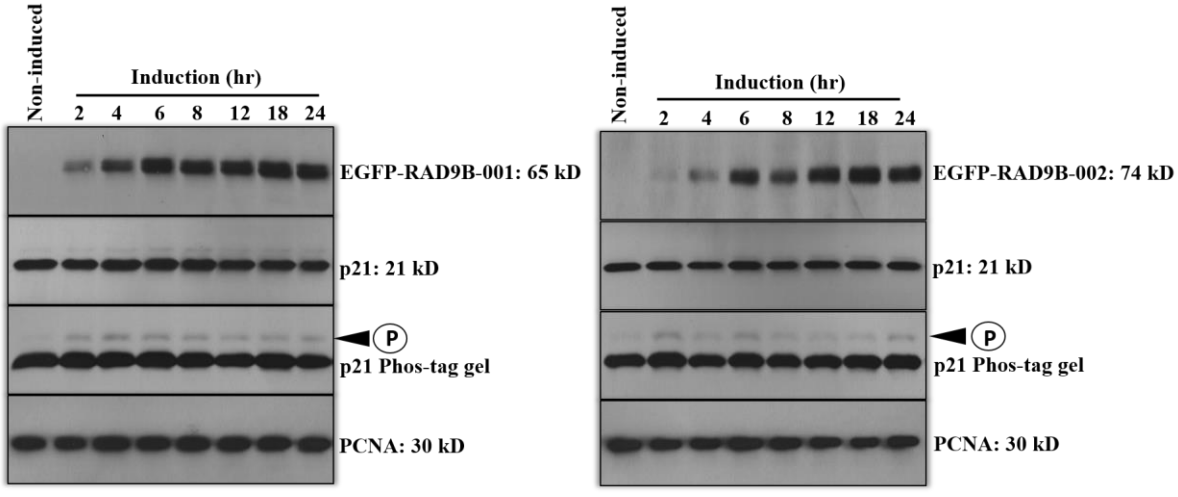

Figure 4.20 Increased p21 phosphorylation upon overexpression of either RAD9B-001 or RAD9B-002. Whole protein was extracted from induced EGFP-RAD9B-001 and EGFP-RAD9B-002 at different times (hr) post induction as indicated. The protein lysate was analysed on SDS-PAGE and immunoblotted with GFP antibody to detect tagged RAD9B-001 and RAD9B-002. Protein from non-induced cell lines was used as a control. The same protein extractions were subjected to either normal SDS-PAGE gels or on phospho-tag electrophoretic separation gels and immunoblotted for p21 protein. The integrated hRad9B and p21 expressions were normalised to the PCNA control.

4.2.14 Over-expression of RAD9B-001 and RAD9B-002 have no influence on the expression of the 9-1-1 complex proteins

The 9-1-1 complex proteins (RAD9, RAD1 and HUS1) are known to activate the checkpoint signalling pathway after being loaded onto damaged DNA (Ohashi et al., 2014; Wu, Shell & Zou, 2005). RAD9B was also found to interact directly with the RAD9A-interacting proteins HUS1 and RAD1 to form a complex similar to the 9-1-1 ring (Perez-Castro & Freire, 2012). However, the functional relationships between RAD9B and the other two 9-1-1 complex subunits is poorly understood. RAD9B over-expression has not yet been reported to influence the expression of any of the other ring proteins. To understand the link between RAD9B and these proteins better, the expression levels of these proteins were analysed in the presence of elevated levels of RAD9B-001 or RAD9B-002 under normal and genotoxic stress conditions. In addition, the localisation of the 9-1-1 complex proteins were also tested in these over-expressed cell lines.

If RAD9B interacts with HUS1 and RAD1 to form a 9-1-1-like complex, this should reduce the expression levels of Rad9A and possibly increase the expression levels of HUS1 and RAD1 upon the over-expression of either RAD9B-001 or RAD9B-002. To utilize this, RAD9, HUS1 and RAD1 expression levels were checked in the induced cell lines under normal and genotoxic conditions. Both the mRNA and protein levels were analysed.

The protein expression of RAD9A, RAD1 and HUS1 were stable and did not change in the over-expression cell lines neither under normal conditions nor when cells were heat treated or exposed to UV light. However, when p21 was used as a control for the UV treatment, it revealed an interesting result as its degradation was reduced in the EGFP-RAD9B-001 and EGFP-Rad9-M50 cell lines, but not in the EGFP-RAD9B-002 cell line. This indicates that RAD9B-001 and Rad9M-50 protect p21 from degradation in the response to UV light. In addition, heat stress resulted in a slight up-regulation of p21 in EGFP-Control and EGFP-Read9-M50 cell lines but not in the RAD9B-001 and RAD9B-002 cell lines (Figure 4.21 & Figure 4.22-A).

After DNA damage, components of the 9-1-1 complex are located in the nucleus where the complex is being loaded onto DNA damaged sites. Here, the localisation of the complex proteins was analysed in over-expressing EGFP-RAD9B-001, EGFP-RAD9B-002, EGFP-

Rad9-M50 and the EGFP-Control cell lines under genotoxic stress. Surprisingly, all three proteins localised to the cytoplasm in normal and genotoxic stress conditions (Figure 4.22-B). Only a faint presence was detected in the nuclear fraction when the western blot films were exposed for a long time. This indicates that only small amounts of these proteins actually form the complex and locate to the nucleus after DNA damage or that the complex is released from chromatin during the extraction. In conclusion, no alteration in the localisation of the 9-1-1 proteins were observed when RAD9B-001, RAD9B-002 or Rad9-M50 was over-expressed.

To check whether the two RAD9B splice variants have an impact at the mRNA levels of the 9-1-1 complex components, q-RT PCR analysis was performed. The results showed that all three components of the 9-1-1 complex had stable expression when RAD9B-001 and RAD9B-002 levels were elevated. The expression of all the targets in the two induced cell lines compared to the expression in the non-induced cells (Control) were almost the same with difference of no more than 0.55 expression fold change, indicating no significant expression changes within the 9-1-1 complex components. The mRNA levels of *p21* were also analysed revealing stable expression in the presence of *RAD9B-001* and *RAD9B-002* elevated mRNA levels (Figure 4.23 & Figure 4.24).

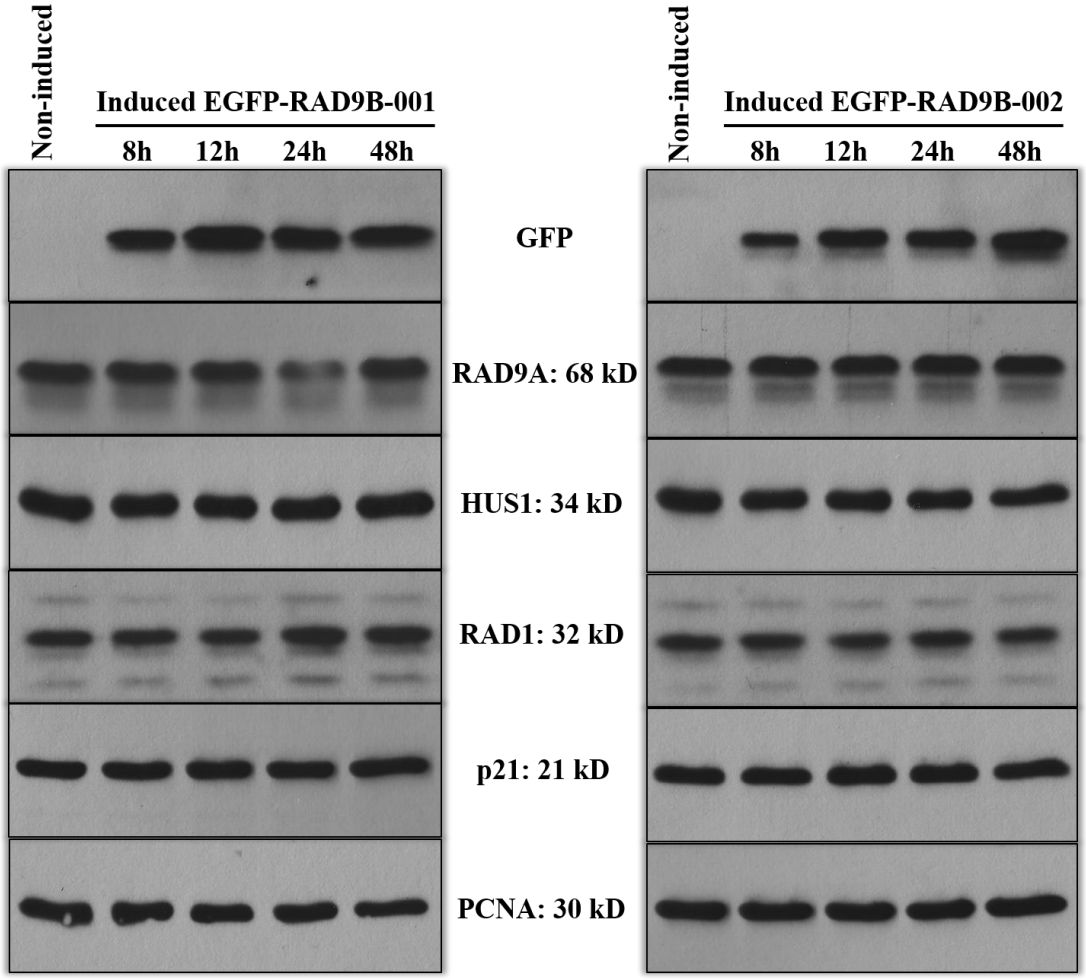

Figure 4.21 9-1-1 complex proteins show stable expression in the presence of high expression levels of RAD9B-001 and RAD9B-002. The EGFP-Rad9B-001 and EGFP-RAD9B-002 cell lines were induced and whole protein was extracted at the indicated times post transfection. The protein extracts were immunoblotted with GFP, RAD9A, HUS1, RAD1 and p21 antibodies. The expression of these proteins was normalised to the expression of the PCNA protein.

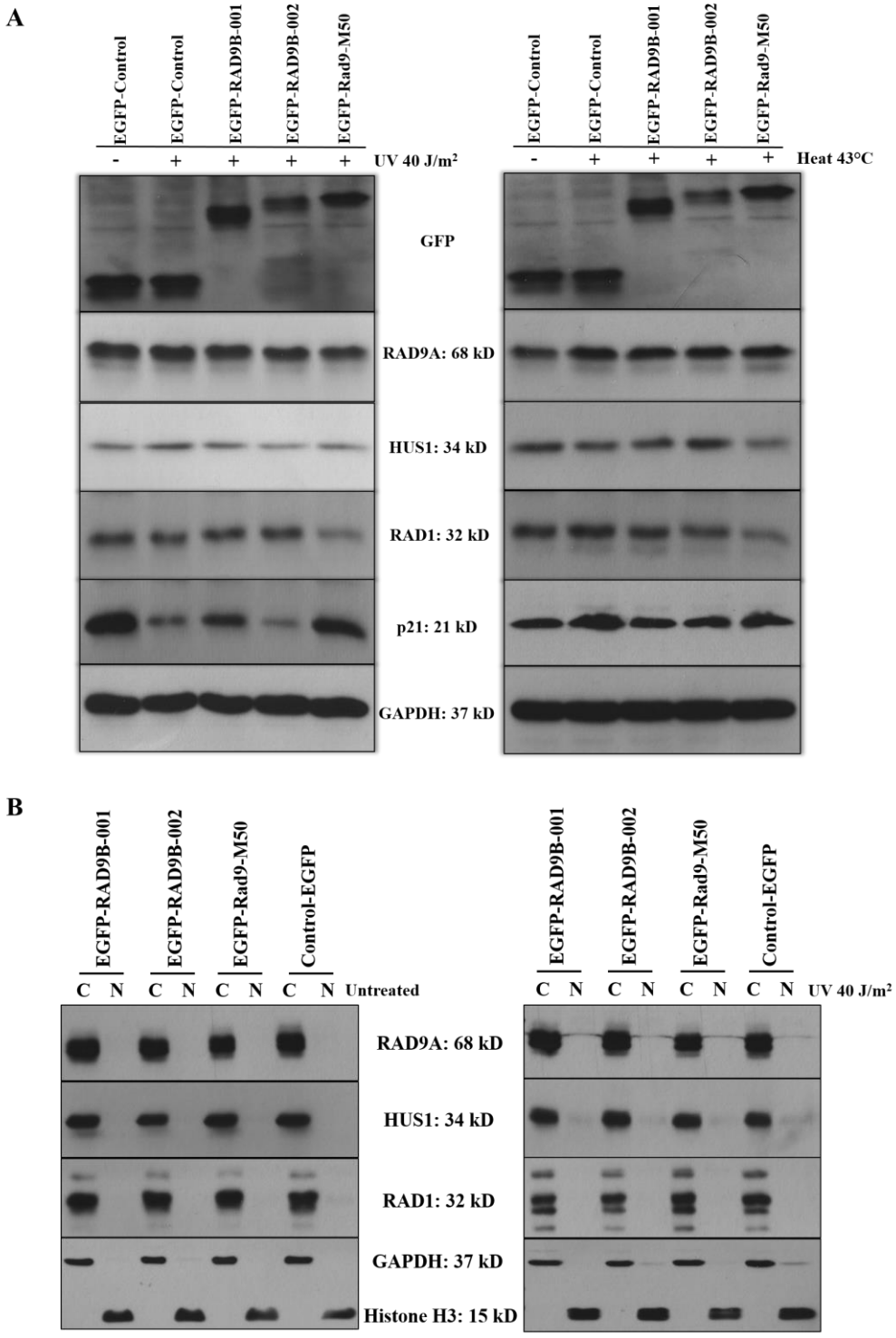

Figure 4.22 Overexpression of RAD9B splice variants or yeast Rad9-M50 do not influence the expression nor the localisation of the 9-1-1 complex protein in response to genotoxic stress. (A) Western blot analysis of RAD9A, HUS1, RAD1 and p21 in response to heat stress and UV light in the constructed over-expressed cell lines. Cells were either heat treated for 1 hr at 43°C or were UV treated (40 J/m^2). Whole protein was extracted from treated cells 1 hr after treatment. (B) Localisation analysis of RAD9A, HUS1 and RAD1 proteins in protein fractionation (cytoplasmic and nuclear) extracted from overexpressed cell lines under normal conditions and after exposure to UV light (40 J/m^2, 1 hr recovery). The GAPDH was used as a quality control for the cytoplasmic fraction whereas the histone H3 was used as a quality control for the nuclear fraction.

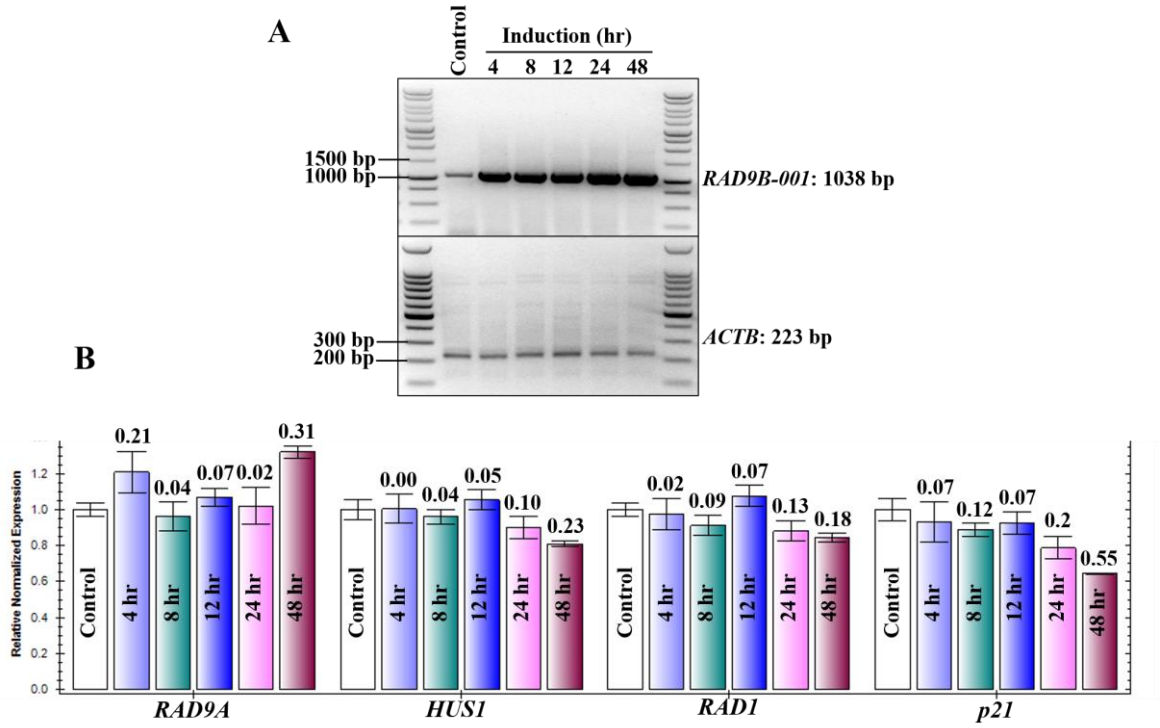

Figure 4.23 qPCR analysis of *RAD9A*, *HUS1*, *RAD1* and *p21* expression in EGFP-RAD9B-001 overexpressed cell line. (A) Total RNA was extracted from the overexpressed EGFP-RAD9B-001 cell line at the indicated times. 200 ng of the RNA was used as a template for the amplification of *RAD9B-001* splice variants using the specific flanking primers. *ACTB* was used as a positive control. (**B**) 1 µg of total RNA was reversed transcribed and the cDNA was used as a template in the qPCR analysis to detect the expression levels of *RAD9A*, *HUS1*, *RAD1* and *p21*. The expression of these genes was normalised to the expression of the *TBP* and *TUBA*.

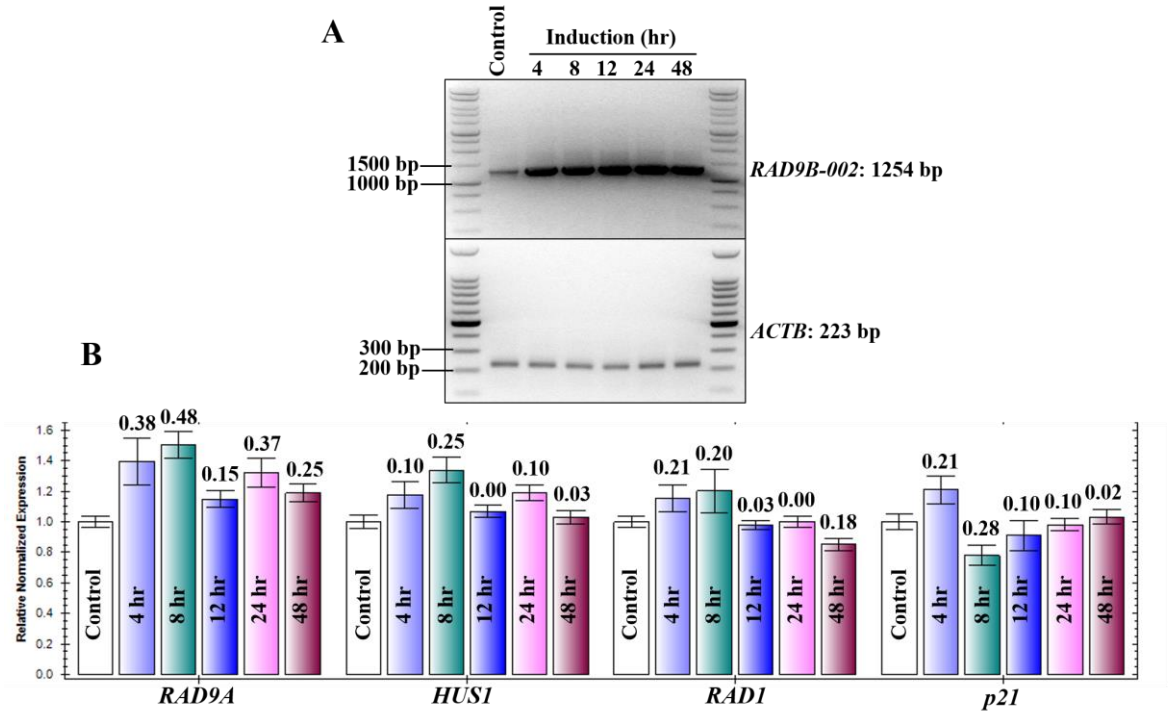

Figure 4.24 qPCR analysis of *RAD9A*, *HUS1*, *RAD1* and *p21* expression in EGFP-RAD9B-002 overexpressed cell line. (A) Total RNA was extracted from the overexpressed EGFP-RAD9B-002 cell line at the indicated times. 200 ng of the RNA was used as a template for the amplification of *RAD9B-002* splice variants using the specific flanking primers. *ACTB* was used as a positive control. (B) 1 µg of total RNA was reversed transcribed and the cDNA was used as a template in the qPCR analysis to detect the expression levels of *RAD9A*, *HUS1*, *RAD1* and *p21*. The expression of these genes was normalised to the expression of the *TBP* and *TUBA*.

4.2.15 RAD9A knockdown by shRNA in HEK293 cells

To further investigate the functional relationship between RAD9A protein and its paralog RAD9B, it was of interest to analyse *RAD9B* expression in the absence of RAD9A. This would address whether RAD9B can complement the loss of RAD9A to form a similar 9-1-1 complex by interacting with HUS1 and RAD1 proteins.

To down-regulate RAD9A, four shRNA cassettes constructed in puromycin plasmids containing a sequence that targets RAD9A were transfected into HEK293 cells. All plasmids were RFP-tagged for the transfection control. As most shRNAs sequences are 25–30% successful, four shRNAs sequences were transiently transfected to investigate the most effective shRNA. To assure a maximum knockdown, a mix of the four shRNAs were also transfected into the same cell line. This particular shRNA system was selected because it uses longer shRNA (29 bp), which is more effective in the down-regulation in addition to its hairpin constructs that allows for long-lasting down-regulation compared to short siRNAs.

The transfection of the individual shRNA plasmids and the four shRNA mixture was done using the Lipofectamine transfection reagent (Invitrogen). Since no validated antibody exists for the detection of RAD9B, the influence of RAD9A knockdown on the expression of RAD9B was tested at the mRNA level. Whole protein and total RNA were extracted 72 hr post-transfection with the shRNAs. Transfected cells displayed puromycin resistance and expressed the red RFP signal only 24 hr post transfection (Figure 4.25-A).

The RT-PCR and Western blot showed that RAD9A was not down-regulated by any of the four transfected shRNA plasmids nor by the mix of plasmids. Assuming the shRNA plasmids are functional, the results indicate that RAD9A inhibition could lead to a cell response against the reduction of RAD9A forcing them to induce more copies of RAD9A to overcome the reduction.

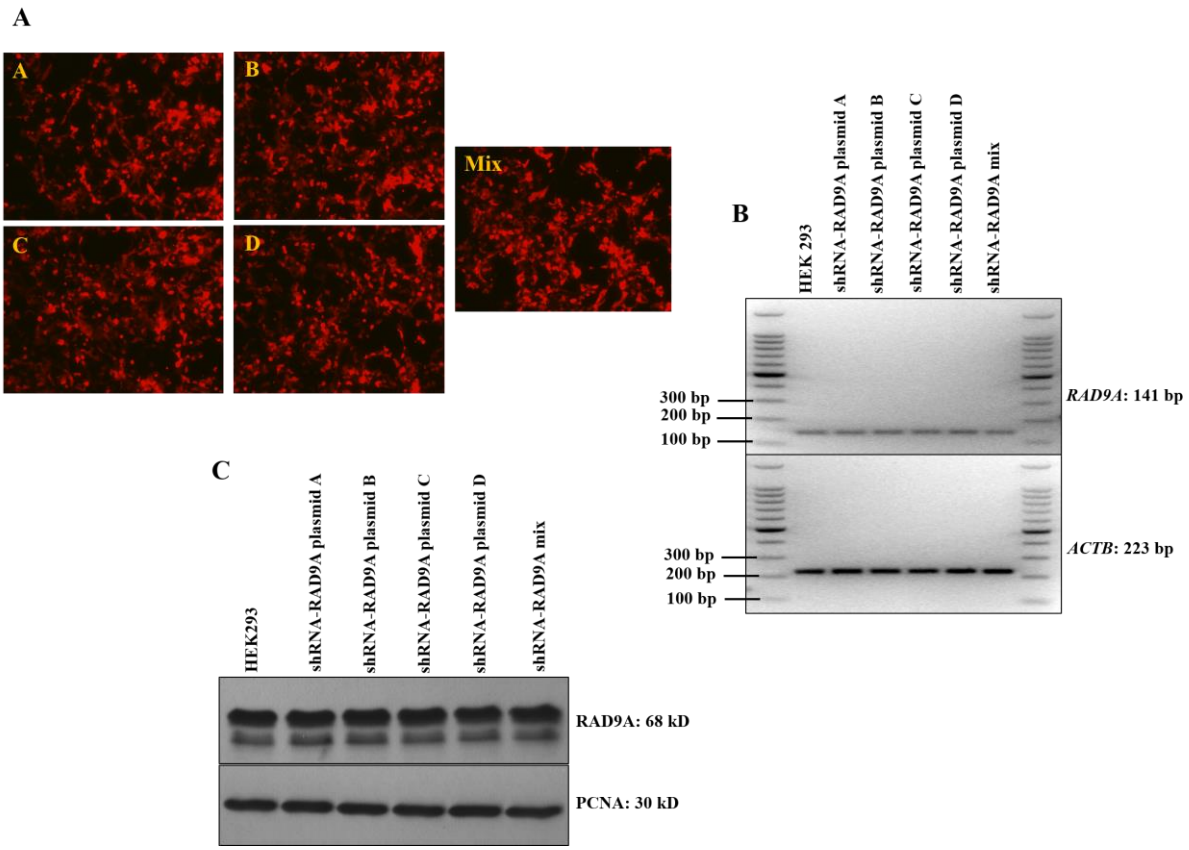

Figure 4.25 RAD9A is not downregulated when using the HuSH shRNA system. The four shRNA plasmids A, B, C and D were transfected into HEK293 cell separately or in conjunction. Total RNA and whole protein were extracted from the HEK293 cells 72 hr post transfection. (A) Expression of the RFP-tag from the shRNA plasmid reflecting the red colour under the microscope only 24 post transfection. (B) Amplification of *RAD9A* by two-step RT-PCR from normal and shRNA-transfected cells. *ACTB* was used as a positive control. (C) Western blot analysis of protein extracted from normal and shRNA-transfected cell immunoblotted with RAD9A antibody. The expression of RAD9A was normalised to the expression of the PCNA protein.

4.2.16 RAD9B-001 and RAD9B-002 do not translocate to the nucleolus in response to UV light

To investigate the functional role of the RAD9B variants and yeast Rad9-M50, their cellular localisation was investigated in HEK293 cells by either protein fractionation analysed by western blot or immuno-localisation using confocal microscopy. In previous studies, over-expressed RAD9B localised to the nucleus under normal conditions (Dufault et al., 2003). RAD9B also was reported to translocate to the nucleolus in the response to DNA damage (Perez-Castro & Freire, 2012). To test whether RAD9B-001 or RAD9B-002 shared a similar cellular location, all engineered cell lines were induced for at least 12 hr, followed by the extraction of the cytoplasmic and nuclear protein fractions.

For the confocal imaging, cells were grown on Poly-D-Lysine glass cover slips and fixed with para-formaldehyde and stained with an anti-GFP antibody.

Unlike the reported localisation of RAD9B, neither RAD9B-001 nor RAD9B-002 localised to the nucleus as they were only found in the cytoplasm when the fractions were analysed on SDS-PAGE. The quality of the protein fractions and the accuracy of the protein fractionation was determined by immunoblotting for cytoplasmic and nuclear specific marker proteins, glyceraldehyde 3-phosphate dehydrogenase (GAPDH) and Lamin B (LMNB), respectively. These control proteins confirmed the quality of the fractionation. However, the GFP-tag can influence the sub-cellular localisation of the recombinant proteins and over-expression can lead to artefacts that cause misleading results, as discussed later.

In Perez-Castro & Freire's study (2012), RAD9B was reported to translocate to the nucleolus in a co-compartmentalisation pattern with p21 after UV irradiation. Therefore, the localisation of this protein was analysed in normal conditions and under UV damage stress. Other proteins in the p21 pathway such as CHK2 or p53, were also analysed. In line with the localisation of RAD9B, p21 was found to localise to the cytoplasm in normal and UV-treated cells (Figure 4.26). The expression of p21 decreased in a time-dependent manner post-treatment as a result of its degradation in response to UV. CHK2 was present in the cytoplasm, but p53 was highly expressed in the cytoplasm and nucleus under normal conditions and in response to UV light.

Immunofluorescence with the confocal microscope was performed to confirm the RAD9B and Rad9-M50 localisation obtained by western blotting and also to verify that their localisation is not an error that occurred during the cytoplasmic and nuclear fraction procedure. The immuno-localisation results were consistent with the results obtained from the protein fractionation analysis. The RAD9B splice variants and Rad9-M50 were detected mainly in the cytoplasm (Figure 4.27). The empty plasmid control also had similar results to the other engineered proteins. Untransfected HEK293 cells were used as a negative control, as they should not induce any GFP signal, hence, the negative cell line did not reflect any GFP fluorescence signal, indicating the validation of florescence staining.

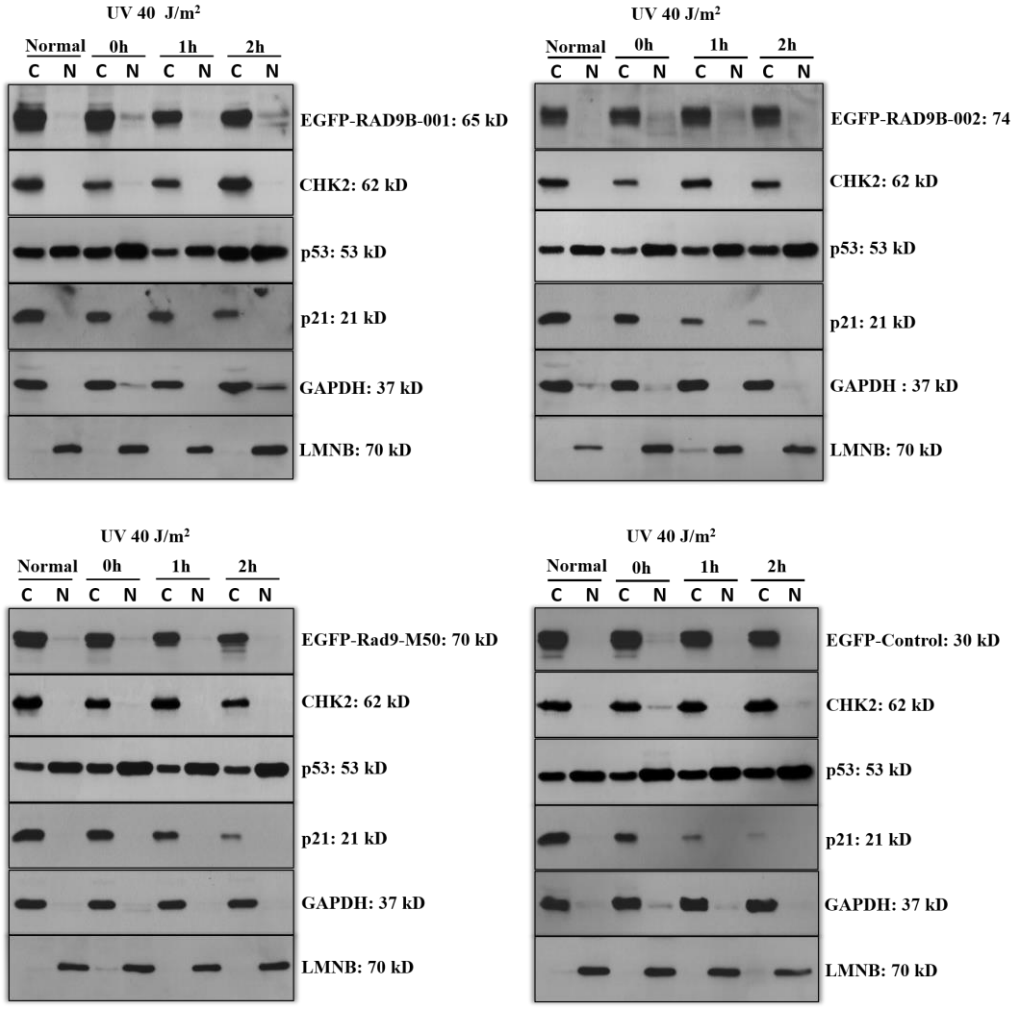

Figure 4.26 Localisation of EGFP-recombinant proteins and cell cycle regulator proteins in normal cells and in response to DNA damage. Two protein fractions (cytoplasmic (C) and nuclear (N)) were extracted from EGFP-RAD9B-001, EGFP-RAD9B-002, EGFP-Rad9-M50 and EGFP-Control cell lines under normal conditions and at different times post DNA damage by UV treatment. The fraction extracts were subjected to SDS-PAGE and immunoblotted with EGFP, CHK2, p53 and p21 antibodies. GAPDH and LMNB were used as positive controls for the cytoplasmic and nuclear fractions, respectively.

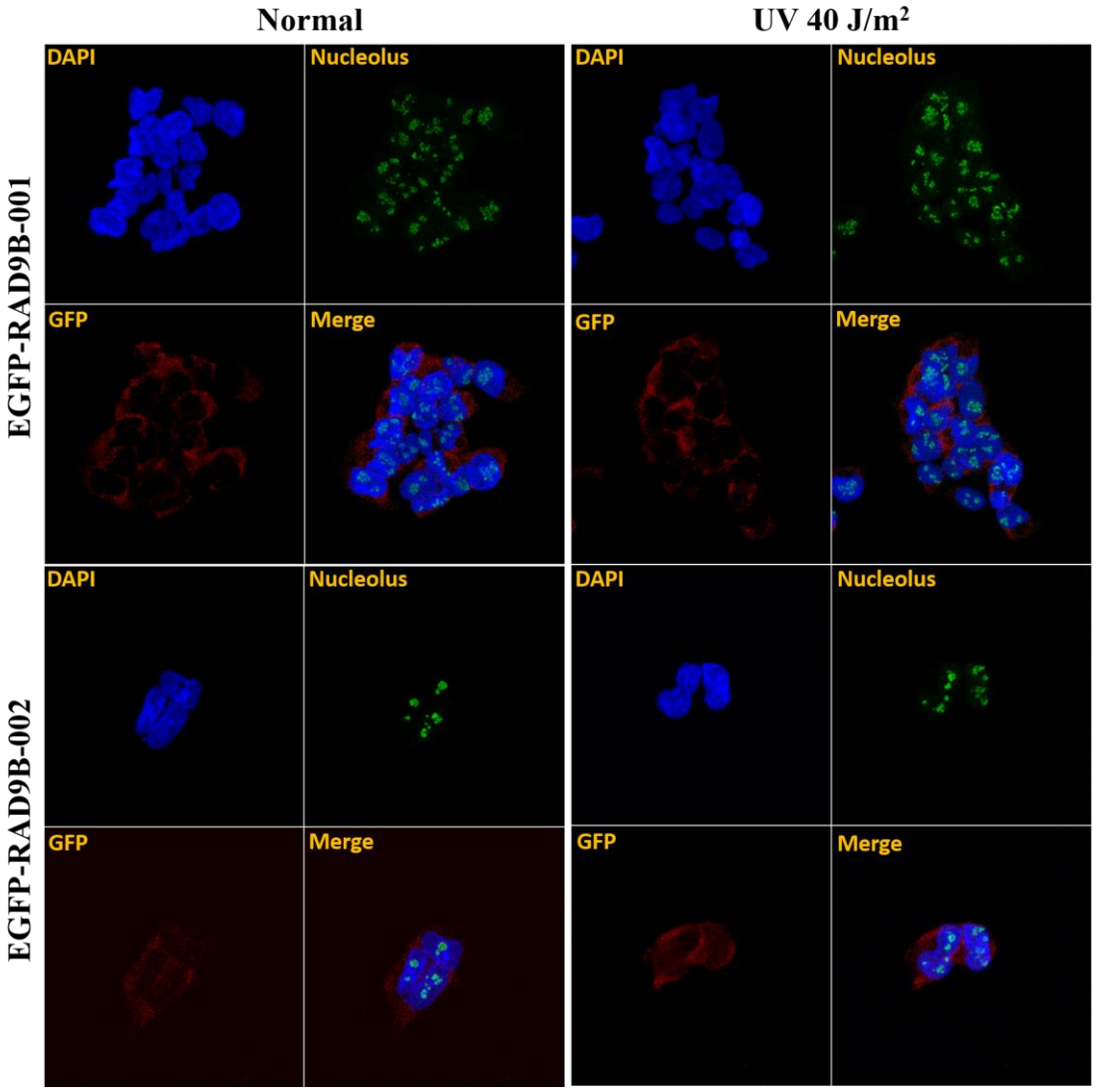
Normal
UV 40 J/m²
EGFP-RAD9B-001
EGFP-RAD9B-002
DAPI
Nucleolus
GFP
Merge
DAPI
Nucleolus
GFP
Merge
DAPI
Nucleolus
GFP
Merge
DAPI
Nucleolus
GFP
Merge

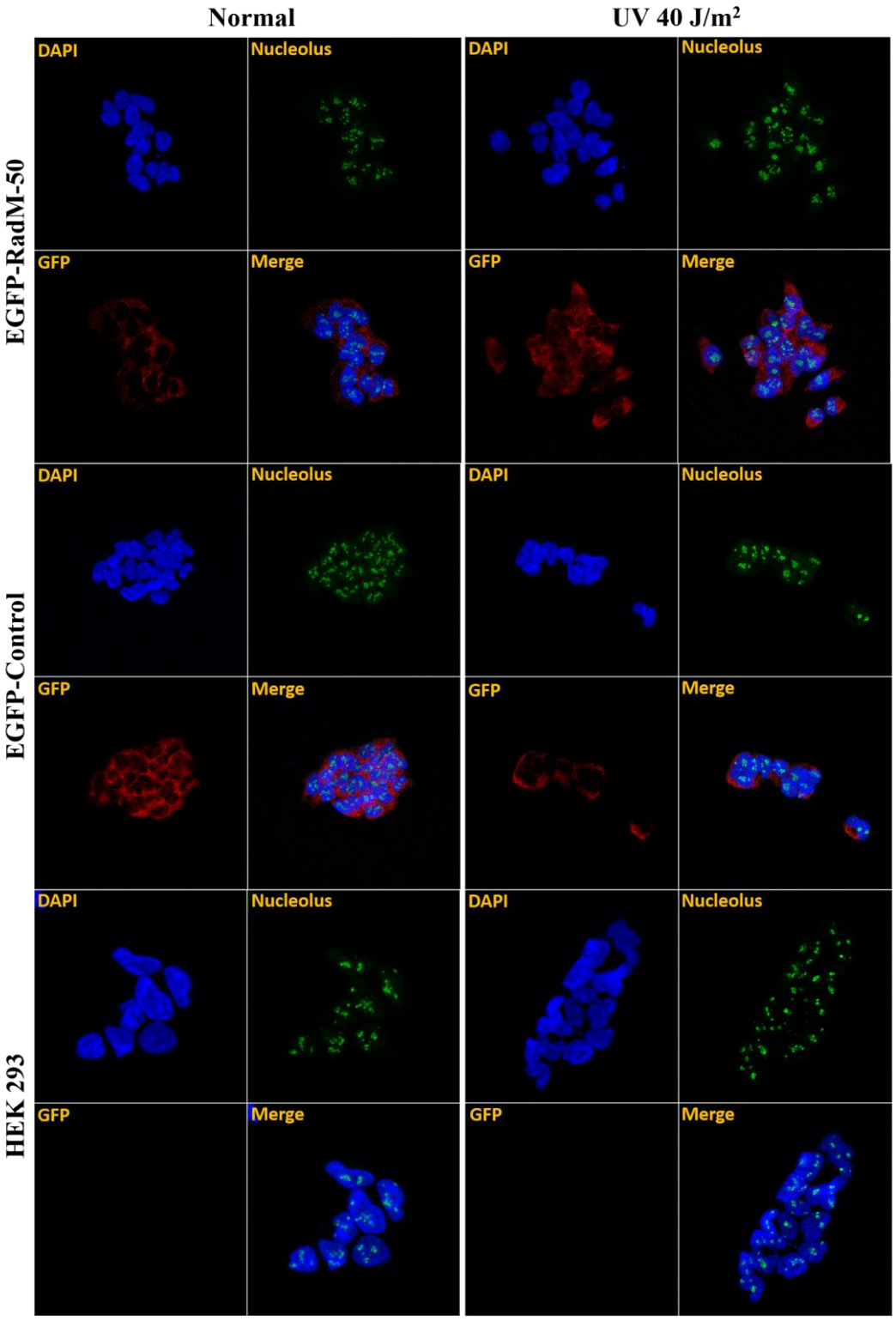

Figure 4.27 RAD9B-001 and RAD9B-002 do not localise to the nucleolus in response to UV light. Cells from the constructed cell lines were grown on coverslips in medium containing doxycycline for at least 12 hr. The cells then were either left untreated (normal) or were UV treated (40 J/m^2) followed by fixation with 4% paraformaldehyde. The cells then were stained with GFP and nucleolus (Anti-Fibrillarin) antibodies in combination with Alexa Fluor (red) and Alexa Fluor 488 (green), respectively, in addition to the nucleus stain DAPI (blue). HEK293 cells were used as a negative control. Images were taken by a Zeiss LSM710 confocal microscope with a 40x objective. Images were processed using Zen lite software.

4.3 Discussion

The key findings of this chapter are: (1) All GFP recombinant proteins reside mainly to the cytoplasm in normal and treated cells. (2) Exposure of the EGFP-RAD9B-001 and EGFP-Rad9B-M50 constructed cell lines to UV light revealed a delay in the degradation of the CDK inhibitor p21 which is not observed for the control or the EGFP-RAD9B-002 constructed cell lines. (3) Over-expression of RAD9B-002 have a negative impact on cell proliferation indicated by the accumulation of sub G1 cell population which may have undergone apoptosis. (4) The reported RAD9B in Perez-Castro Freire's (2012) study is likely to be the RAD9B-001 splice variant since its over-expression results in the reported G1 transient arrest. (5) Elevated levels of RAD9B-001 or RAD9B-002 increase the phosphorylation of p21 kinase inhibitor but do not show any impact on its transcription levels. (6) RAD9B may have a distinct role than RAD9A or the 9-1-1 complex since no alteration in the expression of RAD9A, HUS1 or RAD1 was observed at their mRNA or the protein levels when RAD9B was over-expressed. (7) RAD9B does not seem to be induced by heat stress or neither have an influence on the phosphorylation of CHK1 at elevated temperature.

Like *RAD9B*, *HUS1B*, a paralog of the human cell cycle checkpoint gene *HUS1*, is highly expressed in testis which led to the model that the `B` forms of these proteins are involved in the processing of the programmed DNA breaks during meiosis (Lyndaker et al., 2013). HUS1B plays a distinct role as its over-expression induces clonogenic cell death (Hang et al., 2002). Interestingly, over-expression of RAD9B-002 may have a similar impact on cells as indicated by the accumulation of sub G1 cell population which may have undergone apoptosis (Figure 4.13). Only RAD9A but not HUS1 was reported to cause an effect on cell survival when over-expressed (Broustas & Lieberman, 2012; Hang et al., 2002). It is likely that the expression of *RAD9B* and *HUS1B* is required only under certain conditions or during a specific cell cycle phase. The toxicity and cleavage of RAD9B-002 when over-expressed (Figure 4.12) supports this hypothesis. This toxic effect is very like caused by RAD9B-002 as high levels of EGFP are nontoxic to cells (Okabe et al., 1997), and only a few reports on the side effects of EGFP expression exist (Koike, Yutoku & Koike, 2013; Baens et al., 2006). Moreover, only the RAD9B-002 fusion partner and neither RAD9B-001 nor yeast Rad9-M50 triggers protein cleavage and a sub G1 population.

Since RAD9B-002 and RAD9B-001 only differ in their N-terminal sequence (Figure 4.28), and because this part of the protein is required for the formation of the 9-1-1 ring, it is reasonable to assume that high levels of RAD9B-002 in the 9-1-1 ring may be responsible for the toxic effect.

```
                  10        20        30        40        50        60
RAD9B-002 MAAMLKCVMSGSQVKVFGKAVQALSRISDEFWLDPSKKGLALRCVNSSRSAYGCVLFSPV
          :
RAD9B-001 M------------------------------------------------------------


                   70        80        90       100       110       120
RAD9B-002 FFQHYQWSALVKMSENELDTTLHLKCKLGMKSILPIFRCLNSLERNIEKCRIFTRSDKCK
                     ::::::::::::::::::::::::::::::::::::::::::::::::
RAD9B-001 ------------SENELDTTLHLKCKLGMKSILPIFRCLNSLERNIEKCRIFTRSDKCK
                          10        20        30        40
```

Figure 4.28 Alignment of RAD9B-001 and RAD9B-002. The alignment was created using ALIGN tool (http://xylian.igh.cnrs.fr/bin/align-guess.cgi. Accessed 28 August 2016). The two splice variants differ only at the first 72 amino acids.

Since RAD9A and RAD9B can both assemble with RAD1 and HUS1 in the ring (Perez-Castro & Freire, 2012; Dufault et al., 2003), elevated RAD9B-002 levels may out compete RAD9A and thereby cause cell death. Moreover, it was reported that RAD9A can be cleaved by caspase 3 where its N-terminal localises to the cytosol and binds to BCL-XL to neutralises its anti-apoptotic activity, thus promoting cell death (Broustas & Lieberman, 2012; Komatsu et al., 2000). Therefore, it is possible that the interaction of RAD9B-002 with HUS1 and RAD1 allows the accumulation of a large amount of RAD9A protein outside of the 9-1-1 complex leading to its apoptotic activity, hence the sub-G1 population. In addition, since RAD9B-002 N-terminal shares more homology with RAD9A than its C-terminal, it is also possible that RAD9B-002 interacts directly with BCL-XL and induces cell death in a similar manner to RAD9A.

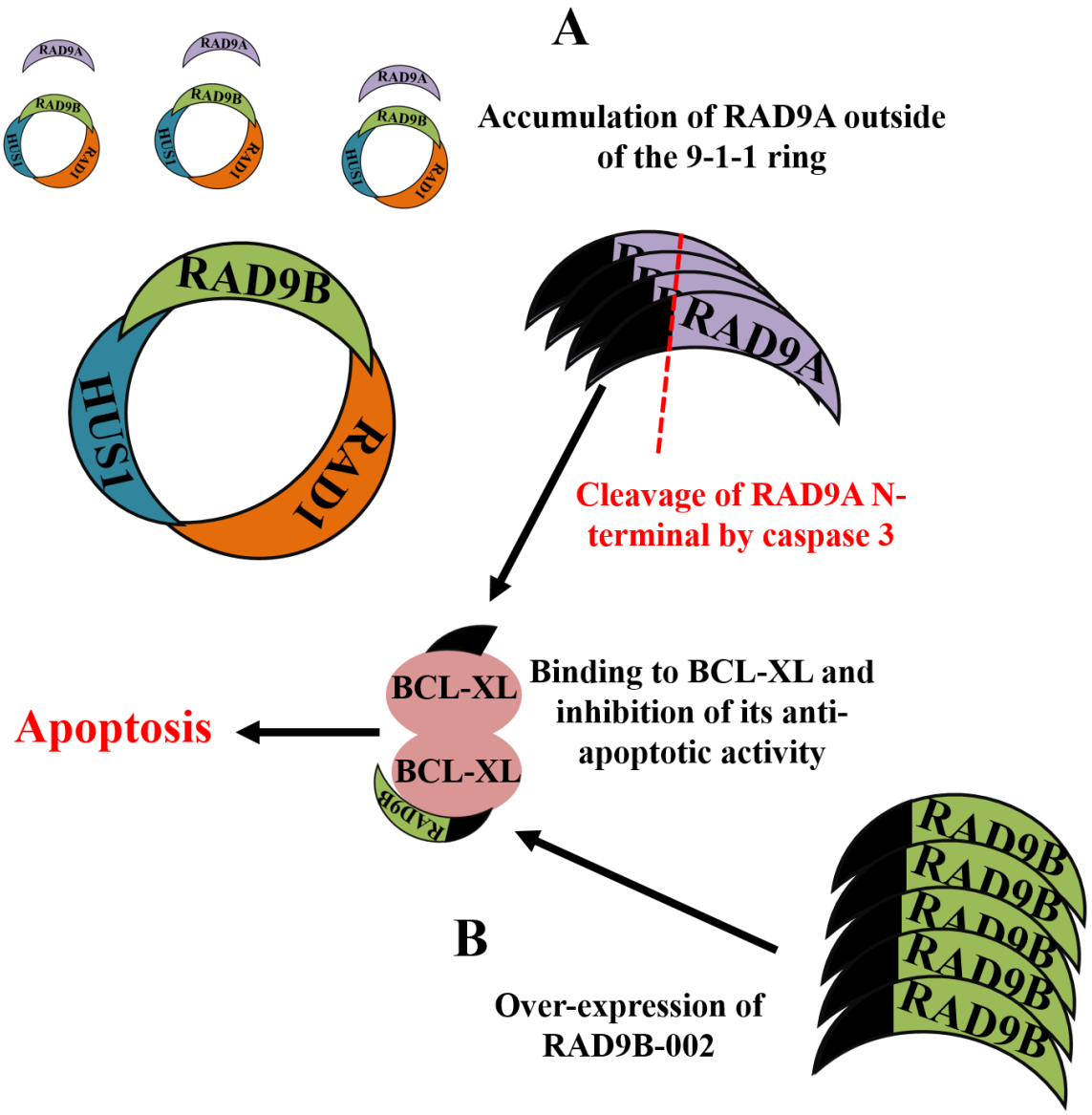

Figure 4.29 Possible induction of apoptosis by the RAD9B-002. (A) Over-expression of RAD9B-002 results in the substitution of RAD9A in the 9-1-1 complex ring leading to the accumulation of RAD9 molecules. The free RAD9A molecules are being cleaved by caspase 3 and the N-terminal of RAD9A translocate to the cytosol where it binds and neutralises the anti-apoptotic activity of BCL-XL and promoting cell death. (B) High elevated levels of RAD9B lead to its interaction with BCL-XL by its N-terminal domain (resembles the N-terminal of RAD9A) and inducing cell death.

Although RAD9B shares an extensive amino acid homology with RAD9A (36% identity, 48% similarity), the two proteins may have different properties. One striking difference between RAD9A and RAD9B is the inability of RAD9B to interact with TOPBP1 in the ATR pathway (Perez-Castro & Freire, 2012). Interestingly, only one of the key phosphorylation sites in the RAD9A tail domain, Ser-387 (Ser-409 in RAD9B-002), is conserved (Dufault et al., 2003). This could be significant since in *S. pombe*, the phosphorylation sites are crucial for the association with TOPBP1 (Rad4/Cut5) (Furuya et al., 2004). When the structure of full-length RAD9B-002 was modelled using the Swiss Model tool and the crystal structure of the N-terminal section (the tail domain is absent) of human RAD9A as a template, RAD9B-002 appears to differ in one domain which is located above the second beta sheets (Figure 4.30). While this section adopts a loop structure in RAD9A, it is significantly larger in RAD9B and adopts some beta sheet elements. In summary, the toxic impact of high RAD9B-002 protein levels could be explained by a competition between RAD9A and RAD9B for the 9-1-1 ring and a negative impact of RAD9B-002 due to its structural changes on DNA damage checkpoint activation. The latter could lead to the accumulation of a sub-G1 cell population and a cleavage event in an attempt of the cells to minimise the negative impact.

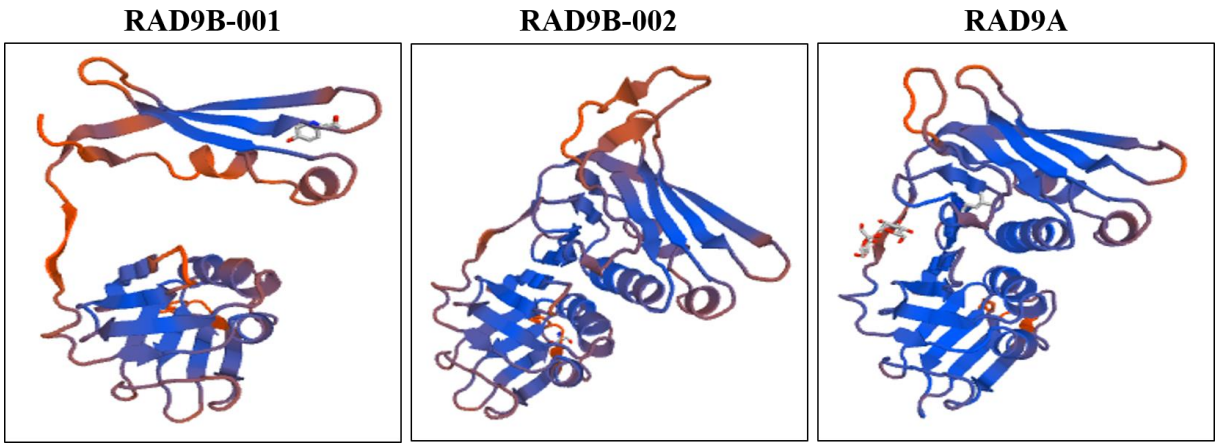

Figure 4.30 RAD9B-001, RAD9B-002 and RAD9A crystal structure. The structure was created using SWISS-MODEL server (https://swissmodel.expasy.org. Accessed 20 July 2016).

Although RAD9B and RAD9A were both previously reported to localise to the nucleus under normal conditions (Perez-Castro & Freire, 2012; Hopkins et al., 2003), in this project RAD9B and RAD9A were primarily localised to cytoplasm under normal conditions as well as in response to UV damage (Figure 4.26). The differences between this study and the published studies may be linked with the affinity tag. While RAD9B and RAD9A were FLAG-tagged and over-expressed in the HeLa or U2OS cell lines in the previous studies, RAD9B was N-terminally EGFP-tagged and over-expressed in the HEK293 cells. It has been reported that GFP can affect the localisation of proteins regardless of whether the GFP tag was attached to the N-terminus or the C-terminus. A study on EB1 (microtubule plus-end tracking protein) localisation found that GFP-EB1 had a different localisation to its untagged counterpart indicating that the GFP-tag can indeed result in misinterpretation (Skube, Chaverri & Goodson, 2010). Regardless of whether the EGFP tag did alter the localisation of the over-expressed RAD9B splice variants, this is unlikely to be the cause of the inconsistency for untagged RAD9A, HUS1 and RAD1 that were also found to localise to the cytoplasm in the cellular fractionation experiments (Figure 4.21). This could however be an artefact of the fractionation method as the 9-1-1 ring may slip off the chromatin during sample preparation. In confocal microscopy studies when the proteins were fixed with para-formaldehyde, RAD9A was confined to the nucleus in HEK293 and in K526 normal and treated cells. Surprisingly, in the same study, protein fractionation analysis of the K526 cells showed that RAD9A was not associated with the nucleus, as RAD9A was released from the chromatin (Burtelow, Kaufmann & Karnitz, 2000).

In this project, over-expression of RAD9B-001 and RAD9B-002 resulted in the increased phosphorylation of p21 when analysed on a phos-tag gel (Figure 4.20). It is unclear whether RAD9B-001 and RAD9B-002 mediated the reported phosphorylation of p21 by AKT kinase which prevents the association of p21 and PCNA to block DNA replication (Rossig et al., 2001). A close link between RAD9B and p21 is further supported by the finding that the UV-induced degradation of p21 is delayed by high protein levels of RAD9B-001 or the yeast Rad9-M50 variant (Figure 4.22-A).

As shown in the next chapter, UV irradiation resulted in the reduction of *RAD9B* mRNA expression (Figure 5.6) indicating that low levels of *RAD9B* are required for the degradation of p21 in the response to UV induced DNA damage. The E3-ligase CRL4 (CDT2) (CUL4-DDB1-CDT2) promotes p21 proteolysis after UV irradiation to enable the translesion DNA eta (POL η) to be recruitment to DNA lesions (Soria et al., 2008) .

The N-terminally truncated variant, RAD9B-001, may adopted a distinct structure when compared to full-length RAD9B-002 (Figure 4.30). Given the absence of the first 72 amino acids, it is unlikely that the shorter protein forms the 9-1-1 ring. It may however be able to assemble with PCNA, which is required for the degradation of p21 (Soria & Gottifredi, 2010) or with the E3 ligase CUL4-DDB1-CDT2 which is involved in p21 degradation. In any case, a delay in p21 degradation in the presence of high RAD9B-001 protein levels would result in UV sensitivity due to the retarded recruitment of DNA lesion bypass polymerases of the Y family (Mansilla et al., 2013). A close link between RAD9B and p21 may also explain the G1 arrest observed upon over-expression of RAD9B-001 (Figure 4.13) as p21 blocks the cyclin-dependent kinases required for G1-S transition (Harper et al., 1993).

Chapter 5: HUMAN RAD9B SPLICE VARIANTS IN RESPONSE TO DNA DAMAGE AND THEIR RELATION TO CHK2 PROTEIN KINASE

5.1 Introduction

So far, the hypothesis that the RAD9B splice variants regulate the dephosphorylation of the CHK1 kinase has not been shown to be true. However, while conducting experiments analysing different checkpoint proteins known for their involvement in the DNA damage response pathways, some alterations have been noted in the phosphorylation of the CHK2 protein but not in the phosphorylation of CHK1, in addition to the changes observed for the CHK2 downstream p21 protein. This chapter summarises the relationship between RAD9B, yeast Rad9 and the proteins of the ATM-CHK2 pathway. As mentioned previously, the ATM protein kinase targets and phosphorylates a number of proteins in response to DSBs including the CHK2 protein kinase. ATM phosphorylates CHK2 at Thr-68 in its N-terminal serine-threonine-glutamine (SQ-TQ) rich motif which triggers the dimerisation of the kinase and its auto-phosphorylation (Smith et al., 2010). Approximately 24 substrates have been identified so far for CHK2 protein kinase in human cells, all of which have been phosphorylated at one or more serine or threonine sites. A number of CHK2 substrates, such as p53, BRCA1, BRCA2 and KAP-1 are also phosphorylated directly by ATM suggesting that CHK2 might play a role in fine tuning ATM kinase (Zannini, Delia & Buscemi, 2014).

Recently, a novel interaction has been reported between CHK2 and the mitotic kinase MPS1. MPS1 was first discovered in yeast and the phenotypic analysis of mutant strains revealed key functions of this kinase in the duplication of the spindle pole body (SPB) (centrosome in humans) (Rose & Fink, 1987). Later, MPS1 was reported to play an important role in the spindle checkpoint. Its over-expression results in the activation of the spindle checkpoint pathway leading to a mitotic cell cycle arrest (Hardwick et al., 1996; Weiss & Winey, 1996) . MPS1 is found in many eukaryotic cells and 11 splice variants of this kinase are recorded in human cells, of which code 8 encode a protein (Ensemble data base). MPS1 has also been found to function in other signalling pathways including the genotoxic stress response.

DNA damage forces the cell cycle to arrest either in G1 or at the G2/M boundary or it directs the cell into apoptosis. In HeLa cells, UV irradiation causes these cervical cancer cells to arrest at the G2/M transition. Interestingly this arrest is completely dependent on the MPS1 protein kinase leading to a direct association between MPS1 and CHK2 resulting in the phosphorylation of CHK2 at Thr-68, the same site targeted by ATM. Phosphorylation of CHK2 requires the N-terminal domain of MPS1 (Yeh et al., 2009; Wei et al., 2005). Activated CHK2 increases MPS1 stability by directly phosphorylating MPS1 at Thr-288, whereby creating a feedback loop required for the G2/M arrest. The phosphorylation of MPS1 is dependent on the FHA and kinase domains of CHK2. Moreover, over-expression of CHK2 kinase increases the expression levels and phosphorylation of MPS1, whereas mutations within its FHA or kinase domain were not capable of inducing the MPS1 kinase (Yeh et al., 2009).

The CHK2 is considered to be a good target for cancer treatment. The main idea is to inactivate pro-survival activities after the DNA damaging treatment, such as cell cycle arrest and DNA repair, or activation of senescence and apoptosis. However, it has been reported that inhibition of CHK2 can increase the resistance of cells to chemotherapy as well as to radiotherapy. This is probably because CHK2 plays a role in the induction of the p53 apoptosis pathway. However, the absence of CHK2 and p53 result in failure to arrest in either the G1/S or G2/M phase after treatment that damages the DNA. Hence, inhibition of only CHK2 protein in p53 deficient tumour cells can sensitise these cells to genotoxic treatments (Jiang et al., 2009). Moreover, CHK2 inhibition has been reported to be beneficial for the treatment of some tumour types, such as pancreatic cancers. Inhibition of CHK2 in four pancreatic cancer cell lines (PaCa-2, Panc-1, BxPC-3 and CFPAC-1) enhanced the anti-tumour effect of gemcitabine (GEM) by significantly increasing the levels of intracellular reactive oxygen species (ROS) (Duong et al., 2013).

This chapter focuses on the response of CHK2 in cells over-expressing RAD9B-001, RAD9B-002 or yeast Rad9-M50 to two important types of DNA damaging agents, namely UV irradiation and H_2O_2. These experiments are informed by the role of human RAD9B and p21 in the response to UV light in the nucleolus (Perez-Castro & Freire, 2012). Also the findings from chapter 4 suggest a UV-specific function of both proteins. Moreover, the focus on oxidative DNA damage was because it is the dominating source of endogenous damage and is a strong stimulator of checkpoint proteins as was reported in multiple studies (Wei et

al., 2005; Yeh et al., 2009; Perez-Castro & Freire, 2012; Yu, Huang & Shieh, 2016; Tubbs & Nussenzweig, 2017). The analysis included two steps: first, the expression of the two splice variants RAD9B-001 and RAD9B-002 is tested at the mRNA level using the one-step RT-PCR assay to understand their expression in the response to the treatments. The same treatments are then applied to the EGFP-RAD9B-001 and EGFP-RAD9B-002 cell lines to analyse CHK2, MPS1, p53 and p21 in the presence of elevated levels of RAD9B-001 and RAD9B-002.

5.2 Results

5.2.1 Analysis of the apoptotic pathway in EGFP-RAD9B-001 and EGFP-RAD9B-002 over-expressing cell lines

The UV radiation dosage that has been used so far (40 J/m^2) does not seem to drive cells into apoptosis. As shown in Figure 5.1-A, cleavage of the PARP protein, which is generally regarded as a sign of apoptosis, does not occur in HEK293 cells under these conditions even 48 hr post-treatment. In line with this interpretation, no changes were observed in the other apoptotic marker BCL-2, with only a slight upregulation of the BAK protein, the expression of which is known to increase in apoptotic cells. The p53 transcription factor is phosphorylated at (Ser-15) up to 48 hr post UV radiation. Interestingly, 24 hours post treatment, almost 30-40% of cells were dead, which corresponds to the high dosage of UV light, and this percentage increased to nearly 60% 48 hr post-treatment. This is reflected in a drop in the phosphorylation of p53 as the cells can no longer recover from the damage. These results suggest that high dosages of UV light causes major damage killing the HEK293 cells independently of the apoptotic pathway.

Therefore, a lower dosage of UV radiation was used (15 J/m^2) to test whether this dosage is able to induce apoptosis in HEK293 cells as this would provide an insight into the possible role of the hRad9B splice variants in apoptosis.

A clear difference between the two doses can be seen in the apoptotic and checkpoint responses (Figure 5.1-B). At the lower dose, HEK293 entered apoptosis 24 hr post-UV irradiation as indicated by the smaller band of the PARP protein which indicates its cleavage. PARP cleavage increases 24hr and 48hr post-treatment. This apoptosis marker was observed

in all four cell lines indicating that this is a response to UV damage rather than a specific outcome of RAD9B-001 or RAD9B-002 over-expression. However, no changes were observed with the other two apoptosis markers BCL-2 and BAK. Unlike the high doses experiment, the p21 protein levels declined at the 12 hr and 24 hr time points and recovered after 48 hr post-treatment.

This drop in p21 correlated well with the phosphorylation of CHK2 at Thr-68 and indicated an ATM-CHK2 checkpoint response. As mentioned previously, p21 is degraded after UV irradiation to free up PCNA for DNA repair and translesion synthesis (Soria & Gottifredi, 2010).

The recovery of p21 expression levels after 48hr signals that cells have completed the UV response as 15 J/m^2 is a sub-lethal UV dose. While these responses were similar in all four cell lines, the p21 expression levels did not seem to recover to the same extent in the presence of high levels of EGFP-RAD9B-002 and yeast Rad9-M50. This suggests a role for the full-length RAD9B-002 and the yeast variant in inhibiting the exit from the UV-induced cell cycle effect.

The cell lines in this experiment were induced for approximately 18 hrs before the treatment. They were also grown in a medium containing doxycycline during the recovery time, in total 66 hrs. It can be seen that all four cell lines showed a drop in EGFP-Rad9 expression including the control cells, even though they were induced for a longer period of time. This may suggest that the UV treatment reduces their expression or results in their removal. The latter is clearly the case for RAD9B-002 which undergoes UV-induced cleavage (Figure 5.1-B).

A

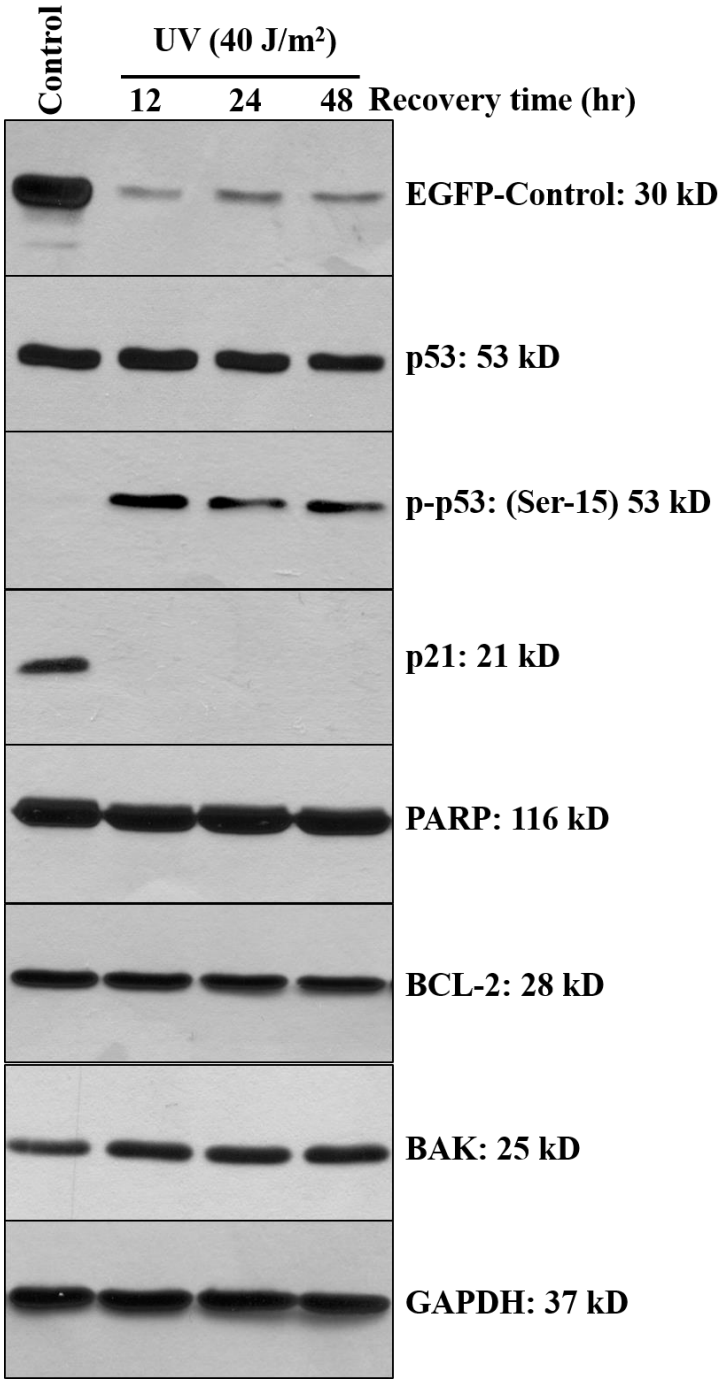
Control
UV (40 J/m2)
12
24
48
Recovery time (hr)
EGFP-Control: 30 kD
p53: 53 kD
p-p53: (Ser-15) 53 kD
p21: 21 kD
PARP: 116 kD
BCL-2: 28 kD
BAK: 25 kD
GAPDH: 37 kD

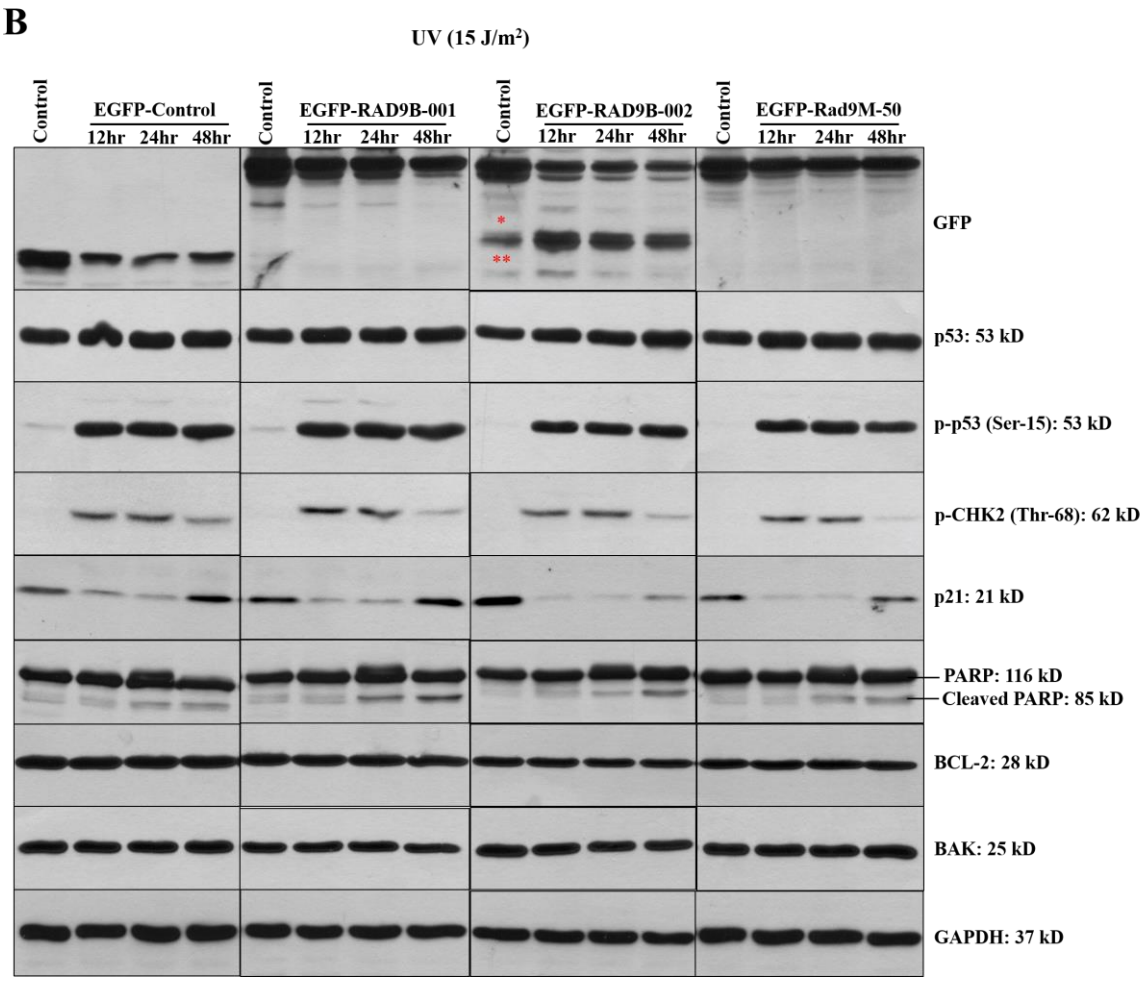

Figure 5.1 Western blot analysis of apoptosis-related proteins after UV damage in the constructed cell lines. (A) The EGFP-Control cell was induced for 18 hr then cells were exposed to a high dose of UV light (40 J/m^2) and whole protein was extracted 12, 24 and 48 hr post treatment. Protein extracts were analysed on the normal SDS-PAGE and immunoblotted for apoptosis-related proteins p53, p-p53, p21, PARP, BCL-2 and BAK and the protein loading control, GAPDH. (B) The four constructed cell lines EGFP-RAD9B-001, EGFP-RAD9B-002, EGFP-Rad9-M50 and the EGFP-Control were induced for 18 hr then were treated with a moderate UV radiation dose (15 J/m^2). Whole protein was extracted from treated cells 12, 24, 48 hr post treatment. Protein extracts were analysed on the normal SDS-PAGE immunoblotted for GFP and for apoptosis-related proteins p53, p-p53, p-CHK2, p21, PARP BCL-2 and BAK and for the GAPDH loading control. (*) indicates the cleaved EGFP-RAD9B-002 (40 kD), (**) indicates the second EGFP-RAD9B-002 cleaved band (27 kD).

5.2.2 Over-expression of RAD9B-001 and RAD9B-002 promotes high phosphorylation of CHK2 kinase.

So far no major differences in the expression of ATM, ATR, CHK1, CHK2 and p53 and p21 have been found as a result of the over-expression of any of the constructed cell lines. To find out whether over-expression of the variants over a longer period triggers a change in the phosphorylation of these checkpoint proteins, samples were taken 8 hr, 12 hr, 24 hr and 48 hr after addition of doxycycline.

As shown in Figure 5.2-A, no changes in the phosphorylation of ATR (Ser-428), ATM (Ser-1981) or CHK1 (Ser-345) were observed. Interestingly, prolonged over-expression of both human RAD9B variants resulted in an increase in CHK2 phosphorylation at Thr-68 (Figure 5.2-A). It is worth noting that the phosphorylation levels of the up-stream kinase ATM did not change indicating that CHK2 is phosphorylated by an alternative kinase which could be MPS1. It is also possible that the CHK2 phosphorylation is linked with the G1 arrests and sub-G1 cell population observed after over-expression of RAD9B-001 or RAD9B-002, respectively (Figure 4.13).

Analysis of p53, revealed an interesting result for RAD9B-001 as its over-expression increased p53 phosphorylation at (Ser-15). This phosphorylation was specific for the RAD9B-001 variant and was not observed upon over-expression of EGFP-RAD9B-002 (Figure 5.2-A). The latter could be linked with the accumulation of a sub-G1 cell population in the induced cell line (Figure 4.13). Finally, no phosphorylation of the CHK1 at Ser-345 was observed in either of the cell lines. These results indicate the possibility that over-expression of RAD9B affects the ATM-CHK2 pathway but not the ATR-CHK1 pathway.

To further investigate the phosphorylation status of CHK2 changes in untreated cells over-expressing the Rad9 variants, their expression was induced for 24hr and soluble protein extracts were loaded onto a 6% phos-tag SDS page. As shown in Figure 5.2-B, Over-expression of EGFP-RAD9B-001 resulted in a strongly reduced mobility of CHK2 indicating an increase in its phosphorylation status.

Over-expression of EGFP-RAD9B-002 caused only a partial over-phosphorylation of CHK2, whereas over-expression of the yeast variant had no impact on CHK2 mobility. Taken

together, these data suggest that elevated levels of the human RAD9B proteins affect CHK2 phosphorylation in untreated cells (Figure 5.2-B).

Based on the increase in CHK2 phosphorylation upon over-expression of the RAD9B-001 and RAD9B-002 and the increase in phosphorylation of p53 as a result of the RAD9B-001 over-expression, a possible physical interaction of the variants with either CHK2 or p53 was examined. To achieve this, immunoprecipitation of the GFP-tagged proteins was performed. Several immunoprecipitation kits were used for the pull down of the over-expressed GFP-tagged proteins, such as GFP magnetic beads, magnetic beads and GFP agarose beads. However, most attempts failed to pull down the RAD9B variants. These negative outcomes might indicate that the RAD9B-001 and RAD9B-002 have interaction partners forming a larger complex making it difficult for the GFP tagged proteins to bind to the beads. Only EGFP-RAD9B-001 was successfully pulled down using the anti-GFP agarose beads. Probing with antibodies for CHK2 and p53 revealed that neither protein binds to this variant indicating that RAD9B-001 causes phosphorylation changes indirectly (Figure 5.2-C).

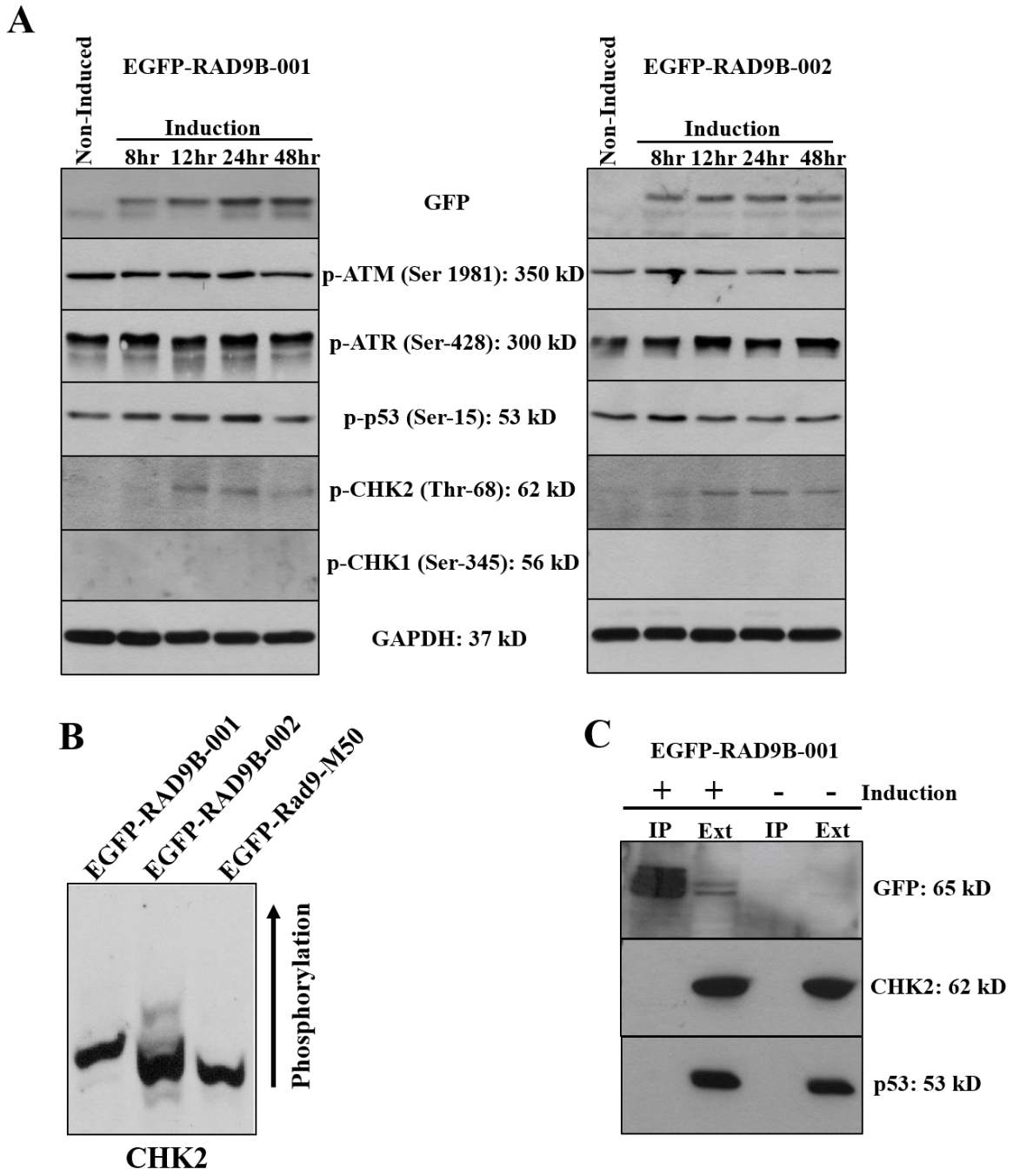

Figure 5.2 High phosphorylation of CHK2 kinase in over-expressed EGFP-RAD9B-001 and EGFP-RAD9B-002 cell lines. (A) The EGFP-RAD9B-001 and EGFP-RAD9B-002 were induced by doxycycline (1µg/ml), and whole protein was extracted from the induced cell lines at the points indicated. Protein extracts were analysed on normal SDS-PAGE and immunoblotted for the checkpoint proteins using phospho-specific antibodies against ATM, ATR, p53, CHK2 and CHK1. The GAPDH was used as the negative control. (B) CHK2 is aberrantly phosphorylated in untreated cells over-expressing human RAD9 variants. Whole protein extracts of untreated cells 24hr after the addition of doxycycline were loaded on a phos-tag gel (6% acrylamide 29:1) and stained with an anti-CHK2 antibody. (C) The EGFP-RAD9B-001 was over-expressed or left non-induced followed by whole protein extraction. The EGFP-RAD9B-001 was immunoprecipitated from the protein extract using the EGFP agarose beads before analysing on western blot for the indicated proteins. (IP): immunoprecipitate, (Ext): total extract.

5.2.3 Possible mediation for CHK2 interaction by the human RAD9B splice variants and the yeast Rad9M-50

To gain more insight into the relationship between the RAD9B splice variants and the phosphorylation of CHK2, protein extracted from UV treated cells was analysed on native polyacrylamide gels. This allows the detection of differences in the native conformation or complex formation of proteins (Nowakowski, Wobig & Petering, 2014). Under native conditions CHK2 migrated in at least 3 forms in untreated EGFP-Control cells while p53 produced 2 bands (Figure 5.3). After UV treatment with 40 J/m^2, p53 increased in EGFP control cells. A similar band pattern was observed in UV treated cells expressing EGFP-RAD9B-001, EGFP-RAD9B-002 or EGFP-Rad9-M50. Therefore, there were no variant specific changes to p53 (Figure 5.3). Interestingly, there was one important difference in the amount of the CHK2 middle form (form 2 in Figure 5.3) which increased very strongly in the presence of all three variants whereas form 3 did not increase as found in the control cell line. The other interesting observation was a faster migrating form of CHK2 in UV treated control cells which was absent in the presence of either RAD9 variant. Taken together this supports the conclusion that over-expression of the Rad9 variants has a specific impact on CHK2 kinase. Unfortunately it is as yet unknown which post-translational modifications contribute to the observed changes in CHK2 mobility.

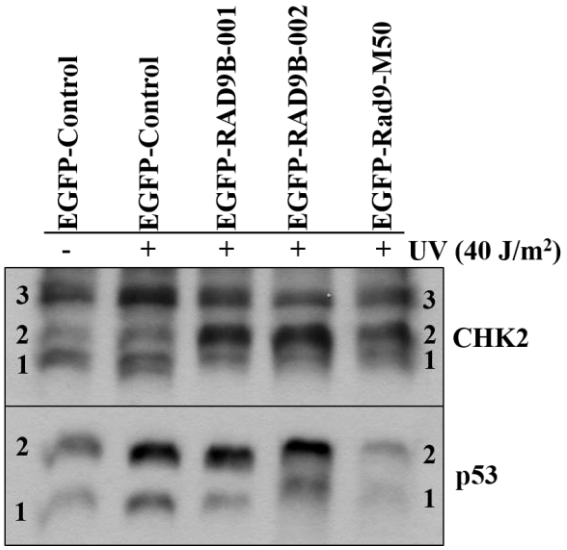

Figure 5.3 Native-PAGE analysis of CHK2 and p53 response to UV radiation in the constructed cell lines. Whole protein was extracted from UV treated (40 J/m^2, 1 hr recovery) over-expressed EGFP-RAD9B-001, EGFP-RAD9B-002 and EGFP-Rad9-M50 and the EGFP-Control cell lines. Extracts were analysed on native-PAGE and probed with antibodies for the CHK2 and p53. The numbers indicate the isoforms.

5.2.4 *RAD9B* mRNA expression in response to UV light

Based on published observations that RAD9B responds to UV light (Perez-Castro & Freire, 2012), the mRNA levels were tested at different time points after UV treatment with 40J/m^2. The expression of *RAD9B* was analysed using the quantitative PCR (qPCR) assay where its levels are normalised to two reference genes (*TUBA* and *PB1*).

The effectiveness of the UV treatment was validated by the degradation of p21. Interestingly, the expression of *RAD9B* dropped immediately after the UV irradiation by 1.80 fold relative to untreated cells, and this decline reached its maximum with a 2.94 fold decline 3 hrs post-treatment (Figure 5.5-A). It is worth mentioning that the primers used for this qPCR are not specific to any of the *RAD9B* splice variants as the primers binds to exon 3 and exon 4 which are conserved in all 5 *RAD9B* splice variants.

Since this qPCR test can not distinguish between the variants, the same RNA samples were analysed by one-step RT-PCR using more specific primers for the full-length mRNA molecules of *RAD9B-001* and *RAD9B-002* (the same two splice variants studied on the protein level in the constructed cell lines). Here the primers used previously for the cloning of *RAD9B-001* and *RAD9B-002* were used. However, the primers that amplified the coding region of the *RAD9B-001*, as shown previously, also bind to *RAD9B-002* and *RAD9B-005*, whereas the primers that amplified the coding region of the *RAD9B-002* bind to *RAD9B-002* and *RAD9B-005* (Figure 5.4).

The RT-PCR test revealed a slight lower expression of both amplified *RAD9B* fragments *RAD9B-001/002/005* and *RAD9B-002/005* in UV-treated samples although the difference in expression was almost undetectable (Figure 5.5-B). This could be because of the small fold changes that are detected in the qPCR analysis arose from primers which detect all *RAD9B* variants. From the same cells, whole protein was extracted and run on a SDS-PAGE to test p21 protein levels. As expected, they dropped in the response to the UV treatment (Figure 5.5-C).

To test whether this response was specific to the non-malignant HEK293 cells, the same treatment was applied to the HeLa (cervical cancer) and Kelly (neuroblastoma) cell lines. The Kelly cell line showed a high sensitivity to UV light as all cells died 24 hrs post-treatment.

This time point could therefore not be included in the analysis. Interestingly, HeLa cells appeared to be more resistant to UV light than either HEK293 or Kelly cells, as almost 90% of cells were alive 24 hrs post-treatment. However, for unknown reasons and in repeat tests no RNA could be obtained for this time point. It appears that mainly *RAD9B-002/005* is down-regulated in both tumour cell lines with an additional decline in the Neuroblastoma cell line (Kelly) (Figure 5.6 & Figure 5.7). These results suggests that *RAD9B* remains expressed after UV damage but at a lower levels compared to untreated cells.

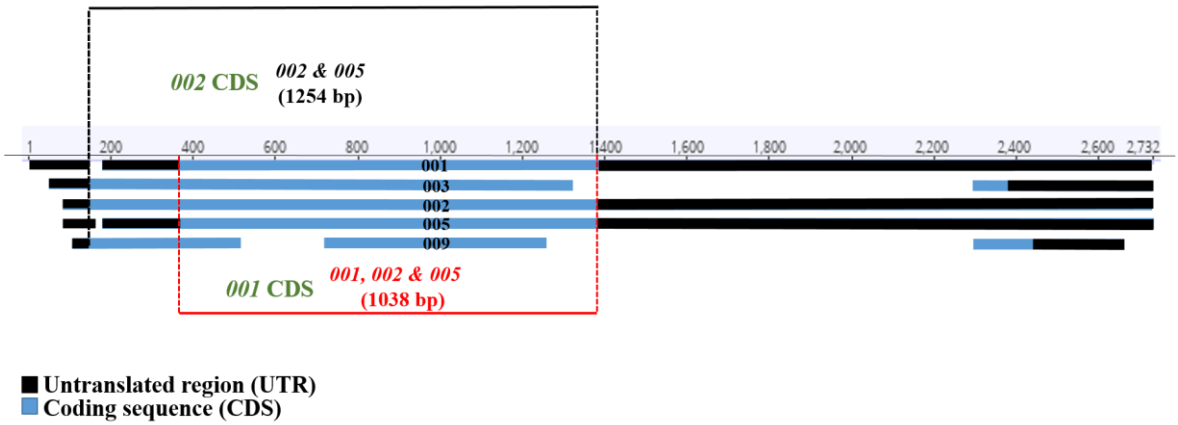

Figure 5.4 Primer design to amplify *RAD9B-001* and *RAD9B-002* CDS. Sites of primer binding across *RAD9B* splice variants amplifying the CDS of *RAD9B-001* and *RAD9B-002*.

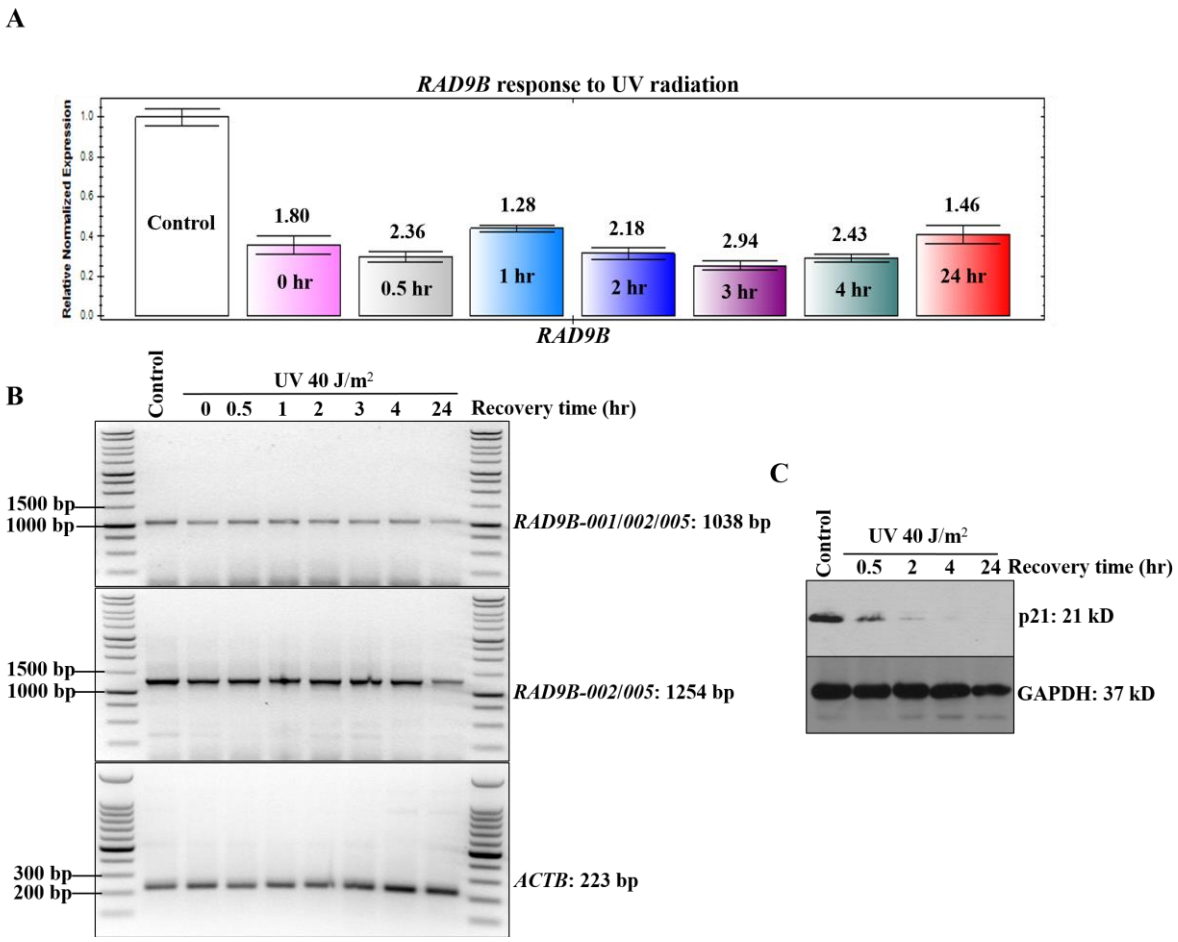

Figure 5.5 Figure *RAD9B* mRNA expression levels drops in response to UV light in HEK293 cells. (A) A bar chart demonstrating the expression of *RAD9B* in response to UV radiation in HEK293 cells as analysed by qPCR. The primers that are used for this qPCR are not specific to any of the *RAD9B* splice variants as the primers bind to exon 3 and exon 4 which are conserved in all 5 *RAD9B* splice variants. The expression of *RAD9B* was normalised to *TUBA* and *PB1* reference genes. The numbers on the top of columns represent the expression fold change compared to expression in the control (untreated cells). (B) RT-PCR of *RAD9B-001/002/005* and *RAD9B-002/005* in response to UV light in HEK293 cells. Cells were treated with UV light (40 J/m^2) and total RNA was extracted at the indicated points. The expression of the *RAD9B* was normalised to the expression of *ACTB*. (C) Whole protein extracted from UV treated cells at the indicated points and immunoblotted for the p21 protein used for the UV treatment control. The GAPDH was used as the protein loading control.

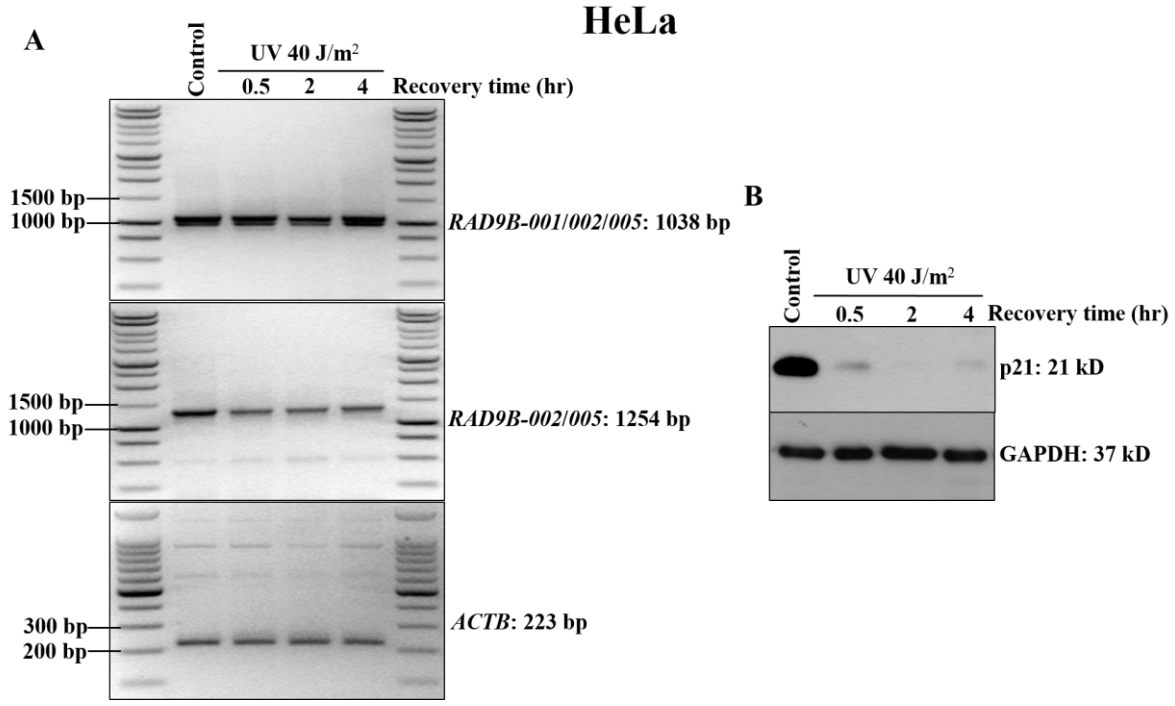

Figure 5.6 Analysis of *RAD9B* mRNA expression in response to UV light in HeLa cells. (A) RT-PCR of *RAD9B-001/002/005* and *RAD9B-002/005* in response to UV light in HeLa cells. Cells were treated with UV light (40 J/m^2) and total RNA was extracted at the indicated points. The expression of the *RAD9B* was normalised to the expression of *ACTB*. (B) Whole protein extracted from UV treated cells at the indicated points and immunoblotted for the p21 protein used for the UV treatment control. The GAPDH was used as the protein loading control.

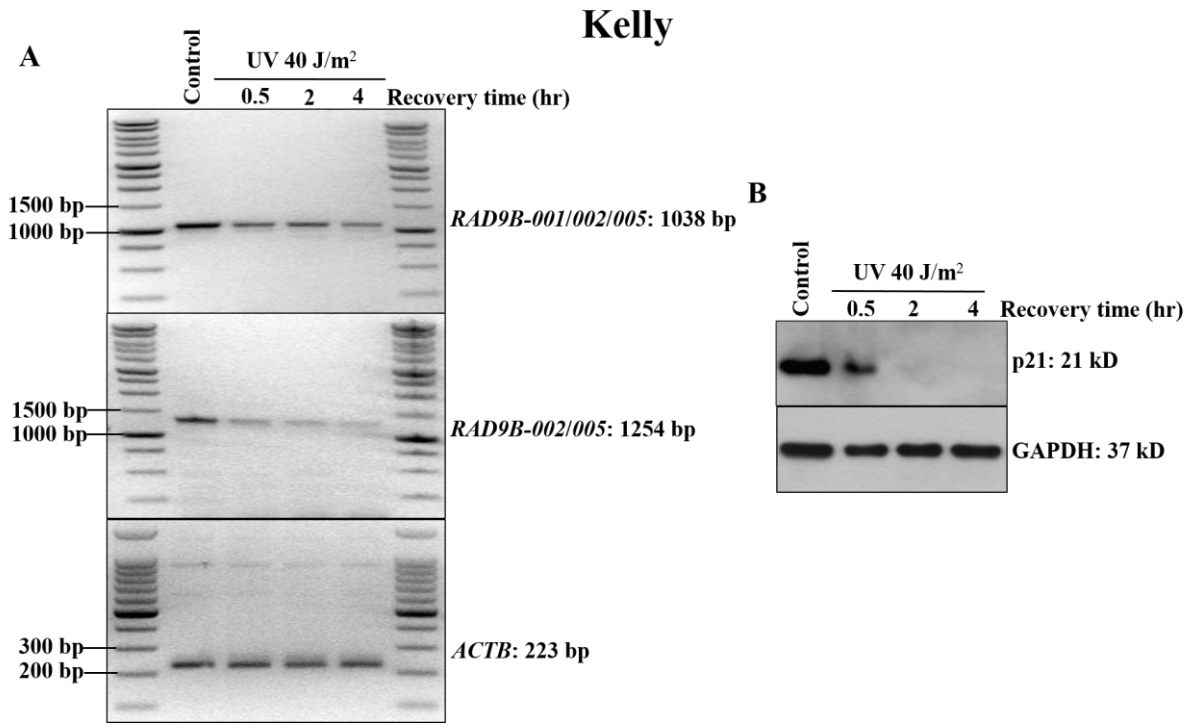

Figure 5.7 Analysis of *RAD9B* mRNA expression in response to UV light in Kelly cells. (A) RT-PCR of *RAD9B-001/002/005* and *RAD9B-002/005* in response to UV light in Kelly cells. Cells were treated with UV light (40 J/m^2) and total RNA was extracted at the indicated points. The expression of *RAD9B* was normalised to the expression of *ACTB*. (B) Whole protein extracted from UV treated cells at the indicated points and immunoblotted for the p21 protein used for the UV treatment control. The GAPDH was used as the protein loading control.

5.2.5 Dephosphorylation of Chk2 protein kinase upon RAD9B-002 over-expression in response to UV radiation.

Based on the results obtained for the aberrant CHK2 phosphorylation as a result of the over-expression of RAD9B-001 and RAD9B-002 (Figure 5.2), the response of the ATM-CHK2 pathway was analysed in the four cell lines: EGFP-Control, EGFP-RAD9B-001, EGFP-RAD9B-002 and EGFP-Rad9-M50. The cell lines were exposed to UV light (40 J/m^2) and whole protein was extracted at 30 min and 2 hr post-treatment.

Analysis of CHK2 revealed two interesting observations. A faster migrating band was observed in most cell lines which increased in abundance during the recovery period with the exception of EGFP-RAD9B-002. The phosphorylation of CHK2 at Thr-68 which increased during the recovery period in the EGFP control cells and in EGFP-RAD9B-001 cells, did not accumulate to the same extend in the remaining to cell lines expressing either EGFP-RAD9B-002 or the yeast variant (Figure 5.8). The identity of the faster migrating CHK2 band is not known, but it could be a splice variant of the kinase (Berge et al., 2010), or CHK2-cleaved band (Golan et al., 2010). In summary, the data confirm a close link between the RAD9B variants and CHK2 and suggest that the UV-induced modification of CHK2 is normal in EGFP-RAD9B-001. In contrast, expression of EGFP-RAD9B-002 or the yeast variant seems to suppress CHK2 modification at Thr-68 in the presence of UV damage.

The analysis of MPS1 revealed additional smaller bands in all cell lines. One of these bands, which appears at a size of 45 kD, is the most intense band and is down-regulated in the EGFP-RAD9B-002 and yeast Rad9 cell lines (Figure 5.8). This down-regulation correlates with the decrease in the faster migrating CHK2 band suggesting that both Rad9 variants may have an impact of the induction of these MPS1 and CHK2 smaller forms.

As observed in the earlier experiments (Figure 4.21), p21 degradation is delayed when RAD9B-001 and RAD9-M50 are over-expressed. These results suggest that RAD9B-001 delays the cellular response to UV damage, which coincides with the degradation of p21 (Soria et al., 2006).

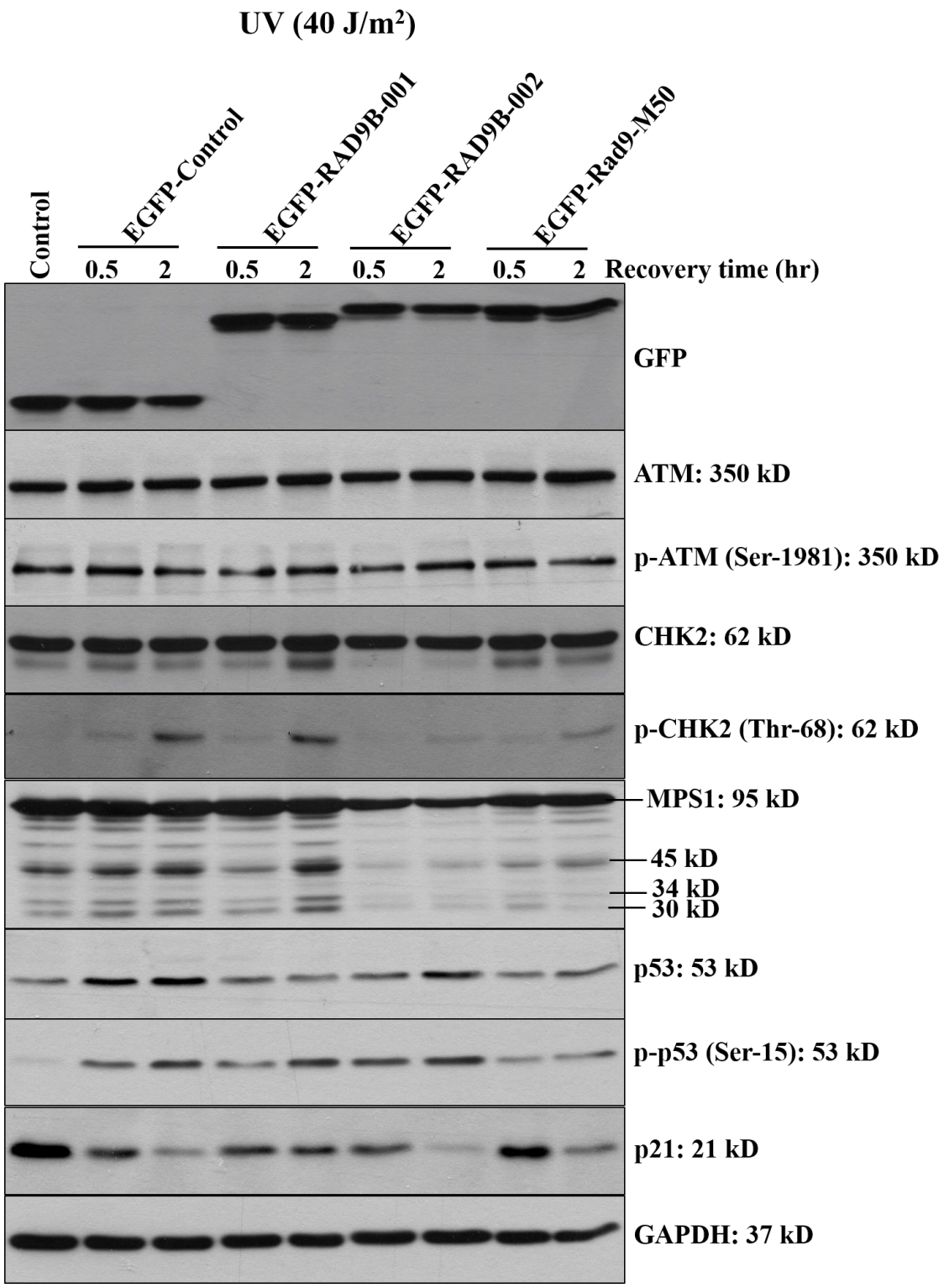

Figure 5.8 Over-expression of EGFP-RAD9B-002 dephosphorylates the CHK2 protein in response to UV light. The four constructed cell lines, EGFP-Control, EGFP-RAD9B-001, EGFP-RAD9B-002 and EGFP-Rad9M50, were over-expressed over-night, followed by UV exposure (40 J/m^2), then cells were left to recover for 30 min and 2 hr. Whole protein was extracted from the recovered cells and subjected to normal SDS-PAGE and immunoblotted with the indicated antibodies. GAPDH was used as a loading control.

5.2.6 *RAD9B* mRNA expression in response to heat stress

In the previous chapter, over-expression of the RAD9B-001 or RAD9B-002 did not show any negative influence on the phosphorylation of CHK1 protein kinase in response to heat stress. This indicated that they play a different role than that of the yeast Rad9-M50. Here, the expression levels of *RAD9B* in the response to heat stress was analysed in HEK293, HeLa and Kelly cells. Heat stress was applied by incubating cells at 43°C for 1 hr followed by a recovery period of up to 24 hr (Figure 5.9). Analysis was performed on the total RNA extracted from the recovered cells by using the one-step RT-PCR.

When HEK293 cells were heat treated, the expression levels of *RAD9B-001/002/005* and *RAD9B-002/005* were reduced 3 hr after the heat treatment, and the expression remained low for up to 24 hr. As shown previously (Figure 4.22-B), p21 expression levels increased in the response to heat stress in HEK293 cells (Figure 5.9-B). The expression of *RAD9B* in response to heat stress was also analysed in the two cancer cell lines, HeLa and Kelly, but with samples taken after shorter recovery times. In HeLa cells, *RAD9B-002/005* expression dropped already 30 min after the end of the heat stress period. The expression remained low up to 24 hr post-treatment. As the primers used detect *RAD9B-002* and *RAD9B-005* it is unclear which of the two genes is down-regulated (Figure 5.10-A). As found in HEK293 cells, p21 expression also increased in the HeLa cells to an even greater extent (Figure 5.10-B). In Kelly cells the expression levels of *RAD9B-001/002/005* and *RAD9B-002/005* remained stable in response to heat stress. Also the expression of p21 remained stable, suggesting that the neuroblastoma cells have a different response to elevated temperatures (Figure 5.11-A & B).

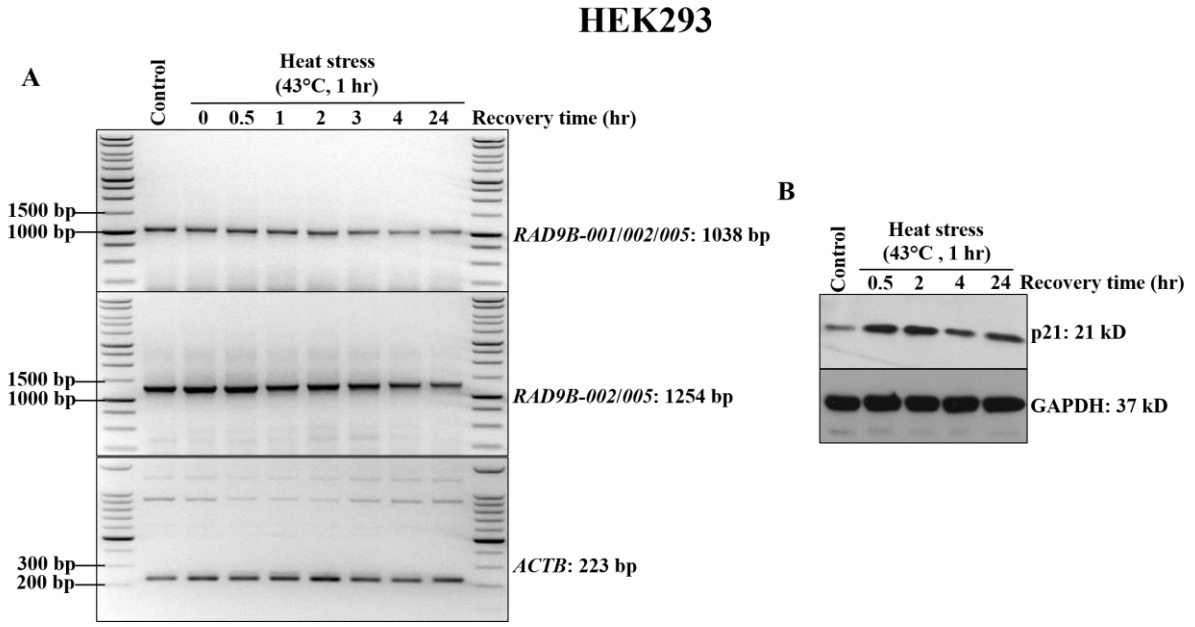

Figure 5.9 Analysis of *RAD9B* response to heat stress in HEK293 cell line. (A) RT-PCR of *RAD9B-001/002/005* and *RAD9B-002/005* in response to heat stress. Cells were incubated at elevated temperature (43°C) for 1 hr and total RNA was extracted at the indicated points. The expression of the *RAD9B* was normalised to the expression *ACTB*. (B) Whole protein was extracted from the heat treated cells at the indicated points and immunoblotted for the p21 protein used as the heat treatment control. The GAPDH was used as a protein loading control.

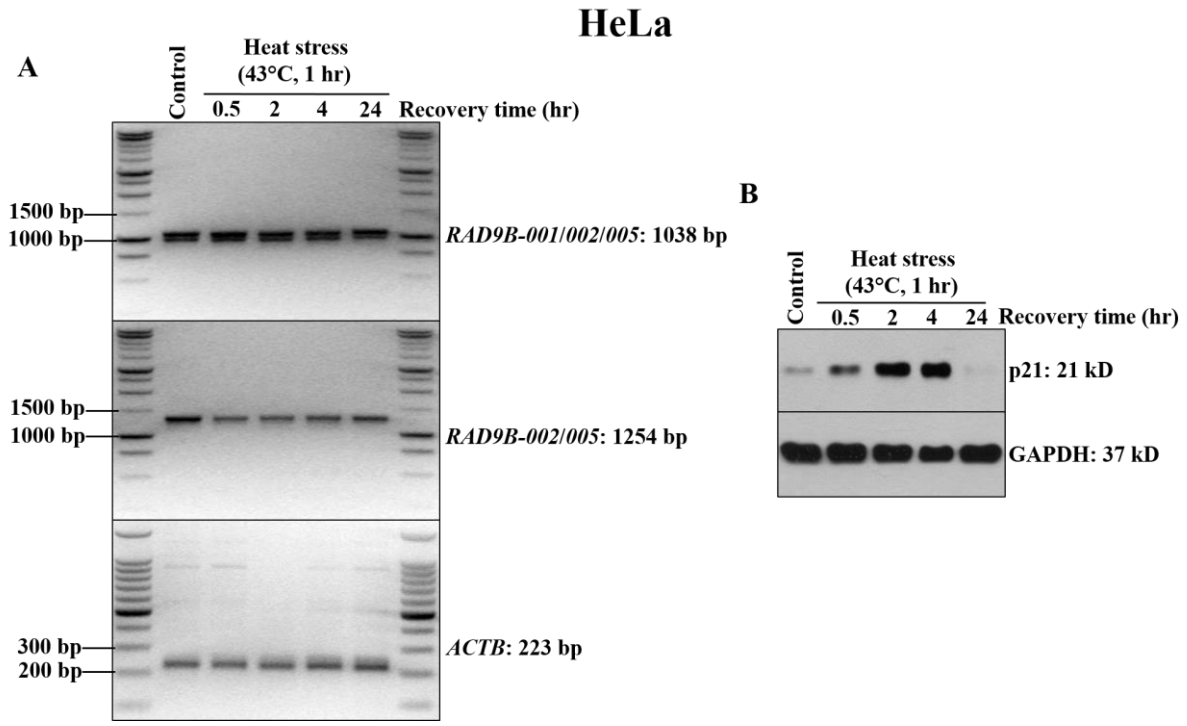

Figure 5.10 Analysis of *RAD9B* response to heat stress in HeLa cell line. RT-PCR of *RAD9B-001/002/005* and *RAD9B-002/005* in response to heat stress. Cells were incubated at an elevated temperature (43°C) for 1 hr and total RNA was extracted at the indicated points. The expression of RAD9B was normalised to the expression *ACTB*. (B) Whole protein was extracted from heat treated cells at the indicated points and immunoblotted for the p21 protein used for as the heat treatment control. The GAPDH was used as a protein loading control.

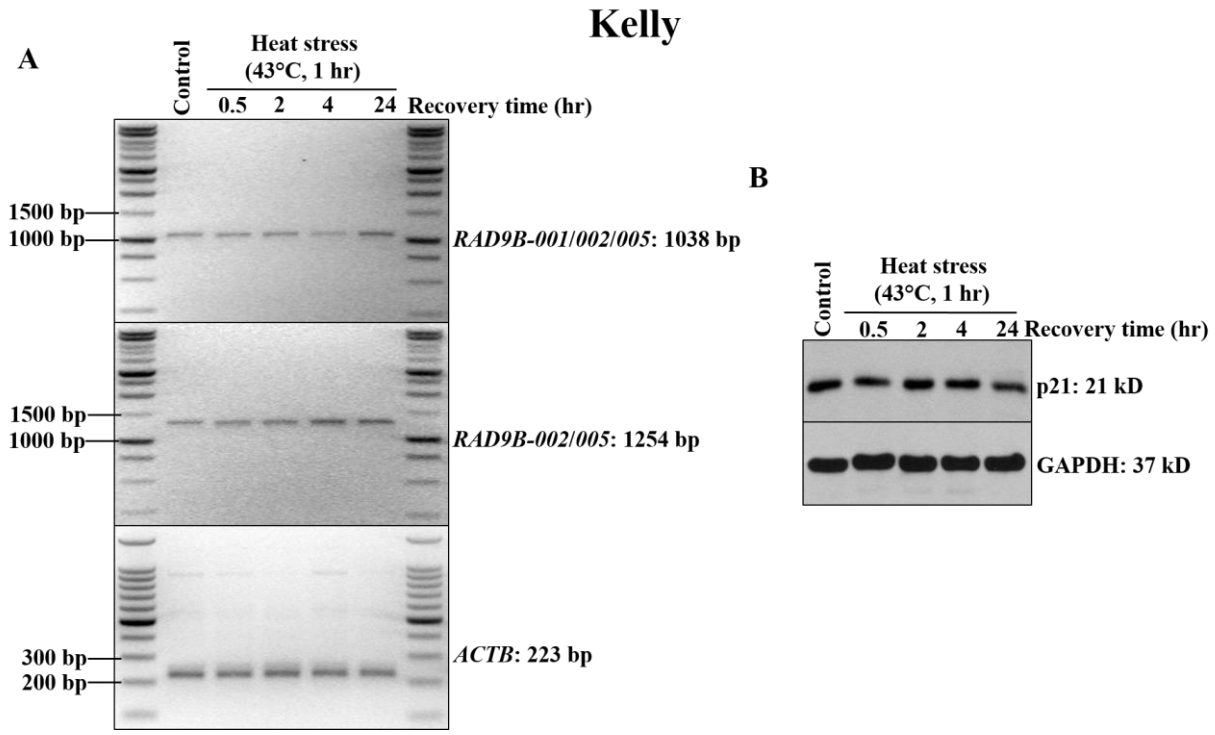

Figure 5.11 Analysis of *RAD9B* response to heat stress in Kelly cell line. (A) RT-PCR of *RAD9B-001/002/005* and *RAD9B-002/005* in response to heat stress. Cells were incubated at elevated temperature (43°C) for 1 hr and total RNA was extracted at the indicated points. The expression of *RAD9B* was normalised to the expression of *ACTB*. (B) Whole protein was extracted from the heat treated cells at the indicated points and immunoblotted for the p21 protein used as the heat treatment control. The GAPDH was used as a protein loading control.

5.2.7 Over-expression of EGFP-RAD9B-001 results in high phosphorylation of CHK2 in the response to heat stress

To test whether expression of the human RAD9B variants has an impact on the modification of CHK2 under heat stress conditions, ATM, CHK2, MPS1, p53 and p21 were analysed after incubation at 43°C for 1 hr. Samples were collected 30 min and 2 hr post-treatment. Since, the CHK2 protein was not found to be phosphorylated in response to heat stress in previous chapter (Figure 4.19), here the concentration of the antibody was doubled to allow for the detection of CHK2 phosphorylation in case it occurred. As shown in Figure 5.12, CHK2 phosphorylation at Thr-68, which was only very slightly induced in the EGFP control cells, was strongly upregulated in cells expressing EGFP-RAD9-001 and to a lesser degree in EGFP-RAD9B-002 expressing cells. This is in line with the hyper-phosphorylation of CHK2 in untreated EGFP-RAD9B-001 cells and to the partial hyper-phosphorylation in EGFP-RAD9B-002 cells (Figure 5.2). Interestingly up to three phosphorylated CHK2 bands were observed. As in the previous experiment (Figure 5.8) the levels of the faster migrating CHK2 band and the 45 kD Mps1 band were decreased in heat-treated EGFP-RAD9B-002 cells (Figure 5.12).

Taken together these findings strengthen the conclusion that over-expression of the shorter 001 variant of human RAD9B has a specific impact on CHK2 phosphorylation especially in untreated or heat treated cells. A similar function is not provided by the related yeast variant. Full-length RAD9B-002 has also an impact on CHK2 modification which is however much reduced compared to its shorter variant. It should be pointed out that the amino acid sequence is identical between RAD9B-001 and RAD9B-002, and that the only difference between the variants is the absence of the N-terminal 72 aa.

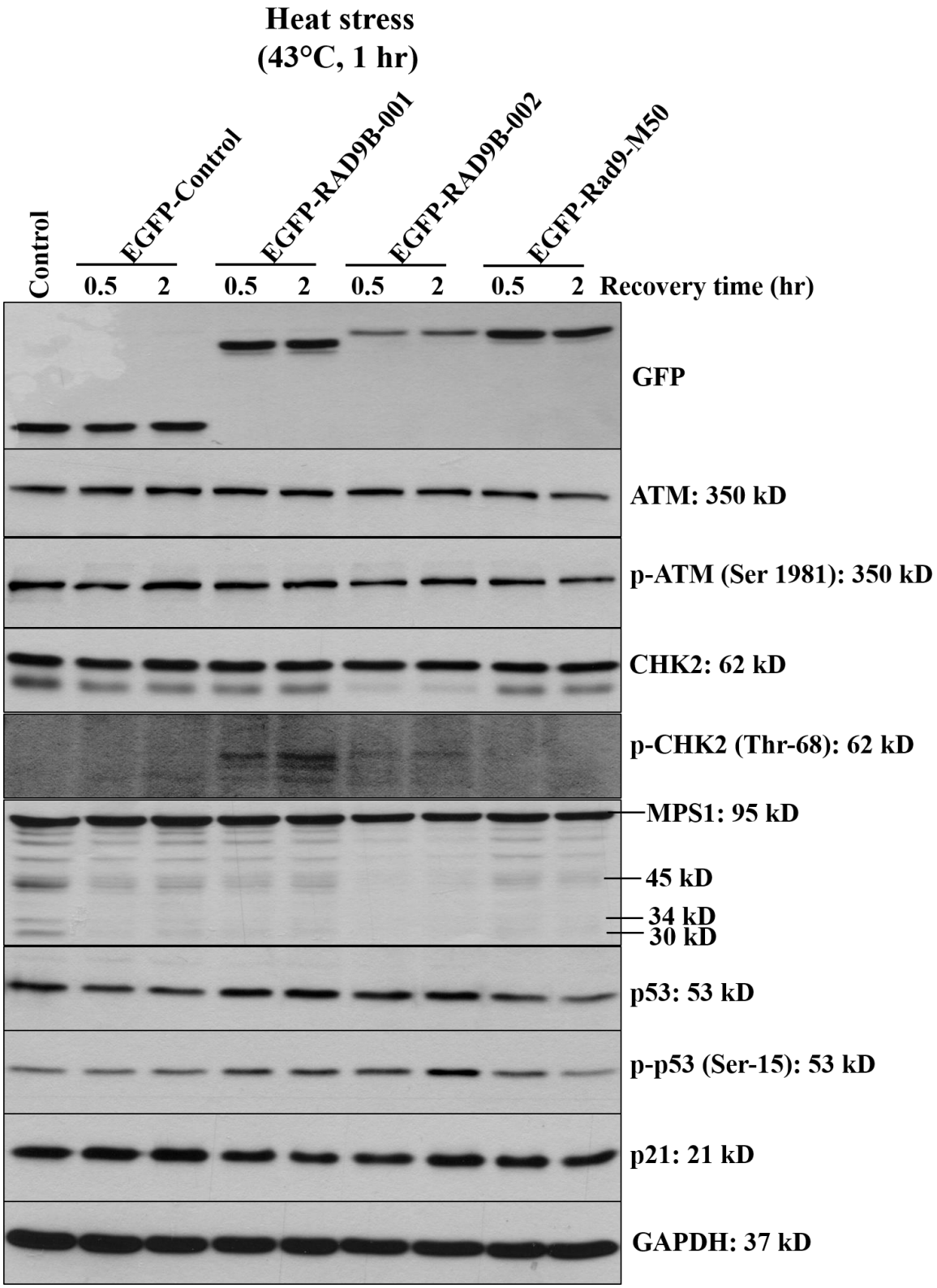

Figure 5.12 Analysis of CHK2 phosphorylation in response to heat stress in the constructed cell lines. The four constructed cell lines, EGFP-Control, EGFP-RAD9B-001, EGFP-RAD9B-002 and EGFP-Rad9-M50, were induced with doxycycline over-night followed by heat treatment (43°C) for 1 hr and cells were then left to recover for 30 min and 2 hr. Whole protein was extracted from the recovered cells and was subject to normal SDS-PAGE immunoblotted with the indicated antibodies. GAPDH was used as a loading control.

5.2.8 *RAD9B-001* and *RAD9B-002* are required after oxidative DNA damage.

Oxidative stress can lead to both DNA single and double strand breaks (Driessens et al., 2009). Therefore, the expression of *RAD9B-001* and *RAD9B-002* was analysed in cells treated with moderate doses of H_2O_2 (500 µM). As in the previous treatments, the transcriptional *RAD9B* response was analysed in the normal cell line (HEK293) and the cancer cell lines (HeLa and Kelly). Of the three cell lines, and similar to the UV treatment, the Kelly cells revealed a high sensitivity to H_2O_2, as the treatment was 100% lethal after less than 24 of incubation with H_2O_2, therefore the response of *RAD9B* was analysed only up 4 hr after addition of the drug.

The *RAD9B-002/005* mRNA expression was found to be mostly stable for up to 24 hr after the addition of H_2O_2 in HEK293 cells (Figure 5.13). Surprisingly, the *RAD9B-001/002/005* expression increased significantly after 1 hr of incubation with H_2O_2 and remained high throughout the rest of the experiment. 24 hr after incubation with H_2O_2 almost 100% of HEK293 cells were alive despite morphological alterations due to the oxidative stress. This suggests that 500 µM H_2O_2 is a sub-lethal dose for HEK293 cells.

In HeLa cells, the *RAD9B-001/002/005* mRNA expression peaked between 2hr and 4hr with a transient drop at the 30min time point. The levels of *RAD9B-002/005* did not change (Figure 5.14).

Kelly cells did not reveal a change of any mRNA levels. There was only a drop after 4 hr which could be linked with their high sensitivity to oxidative stress (Figure 5.15).

In both the HeLa and Kelly cell lines, p21 was quickly degraded after the addition of H_2O_2. The degradation of p21 in both cell lines was irreversible indicating that these cancer cell lines might have had an instant response to oxidative stress. However, different results for p21 were observed in the HEK293 cell line. Here, the p21 protein was degraded after the start of the treatment, as in HeLa and Kelly cells, but the levels recovered significantly 24 hr after incubation with H_2O_2.

These results indicate that the *RAD9B* splice variants are required for the response to oxidative stress in HEK293 and HeLa cells. In addition, these results show clearly how different cells can respond the same type of cellular stress.

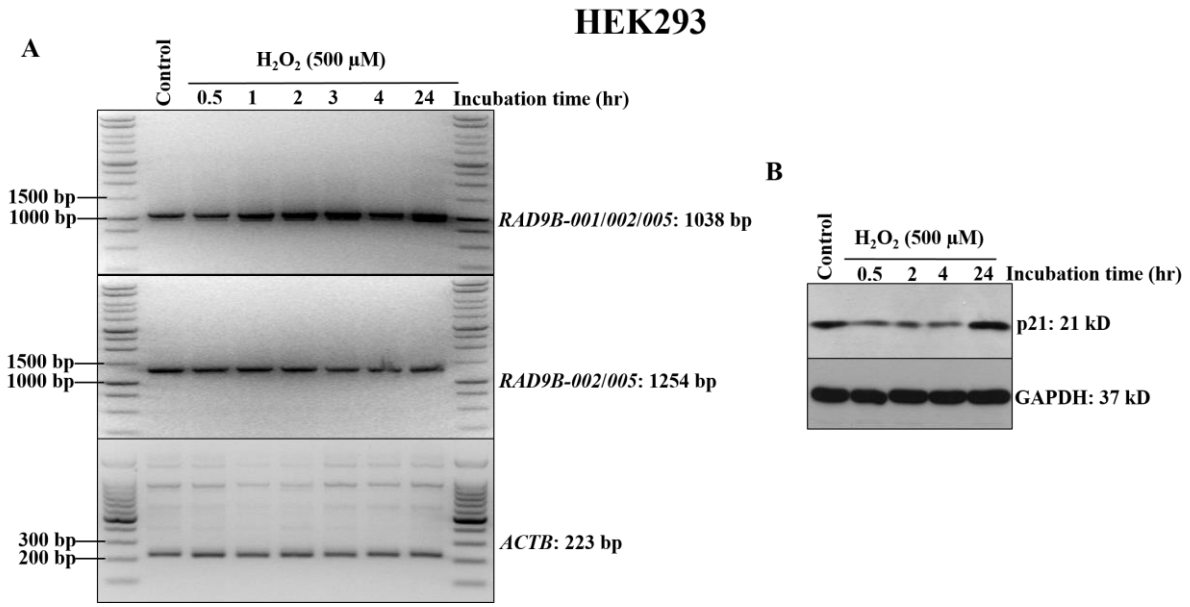

Figure 5.13 *RAD9B-001* mRNA expression levels increase in response to H_2O_2 in HEK293 cells. (A) Expression levels of *RAD9B-001/002/005* and *RAD9B-002/005* in response to H_2O_2. Cells were incubated with 500 µM and total RNA was extracted from normal (control) and treated cells at the indicated time points. The expression levels of *RAD9B-001/002/005* and *RAD9B-002/005* were detected in normal and treated cells using the one step RT-PCR. The expression of the *RAD9B* splice variants was normalised to the expression *ACTB*. (B) Whole protein was extracted from H_2O_2 treated cells at the indicated time points and immunoblotted for the p21 protein used as the H_2O_2 treatment control. The GAPDH was used as a protein loading control.

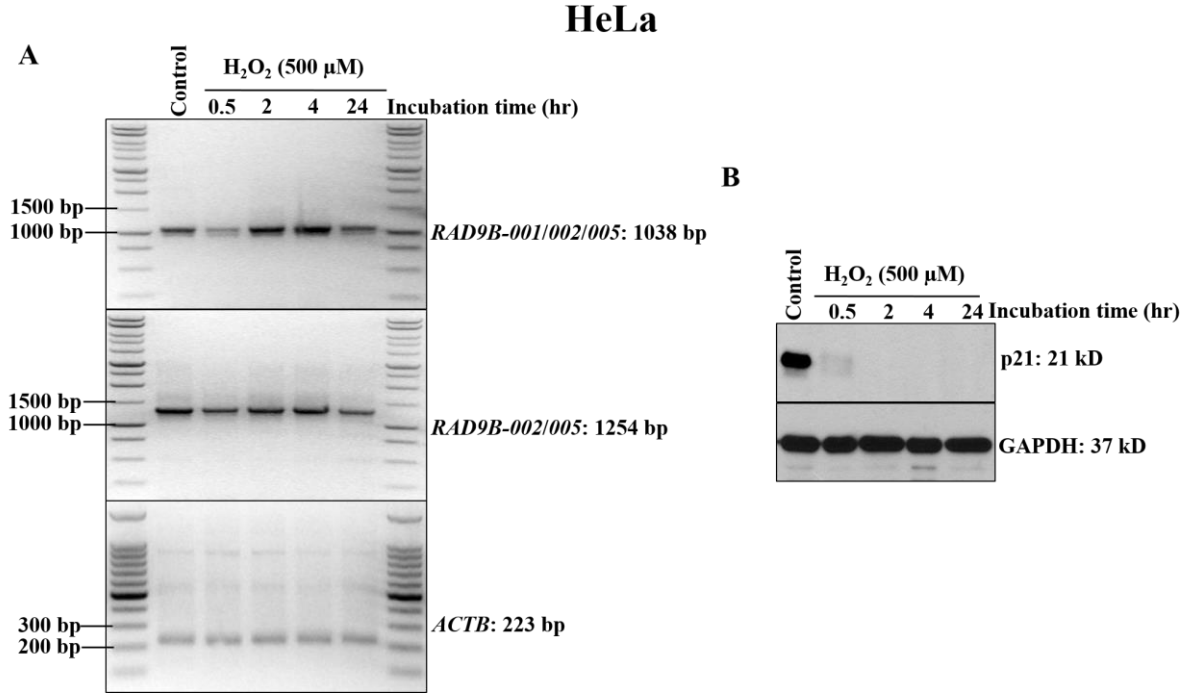

Figure 5.14 *RAD9B-001* mRNA expression level increases in response to H_2O_2 in HeLa cells.
(A) Expression levels of *RAD9B-001/002/005* and *RAD9B-002/005* in response to H_2O_2. Cells were incubated with 500 µM H_2O_2 and total RNA was extracted from normal (control) and treated cells at the indicated time points. The expression levels of *RAD9B-001*/*002*/*005* and *RAD9B-002*/*005* were detected in normal and treated cells using the one step RT-PCR. The expression of the *RAD9B* splice variants was normalised to the expression of *ACTB*. (B) Whole protein was extracted from H_2O_2 treated cells at the indicated time points and immunoblotted for the p21 protein used as H_2O_2 treatment control. The GAPDH was used as a protein loading control.

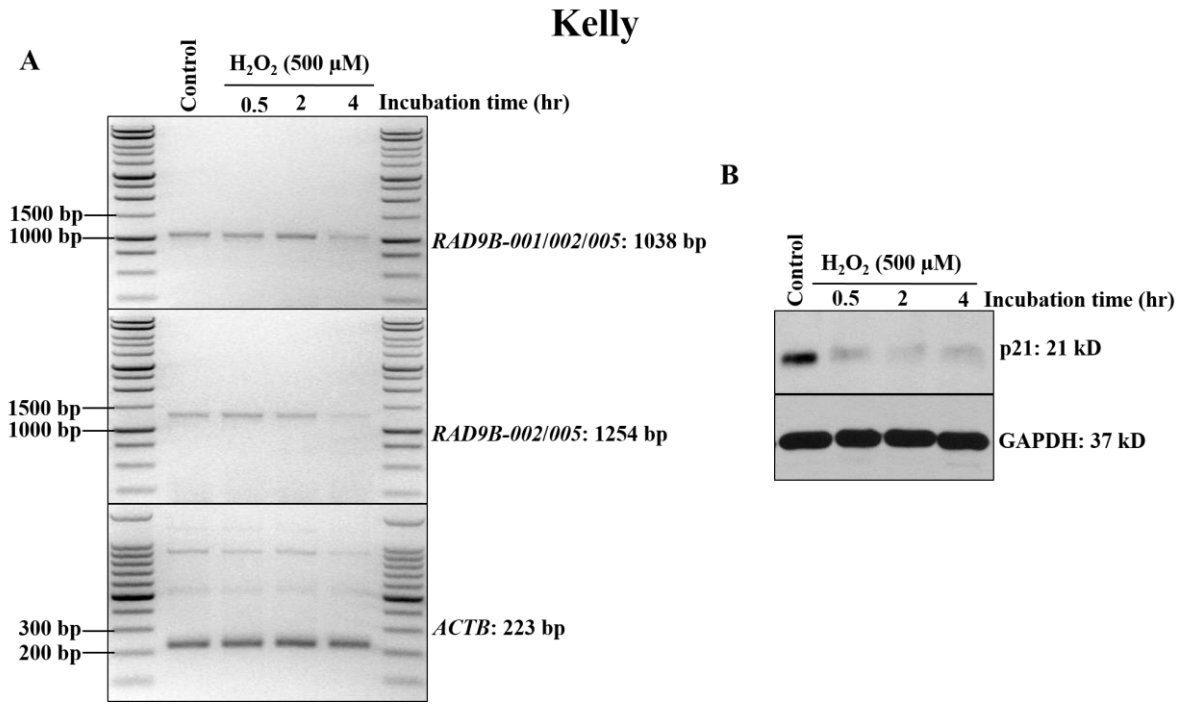

Figure 5.15 Analysis of *RAD9B* splice variants in response to H_2O_2 in the Kelly cell line. (A) Expression levels of *RAD9B-001/002/005* and *RAD9B-002/005* in response to H_2O_2. Cells were incubated with 500 µM H_2O_2 and total RNA was extracted from normal (control) and treated cells at the indicated time points. The expression levels of *RAD9B* splice variants were detected in normal and treated cells using the one step RT-PCR. The expression of the *RAD9B* splice variants was normalised to the expression of *ACTB*. (B) Whole protein was extracted from H_2O_2 treated cells at the indicated time points and immunoblotted for the p21 protein used as H_2O_2 treatment control. The GAPDH was used as a protein loading control.

5.2.9 Over-expression of EGFP-RAD9B-001 results in increased phosphorylation of Chk2 in response to H_2O_2.

On the basis of the results described previously (Figure 5.13), H_2O_2 appears to be an inducer of the *RAD9B-001* splice variant, therefore, the role of this variant in response to H_2O_2 was investigated further in the EGFP-RAD9B-001 constructed cell line. The analysis of CHK2 phosphorylation at Thr-68 revealed a strong response to oxidative stress in cells over-expressing EGFP-RAD9B-001 (Figure 5.16). While CHK2 was phosphorylated after 2 hr and 4 hr in the presence of hydrogen peroxide in the EGFP control cell line, the levels were strongly increased in the presence of EGFP-RAD9B-001 and to a lesser extent in the presence of the yeast variant (Figure 5.3). Interestingly, the high phosphorylation of CHK2 in the EGFP-RAD9B-001 cell line correlates with increased *RAD9B-001* mRNA levels in response to H_2O_2 (Figure 5.13). The other interesting observation was the very low CHK2 phosphorylation levels in the presence of EGFP-RAD9B-002 which could indicate that this variant suppresses CHK2 modification as observed in
Figure **5.8**.

As shown previously, the p21 protein levels dropped in the response to H_2O_2. Surprisingly, expression of EGFP-RAD9B-002 at the 2 hr time point showed unusually high p21 levels (Figure 5.16).

When the H_2O_2 treated samples were analysed on a phos-tag SDS page, neither RAD9B-001 nor RAD9B-002 revealed any changes in their phosphorylation status after 2 hr and 4 hr of incubation with H_2O_2. However, the yeast Rad9-M50 variant became phosphorylated in response to H_2O_2 (Figure 5.17). This indicates that human cells recognise the yeast variant during the response to oxidative stress.

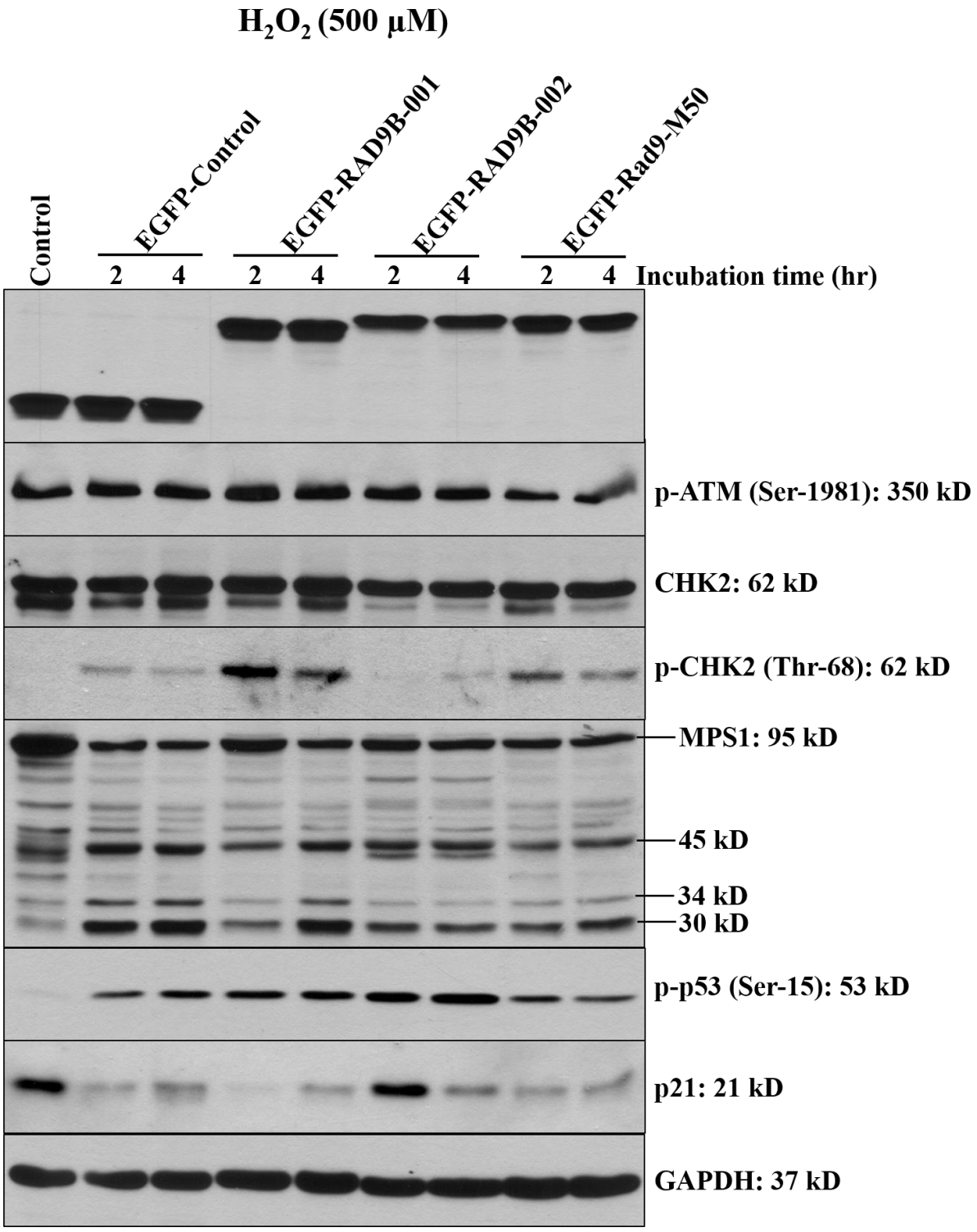

Figure 5.16 Exposure of EGPF-RAD9B-001 and EGFP-RAD9B-002 to H_2O_2 reveals different status in the phosphorylation of CHK2. Representative western blot shows levels of ATM, p-ATM, CHK2, p-CHK2, MPS1, p-p53 and p21 obtained from the over-expressed constructed cell lines exposed to H_2O_2 (500 μM) for 2 hr and 4 hr. GAPDH was used as a positive control.

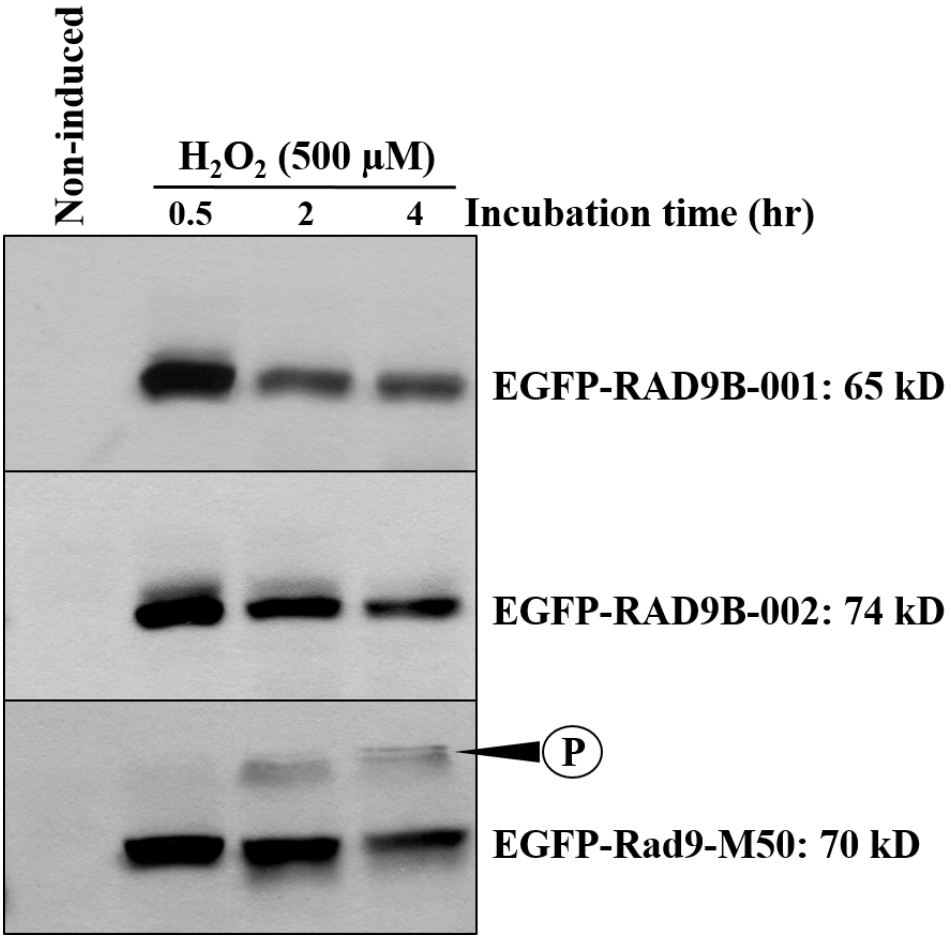

Figure 5.17 Separation of EGFP-RAD9B-001, RAD9B-002 and EGFP-Rad9-M50 H_2O_2 treated samples on phos-tag SDS-PAGE. Cell lines were incubated with H_2O_2 (500 µM) for 2 and 4 hr. Whole protein extracted from normal and treated cells was analysed on phos-tag SDS-PAGE. Only the Rad9-M50 revealed an additional top band in response to H_2O_2, reflecting the phosphorylation isoform.

5.2.10 Dephosphorylation of CHK2 by hRad9B-002 in response to H_2O_2 may be dependent on MPS1 protein.

To investigate the possible role of RAD9B-002 in dephosphorylating the CHK2 kinase in response to H_2O_2 and to find out whether the dephosphorylation is dependent on MPS1 kinase, the phosphorylation status of CHK2 kinase was analysed in the presence and absence of the MPS1 inhibitor (AZ 3146, Selleck Chemicals) in response to H_2O_2 in the over-expressing RAD9B-002 cell line. To inhibit the Mps1, cells were incubated with 2µM of AZ 3146 for 72 hr. Cells were then exposed to 500µM H_2O_2 for 2 hr.

Western blot analysis revealed that CHK2 is indeed a target of MPS1 kinase as its phosphorylation was reduced upon inhibition of MPS1 under oxidative stress conditions. As observed previously, induction of EGFP-RAD9B-002 reduced CHK2 phosphorylation in the presence of hydrogen peroxide. Interestingly, the reduction was partly released upon inhibition of MPS1 (Figure 5.18). These results indicate that CHK2 kinase is de-phosphorylated in EGFP-RAD9B cells in a manner partly dependent on MPS1 kinase. Moreover, CHK2 protein levels also seemed to be reduced when MPS1 protein was blocked in both the induced and non-induced EGFP-RAD9B-002 cell line.

The main band of the MPS1 (95 kD) was not affected by either its inhibition or the over-expression of EGFP-RAD9B-002. However, the 45 kD band, which increased in intensity upon induction of the RAD9B variant, was affected by Mps1 inhibition (Figure 5.18). This implies that the induction of RAD9B-002 increases this 45 kD band in a manner dependent on MPS1 kinase. If this smaller band is a cleavage product of MPS1, RAD9B-002 may affect this cleavage but only when MPS1 is active (Figure 5.18). Taking this together, RAD9B-002 may function in relationship with MPS1 in the regulation of CHK2 phosphorylation.

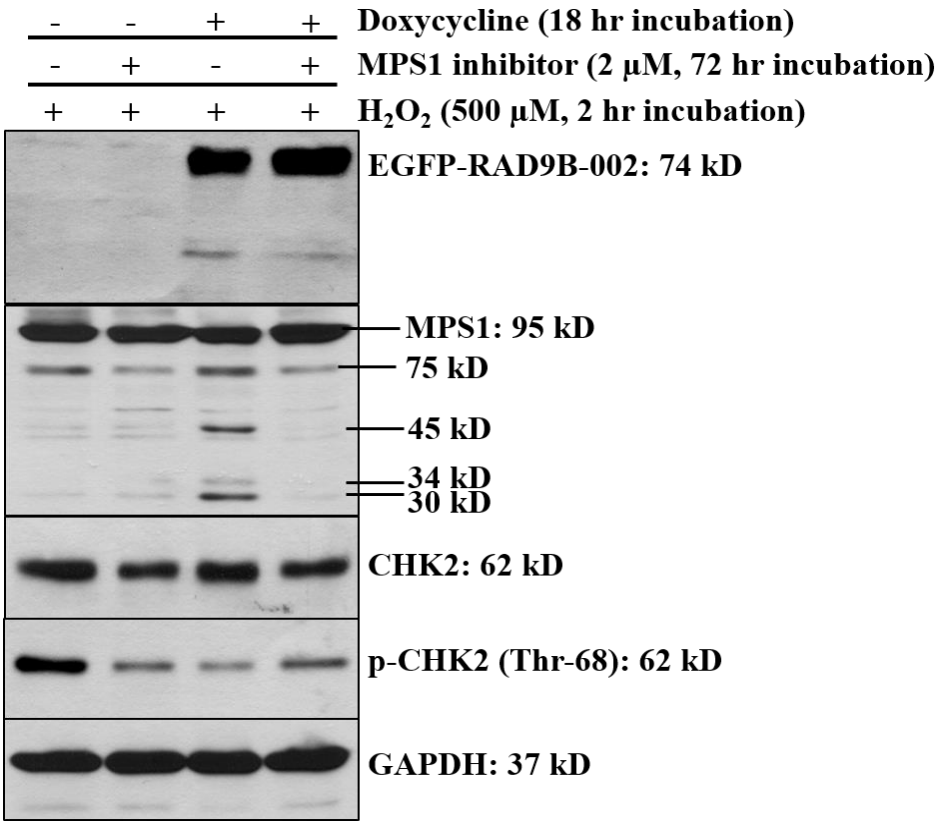

Figure 5.18 Analysis of CHK2 phosphorylation in response to H_2O_2 after inhibition of MPS1 kinase in over-expressed EGFP-RAD9B-002 cell line. EGFP-RAD9B-002 cells were either incubated with MPS1 inhibitor (2µM) for 72 hr or were left untreated. The EGFP-RAD9B-002 cell line then was either induced with doxycycline (1 µg/ml) or left without induction. The cells then were incubated with H_2O_2 (500 µM) for 2 hr and whole protein was extracted and subjected to SDS-PAGE, immunoblotted with GFP, MPS1, CHK2 and p-CHK2 antibodies. GAPDH was used as a loading control.

6.3 Discussion

The key findings of this chapter are as: (1) elevated levels of RAD9B-001 and to a lesser extent RAD9B-002 result in high phosphorylation of CHK2 kinase in untreated cells. (2) Over-expression of RAD9B-002 inhibit the phosphorylation of CHK2 at Thr-68 in the response to UV light and oxidative stress caused by H_2O_2 in an ATM-independent manner. This influence on the phosphorylation of CHK2 seems to be dependent on the mitotic MPS1 kinase. (3) An opposite role was detected for the RAD9B-001 variant in controlling the phosphorylation of CHK2 in the response to H_2O_2. CHK2 appeared highly phosphorylated compared to the treated control cell line. This increased phosphorylation at Thr-68 is in line with the increased mRNA expression of *RAD9B-001* in response to H_2O_2.

Over-expression of RAD9B-001 or RAD9B-002 results in the elevated phosphorylation of CHK2 kinase under normal conditions in a manner which appears independent of ATM (Figure 5.2). Similar results were obtained in the previous chapter with p21 phosphorylation. Moreover, over-expression of RAD9B-001 caused a transient G1 arrest which has also been reported upon over-expression of p21 (Mansilla et al., 2013).

CHK2 kinase is phosphorylated at Thr-68 by ATM in the response to DNA damage. ATM activation depends on the type of DNA lesion. When DNA breaks occur, ATM is recruited to the break by NBS1 in the RAD50-MRE11-NBS1 complex and undergoes autophosphorylation at Ser-367, Ser-1893, Ser-1981 and Ser-2996 and TIP60-dependent acetylation at K3016 (Stracker et al., 2013). However, in the response to oxidative stress, ATM forms an active homodimer upon oxidation of cysteine residues. Both conditions result in the phosphorylation of CHK2 kinase. Interestingly, over-expression of RAD9B-001 and to a lesser extend RAD9B-002 results in the hyper-phosphorylation of CHK2 in untreated HEK293 cells (Figure 5.2). This indicates that the phosphorylation of CHK2 is a result of either the presence of DNA damage caused by the over-expression or the recruitment of a kinase to CHK2.

The partial hyper-phosphorylation of CHK2 in untreated RAD9B-002 cells could be linked with the appearance of the sub-G1 cell population which may have undergone cell death in the response to chromatin abnormalities.

It is however interesting that ATM phosphorylation was not elevated at Ser-1981 (Figure 5.2) which indicates that another kinase targets CHK2 under these conditions. Over-expression of RAD9B-001, the shorter variant, did only transiently arrest cells in G1 but caused high CHK2 phosphorylation in untreated cells (Figure 5.2). This implies that the shorter variant also targets another kinase to CHK2 as no changes to ATM phosphorylation at Ser-1981 were observed (Figure 5.2).

Interestingly, when RAD9B-002 was over-expressed in response to UV radiation, the CHK2 Thr-68 phosphorylation was significantly reduced compared to the high phosphorylation in the control cell line (Figure 5.8). UV-irradiated cells have increased levels of the tumour suppresser p53, but over expression of RAD9B-002 had no impact on p53 under these conditions (Figure 5.8) suggesting that the changes to CHK2 modification are not channelled into the p53 pathway. The delay of p21 degradation by high RAD9B-001 and yeast Rad9-M50 protein levels (Figure 5.8) do however not correlate with the hyper-phosphorylation of CHK2 as this is absent in cells with high levels of the yeast variant . This shows that the impact on p21 degradation in the response to UV is independent of the changes to CHK2 Thr-68 phosphorylation.

The experiments this chapter revealed a possible functional link between the RAD9B and MPS1 kinase. MPS1 kinase plays a role in the cell response to UV radiation, oxidative stress and during mitosis at the centrosome (Marquardt et al., 2016). Cells with down-regulated MPS1 showed a reduction in the phosphorylation of CHK2 at Thr-68 and a G2/M arrest defect after UV radiation with a population of sub-G1 cells (Wei et al., 2005). Interestingly, MPS1 levels in addition to its smaller forms were reduced upon over-expression of EGFP-RAD9B-002 in response to UV radiation, while this reduction correlated with a reduction in the phosphorylation of CHK2 (Figure 5.8). It is therefore likely that elevated levels of RAD9B-002 affect MPS1 kinase in response to UV damage which consequently results in a reduction in CHK2 Thr-68 phosphorylation. This is in line with the ability of MPS1 to target Thr-68 (Wei et al., 2005) and its activation in response to DNA damage caused by UV light (Huang & Shieh, 2016; Zhang et al., 2013).

In response to the oxidative stress caused by H_2O_2, both kinases, ATM and CHK2, in addition to histone H2AX serine-139 modification are activated. The phosphorylation of these proteins was detected mostly in S phase (Zhao et al., 2008). When oxidative stress was triggered in the RAD9B cell lines, the CHK2 phosphorylation at Thr-68 was significantly reduced upon RAD9B-002 over-expression, but increased phosphorylation was detected in the RAD9B-001 over-expressing cell line (Figure 5.16). As summarised in the chapter 3, *RAD9B-002* mRNA expression levels were reduced when cells underwent the G1-S transition which indicates that RAD9B-002 interferes with this cell cycle stage. Alternatively, it may also indicate that RAD9B-002 is not expressed during S phase. Taking this together, it may be possible that forced elevated levels of RAD9B-002 result in a drop in the CHK2 phosphorylation during S phase.

The MPS1 inhibitor experiment (Figure 5.18) is in line with this suggestion as CHK2 Thr-68 phosphorylation levels are reduced upon the down-regulation of MPS1 activity. Interestingly, the negative impact of RAD9B-002 over-expression on CHK2-Thr-68 modification is mitigated upon inhibition of MPS1 which implies that the variant depends on high MPS1 activity to block or dephosphorylate CHK2-Thr-68. Given that MPS1 activity is essential for the spindle attachment checkpoint at the kinetochore during mitosis (Isokane et al., 2016), it could be that elevated RAD9B-002 levels affect CHK2-Thr-68 modification during mitosis. Thr-68 phosphorylated CHK2 is localised to the centrosome where it can be phosphorylated by Polo like kinase 1 (PLK1) (Tsvetkov et al., 2003). Human MPS1 kinase is required for centrosome duplication during S phase through regulation by CDK2 which phosphorylates MPS1 directly and this phosphorylation suppresses the protostome-mediated degradation of MPS1 (Cui et al., 2010; Kasbek, Yang & Fisk, 2009). Since CHK2 phosphorylates MPS1 at Thr-288 in the response to IR which leads to G2/M arrest (Yeh et al., 2009; Wei et al., 2005), it is possible that RAD9B-002 interferes with a kinase system at the centrosome and/or the kinetochore during mitosis which consists of CHK2, MPS1 and PLK1. Since the data for the different treatments revealed that over-expression of RAD9B-002 reduced the amount of a smaller, 45 kD band of MPS1, the variant may also suppress the proteasome-mediated degradation of MPS1 during G1 and S phase and thereby indirectly affect the centrosome. As shown in the model (Figure 5.19), the best explanation of the results is provided by a negative impact of RAD9B-002 on PLK1 kinase.

The key observation is that inhibition of MPS1 kinase partly restores CHK2-Thr-68 phosphorylation by reducing the ability of RAD9B-002 to negatively impact on it (Figure 5.18). This strongly indicates that MPS1 is not blocked by the variant but that MPS1 is required to stimulate a protein which is the target of RAD9B-002. If RAD9B-002 were to directly block MPS1, its over-expression and the inhibition of MPS1 should have an additive impact on CHK2-Thr-68 phosphorylation causing a much stronger reduction which is not the case. It is therefore more likely that RAD9B-002 blocks CHK2-Thr-68 modification by down-regulating PLK1 kinase or another kinase which can target CHK2-Thr-68. This view is supported by a close functional relationship between MPS1 and PLK1 kinase (von Schubert et al., 2015).

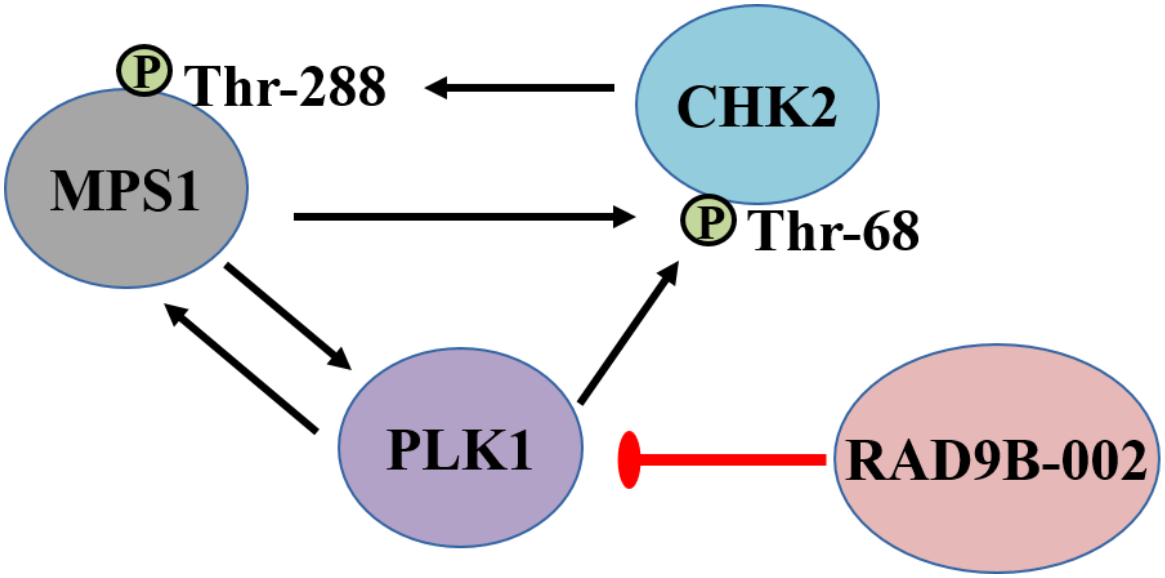

Figure 5.19 Possible down-regulation of polo like kinase (PLK1) by RAD9B-002. Over-expression of RAD9B-002 may reduce CHK2-T68 phosphorylation in the presence of UV light and oxidative DNA damage by down-regulating PLK1. This down-regulation may require the activity of MPS1 at the kinetochore or centromere.

A role of RAD9B-002 at the centromere may also explain the accumulation of sub-G1 cells and the strong growth reduction upon its over expression. It would be interesting to test whether mitotic markers are accumulated in these cells and whether the biology of PLK1 is affected.

Chapter 6: GENERAL DISCUSSION

The current study focused on the role of the RAD9B splice variants in human cells. The study analysed the endogenous *RAD9B* expression at the mRNA level, since no commercial product is currently available to detect the RAD9B protein. In addition, the study analysed the effects of the over-expression of RAD9B-001 variant and full-length RAD9B-002 on the progression of the cell cycle and on the checkpoint pathways in the response to different types of DNA damage. The study discovered a number of interesting findings for each of the two RAD9B splice variants and revealed a possible relation between them. Table 6.1 summarises the over-expression effects of the RAD9B splice variants on cell proliferation and checkpoint proteins.

Table 6.1 Summary of the over-expression phenotypes

Rad9 Variant	**Cell Cycle Effect**	**CHK2-Phosph**	**CHK2-Phosph UV Light**	**Cleavage of Rad9 variant**	**p21 Deg UV Light**	**p21-Phosph**	**CHK2-Phosph H_2O_2**	**p21 Deg Oxidative stress**
RAD9B 001 (345aa)	G1 arrest	Hyper	Normal	None	Delayed	Yes	Hyper	Not delayed
RAD9B 002 (417aa)	Sub-G1 population	Partially hyper	Reduced	Cleaved	Not delayed	Yes	Reduced	Delayed
Yeast Rad9 (377aa)	None	None	Reduced	None	Delayed	None	Normal	Not delayed

*__deg__: degradation.*__phosph__: phosphorylation.

6.1 Low expression of *RAD9A* and *RAD9B*

Previous studies on *RAD9B* expression were mainly based on the northern blot technique rather than the RT-PCR assay which is more sensitive (Hopkins et al., 2003, Dufault et al., 2003). The northern blot has great specificity and allows for the detection of potential spliced transcripts of a gene in addition to giving a clear indication of the abundance of the particular gene. The disadvantage of using the northern blot assay is that it is not sufficiently accurate for the detection of weakly expressed genes. In such a situation, RT-PCR is the better option. In this project, RT-PCR analysis revealed contrary results for the expression of *RAD9B* splice

variants compared to previous published works. While earlier work identified three RAD9B transcripts in testis, skeletal muscle and heart, the more sensitive RT-PCR test revealed expression in most tested human tissues. However, *RAD9B* expression was extremely weak and the full length transcripts were only detected when the high sensitivity RT-PCR kits were used. The presence of *RAD9B* transcription across a wide range of human tissues indicates that the protein plays an essential role in different cell types in the body.

Interestingly, a study on Rad9 expression in *S. pombe* cells found that *Rad9* is expressed at a very low level and it was difficult to clone the cDNA (Murray et al., 1991). Work in budding yeast (*S. cerevisiae*) revealed that most genes involved in DNA repair have low expression (Friedberg, 1988). During evolution, low expression levels may have protected cells from the aberrant activation of the DDR genes. For example, high levels of RAD9A could induce apoptosis like elevated levels of HUS1B (Lee, Hirai & Wang, 2003; Hang et al., 2002). Expression of RAD9B seems to oscillate throughout the cell cycle as shown by the specific increase in *RAD9B* mRNA during the G1 phase (Figure 3.11). It should however be noted that high mRNA levels do not automatically translate into high protein levels as additional regulations are in place in the cell to control protein synthesis. It is also possible that the transcribed mRNA fulfils structural or regulatory functions independently from its role in translation (Kloc, Foreman & Reddy, 2011).

Many DDR genes are up-regulated in the presence of DNA lesions. For example, expression of p21 upon ionising radiation promotes a G1 cell cycle arrest (Abbas & Dutta, 2009). These conditions may also increase the levels of alternative transcripts of DNA repair or checkpoint genes (Forrester et al., 2012). This is consistent with the findings in this work that oxidative damage increases the expression of *RAD9B-001* (Figure 5.13).

Compared to *RAD9B*, expression of *RAD9A* is higher but still at a low level compared to many other genes, *Rad9A* is expressed in a wide variety of tissues and cell lines. A northern blot analysis using 16 different normal tissues showed expression of *RAD9A* in all tissues, whereas expression of *RAD9B* was only detected in testis, skeletal muscle and heart. The mouse *Rad9b* gene revealed a similar very low expression pattern to the human *RAD9B* (Hopkins et al., 2003). This difference suggests that cells tolerate only very low levels of RAD9B and that RAD9B may be responsible for infrequent events or events which occur only in a sub-compartment of the cell. This notion is in line with the role of RAD9B in the

nucleolus after UV irradiation (Perez-CastroFreire, 2012) and the observation in this work that over-expression of RAD9B-001 delays cells in G1 (Figure 4.13 & 4.14). It is noteworthy that RAD9A is well known for its role in the activation of the ATR-CHK1 pathway at DNA lesions with single-stranded DNA but has no direct impact on the ATM-CHK2 system at broken chromosomes which did not undergo end resection (Ohashi et al., 2014). The results presented here suggest that RAD9B impacts on the modification of CHK2 kinase but not of CHK1. This would place RAD9B in the context of the ATM-CHK2 pathway and may explain why gene duplication was necessary during the evolution of multicellular organisms. In single cell organisms like the fission yeast ATR (Rad3) activates both Chk1 and Chk2 which would make a second Rad9 protein dedicated to the ATM (Tel1)-Chk2 system obsolete.

6.2 The role of RAD9A and RAD9B in tumorigenesis

To find out whether changes in the *RAD9B* gene are associated with cancer development, the 148 cancer studies curated in the cBioPortal database were searched for *RAD9B* alterations (http://www.cbioportal.org. Accessed 11 February 2017). As shown in Figure 6.1, 59 studies reported changes in this gene, which were on average less frequent when compared with other cancer promoting genes. It was however interesting to see that the majority of changes are amplifications of the *RAD9B* gene. In line with the earlier discussion on the low expression level of *RAD9B*, this implies that cancer cells may benefit from higher levels of RAD9B. The highest number of cases (19) were reported in the Neuroendocrine Prostate Cancer (NEPC) (Trento/Cornell/Broad 2016) study (Beltran et al., 2016). It was very interesting to find that mutations in three genes, *PSD1* (significance 3.2), *FANCI* (significance 2.3) and *PDP1* (significance 1.2) had a high co-occurrence rate with the amplification of the *RAD9B* gene (Figure 6-2). The *PSD1* gene encodes a Pleckstrin homology and SEC7 domain-containing protein that functions as a guanine nucleotide exchange factor. It regulates signal transduction by activating ADP-ribosylation factor 6 (ARF6). ARF6 is involved in cell migration and the formation of metastasis (Sabe, 2003).

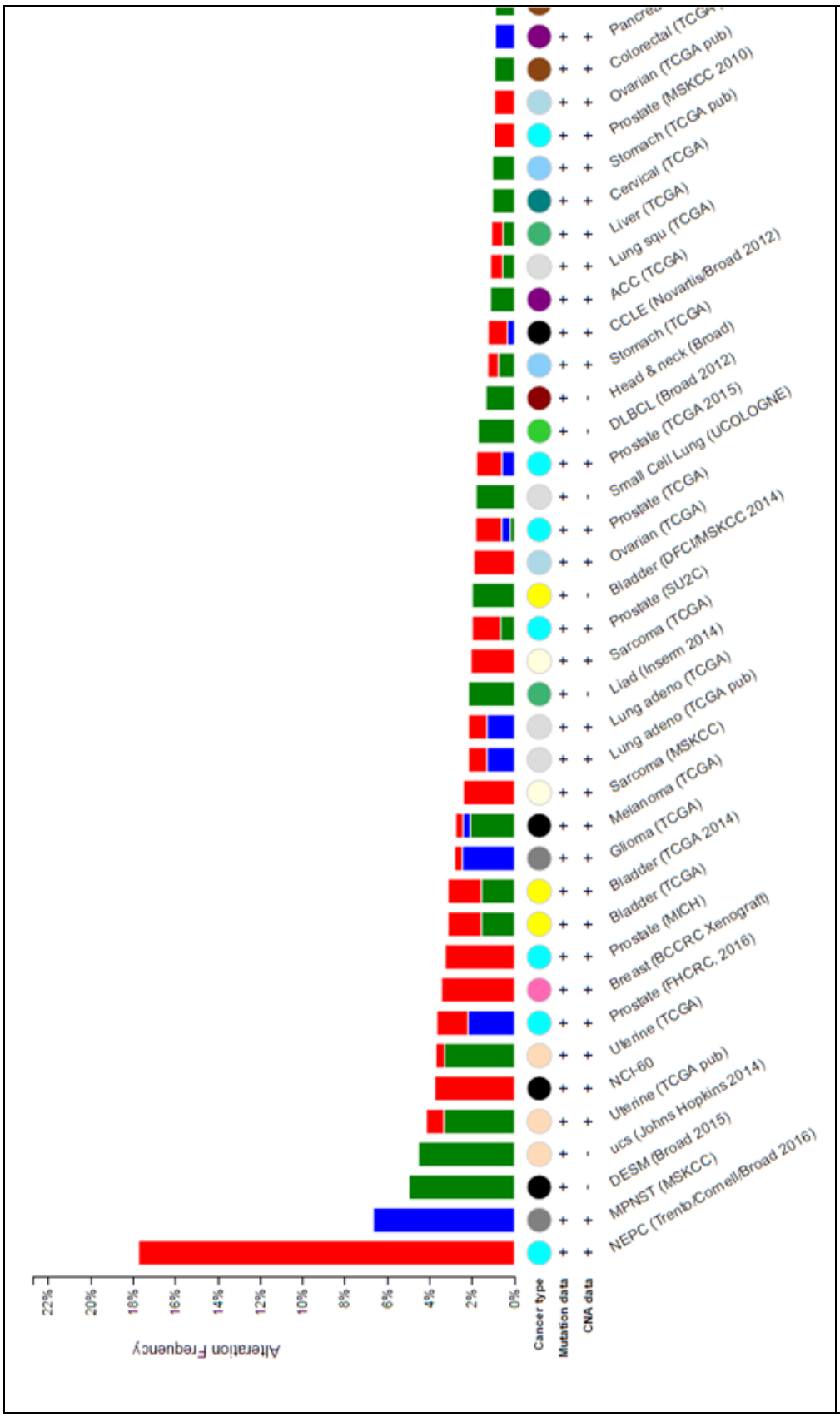

Figure 6.1 Genomic alterations of the human *RAD9B* gene. The analysis of 148 cancer studies curated in the CBioPortal database revealed 59 studies in which genetic changes to the *RAD9B* gene were detected. Interestingly the majority of alterations were amplifications of the gene (red color), whereas single nucleotide mutations (green) and gene deletions (blue) were less frequent. The highest number of patients with amplifications (19 cases) were detected in the Neuroendocrine Prostate Cancer (NEPC) (Trento/Cornell/Broad 2016) study (first red bar on the left). (http://www.cbioportal.org. Accessed 11 February 2017).

FANCI is a member of the Fanconi anemia protein complex. It is required for the repair of DNA double-strand breaks by homologous recombination and in the repair of interstrand DNA cross-links (Boisvert & Howlett, 2014). *PDP1* encodes the Pyruvate Dehydrogenase Phosphatase Catalytic Subunit 1 which has phosphatase activity and locates to the matrix of the mitochondria (Vassylyev & Symersky, 2007).

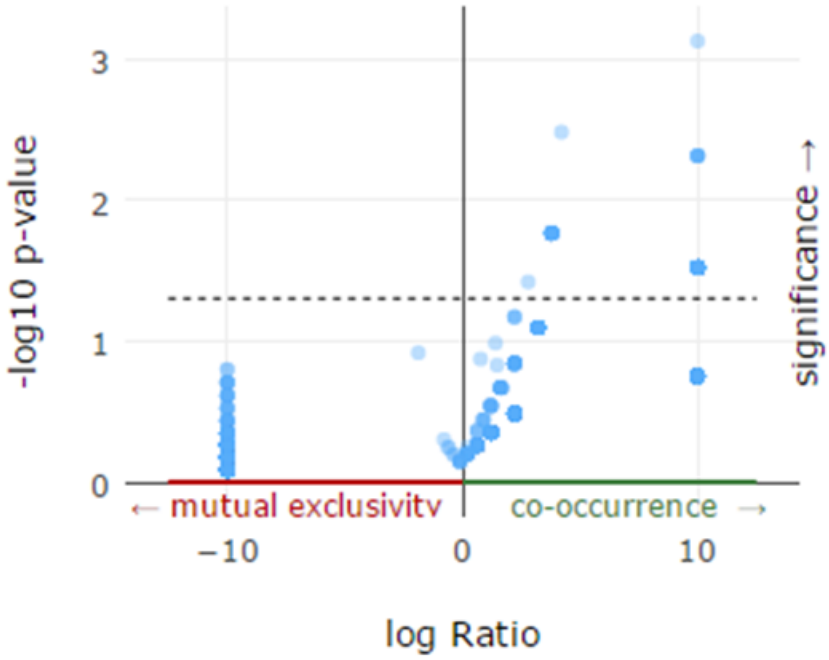

Figure 6.2 Genetic mutations which co-occur with the amplification of the *RAD9B* gene. Mutations in the three genes co-occur with *RAD9B* amplification (the three blue dotes at log 10 Ratio above the dotted line with high significance). The genes are *PSD1* (significance 3.2), *FANCI* (significance 2.3) and *PDP1* (significance 1.2). (http://www.cbioportal.org. Accessed 11 February 2017).

The gene with the highest probability of being co-amplified with RAD9B is *EFNA5* (Figure 6-3). The EFNA5 protein is a tyrosine kinase cell surface receptor which is involved in normal hematopoietic development and tumorigenesis (Kuang et al., 2010).

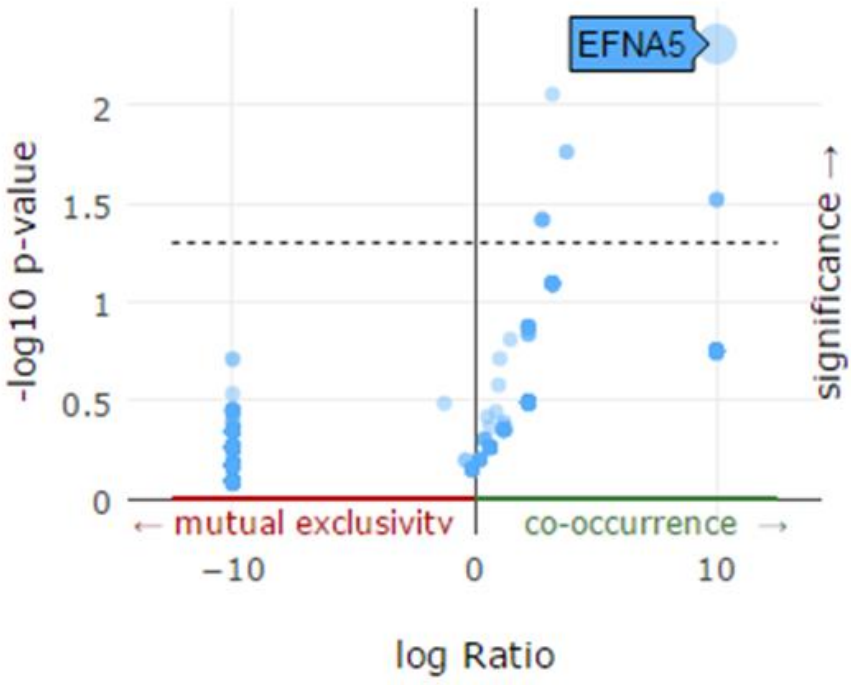

Figure 6.3 Genetic amolifications which co-occur with the amplification of the *RAD9B* gene. The highest probability of co-amplification has the *EFAN5* gene. (http://www.cbioportal.org. Accessed 11 February 2017).

Using the Catalogue of Somatic Mutations in Cancer (COSMIC) database (http://cancer.sanger.ac.uk/cosmic. Accessed 11 February 2017), the number of somatic point mutations in *RAD9B* was analysed. The database curates currently 36 somatic mutations in the N-terminal 260 amino acid long PCNA-like domain of RAD9B. The majority, 72% (26 mutations), are missense mutations. The mutation D141N displays the highest frequency.

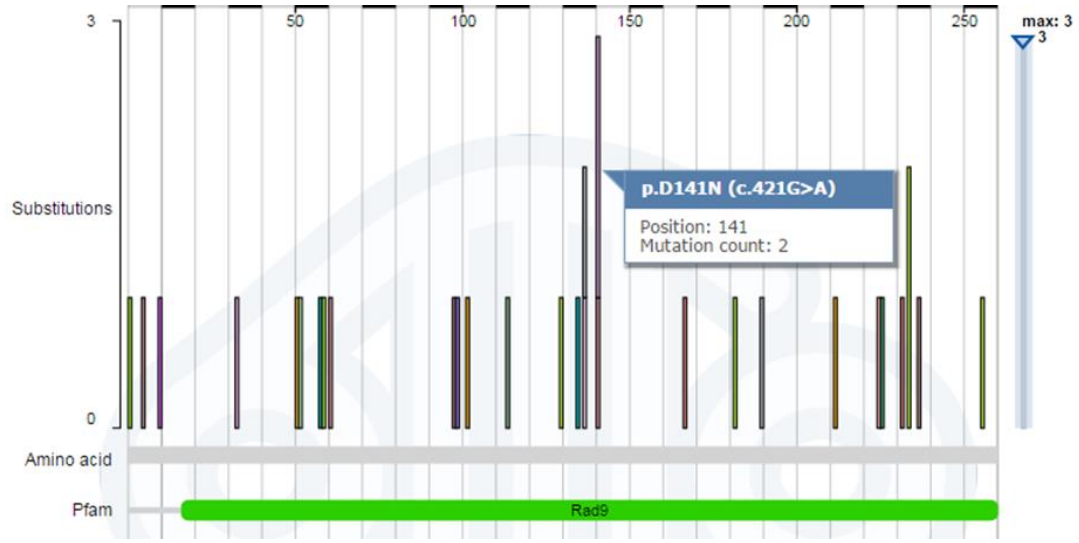

Figure 6.4 Somatic point mutations in human *RAD9B*. The COSMIC database currates currently 36 somatic mutations in the N-terminal 260 amino acid long PCNA-like domain. 72% (26 mutations) are missense mutations shown in this diagram. The mutation D141N displays the highest frequency. (http://cancer.sanger.ac.uk/cosmic. Accessed 11 February 2017).

The total number of somatic mutations in *RAD9B* are extremely low demonstrating a mutation frequency of less than 1% for all tested tissues. This suggests that these mutations are unlikely to be causatively linked with the development of cancer. It is more likely that they are passenger mutations that arise due to an increase in genomic instability in cancer tissues (Pon & Marra, 2015).

While aberrant expression of human *RAD9A* has been linked to several cancers, including skin, lung, prostate, thyroid and breast tumorigenesis, there is very limited evidence that RAD9B is a driver of malignant growth. High expression levels of *RAD9A* were detected in breast tumours, where 52.1% of breast tumours over-expressed *RAD9A* mRNA, and knock-down of RAD9A protein levels in the MCF-7 breast cancer cell line inhibited their proliferation. This suggests a link between high RAD9A abundance and growth control (Lieberman et al., 2011; Cheng et al., 2005). In a study on *RAD9A* expression in prostate cancer tissue, a strong correlation between RAD9A protein levels and the stage of prostate cancer was reported. Of all prostate cancer samples that were tested, 40.01% were positive for Rad9A expression. In contrast, only 3.8% of normal prostate tissues revealed weak expression of Rad9A. This aberrant expression of *RAD9A* has been linked to a methylation event of a transcription repressor located in the second intron of *RAD9A*, which is responsible for its

high abundance (Zhu, Zhang & Lieberman, 2008; Cheng et al., 2005). A high abundance of *RAD9A* was also reported in three prostate cancer cell lines, namely CWR22, DU145 and PC-3. Only one study has reported the expression of *RAD9B* in several cancer cell lines, such as K562 (myelogenous leukaemia), OVCAR5 (ovarian adenocarcinoma) and HeLa (human cervix epithelioid carcinoma) (Hopkins et al., 2003). The expression of *RAD9B* in HeLa cells in addition to brain neuroblastoma cells (Kelly) was also confirmed in this study.

6.3 The toxicity of RAD9B-002 over-expression

As discussed previously (Figure 4.28), a possible explanation for the appearance of a sub-G1 cell population in cells over-expressing RAD9B-002 is provided by the link between RAD9A and the apoptotic pathway. High protein levels of full-length RAD9B-002 may release RAD9A from the 9-1-1 complex resulting in its accumulation in the cytoplasm where it could induce apoptosis by interacting with the anti-apoptotic protein BCL-XL. In addition, RAD9B may directly interact with BCL-XL through its N-terminal domain, in a similar way as shown for the corresponding domain of RAD9A (Lee, Hirai & Wang, 2003). While the first possibility is supported by the high homology between the N-terminal section of RAD9A and RAD9B, the second possibility is in line with the presence of a BCL-2 homology 3 (BH3) domains in RAD9A and RAD9B. This is one of four domains (BH1, BH2. BH3 and BH4) which are conserved among BCL-2 family members and required for their interactions and functions in controlling cell death. While the BH1 and BH2 domains are conserved in anti-apoptotic members, the BH3 domain is present in pro-apoptotic proteins. RAD9A is known to interact via its BH3 domain with the anti-apoptotic proteins BCL-2 and BCL-XL to inhibit their role and to initiate cell death. Since this region is also conserved in RAD9B, it is likely that RAD9B plays a similar role to RAD9A in initiating cell death, a conclusion which is supported by the toxicity of RAD9B-002 when over expressed (Hopkins et al., 2003; Komatsu et al., 2000).

6.4 The role of RAD9B-001 and RAD9B-002 in cell cycle regulation, DNA damage response and cell death

6.4.1 Is p21 modification by RAD9B-001 or RAD9B-002 direct?

The role of p21 in binding to the G1-cyclin-CDK complexes and causing a G1 cell cycle arrest is well known (Harper et al., 1995). Moreover, low expression levels of p21 are required for CDK activity, although basal levels of p21 are insufficient in inhibiting CDK activity (Soria & Gottifredi, 2010; Dotto, 2000).

The GTP-binding protein 1 (NGP-1), also known as guanine nucleotide-binding protein-like 2 (GNL2), is a member of the HSR1-MMR1 family of GTPases, was reported to act as a regulator of the G1-S transition. NGP-1 is expressed in various cancers with up-regulation in certain cancers such as breast, colon and colorectal tumours. The over-expression of NGP-1 increases cell proliferation and DNA replication (Datta et al., 2015). Over-expression of NGP-1 also increases the levels of p53 and p21. These findings were surprising since p53 and p21 are known to be suppressors of cell proliferation. The same study showed good evidence that NGP-1 mediates cell cycle progression through the p53 protein and its downstream target p21 and the interaction between p21 and the cyclin D1-CDK4 complex which results in the hyperphosphorylation of the retinoblastoma RB protein. This hyperphosphorylation leads to the up-regulation of the E2F1 transcription factors required for the G1-S transition (Datta et al., 2015). Despite the role of p21 in the inhibition of cyclin D1-CDK4 complex activity, p21 can enhance the activity of this complex by acting as an adaptor protein to assemble and programme the complex to perform specific functions (La & Baer et al., 1997). The research reported here shows that the expression levels of RAD9B-002/005 drop during the G1/S cell cycle transition in HEK293 cells (Figure 3.12). Furthermore, the results showed that the over-expression of EGFP-RAD9B-002 slows cell growth (Figure 4.14), suggesting that elevated RAD9B protein levels negatively impact the G1-S transition in HEK293 cells. Such a misregulation of the G1-S transition can affect cell proliferation and lead to oncogenesis (Bertoli, Skotheim & de Bruin, 2013). This is in line with the reported over-expression of the NGP-1 protein in cancers, which leads to a faster G1-S transition. The drop in *RAD9B-002/005* mRNA levels required for the G1-S transition in normal cells could be linked with the high phosphorylation of p21 upon the over-expression of EGFP-RAD9B-002. Elevated levels of full-length RAD9B-002 could stimulate a kinase that phosphorylates p21 during the

cell cycle G1/S transition. A poosible kinase is AKT kinase as it modifies p21 to prevent its association with PCNA which blocks DNA replication (Rossig et al., 2001). How RAD9B-002 impacts on AKT is not known, but one possible link is provided by the functional link between TOPBP1 (Crb2), AKT and E2F1. Akt phosphorylates TOPBP1 thereby promoting the oligomerization of TOPBP1 and its association with E2F1 which initiates cell death at the G1/S transition (Liu et al., 2006). A stimulation of this AKT-TOPBP1-E2F1 pathway may also be an alternative explanation for the accumulation of a sub-G1 cell population upon over-expression of RAD9B-002 (Figure 4.13). In summary, these results suggest a negative impact of RAD9B-002 on G1/S transition and cell survival that is linked with the phosphorylation of p21. Moreover, *RAD9B-002/005* mRNA levels are significantly high in HeLa cancer cells (Figure 3.12); supporting a possible link between RAD9B and the NGP-1 G1/S escalator protein which also regulates p21 levels.

The p21 protein is thought to have a dual function in oncogenesis depending on its cellular localisation. It acts as a tumour suppressor when it localises to the nucleus after DNA damage but is oncogenic when it localises to the cytoplasm. Further, p21 accumulates in the nucleus after DNA damage to induce cell cycle arrest (Abella et al., 2010). Interestingly, p21 localises also to the nucleolus after DNA damage independently of p53 and ATM (Perez-Castro & Freire, 2012; Abella et al., 2010). As aforementioned, RAD9B was also reported to localise to the nucleolus in special spherical structures in the response to UV light. However, the roles of RAD9B and p21 in this localisation remain unclear. Since the nucleolus provides the environment for the assembly of ribosomes, it is possible that the function of RAD9B is related to maintaining ribosomal rDNA integrity after UV damage (Calkins, Iglehart & Lazaro, 2013). This localisation of RAD9B requires its C-terminal domain and is dependent on ATR and JNK kinase signalling, as the inhibition of these signalling pathways results in the reduced migration of RAD9B to the disturbed nucleolus (Perez-Castro & Freire, 2012). As mentioned previously, the over-expression of RAD9B-001, but not RAD9B-002, results in a transient G1 cell cycle arrest as reported for the over-expression of RAD9B in the study by Perez-Castro and colleagues (Perez-CastroFreire, 2012).

Since the authors did not clearly state which RAD9B variant was over-expressed, it is very likely that they studied the shorter RAD9B-001 and not the full-length RAD9B-002. Although the over-expression of both, RAD9B-001 and RAD9B-002, results in the

hyperphosphorylation of p21, it is clear that both variants perform distinct functions. For example, high levels of RAD9B-001 result in a profound hyper-phosphorylation of CHK2 in untreated cells and delay the UV-induced degradation of p21, whereas over-expression of RAD9B-002 only partly increases CHK2 phosphorylation and does not delay p21 degradation in response to UV light (Table 6.1). These differences could be explained by a specific role of RAD9B-001 in the maintenance of the ribosomal DNA in the nucleolus where p21 and RAD9B-001 may collaborate.

In addition, p21 causes a G1 cell cycle arrest when over-expressed, similarly to RAD9B-001 (Mansilla et al., 2013). Also RAD9B-001 is up-regulated in senescent cells (Figure 3.10-C) as it is the case for p21 (Park, Lim & Jang, 2011) where the activation of senescent p21 is p53 tumour suppressor-dependent (Campisi, 2013). This could explain the increased phosphorylation of p53 when RAD9B-001 is over-expressed (Figure 5.2) which is not observed when RAD9B-002 is over expressed. Taken together, these findings strongly indicate that both full-length RAD9B-002 and its shorter variant RAD9B-001 are functionally linked with the p21 pathways but possibly under different circumstances or in distinct cellular compartments.

6.4.2 P21 degradation after exposure to UV light

The p21 protein response to DNA damage depends on the extent of the damage. With low DNA damage, p21 expression levels increase resulting in the inhibition of CDK activation. This consequently leads to a cell cycle arrest allowing for anti-apoptotic activities and DNA repair. However, when DNA is extensively damaged, p21 expression levels decrease and the cells undergo apoptosis (Cmielova & Rezacova, 2011).

p21 can be down-regulated by some types of DNA damage; for example, it is degraded in the response to UV irradiation. Degradation of p21 is dependent on the E3-ubiquitin ligase CRL4/CDT2 in the response to UV light (Nishitani et al., 2008).

The E3 ubiquitin ligase couples protein degradation to DNA replication and recognises its substrate when bound to PCNA (Havens & Walter, 2011). Its activity is important to prevent re-replication within one cell cycle and to respond to DNA damage. The forced stabilisation of p21 after UV irradiation impairs DNA replication and genomic stability, resulting in the

accumulation of replication stress markers. The release of PCNA from the PCNA-p21 complex in the response to UV light promotes PCNA-dependent DNA repair by allowing the recruitment of other PCNA partners, such as the Y-family DNA polymerases to bind (Mansilla et al., 2013). This polymerase switch defines DNA translesion synthesis (TLS). The TLS polymerases replicate damaged DNA templates to avoid the stalling of DNA replication forks as this would cause DNA double-strand breaks. Polymerases from the Y family show a critical, evolutionary role as they exist in all three kingdoms of life. However, it has been proposed that they perform tumour suppressive functions since higher organisms express a larger number of these TLS polymerases. One of the main disorders in patients with impaired TLS is xeroderma pigmentosum variant (XPV) syndrome which is characterised by a genetic predisposition to sunlight-induced skin cancer due to autosomal recessive mutation in TLS polymerases and associated factors (Knobel & Marti, 2011; Stallons & McGregor, 2010; Ohmori et al., 2001; Cordonnier, Lehmann & Fuchs, 1999).

The results in Figure 5.5-A & B shows that importance of regulating the levels of RAD9B in response to UV irradiation. Furthermore, the results in Figure 5.8 show that after UV radiation, p21 degradation is delayed by high levels of RAD9B-001, and interestingly, the *S. pombe* Rad9-M50 variant. Since both N-terminally truncated variants slow down p21 degradation, they may bind either to PCNA or to p21 to block the formation of the PCNA-p21 complex, which is essential for the $CRL4^{CDT2}$ E3 ubiquitin ligase to recognise p21 (Figure 6.5). Since RAD9B-001 is thought to physically interact with p21 (Perez-Castro & Freire, 2012), it is likely that the physical interaction of RAD9B-001 and SpRad9-M50 with p21 prevents the formation of the p21-PCNA complex. Alternatively, it is also possible that the Rad9 variants interact directly with the E3 ligase $CRL4^{CDT2}$ to prevent p21 degradation (Soria et al., 2008). However, the possibility of a direct interaction between RAD9B-001 and p21 is the strongest (Figure 6.5). Since full-length RAD9B-002 does not delay the degradation of p21 after UV-light exposure, removal of the N-terminal domain by alternative splicing may be essential for RAD9B to regulate p21 degradation. The latter would also explain why the yeast Rad9 variant can slow down p21 degradation. Furthermore, it strongly indicates that the domain required for this regulation is conserved in the yeast protein. The PCNA binding domain resides in the last 22 C-terminal amino acids of human p21 (Gulbis et al., 1996), and since RAD9A and RAD9B share some similarity with PCNA (Xu et al., 2009), it may be the case that p21 binds to RAD9B-001 or SpRad9-M50 via the same domain. It is also worth

pointing out that the different effects of RAD9B-001 and RAD9B-002 on the p21 protein in response to UV light also indicate that the phosphorylation of p21 during the over-expression of either variant result in distinct roles for p21. At a minimum, the regulation of RAD9B-001 levels in response to UV irradiation and possibly other reagents causing stalled replication forks is an essential mechanism for p21 degradation and TLS function.

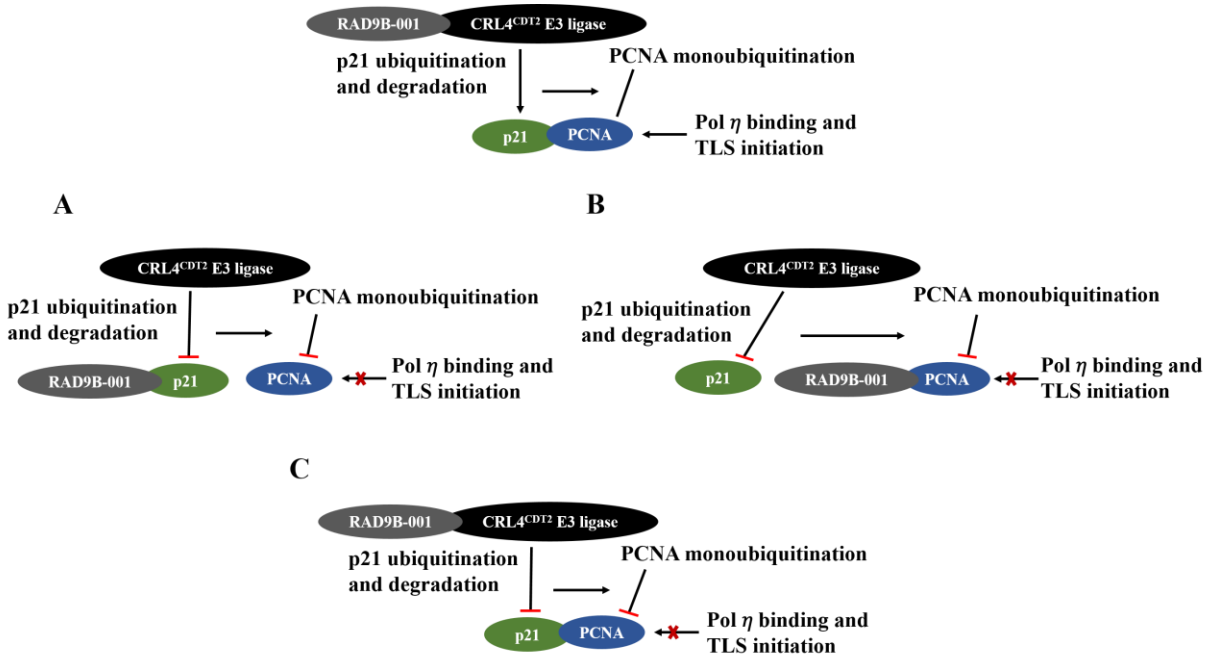

Figure 6.5 Inhibition of DNA translesion synthesis (TLS) by RAD9B-001 over-expression. Following UV irradiation, p21 binds to PCNA, which results in p21 ubiquitination by the $CRL4^{CDT2}$ E3 ligase complex; this, in turn, results in p21 degradation. The release of PCNA from the p21-PCNA complex allows for PCNA monoubiquitination, an important process in switching from normal replication polymerase binding to TLS polymerase η (POL η). POL η is then located at damaged sites by PCNA where the TLS mechanism is initiated. The TLS mechanism can be inhibited by impaired p21 degradation in the presence of high levels of RAD9B-001 via three possible mechanisms, as follows: (A) RAD9B-001 physically interacts with p21 and inhibits p21-PCNA coupling; (B) due to the high homology between RAD9B-001 and the interacting PCNA partner RAD9A, RAD9B-001 interacts with PCNA and prevents PCNA-p21 coupling; or (C) RAD9B-001 interacts with the $CRL4^{CDT2}$ E3 ligase complex and impairs p21 ubiquitination. The possibilities A or B or C result in preventing p21 degradation, and as a consequence, impaired TLS initiation. However, hypothesis A is the strongest, since RAD9B and p21 were reported to physically interact.

This other intriguing observation is the inverse relationship between RAD9B-001 and RAD9B-002 on p21 degradation. While high levels of RAD9B-001 delay p21 degradation in the response to UV light, elevated RAD9B-002 levels block p21 degradation in the presence

of oxidative stress (Table 6.1). Only a few studies exist in the literature on the decline in p21 expression in the response to oxidative stress. They suggest that p21 is targeted by an E3 ubiquitin ligase which may be distinct from the PCNA-coupled process. Since MPS1 levels are reported to be regulated through the cell cycle by the anaphase-promoting complex (APC) E3 ligase (Palframan et al., 2006), it is possible that MPS1 and p21 are regulated in a similar manner in response to H_2O_2, Indeed, p21 is degraded during mitosis in a CDK2-dependent manner by the APC (Yamada et al., 2011). Moreover, since MPS1 and p21 proteolysis are affected by the high levels of hRad9B-002, it is highly likely that RAD9B-002 negatively interferes with the CDC2 pathway and consequently influences APC activity. Hence, RAD9B-001 and RAD9B-002 may affect p21 stability through the PCNA and APC pathways, respectively.

6.4.3 CHK2 hyperphosphorylation by RAD9B-001

In the response to DNA damage, CHK2 stabilises the p53 tumour-suppressor protein leading to a G1 cell cycle arrest (Chehab et al., 2000). CHK2 is also involved in the G2/M arrest (Zannini, Delia & Buscemi, 2014). During the G1/S cell cycle arrest, ATM and CHK2 stabilise p53 which leads to the up-regulation of p21 expression, resulting in the inhibition of CDK complexes and consequent blocking of the G1/S transition (Chehab et al., 2000; Hirao et al., 2000). The over-expression of CHK2 was also reported to result in a G1/S arrest (Chehab et al., 2000). In this study, the over-expression of RAD9B-001 caused the strong hyperphosphorylation of CHK2 and increased p53 phosphorylation 12 hours after inducing the expression of RAD9B-001 in untreated cells (Figure 5.2). Up to 12 hours post RAD9B-001 induction, no G1 arrest was observed when the samples were analysed in a fax machine (Figure 4.13) as the G1 arrest appeared only 24 hours after induction. This indicates that the increased phosphorylation of CHK2 and p53 is not a result of the G1 arrest but caused by the over-expression of RAD9B-001. Interestingly, over-expression of Rad9-M50 did not affect CHK2 phosphorylation (Figure 5.2) implying that this function is distinct from the delayed degradation of p21.

These results strongly evidence that RAD9B-001 acts upstream of CHK2 and plays a role in activating the CHK2-p53 pathway, subsequently leading to G1 arrest. Since the accumulation of the p21 protein is essential for the inhibition of the CDK complexes to stop cell cycle progression, and since p21 levels did not increase upon over-expression of RAD9B-001

(Figure 4.20), an alternative G1/S arrest pathway may exist. One possible example is the binding of the active p53 protein to the 5' region of *CDK4* mRNA to inhibit its translation thereby leading to a G1 arrest (Miller et al., 2000). Further support for a close link between RAD9B-001 and the CHK2-p53 pathway is provided by the hyperphosphorylation of CHK2 in the response to H_2O_2 in the RAD9B-001 cell line (Figure 5.16) along with the increased expression of endogenous RAD9B-001 in the response to H_2O_2. How high levels of RAD9B-001 trigger the phosphorylation of CHK2 is not yet clear. Since the ATM-CHK2 pathway is typically activated when ATM is recruited to DNA double-strand breaks (Falck, Coates & Jackson, 2005), elevated levels of RAD9B-001 could cause such breaks maybe via its interaction with the PCNA-p21 system during DNA replication.

6.4.4 CHK2 phosphorylation by RAD9B-002 in untreated cells

While high levels of RAD9B-001 cause a strong hyper-phosphorylation of CHK2 in otherwise untreated cells, elevated levels of the full-length RAD9B-002 protein are much less effective (Figure 5.2-B). It is therefore likely that CHK2 phosphorylation caused by RAD9B-002 occurs in a different manner to RAD9B-001. Since the over-expression of RAD9B-002 results in the increased phosphorylation of CHK2 in an ATM-independent manner (Figure 5.2-A), another kinase may be involved. As aforementioned, MPS1 is a mitotic kinase that is required for error-free mitotic progression in eukaryotes (Tyler et al., 2009). In human cells, MPS1 levels are regulated in a cell cycle-dependent manner by the ubiquitin ligase/proteasome pathway during late mitosis and in G1 (Cui et al., 2010). Interestingly, cleavage of MPS1 was observed in all protein samples analysed in this project (Figure 5.8). The MPS1 kinase is required for centrosome duplication during the S phase where it is phosphorylated by CDK2 as this phosphorylation suppresses the proteostome-mediated degradation of MPS1.

The CDK2-regulated MSP1 degradation pathway is specific to the centrosome since the inhibition of the phosphorylation of MPS1 causes the loss of the kinase specifically from the centrosome but not from other locations (Kasbek et al., 2007). MPS1 activity is essential for the coordinated duplication of the centrosome as the suppression of MPS1 degradation results in centrosome re-duplication associated with the abnormal, multipolar mitotic cell division found in some cancers (Kasbek, Yang & Fisk, 2009).

A few potential mechanisms for the suppression of MPS1 degradation exist in the literature, including an increase in CDK2 activity, which inhibits the degradation of MPS1 at the centrosomes, or the inhibition of degradation machinery itself, which inhibits the proteasome (Kasbek, Yang & Fisk, 2009). As mentioned previously, in all the experiments, MPS1 is less degraded upon over-expression of RAD9B-002 (Figure 5.8, Figure 5.12). These results suggest that RAD9B-002 has a negative impact on the degradation of MPS1 maybe at the centrosome as a result of its interference with the CDC2-MPS1 pathway. The effect of RAD9B-002 on the CDC2 pathway is supported by the high phosphorylation levels of CDC2 main regulator p21 in the cell line over-expressing RAD9B-002. This could be a good explanation for the weak abundancy of RAD9B-002 in general and specifically during the time of centrosome duplication at the G1-S transition (Figure 3.12) to ensure an accurate centrosome duplication and cell cycle division. A centrosomal role of RAD9B-002 may also explain the increased phosphorylation of CHK2 upon the over-expression of the variant as CHK2 co-localises with MPS1 at the centrosome in a DNA damage independent manner (Golan et al., 2010). CHK2 is required to stabilise MPS1 at the kinetochors during mitosis and MPS1 can phosphorylate Chk2 at Thr-68 in the response to DNA damage (PetsalakiZachos, 2014, Wei et al., 2005).

6.4.5 Why is CHK2 phosphorylation reduced by RAD9B-002 in the response to DNA damage?

Although high levels of RAD9B-002 cause an increase in CHK2 phosphorylation in undamaged cells (Figure 5.2), CHK2 phosphorylation at Thr-68 is inhibited in the response to UV and oxidative stress in the RAD9B-002 cell line (Figure 5.8 & Figure 5.18). This suggests that RAD9B-002 impacts on CHK2 phosphorylation is a rather specific manner. A study of CHK2 phosphorylation in response to oxidative stress showed that the phosphorylation signal was highest in S-phase cells, less in G1- phase cells and the least in G2/M-phase cells (Zhao et al., 2008). It is likely that the forced elevation of RAD9B-002 interferes and blocks the phosphorylation of CHK2 during the S phase under DNA conditions.

It is also likely that the CHK2 phosphorylation events in undamaged cells could occur in different cellular compartments such as at the centrosomes or the kinetochore (Golan et al.,

2010), whereas the DNA damage induced phosphorylation is expected to take place at the chromatin. The suppression of the smaller CHK2 band by the over-expression of RAD9B-002 also could be linked with its centrosomal role, as this cleaved CHK2 form was also found to localise to the centrosome (Golan et al., 2010). The data in (Figure 5.18) shows that the pharmacological down-regulation of MPS1 decrease CHK2 phosphorylation in the response to H_2O_2 which is in line with the ability of MPS1 to target CHK2-T68 in the presence of DNA damage. However, a combination of the down-regulation of MPS1 and the over-expression of RAD9B-002 shows a slight recovery of CHK2-T68 phosphorylation which supports the model that RAD9B-002 targets MPS1 by blocking Polo-like kinase PLK1 at the centrosome (Figure 5.19). In summary, RAD9B-002 may target CHK2 at the centrosome, at the kinetochore and/or at the chromatin as the kinase localises to all three structures (Yeh et al., 2014; Li & Stern, 2005; Tsvetkov et al., 2003). More experimental work is however required to investigate the relationship between RAD9B-002 and CHK2 further.

6.5 Conclusion

This project provides, for the first time, an insight into the diverse roles of the splice variants of the human *RAD9B* gene which regulate the CHK2-p53-p21 G1/S signalling module in quite different ways. While over-expression of the full-length protein RAD9B-002 induces cell death in G1 and delays p21 degradation in the response to oxidative stress, over-expression of its N-terminally deleted variant RAD9B-001 only transiently arrests G1 progression and only delays p21 degradation in the presence of UV induced DNA damage. Both proteins have an impact on CHK2 phosphorylation levels, probably through distinct mechanisms. Taken together, the results presented here suggest that RAD9B acts on CHK2 kinase, whereas RAD9A regulates CHK1 kinase. Since the clear division between ATR-CHK1 and ATM-CHK2 DNA damage signalling emerged after the development of multicellular organism, it is possible that RAD9B evolved from an early gene duplication event to enable multicellular organisms to regulate CHK1 and CHK2 independently. The work also provides evidence that RAD9B may regulate the modification of CHK2 by the mitotic kinase MPS1 which controls the spindle attachment checkpoint in mitosis and the duplication of the centrosome in G1/S.

6.6 Future work

The reliance on engineered EGFP-RAD9B fusion proteins which are over-expressed in the presence of the endogenous RAD9 proteins may limit the interpretation of this work. Two strategies could be applied to resolve this issue. The endogenous RAD9B gene could be deleted using the Crispr/Cas9 technology as this would render cells dependent on the engineered proteins. This would allow to study RAD9B in the absence of the endogenous splice variants. This approach may however be limited if any of the RAD9B variants were to be essential for cell viability.

The second approach could aim to raise variant specific antibodies or an antibody that recognises more RAD9B variants. Currently none of the commercially available antibodies recognises endogenous RAD9B, possibly because of the low expression levels. Also the high degree of identity at protein level may make it difficult to raise variant specific antibodies. Future work could focus on the functional relationships between RAD9B-002, PLK1, MPS1 and CHK2, and their role at the centrosome. This could be achieved by using confocal microscopy to analyse RAD9B-002 localisation in G1, S and G2 in synchronised cells. It would also be interesting to search for possible interaction partners of RAD9B-002 through immunoprecipitation in these cell cycle phases.

References

Abbas, T. & Dutta, A. 2009. p21 in cancer: intricate networks and multiple activities. *Nature Reviews Cancer.* 9 (6). pp. 400-414.

Abella, N., Brun, S., Calvo, M., Tapia, O., Weber, J.D., Berciano, M.T., Lafarga, M., Bachs, O. & Agell, N. 2010. Nucleolar disruption ensures nuclear accumulation of p21 upon DNA damage. *Traffic.* 11 (6). pp. 743-755.

Ahmad, Y., Boisvert, F.M., Lundberg, E., Uhlen, M. & Lamond, A.I. 2012. Systematic analysis of protein pools, isoforms, and modifications affecting turnover and subcellular localization. *Molecular & Cellular Proteomics.* 11 (3). pp. M111.013680.

Ahn, J.Y., Li, X., Davis, H.L. & Canman, C.E. 2002. Phosphorylation of threonine 68 promotes oligomerization and autophosphorylation of the Chk2 protein kinase via the forkhead-associated domain. *Journal of Biological Chemistry.* 277 (22). pp. 19389-19395.

Ahn, J.Y., Schwarz, J.K., Piwnica-Worms, H. & Canman, C.E. 2000. Threonine 68 phosphorylation by ataxia telangiectasia mutated is required for efficient activation of Chk2 in response to ionizing radiation. *Cancer Research.* 60 (21). pp. 5934-5936.

Alló, M., Buggiano, V., Fededa, J.P., Petrillo, E., Schor, I., de la Mata, M., Agirre, E., Plass, M., Eyras, E. & Elela, S.A. 2009. Control of alternative splicing through siRNA-mediated transcriptional gene silencing. *Nature Structural & Molecular Biology.* 16 (7). pp. 717-724.

Arsic, N., Gadea, G., Lagerqvist, E.L., Busson, M., Cahuzac, N., Brock, C., Hollande, F., Gire, V., Pannequin, J. & Roux, P. 2015. The p53 isoform Δ133p53β promotes cancer stem cell potential. *Stem Cell Reports.* 4 (4). pp. 531-540.

Baens, M., Noels, H., Broeckx, V., Hagens, S., Fevery, S., Billiau, A.D., Vankelecom, H. & Marynen, P. 2006. The dark side of EGFP: defective polyubiquitination. *PloS One.* 1 (1). pp. e54.

Bahassi, E.M., Myer, D.L., McKenney, R.J., Hennigan, R.F. & Stambrook, P.J. 2006. Priming phosphorylation of Chk2 by polo-like kinase 3 (Plk3) mediates its full activation by ATM and a downstream checkpoint in response to DNA damage. *Mutation Research/Fundamental and Molecular Mechanisms of Mutagenesis.* 596 (1). pp. 166-176.

Bai, H., Madabushi, A., Guan, X. & Lu, A. 2010. Interaction between human mismatch repair recognition proteins and checkpoint sensor Rad9-Rad1-Hus1. *DNA Repair.* 9 (5). pp. 478-487.

Balakrishnan, L., Brandt, P.D., Lindsey-Boltz, L.A., Sancar, A. & Bambara, R.A. 2009. Long patch base excision repair proceeds via coordinated stimulation of the multienzyme DNA repair complex. *Journal of Biological Chemistry.* 284 (22). pp. 15158-15172.

Bartek, J. & Lukas, J. 2003. Chk1 and Chk2 kinases in checkpoint control and cancer. *Cancer Cell.* 3 (5). pp. 421-429.

Bell, L. & Ryan, K. 2004. Life and death decisions by E2F-1. *Cell Death & Differentiation.* 11 (2). pp. 137-142.

Beltran, H., Prandi, D., Mosquera, J.M., Benelli, M., Puca, L., Cyrta, J., Marotz, C., Giannopoulou, E., Chakravarthi, B.V. & Varambally, S. 2016. Divergent clonal evolution of castration-resistant neuroendocrine prostate cancer. *Nature Medicine.*

Ben-Porath, I. & Weinberg, R.A. 2005. The signals and pathways activating cellular senescence. *International Journal of Biochemistry & Cell Biology.* 37 (5). pp. 961-976.

Berge, E.O., Staalesen, V., Straume, A.H., Lillehaug, J.R. & Lønning, P.E. 2010. Chk2 splice variants express a dominant-negative effect on the wild-type Chk2 kinase activity. *Biochimica et Biophysica Acta-Molecular Cell Research.* 1803 (3). pp. 386-395.

Berget, S.M., Moore, C. & Sharp, P.A. 1977. Spliced segments at the 5' terminus of adenovirus 2 late mRNA. *Proceedings of the National Academy of Sciences of the United States of America.* 74 (8). pp. 3171-3175.

Bertoli, C., Skotheim, J.M. & de Bruin, R.A. 2013. Control of cell cycle transcription during G1 and S phases. *Nature Reviews Molecular Cell Biology.* 14 (8). pp. 518-528.

Blanco, F.J., Grande, M.T., Langa, C., Oujo, B., Velasco, S., Rodriguez-Barbero, A., Perez-Gomez, E., Quintanilla, M., Lopez-Novoa, J.M. & Bernabeu, C. 2008. S-endoglin expression is induced in senescent endothelial cells and contributes to vascular pathology. *Circulation Research.* 103 (12). pp. 1383-1392.

Boisvert, R.A. & Howlett, N.G. 2014. The Fanconi anemia ID2 complex: dueling saxes at the crossroads. *Cell Cycle.* 13 (19). pp. 2999-3015.

Boutz, P.L., Stoilov, P., Li, Q., Lin, C.H., Chawla, G., Ostrow, K., Shiue, L., Ares, M.,Jr & Black, D.L. 2007. A post-transcriptional regulatory switch in polypyrimidine tract-binding proteins reprograms alternative splicing in developing neurons. *Genes & Development.* 21 (13). pp. 1636-1652.

Broustas, C.G. & Lieberman, H.B. 2012. Contributions of Rad9 to tumorigenesis. *Journal of Cellular Biochemistry.* 113 (3). pp. 742-751.

Buchholz, F., Ringrose, L., Angrand, P.O., Rossi, F. & Stewart, A.F. 1996. Different thermostabilities of FLP and Cre recombinases: implications for applied site-specific recombination. *Nucleic Acids Research.* 24 (21). pp. 4256-4262.

Bunz, F., Dutriaux, A., Lengauer, C., Waldman, T., Zhou, S., Brown, J.P., Sedivy, J.M., Kinzler, K.W. & Vogelstein, B. 1998. Requirement for p53 and p21 to sustain G2 arrest after DNA damage. *Science.* 282 (5393). pp. 1497-1501.

Burtelow, M.A., Kaufmann, S.H. & Karnitz, L.M. 2000. Retention of the human Rad9 checkpoint complex in extraction-resistant nuclear complexes after DNA damage. *Journal of Biological Chemistry.* 275 (34). pp. 26343-26348.

Buscemi, G., Carlessi, L., Zannini, L., Lisanti, S., Fontanella, E., Canevari, S. & Delia, D. 2006. DNA damage-induced cell cycle regulation and function of novel Chk2 phosphoresidues. *Molecular and Cellular Biology.* 26 (21). pp. 7832-7845.

Campisi, J. & di Fagagna, F.d. 2007. Cellular senescence: when bad things happen to good cells. *Nature reviews Molecular Cell Biology.* 8 (9). pp. 729-740.

Campisi, J. 2013. Aging, cellular senescence, and cancer. *Annual Review of Physiology.* 75 pp. 685-705.

Caspari, T. & Hilditch, V. 2015. Two Distinct Cdc2 pools regulate cell cycle progression and the DNA damage response in the fission yeast *S. pombe*. *PloS One.* 10 (7). pp. e0130748.

Cheng, C.K., Chow, L.W., Loo, W.T., Chan, T.K. & Chan, V. 2005. The cell cycle checkpoint gene Rad9 is a novel oncogene activated by 11q13 amplification and DNA methylation in breast cancer. *Cancer Research.* 65 (19). pp. 8646-8654.

Child, E.S. & Mann, D.J. 2006. The intricacies of p21 phosphorylation: protein/protein interactions, subcellular localization and stability. *Cell Cycle.* 5 (12). pp. 1313-1319.

Chow, L.T., Gelinas, R.E., Broker, T.R. & Roberts, R.J. 1977. An amazing sequence arrangement at the 5′ ends of adenovirus 2 messenger RNA. *Cell.* 12 (1). pp. 1-8.

Ciccia, A. & Elledge, S.J. 2010. The DNA damage response: making it safe to play with knives. *Molecular Cell.* 40 (2). pp. 179-204.

Cimprich, K.A. & Cortez, D. 2008. ATR: an essential regulator of genome integrity. *Nature Reviews Molecular Cell Biology.* 9 (8). pp. 616-627.

Cordonnier, A.M., Lehmann, A.R. & Fuchs, R.P. 1999. Impaired translesion synthesis in xeroderma pigmentosum variant extracts. *Molecular and Cellular Biology.* 19 (3). pp. 2206-2211.

Craig, N.L. 1988. The mechanism of conservative site-specific recombination. *Annual Review of Genetics.* 22 (1). pp. 77-105.

Cui, Y., Cheng, X., Zhang, C., Zhang, Y., Li, S., Wang, C. & Guadagno, T.M. 2010. Degradation of the human mitotic checkpoint kinase Mps1 is cell cycle-regulated by APC-cCdc20 and APC-cCdh1 ubiquitin ligases. *Journal of Biological Chemistry.* 285 (43). pp. 32988-32998.

Driessens, N., Versteyhe, S., Ghaddhab, C., Burniat, A., De Deken, X., Van Sande, J., Dumont, J.E., Miot, F. & Corvilain, B. 2009. Hydrogen peroxide induces DNA single- and double-strand breaks in thyroid cells and is therefore a potential mutagen for this organ. *Endocrine-Related Cancer.* 16 (3). pp. 845-856.

Dufault, V.M., Oestreich, A.J., Vroman, B.T. & Karnitz, L.M. 2003. Identification and characterization of RAD9B, a paralog of the RAD9 checkpoint gene. *Genomics.* 82 (6). pp. 644-651.

Duong, H., Hong, Y.B., Kim, J.S., Lee, H., Yi, Y.W., Kim, Y.J., Wang, A., Zhao, W., Cho, C.H. & Seong, Y. 2013. Inhibition of checkpoint kinase 2 (CHK2) enhances sensitivity of pancreatic adenocarcinoma cells to gemcitabine. *Journal of Cellular and Molecular Medicine.* 17 (10). pp. 1261-1270.

Forrester, H.B., Li, J., Hovan, D., Ivashkevich, A.N. & Sprung, C.N. 2012. DNA repair genes: alternative transcription and gene expression at the exon level in response to the DNA damaging agent, ionizing radiation. *PLoS One.* 7 (12). pp. e53358.

Friedberg, E.C. 1988. Deoxyribonucleic acid repair in the yeast Saccharomyces cerevisiae. *Microbiological Reviews.* 52 (1). pp. 70-102.

Furuya, K., Poitelea, M., Guo, L., Caspari, T. & Carr, A.M. 2004. Chk1 activation requires Rad9 S/TQ-site phosphorylation to promote association with C-terminal BRCT domains of Rad4TOPBP1. *Genes & Development.* 18 (10). pp. 1154-1164.

g Hardwick, K., Weiss, E., Luca, F.C., Winey, M. & Murray, A.W. 1996. Activation of the budding yeast spindle assembly checkpoint without mitotic spindle disruption. *Science.* 273 (5277). pp. 953.

Gapp, K., Woldemichael, B., Bohacek, J. & Mansuy, I. 2014. Epigenetic regulation in neurodevelopment and neurodegenerative diseases. *Neuroscience.* 264 pp. 99-111.

Gautschi, O., Heighway, J., Mack, P.C., Purnell, P.R., Lara, P.N.,Jr & Gandara, D.R. 2008. Aurora kinases as anticancer drug targets. *Clinical Cancer Research.* 14 (6). pp. 1639-1648.

Giglia-Mari, G., Zotter, A. & Vermeulen, W. 2011. DNA damage response. *Cold Spring Harbor Perspectives in Biology.* 3 (1). pp. a000745.

Godovac-Zimmermann, J., Kleiner, O., Brown, L.R. & Drukier, A.K. 2005. Perspectives in spicing up proteomics with splicing. *Proteomics.* 5 (3). pp. 699-709.

Golan, A., Pick, E., Tsvetkov, L., Nadler, Y., Kluger, H. & Stern, D.F. 2010. Centrosomal Chk2 in DNA damage responses and cell cycle progession. *Cell Cycle.* 9 (13). pp. 2647-2656.

Gomel, R., Xiang, C., Finniss, S., Lee, H.K., Lu, W., Okhrimenko, H. & Brodie, C. 2007. The localization of protein kinase Cdelta in different subcellular sites affects its proapoptotic and antiapoptotic functions and the activation of distinct downstream signaling pathways. *Molecular Cancer Research.* 5 (6). pp. 627-639.

Green, D.R. 2006. At the gates of death. *Cancer Cell.* 9 (5). pp. 328-330.

Hang, H., Zhang, Y., Dunbrack, R.L., Wang, C. & Lieberman, H.B. 2002. Identification and characterization of a paralog of human cell cycle checkpoint gene HUS1. *Genomics.* 79 (4). pp. 487-492.

Harper, J.W., Adami, G.R., Wei, N., Keyomarsi, K. & Elledge, S.J. 1993. The p21 Cdk-interacting protein Cip1 is a potent inhibitor of G1 cyclin-dependent kinases. *Cell.* 75 (4). pp. 805-816.

Hasanzadeh_Nazarabadi, M., Hamzehloie, T., Mojarrad, M. & Shekouhi, S. 2012. The role of tumor protein 53 mutations in common human cancers and targeting the murine double minute 2–p53 interaction for cancer therapy. *Iranian Journal of Medical Sciences.* 37 (1). pp. 3-8.

Hassan, M., Watari, H., AbuAlmaaty, A., Ohba, Y. & Sakuragi, N. 2014. Apoptosis and molecular targeting therapy in cancer. *BioMed Research International.* 2014 pp. 150845.

Hayes, O., Ramos, B., Rodriguez, L., Aguilar, A., Badia, T. & Castro, F. 2005. Cell confluency is as efficient as serum starvation for inducing arrest in the G0/G1 phase of the cell cycle in granulosa and fibroblast cells of cattle. *Animal Reproduction Science.* 87 (3). pp. 181-192.

Heyn, H. & Esteller, M. 2012. DNA methylation profiling in the clinic: applications and challenges. *Nature Reviews Genetics.* 13 (10). pp. 679-692.

Hinkson, I.V. & Elias, J.E. 2011. The dynamic state of protein turnover: It's about time. *Trends in Cell Biology.* 21 (5). pp. 293-303.

Ho, M.R., Tsai, K.W., Chen, C.H. & Lin, W.C. 2011. dbDNV: a resource of duplicated gene nucleotide variants in human genome. *Nucleic Acids Research.* 39 (Database issue). pp. D920-5.

Hopkins, K.M., Wang, X., Berlin, A., Hang, H., Thaker, H.M. & Lieberman, H.B. 2003. Expression of mammalian paralogues of HRAD9 and Mrad9 checkpoint control genes in normal and cancerous testicular tissue. *Cancer Research.* 63 (17). pp. 5291-5298.

Hu, H., Bliss, J.M., Wang, Y. & Colicelli, J. 2005. RIN1 is an ABL tyrosine kinase activator and a regulator of epithelial-cell adhesion and migration. *Current Biology.* 15 (9). pp. 815-823.

Hu, Z., Liu, Y., Zhang, C., Zhao, Y., He, W., Han, L., Yang, L., Hopkins, K.M., Yang, X., Lieberman, H.B. & Hang, H. 2008. Targeted deletion of Rad9 in mouse skin keratinocytes enhances genotoxin-induced tumor development. *Cancer Research.* 68 (14). pp. 5552-5561.

Isokane, M., Walter, T., Mahen, R., Nijmeijer, B., Heriche, J.K., Miura, K., Maffini, S., Ivanov, M.P., Kitajima, T.S., Peters, J.M. & Ellenberg, J. 2016. ARHGEF17 is an essential spindle assembly checkpoint factor that targets Mps1 to kinetochores. *Journal of Cell Biology.* 212 (6). pp. 647-659.

Jackson, S.P. & Bartek, J. 2009. The DNA-damage response in human biology and disease. *Nature.* 461 (7267). pp. 1071-1078.

Janes, S., Schmidt, U., Ashour Garrido, K., Ney, N., Concilio, S., Zekri, M. & Caspari, T. 2012. Heat induction of a novel Rad9 variant from a cryptic translation initiation site reduces mitotic commitment. *Journal of Cell Science.* 125 (Pt 19). pp. 4487-4497.

Jazayeri, A., Falck, J., Lukas, C., Bartek, J., Smith, G.C., Lukas, J. & Jackson, S.P. 2006. ATM-and cell cycle-dependent regulation of ATR in response to DNA double-strand breaks. *Nature Cell Biology.* 8 (1). pp. 37-45.

Jiang, H., Reinhardt, H.C., Bartkova, J., Tommiska, J., Blomqvist, C., Nevanlinna, H., Bartek, J., Yaffe, M.B. & Hemann, M.T. 2009. The combined status of ATM and p53 link tumor development with therapeutic response. *Genes & Development.* 23 (16). pp. 1895-1909.

Johnson, J.M., Castle, J., Garrett-Engele, P., Kan, Z., Loerch, P.M., Armour, C.D., Santos, R., Schadt, E.E., Stoughton, R. & Shoemaker, D.D. 2003. Genome-wide survey of human alternative pre-mRNA splicing with exon junction microarrays. *Science.* 302 (5653). pp. 2141-2144.

Kai, M. 2013. Role of the Checkpoint Clamp in DNA Damage Response. *Biomolecules.* 3 (1). pp. 75-84.

Kasbek, C., Yang, C. & Fisk, H.A. 2009. Mps1 as a link between centrosomes and genomic instability. *Environmental and Molecular Mutagenesis.* 50 (8). pp. 654-665.

Kelemen, O., Convertini, P., Zhang, Z., Wen, Y., Shen, M., Falaleeva, M. & Stamm, S. 2013. Function of alternative splicing. *Gene.* 514 (1). pp. 1-30.

Kim, H. & Colaiácovo, M.P. 2014. ZTF-8 interacts with the 9-1-1 complex and is required for DNA damage response and double-strand break repair in the *C. elegans* germline. *PLoS Genetics.* 10 (10). pp. e1004723.

Kim, J., Fukukawa, C., Ueda, K., Nishidate, T., Katagiri, T. & Nakamura, Y. 2010. Involvement of C12orf32 overexpression in breast carcinogenesis. *International Journal of Oncology.* 37 (4). pp. 861-867.

Kloc, M., Foreman, V. & Reddy, S.A. 2011. Binary function of mRNA. *Biochimie.* 93 (11). pp. 1955-1961.

Knobel, P.A. & Marti, T.M. 2011. Translesion DNA synthesis in the context of cancer research. *Cancer cell international.* 11 (1). pp. 39.

Koike, M., Yutoku, Y. & Koike, A. 2013. Ku80 attentuates cytotoxicity induced by green fluorescent protein transduction independently of non-homologous end joining. *FEBS Open Bio.* 3 (1). pp. 46-50.

Komatsu, K., Hopkins, K.M., Lieberman, H.B. & Wang, H. 2000. *Schizosaccharomyces pombe* Rad9 contains a BH3-like region and interacts with the anti-apoptotic protein Bcl-2. *FEBS Letters.* 481 (2). pp. 122-126.

Komatsu, K., Miyashita, T., Hang, H., Hopkins, K.M., Zheng, W., Cuddeback, S., Yamada, M., Lieberman, H.B. & Wang, H. 2000. Human homologue of *S. pombe* Rad9 interacts with BCL-2/BCL-x L and promotes apoptosis. *Nature Cell Biology.* 2 (1). pp. 1-6.

Kosoy, A. & O'Connell, M.J. 2008. Regulation of Chk1 by its C-terminal domain. *Molecular Biology of the Cell.* 19 (11). pp. 4546-4553.

Krämer, A., Mailand, N., Lukas, C., Syljuåsen, R.G., Wilkinson, C.J., Nigg, E.A., Bartek, J. & Lukas, J. 2004. Centrosome-associated Chk1 prevents premature activation of cyclin-B–Cdk1 kinase. *Nature Cell Biology.* 6 (9). pp. 884-891.

Kuang, S.Q., Bai, H., Fang, Z.H., Lopez, G., Yang, H., Tong, W., Wang, Z.Z. & Garcia-Manero, G. 2010. Aberrant DNA methylation and epigenetic inactivation of Eph receptor tyrosine kinases and ephrin ligands in acute lymphoblastic leukemia. *Blood.* 115 (12). pp. 2412-2419.

Kumari, A., Iwasaki, T., Pyndiah, S., Cassimere, E., Palani, C. & Sakamuro, D. 2015. Regulation of E2F1-induced apoptosis by poly (ADP-ribosyl) ation. *Cell Death & Differentiation.* 22 (2). pp. 311-322.

LaGory, E.L., Sitailo, L.A. & Denning, M.F. 2010. The protein kinase Cdelta catalytic fragment is critical for maintenance of the G2/M DNA damage checkpoint. *Journal of Biological Chemistry.* 285 (3). pp. 1879-1887.

Lee, A.W., Champagne, N., Wang, X., Su, X.D., Goodyer, C. & Leblanc, A.C. 2010. Alternatively spliced caspase-6B isoform inhibits the activation of caspase-6A. *Journal of Biological Chemistry.* 285 (42). pp. 31974-31984.

Lee, M.W., Hirai, I. & Wang, H. 2003. Caspase-3-mediated cleavage of Rad9 during apoptosis. *Oncogene.* 22 (41). pp. 6340-6346.

Leloup, C., Hopkins, K.M., Wang, X., Zhu, A., Wolgemuth, D.J. & Lieberman, H.B. 2010. Mouse Rad9b is essential for embryonic development and promotes resistance to DNA damage. *Developmental Dynamics.* 239 (11). pp. 2837-2850.

Letai, A., Bassik, M.C., Walensky, L.D., Sorcinelli, M.D., Weiler, S. & Korsmeyer, S.J. 2002. Distinct BH3 domains either sensitize or activate mitochondrial apoptosis, serving as prototype cancer therapeutics. *Cancer Cell.* 2 (3). pp. 183-192.

Li, J., Williams, B.L., Haire, L.F., Goldberg, M., Wilker, E., Durocher, D., Yaffe, M.B., Jackson, S.P. & Smerdon, S.J. 2002. Structural and functional versatility of the FHA domain in DNA-damage signaling by the tumor suppressor kinase Chk2. *Molecular Cell.* 9 (5). pp. 1045-1054.

Lieberman, H.B. 2006. Rad9, an evolutionarily conserved gene with multiple functions for preserving genomic integrity. *Journal of Cellular Biochemistry.* 97 (4). pp. 690-697.

Lieberman, H.B., Bernstock, J.D., Broustas, C.G., Hopkins, K.M., Leloup, C. & Zhu, A. 2011. The role of RAD9 in tumorigenesis. *Journal of Molecular Cell Biology.* 3 (1). pp. 39-43.

Lin, S. & Fu, X.D. 2007. SR proteins and related factors in alternative splicing. *Advances in Experimental Medicine and Biology.* 623 pp. 107-122.

Louis, E.J. 2007. Evolutionary genetics: making the most of redundancy. *Nature.* 449 (7163). pp. 673-674.

Lu, Y.F., Goldstein, D.B., Angrist, M. & Cavalleri, G. 2014. Personalized medicine and human genetic diversity. *Cold Spring Harbor Perspectives in Medicine.* 4 (9). pp. a008581.

Lubec, G. & Afjehi-Sadat, L. 2007. Limitations and pitfalls in protein identification by mass spectrometry. *Chemical Reviews.* 107 (8). pp. 3568-3584.

Lynch, K.W. 2007. Regulation of alternative splicing by signal transduction pathways. *Advances in Experimental Medicine and Biology.* 623 pp. 161-174.

Lynch, M. & Conery, J.S. 2000. The evolutionary fate and consequences of duplicate genes. *Science.* 290 (5494). pp. 1151-1155.

Lyndaker, A., Vasileva, A., Wolgemuth, D.J., Weiss, R. & Lieberman, H. 2013. Clamping down on mammalian meiosis. *Cell Cycle.* 12 (19). pp. 3135-3334.

Lyndaker, A.M., Lim, P.X., Mleczko, J.M., Diggins, C.E., Holloway, J.K., Holmes, R.J., Kan, R., Schlafer, D.H., Freire, R. & Cohen, P.E. 2013. Conditional inactivation of the DNA damage response gene Hus1 in mouse testis reveals separable roles for components of the RAD9-RAD1-HUS1 complex in meiotic chromosome maintenance. *PLoS Genetics.* 9 (2). pp. e1003320.

Ma, H.T. & Poon, R.Y. 2011. Cell Cycle Synchronization: Methods and Protocols. *Humana Press.* pp. 151-161.

Ma, J., Ward, C.C., Jungreis, I., Slavoff, S.A., Schwaid, A.G., Neveu, J., Budnik, B.A., Kellis, M. & Saghatelian, A. 2014. Discovery of human sORF-encoded polypeptides (SEPs) in cell lines and tissue. *Journal of Proteome Research.* 13 (3). pp. 1757-1765.

Magadum, S., Banerjee, U., Murugan, P., Gangapur, D. & Ravikesavan, R. 2013. Gene duplication as a major force in evolution. *Journal of Genetics.* 92 (1). pp. 155-161.

Mailand, N., Falck, J., Lukas, C., Syljuasen, R.G., Welcker, M., Bartek, J. & Lukas, J. 2000. Rapid destruction of human Cdc25A in response to DNA damage. *Science.* 288 (5470). pp. 1425-1429.

Makeyev, E.V., Zhang, J., Carrasco, M.A. & Maniatis, T. 2007. The MicroRNA miR-124 promotes neuronal differentiation by triggering brain-specific alternative pre-mRNA splicing. *Molecular Cell.* 27 (3). pp. 435-448.

Manic, G., Obrist, F., Sistigu, A. & Vitale, I. 2015. Trial Watch: Targeting ATM–CHK2 and ATR–CHK1 pathways for anticancer therapy. *Molecular & Cellular Oncology.* 2 (4). pp. e1012976.

Mansilla, S.F., Soria, G., Vallerga, M.B., Habif, M., Martinez-Lopez, W., Prives, C. & Gottifredi, V. 2013. UV-triggered p21 degradation facilitates damaged-DNA replication and preserves genomic stability. *Nucleic Acids Research.* 41 (14). pp. 6942-6951.

Marquardt, J.R., Perkins, J.L., Beuoy, K.J. & Fisk, H.A. 2016. Modular elements of the TPR domain in the Mps1 N terminus differentially target Mps1 to the centrosome and kinetochore. *Proceedings of the National Academy of Sciences of the United States of America.* 113 (28). pp. 7828-7833.

Martinez-Contreras, R., Cloutier, P., Shkreta, L., Fisette, J., Revil, T. & Chabot, B. 2008. 8 hnRNP proteins and splicing control. *Advances in Experimental Medicine & Biology.* 623 pp. 123.

Mattia, M., Gottifredi, V., McKinney, K. & Prives, C. 2007. p53-Dependent p21 mRNA elongation is impaired when DNA replication is stalled. *Molecular and Cellular Biology.* 27 (4). pp. 1309-1320.

Miyashita, T., Krajewski, S., Krajewska, M., Wang, H.G., Lin, H.K., Liebermann, D.A., Hoffman, B. & Reed, J.C. 1994. Tumor suppressor p53 is a regulator of bcl-2 and bax gene expression in vitro and in vivo. *Oncogene.* 9 (6). pp. 1799-1805.

Moldovan, G., Pfander, B. & Jentsch, S. 2007. PCNA, the maestro of the replication fork. *Cell.* 129 (4). pp. 665-679.

Mosley, J.D. & Keri, R.A. 2006. Splice variants of mIAP1 have an enhanced ability to inhibit apoptosis. *Biochemical and Biophysical Research Communications.* 348 (3). pp. 1174-1183.

Muñoz-Espín, D., Cañamero, M., Maraver, A., Gómez-López, G., Contreras, J., Murillo-Cuesta, S., Rodríguez-Baeza, A., Varela-Nieto, I., Ruberte, J. & Collado, M. 2013. Programmed cell senescence during mammalian embryonic development. *Cell.* 155 (5). pp. 1104-1118.

Murray, J.M., Carr, A.M., Lehmann, A.R. & Watts, F.Z. 1991. Cloning and characterisation of the rad9 DNA repair gene from *Schizosaccharomyces pombe*. *Nucleic Acids Research.* 19 (13). pp. 3525-3531.

Ngo, G.H., Balakrishnan, L., Dubarry, M., Campbell, J.L. & Lydall, D. 2014. The 9-1-1 checkpoint clamp stimulates DNA resection by Dna2-Sgs1 and Exo1. *Nucleic Acids Research.* 42 (16). pp. 10516-10528.

Nilsen, T.W. & Graveley, B.R. 2010. Expansion of the eukaryotic proteome by alternative splicing. *Nature.* 463 (7280). pp. 457-463.

Nowakowski, A.B., Wobig, W.J. & Petering, D.H. 2014. Native SDS-PAGE: high resolution electrophoretic separation of proteins with retention of native properties including bound metal ions. *Metallomics.* 6 (5). pp. 1068-1078.

Ohashi, E., Takeishi, Y., Ueda, S. & Tsurimoto, T. 2014. Interaction between Rad9–Hus1–Rad1 and TopBP1 activates ATR–ATRIP and promotes TopBP1 recruitment to sites of UV-damage. *DNA Repair.* 21 pp. 1-11.

Ohmori, H., Friedberg, E.C., Fuchs, R.P., Goodman, M.F., Hanaoka, F., Hinkle, D., Kunkel, T.A., Lawrence, C.W., Livneh, Z. & Nohmi, T. 2001. The Y-family of DNA polymerases. *Molecular Cell.* 8 (1). pp. 7-8.

Ohno, S. 1970. Duplication for the sake of producing more of the same. *Evolution by Gene Duplication*. pp. 59-65.

Okabe, M., Ikawa, M., Kominami, K., Nakanishi, T. & Nishimune, Y. 1997. 'Green mice'as a source of ubiquitous green cells. *FEBS Letters.* 407 (3). pp. 313-319.

Ou, Y.H., Chung, P.H., Sun, T.P. & Shieh, S.Y. 2005. p53 C-terminal phosphorylation by CHK1 and CHK2 participates in the regulation of DNA-damage-induced C-terminal acetylation. *Molecular Biology of the Cell.* 16 (4). pp. 1684-1695.

Pabla, N., Bhatt, K. & Dong, Z. 2012. Checkpoint kinase 1 (Chk1)-short is a splice variant and endogenous inhibitor of Chk1 that regulates cell cycle and DNA damage checkpoints. *Proceedings of the National Academy of Sciences of the United States of America.* 109 (1). pp. 197-202.

Pan, Q., Shai, O., Lee, L.J., Frey, B.J. & Blencowe, B.J. 2008. Deep surveying of alternative splicing complexity in the human transcriptome by high-throughput sequencing. *Nature Genetics.* 40 (12). pp. 1413-1415.

Parrilla-Castellar, E.R., Arlander, S.J. & Karnitz, L. 2004. Dial 9–1–1 for DNA damage: the Rad9–Hus1–Rad1 (9–1–1) clamp complex. *DNA Repair.* 3 (8). pp. 1009-1014.

Peng, C.Y., Graves, P.R., Thoma, R.S., Wu, Z., Shaw, A.S. & Piwnica-Worms, H. 1997. Mitotic and G2 checkpoint control: regulation of 14-3-3 protein binding by phosphorylation of Cdc25C on serine-216. *Science.* 277 (5331). pp. 1501-1505.

Perez-Castro, A.J. & Freire, R. 2012. Rad9B responds to nucleolar stress through ATR and JNK signalling, and delays the G1-S transition. *Journal of Cell Science.* 125 (Pt 5). pp. 1152-1164.

Petsalaki, E. & Zachos, G. 2014. Chk2 prevents mitotic exit when the majority of kinetochores are unattached. *Journal of Cell Biology.* 205 (3). pp. 339-356.

Pichiorri, F., Ishii, H., Okumura, H., Trapasso, F., Wang, Y. & Huebner, K. 2008. Molecular parameters of genome instability: roles of fragile genes at common fragile sites. *Journal of Cellular Biochemistry.* 104 (5). pp. 1525-1533.

Pon, J.R. & Marra, M.A. 2015. Driver and passenger mutations in cancer. *Annual Review of Pathology: Mechanisms of Disease.* 10 pp. 25-50.

Rappsilber, J. & Mann, M. 2002. What does it mean to identify a protein in proteomics? *Trends in Biochemical Sciences.* 27 (2). pp. 74-78.

Roninson, I.B. 2002. Oncogenic functions of tumour suppressor p21 Waf1/Cip1/Sdi1: association with cell senescence and tumour-promoting activities of stromal fibroblasts. *Cancer Letters.* 179 (1). pp. 1-14.

Roos-Mattjus, P., Hopkins, K.M., Oestreich, A.J., Vroman, B.T., Johnson, K.L., Naylor, S., Lieberman, H.B. & Karnitz, L.M. 2003. Phosphorylation of human Rad9 is required for genotoxin-activated checkpoint signaling. *Journal of Biological Chemistry.* 278 (27). pp. 24428-24437.

Rose, M.D. & Fink, G.R. 1987. KAR1, a gene required for function of both intranuclear and extranuclear microtubules in yeast. *Cell.* 48 (6). pp. 1047-1060.

Rossig, L., Jadidi, A.S., Urbich, C., Badorff, C., Zeiher, A.M. & Dimmeler, S. 2001. Akt-dependent phosphorylation of p21(Cip1) regulates PCNA binding and proliferation of endothelial cells. *Molecular and Cellular Biology.* 21 (16). pp. 5644-5657.

Rumbajan, J.M., Yamaguchi, Y., Nakabayashi, K., Higashimoto, K., Yatsuki, H., Nishioka, K., Matsuoka, K., Aoki, S., Toda, S. & Takeda, S. 2016. The HUS1B promoter is hypomethylated in the placentas of low-birth-weight infants. *Gene.* 583 (2). pp. 141-146.

Sabe, H. 2003. Requirement for Arf6 in cell adhesion, migration, and cancer cell invasion. *Journal of Biochemistry.* 134 (4). pp. 485-489.

Sánchez Rodríguez, L. 2008. Sex-determining mechanisms in insects. *International Journal of Developmental Biology.* 52(7), pp.837-856

Sauer, B. 1994. Site-specific recombination: developments and applications. *Current Opinion in Biotechnology.* 5 (5). pp. 521-527.

Sevignani, C., Calin, G.A., Siracusa, L.D. & Croce, C.M. 2006. Mammalian microRNAs: a small world for fine-tuning gene expression. *Mammalian Genome.* 17 (3). pp. 189-202.

Sharp, P.A. 2005. The discovery of split genes and RNA splicing. *Trends in Biochemical Sciences.* 30 (6). pp. 279-280.

Shieh, S.Y., Ahn, J., Tamai, K., Taya, Y. & Prives, C. 2000. The human homologs of checkpoint kinases Chk1 and Cds1 (Chk2) phosphorylate p53 at multiple DNA damage-inducible sites. *Genes & Development.* 14 (3). pp. 289-300.

Shin, C. & Manley, J.L. 2004. Cell signalling and the control of pre-mRNA splicing. *Nature Reviews Molecular Cell Biology.* 5 (9). pp. 727-738.

Shkreta, L. & Chabot, B. 2015. The RNA splicing response to DNA damage. *Biomolecules.* 5 (4). pp. 2935-2977.

Siliciano, J.D., Canman, C.E., Taya, Y., Sakaguchi, K., Appella, E. & Kastan, M.B. 1997. DNA damage induces phosphorylation of the amino terminus of p53. *Genes & Development.* 11 (24). pp. 3471-3481.

Skube, S.B., Chaverri, J.M. & Goodson, H.V. 2010. Effect of GFP tags on the localization of EB1 and EB1 fragments in vivo. *Cytoskeleton.* 67 (1). pp. 1-12.

Slavoff, S.A., Heo, J., Budnik, B.A., Hanakahi, L.A. & Saghatelian, A. 2014. A human short open reading frame (sORF)-encoded polypeptide that stimulates DNA end joining. *Journal of Biological Chemistry.* 289 (16). pp. 10950-10957.

Slavoff, S.A., Mitchell, A.J., Schwaid, A.G., Cabili, M.N., Ma, J., Levin, J.Z., Karger, A.D., Budnik, B.A., Rinn, J.L. & Saghatelian, A. 2013. Peptidomic discovery of short open reading frame–encoded peptides in human cells. *Nature Chemical Biology.* 9 (1). pp. 59-64.

Smith, J., Mun Tho, L., Xu, N. & Gillespie, D.A. 2010. The ATM-Chk2 and ATR-Chk1 pathways in DNA damage signaling and cancer. *Advances in Cancer Research.* 108 (C). pp. 73-112.

Soria, G. & Gottifredi, V. 2010. PCNA-coupled p21 degradation after DNA damage: The exception that confirms the rule? *DNA Repair.* 9 (4). pp. 358-364.

Soria, G., Podhajcer, O., Prives, C. & Gottifredi, V. 2006. P21Cip1/WAF1 downregulation is required for efficient PCNA ubiquitination after UV irradiation. *Oncogene.* 25 (20). pp. 2829-2838.

Soria, G., Speroni, J., Podhajcer, O.L., Prives, C. & Gottifredi, V. 2008. p21 differentially regulates DNA replication and DNA-repair-associated processes after UV irradiation. *Journal of Cell Science.* 121 (Pt 19). pp. 3271-3282.

Sossey-Alaoui, K., Li, X. & Cowell, J.K. 2007. c-Abl-mediated phosphorylation of WAVE3 is required for lamellipodia formation and cell migration. *Journal of Biological Chemistry.* 282 (36). pp. 26257-26265.

Staalesen, V., Falck, J., Geisler, S., Bartkova, J., Børresen-Dale, A., Lukas, J., Lillehaug, J.R., Bartek, J. & Lønning, P.E. 2004. Alternative splicing and mutation status of CHEK2 in stage III breast cancer. *Oncogene.* 23 (52). pp. 8535-8544.

Stallons, L.J. & McGregor, W.G. 2010. Translesion synthesis polymerases in the prevention and promotion of carcinogenesis. *Journal of Nucleic Acids.* 2010 pp. 10.4061/2010/643857.

Storer, M., Mas, A., Robert-Moreno, A., Pecoraro, M., Ortells, M.C., Di Giacomo, V., Yosef, R., Pilpel, N., Krizhanovsky, V. & Sharpe, J. 2013. Senescence is a developmental mechanism that contributes to embryonic growth and patterning. *Cell.* 155 (5). pp. 1119-1130.

Stracker, T.H., Roig, I., Knobel, P.A. & Marjanovic, M. 2013. The ATM signaling network in development and disease. *Frontiers in Genetics.* 4. pp. 37.

Strebhardt, K. & Ullrich, A. 2006. Targeting polo-like kinase 1 for cancer therapy. *Nature Reviews Cancer.* 6 (4). pp. 321-330.

Sugnet, C.W., Kent, W.J., Ares, M. & Haussler, D. 2004. Transcriptome and genome conservation of alternative splicing events in humans and mice. *Pacific Symposium on Biocomputing.* 9. pp. 66.

Sur, S., Pagliarini, R., Bunz, F., Rago, C., Diaz, L.A.,Jr, Kinzler, K.W., Vogelstein, B. & Papadopoulos, N. 2009. A panel of isogenic human cancer cells suggests a therapeutic approach for cancers with inactivated p53. *Proceedings of the National Academy of Sciences of the United States of America.* 106 (10). pp. 3964-3969.

Suzuki, H., Yabuta, N., Okada, N., Torigata, K., Aylon, Y., Oren, M. & Nojima, H. 2013. Lats2 phosphorylates p21/CDKN1A after UV irradiation and regulates apoptosis. *Journal of Cell Science.* 126 (Pt 19). pp. 4358-4368.

Tanaka, Y., Maniwa, Y., Bermudez, V.P., Nishio, W., Ohbayashi, C., Okita, Y., Hurwitz, J., Hayashi, Y. & Yoshimura, M. 2010. Nonsynonymous single nucleotide polymorphisms in DNA damage repair pathways and lung cancer risk. *Cancer.* 116 (4). pp. 896-902.

Tschan, M.P., Fischer, K.M., Fung, V.S., Pirnia, F., Borner, M.M., Fey, M.F., Tobler, A. & Torbett, B.E. 2003. Alternative splicing of the human cyclin D-binding Myb-like protein (hDMP1) yields a truncated protein isoform that alters macrophage differentiation patterns. *Journal of Biological Chemistry.* 278 (44). pp. 42750-42760.

Tsvetkov, L., Xu, X., Li, J. & Stern, D.F. 2003. Polo-like kinase 1 and Chk2 interact and co-localize to centrosomes and the midbody. *Journal of Biological Chemistry.* 278 (10). pp. 8468-8475.

Turner, T. & Caspari, T. 2014. When heat casts a spell on the DNA damage checkpoints. *Open biology.* 4 (3). p.140008.

Tuul, M., Kitao, H., Iimori, M., Matsuoka, K., Kiyonari, S., Saeki, H., Oki, E., Morita, M. & Maehara, Y. 2013. Rad9, Rad17, TopBP1 and claspin play essential roles in heat-induced activation of ATR kinase and heat tolerance. *PLoS One.* 8 (2). pp. e55361.

van Vugt, M.A., Gardino, A.K., Linding, R., Ostheimer, G.J., Reinhardt, H.C., Ong, S., Tan, C.S., Miao, H., Keezer, S.M. & Li, J. 2010. A mitotic phosphorylation feedback network connects Cdk1, Plk1, 53BP1, and Chk2 to inactivate the G 2/M DNA damage checkpoint. *PLoS Biology.* 8 (1). pp. e1000287.

Vassylyev, D.G. & Symersky, J. 2007. Crystal structure of pyruvate dehydrogenase phosphatase 1 and its functional implications. *Journal of Molecular Biology.* 370 (3). pp. 417-426.

Vaux, D.L. 1998. Immunopathology of apoptosis—introduction and overview. *Springer Seminars in Immunopathology*. 19 (3). pp. 271-278.

von Schubert, C., Cubizolles, F., Bracher, J.M., Sliedrecht, T., Kops, G.J. & Nigg, E.A. 2015. Plk1 and Mps1 cooperatively regulate the spindle assembly checkpoint in human cells. *Cell Reports.* 12 (1). pp. 66-78.

Wahl, M.C., Will, C.L. & Lührmann, R. 2009. The spliceosome: design principles of a dynamic RNP machine. *Cell.* 136 (4). pp. 701-718.

Wang, E.T., Sandberg, R., Luo, S., Khrebtukova, I., Zhang, L., Mayr, C., Kingsmore, S.F., Schroth, G.P. & Burge, C.B. 2008. Alternative isoform regulation in human tissue transcriptomes. *Nature.* 456 (7221). pp. 470-476.

Wang, K., Cao, K. & Hannenhalli, S. 2015. Chromatin and genomic determinants of alternative splicing. *Proceedings of the 6th ACM Conference on Bioinformatics, Computational Biology and Health Informatics.* pp. 345-354.

Wang, L., Hsu, C.L., Ni, J., Wang, P.H., Yeh, S., Keng, P. & Chang, C. 2004. Human checkpoint protein hRad9 functions as a negative coregulator to repress androgen receptor transactivation in prostate cancer cells. *Molecular and Cellular Biology.* 24 (5). pp. 2202-2213.

Wang, L., Pan, J., Wang, T., Song, M. & Chen, W. 2013. Pathological cyclic strain-induced apoptosis in human periodontal ligament cells through the RhoGDIα/caspase-3/PARP pathway. *PloS One.* 8 (10). pp. e75973.

Wang, X., Chu, H., Lv, M., Zhang, Z., Qiu, S., Liu, H., Shen, X., Wang, W. & Cai, G. 2016. Structure of the intact ATM/Tel1 kinase. *Nature Communications.* 7.

Wei, J.H., Chou, Y.F., Ou, Y.H., Yeh, Y.H., Tyan, S.W., Sun, T.P., Shen, C.Y. & Shieh, S.Y. 2005. TTK/hMps1 participates in the regulation of DNA damage checkpoint response by phosphorylating CHK2 on threonine 68. *The Journal of Biological Chemistry.* 280 (9). pp. 7748-7757.

Weiss, E. & Winey, M. 1996. The *Saccharomyces cerevisiae* spindle pole body duplication gene MPS1 is part of a mitotic checkpoint. *The Journal of Cell Biology.* 132 (1-2). pp. 111-123.

Wu, C., Huang, K., Yang, T., Li, Y., Wen, C., Hsu, S. & Chen, T. 2015. The Topoisomerase 1 Inhibitor Austrobailignan-1 Isolated from Koelreuteria henryi Induces a G2/M-Phase Arrest and Cell Death Independently of p53 in Non-Small Cell Lung Cancer Cells. *PloS One.* 10 (7). pp. e0132052.

Wu, X., Shell, S.M. & Zou, Y. 2005. Interaction and colocalization of Rad9/Rad1/Hus1 checkpoint complex with replication protein A in human cells. *Oncogene.* 24 (29). pp. 4728-4735.

Xie, J. & Black, D.L. 2001. A CaMK IV responsive RNA element mediates depolarization-induced alternative splicing of ion channels. *Nature.* 410 (6831). pp. 936-939.

Xu, M., Bai, L., Gong, Y., Xie, W., Hang, H. & Jiang, T. 2009. Structure and functional implications of the human rad9-hus1-rad1 cell cycle checkpoint complex. *The Journal of Biological Chemistry.* 284 (31). pp. 20457-20461.

Xu, X., Tsvetkov, L.M. & Stern, D.F. 2002. Chk2 activation and phosphorylation-dependent oligomerization. *Molecular and Cellular Biology.* 22 (12). pp. 4419-4432.

Yearim, A., Gelfman, S., Shayevitch, R., Melcer, S., Glaich, O., Mallm, J., Nissim-Rafinia, M., Cohen, A.S., Rippe, K. & Meshorer, E. 2015. HP1 is involved in regulating the global impact of DNA methylation on alternative splicing. *Cell Reports.* 10 (7). pp. 1122-1134.

Yeh, Y., Huang, Y., Lin, T. & Shieh, S. 2009. The cell cycle checkpoint kinase CHK2 mediates DNA damage-induced stabilization of TTK/hMps1. *Oncogene.* 28 (10). pp. 1366-1378.

Yogalingam, G. & Pendergast, A.M. 2008. Abl kinases regulate autophagy by promoting the trafficking and function of lysosomal components. *The Journal of Biological Chemistry.* 283 (51). pp. 35941-35953.

Yoshida, K., Wang, H.G., Miki, Y. & Kufe, D. 2003. Protein kinase Cdelta is responsible for constitutive and DNA damage-induced phosphorylation of Rad9. *EMBO Journal.* 22 (6). pp. 1431-1441.

Yu, Z.C., Huang, Y.F. & Shieh, S.Y. 2016. Requirement for human Mps1/TTK in oxidative DNA damage repair and cell survival through MDM2 phosphorylation. *Nucleic Acids Research.* 44 (3). pp. 1133-1150.

Zannini, L., Delia, D. & Buscemi, G. 2014. CHK2 kinase in the DNA damage response and beyond. *Journal of Molecular Cell Biology.* 6 (6). pp. 442-457.

Zhang, X., Ling, Y., Wang, W., Zhang, Y., Ma, Q., Tan, P., Song, T., Wei, C., Li, P. & Liu, X. 2013. UV-C irradiation delays mitotic progression by recruiting Mps1 to kinetochores. *Cell Cycle.* 12 (8). pp. 1292-1302.

Zhao, H., Traganos, F., Albino, A.P. & Darzynkiewicz, Z. 2008. Oxidative stress induces cell cycle-dependent Mre11 recruitment, ATM and Chk2 activation and histone H2AX phosphorylation. *Cell Cycle.* 7 (10). pp. 1490-1495.

Zhao, H., Watkins, J.L. & Piwnica-Worms, H. 2002. Disruption of the checkpoint kinase 1/cell division cycle 25A pathway abrogates ionizing radiation-induced S and G2 checkpoints. *Proceedings of the National Academy of Sciences of the United States of America.* 99 (23). pp. 14795-14800.

Zhao, L. & Washington, M.T. 2017. Translesion Synthesis: Insights into the Selection and Switching of DNA Polymerases. *Genes.* 8 (1). pp. 24.

Zhao, Y., Ma, X., Wang, J., Chen, S., Yuan, H., Xu, A., Hang, H. & Wu, L. 2015. The Roles of p21Waf1/CIP1 and Hus1 in Generation and Transmission of Damage Signals Stimulated by Low-Dose Alpha-Particle Irradiation. *Radiation Research.* 184 (6). pp. 578-585.

Zhu, A., Zhang, C.X. & Lieberman, H.B. 2008. Rad9 has a functional role in human prostate carcinogenesis. *Cancer Research.* 68 (5). pp. 1267-1274.

Appendices

Appendix 1

RT-PCR analysis of human RAD9B splice variants in normal tissues

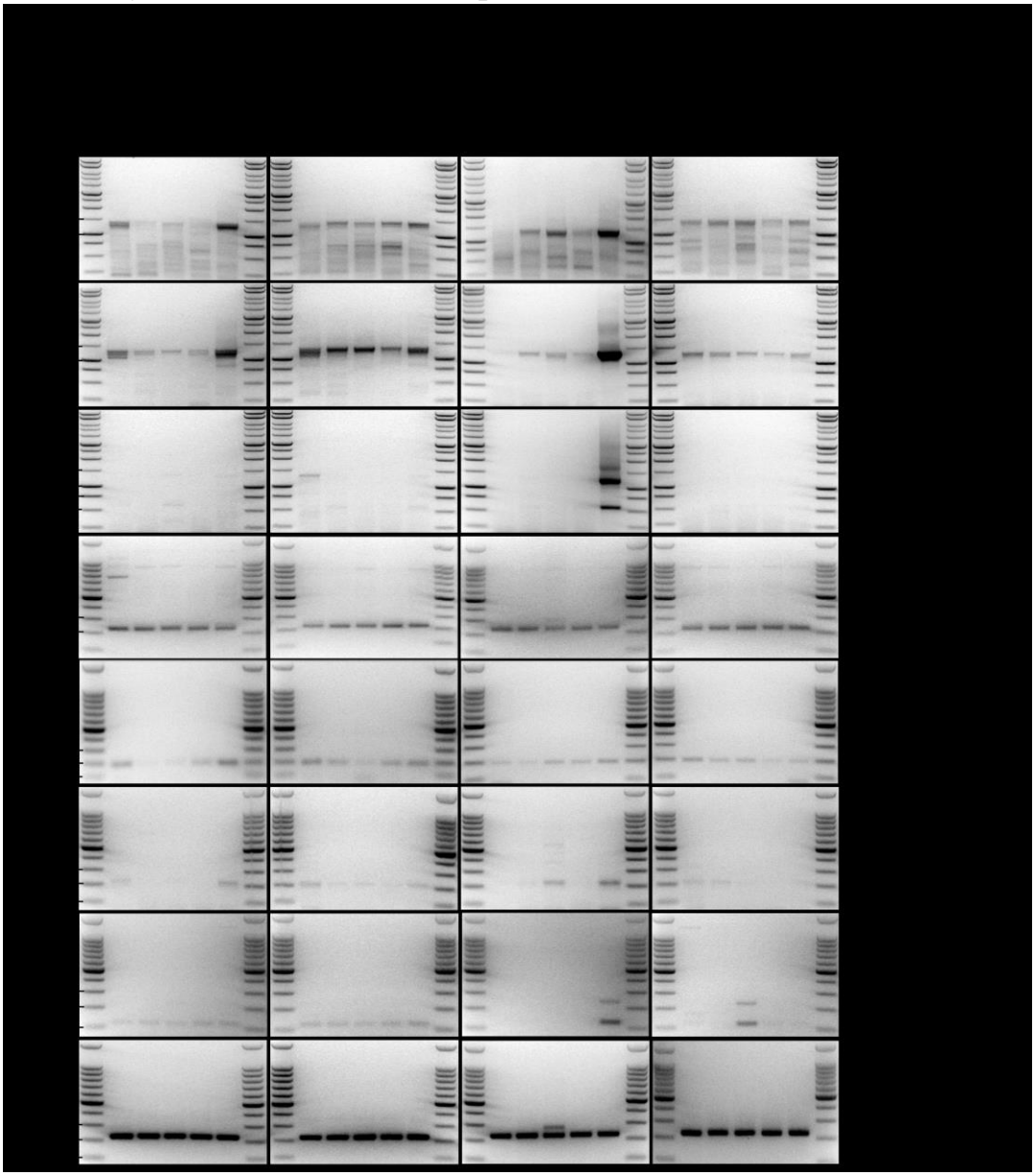

RT-PCR analysis of the *RAD9B* mRNA across several normal human tissues. (A) 200 ng of total human RNA (Human Total RNA Master Panel II, Clontech Laboratories) was reverse transcribed and amplified by Bioline One-Step RT-PCR kit using specific primers for *RAD9B-001*, 002/005, 003 and 009. Then 10 µl of the RT-PCR reactions were run on 0.8% agarose gels. (B) 1 µg of RNA from the Human Total RNA Master Panel II (Clontech Laboratories) was reverse transcribed into cDNA by a Bioline cDNA synthesis kit, followed by RT-PCR to amplify short regions of *RAD9B-001*, 002/005, 003 and 009 using Bioline Red Mix polymerase. Then 20 µl of the RT-PCR reactions were loaded on 1.5% agarose gels for all variants, except for *009*. The *009* variant was run on 2% agarose gels. *ACTB* was used as a positive control for the one-step and two-step RT-PCRs. For *ACTB*, 10 µl of the reaction was run on 1.5% agarose gels. All images were taken by the Bio-Rad Documentation System. The name and expected amplicon size of each gene is shown to the right.

Appendix 2

Alignment of the five *RAD9B* splice variants *001*, *002*, *003*, *005* and *009*

```
RAD9B-001      AAAGCCGTTTGGGAACTTGTGGAGGCGGGGTGGTAGAGTGCAGAGACGAGATCGCGAAGC 60
RAD9B-002      ------------------------------------------------------------ 0
RAD9B-003      ----------------------------------------GCAGAGACGAGATCGCGAAGC 21
RAD9B-005      ------------------------------------------------------------ 0
RAD9B-009      ------------------------------------------------------------ 0

RAD9B-001      TTTGAAAAGCGCGGGCAACATCCGGGCACCTGGGCCGTCGAGCTGAGGCGCGCCTTCCGA 120
RAD9B-002      ------------------------------GGGCCGTCGAGCTGAGGCGCGCCTTCCGA 29
RAD9B-003      TTTGAAAAGCGCGGGCAACATCCGGGCACCTGGGCCGTCGAGCTGAGGCGCGCCTTCCGA 81
RAD9B-005      ------------------------------GGGCCGTCGAGCTGAGGCGCGCCTTCCGA 29
RAD9B-009      ----------------------------------------------------TTCCGA 6
                                                                      ******

RAD9B-001      GCCTGCTTTTTAGGGCGGATGGCAGCC----------------------------ATGC 151
RAD9B-002      GCCTGCTTTTTAGGGCGGATGGCAGCCATGCTGAAGTGCGTGATGAGCGGCAGTCAGGTG 89
RAD9B-003      GCCTGCTTTTTAGGGCGGATGGCAGCCATGCTGAAGTGCGTGATGAGCGGCAGTCAGGTG 141
RAD9B-005      GCCTGCTTTTTAGGGCGGATGGCAGCCATGCTGAAGTGCGTGATGAGCGGCAGTC----- 84
RAD9B-009      GCCTGCTTTTTAGGGCGGATGGCAGCCATGCTGAAGTGCGTGATGAGCGGCAGTCAGGTG 66
               **************************

RAD9B-001      TGAATATTTGGGAAAGCAGTTCAAGCTCTATCACGAATTAGTGACGAGTTCTGGCTAGAC 211
RAD9B-002      AAAGTATTTGGGAAAGCAGTTCAAGCTCTATCACGAATTAGTGACGAGTTCTGGCTAGAC 149
RAD9B-003      AAAGTATTTGGGAAAGCAGTTCAAGCTCTATCACGAATTAGTGACGAGTTCTGGCTAGAC 201
RAD9B-005      --AGTATTTGGGAAAGCAGTTCAAGCTCTATCACGAATTAGTGACGAGTTCTGGCTAGAC 142
RAD9B-009      AAAGTATTTGGGAAAGCAGTTCAAGCTCTATCACGAATTAGTGACGAGTTCTGGCTAGAC 126
                 * ************************************************

RAD9B-001      CCATCTAAAAAAGGTCTTGCTCTAAGATGTGTGAATTCTTCTCGGTCAGCATATGGATGT 271
RAD9B-002      CCATCTAAAAAAGGTCTTGCTCTAAGATGTGTGAATTCTTCTCGGTCAGCATATGGATGT 209
RAD9B-003      CCATCTAAAAAAGGTCTTGCTCTAAGATGTGTGAATTCTTCTCGGTCAGCATATGGATGT 261
RAD9B-005      CCATCTAAAAAAGGTCTTGCTCTAAGATGTGTGAATTCTTCTCGGTCAGCATATGGATGT 202
RAD9B-009      CCATCTAAAAAAGGTCTTGCTCTAAGATGTGTGAATTCTTCTCGGTCAGCATATGGATGT 186
               ************************************************************

RAD9B-001      GTCCTGTTCTCTCCTGTGTTTTTTCAGCATTATCAATGGTCAGCTTTAGTGAAAATGAGT 331
RAD9B-002      GTCCTGTTCTCTCCTGTGTTTTTTCAGCATTATCAATGGTCAGCTTTAGTGAAAATGAGT 269
RAD9B-003      GTCCTGTTCTCTCCTGTGTTTTTTCAGCATTATCAATGGTCAGCTTTAGTGAAAATGAGT 321
RAD9B-005      GTCCTGTTCTCTCCTGTGTTTTTTCAGCATTATCAATGGTCAGCTTTAGTGAAAATGAGT 262
RAD9B-009      GTCCTGTTCTCTCCTGTGTTTTTTCAGCATTATCAATGGTCAGCTTTAGTGAAAATGAGT 246
               ************************************************************

RAD9B-001      GAAAATGAACTTGACACAACACTGCATTTAAAATGCAAATTGGGAATGAAGTCAATTTTG 391
RAD9B-002      GAAAATGAACTTGACACAACACTGCATTTAAAATGCAAATTGGGAATGAAGTCAATTTTG 329
RAD9B-003      GAAAATGAACTTGACACAACACTGCATTTAAAATGCAAATTGGGAATGAAGTCAATTTTG 381
RAD9B-005      GAAAATGAACTTGACACAACACTGCATTTAAAATGCAAATTGGGAATGAAGTCAATTTTG 322
RAD9B-009      GAAAATGAACTTGACACAACACTGCATTTAAAATGCAAATTGGGAATGAAGTCAATTTTG 306
               ************************************************************

RAD9B-001      CCCATCTTTAGATGTCTGAATTCCCTTGAAAGAAATATAGAGAAGTGCAGAATATTCACC 451
RAD9B-002      CCCATCTTTAGATGTCTGAATTCCCTTGAAAGAAATATAGAGAAGTGCAGAATATTCACC 389
RAD9B-003      CCCATCTTTAGATGTCTGAATTCCCTTGAAAGAAATATAGAGAAGTGCAGAATATTCACC 441
RAD9B-005      CCCATCTTTAGATGTCTGAATTCCCTTGAAAGAAATATAGAGAAGTGCAGAATATTCACC 382
RAD9B-009      CCCATCTTTAGATGTCTGAATTCCCTTGAAAGAAATATAGAGAAGTGCAGAATATTCACC 366
               ************************************************************

RAD9B-001      AGATCTGATAAATGCAAAGTAGTTATTCAATTCTTCTACAGACATGGTATTAAAAGAACT 511
RAD9B-002      AGATCTGATAAATGCAAAGTAGTTATTCAATTCTTCTACAGACATGGTATTAAAAGAACT 449
RAD9B-003      AGATCTGATAAATGCAAAGTAGTTATTCAATTCTTCTACAGACATGGTATTAAAAGAACT 501
RAD9B-005      AGATCTGATAAATGCAAAGTAGTTATTCAATTCTTCTACAGACATGGTATTAAAAGAACT 442
```

```
RAD9B-009      AGATCTGATAAATGCAAAGTAGTTATTCAATTCTTCTACAGACATG---------------- 412
               ****************************************

RAD9B-001      CATAATATATGTTTTCAAGAAAGTCAGCCTTTGCAAGTTATTTTTGACAAGAATGTTTGT 571
RAD9B-002      CATAATATATGTTTTCAAGAAAGTCAGCCTTTGCAAGTTATTTTTGACAAGAATGTTTGT 509
RAD9B-003      CATAATATATGTTTTCAAGAAAGTCAGCCTTTGCAAGTTATTTTTGACAAGAATGTTTGT 561
RAD9B-005      CATAATATATGTTTTCAAGAAAGTCAGCCTTTGCAAGTTATTTTTGACAAGAATGTTTGT 502
RAD9B-009      ------------------------------------------------------------ 412


RAD9B-001      ACTAATACGCTAATGATTCAACCAAGATTGCTTGCTGATGCCATTGTTCTTTTTACATCA 631
RAD9B-002      ACTAATACGCTAATGATTCAACCAAGATTGCTTGCTGATGCCATTGTTCTTTTTACATCA 569
RAD9B-003      ACTAATACGCTAATGATTCAACCAAGATTGCTTGCTGATGCCATTGTTCTTTTTACATCA 621
RAD9B-005      ACTAATACGCTAATGATTCAACCAAGATTGCTTGCTGATGCCATTGTTCTTTTTACATCA 562
RAD9B-009      ------------------------------------------------------------ 412


RAD9B-001      AGTCAAGAGGAAGTTACTCTTGCTGTTACTCCACTGAATTTTTGCCTCAAGAGTTCTAAT 691
RAD9B-002      AGTCAAGAGGAAGTTACTCTTGCTGTTACTCCACTGAATTTTTGCCTCAAGAGTTCTAAT 629
RAD9B-003      AGTCAAGAGGAAGTTACTCTTGCTGTTACTCCACTGAATTTTTGCCTCAAGAGTTCTAAT 681
RAD9B-005      AGTCAAGAGGAAGTTACTCTTGCTGTTACTCCACTGAATTTTTGCCTCAAGAGTTCTAAT 622
RAD9B-009      ------------------------------------------------------------ 412


RAD9B-001      GAGGAATCAATGGATTTGAGCAATGCTGTACACAGTGAGATGTTTGTTGGCTCAGATGAG 751
RAD9B-002      GAGGAATCAATGGATTTGAGCAATGCTGTACACAGTGAGATGTTTGTTGGCTCAGATGAG 689
RAD9B-003      GAGGAATCAATGGATTTGAGCAATGCTGTACACAGTGAGATGTTTGTTGGCTCAGATGAG 741
RAD9B-005      GAGGAATCAATGGATTTGAGCAATGCTGTACACAGTGAGATGTTTGTTGGCTCAGATGAG 682
RAD9B-009      -------------ATTTGAGCAATGCTGTACACAGTGAGATGTTTGTTGGCTCAGATGAG 459
                           ********************************************

RAD9B-001      TTTGACTTCTTTCAAATTGGAATGGACACTGAGATAACATTTTGTTTCAAAGAATTGAAG 811
RAD9B-002      TTTGACTTCTTTCAAATTGGAATGGACACTGAGATAACATTTTGTTTCAAAGAATTGAAG 749
RAD9B-003      TTTGACTTCTTTCAAATTGGAATGGACACTGAGATAACATTTTGTTTCAAAGAATTGAAG 801
RAD9B-005      TTTGACTTCTTTCAAATTGGAATGGACACTGAGATAACATTTTGTTTCAAAGAATTGAAG 742
RAD9B-009      TTTGACTTCTTTCAAATTGGAATGGACACTGAGATAACATTTTGTTTCAAAGAATTGAAG 519
               ************************************************************

RAD9B-001      GGAATACTGACATTTTCAGAAGCTACACATGCTCCTATATCCATTTATTTTGATTTCCCT 871
RAD9B-002      GGAATACTGACATTTTCAGAAGCTACACATGCTCCTATATCCATTTATTTTGATTTCCCT 809
RAD9B-003      GGAATACTGACATTTTCAGAAGCTACACATGCTCCTATATCCATTTATTTTGATTTCCCT 861
RAD9B-005      GGAATACTGACATTTTCAGAAGCTACACATGCTCCTATATCCATTTATTTTGATTTCCCT 802
RAD9B-009      GGAATACTGACATTTTCAGAAGCTACACATGCTCCTATATCCATTTATTTTGATTTCCCT 579
               ************************************************************

RAD9B-001      GGGAAACCTCTGGCTTTGAGTATTGATGATATGTTAGTGGAAGCTAACTTTATTTTGGCC 931
RAD9B-002      GGGAAACCTCTGGCTTTGAGTATTGATGATATGTTAGTGGAAGCTAACTTTATTTTGGCC 869
RAD9B-003      GGGAAACCTCTGGCTTTGAGTATTGATGATATGTTAGTGGAAGCTAACTTTATTTTGGCC 921
RAD9B-005      GGGAAACCTCTGGCTTTGAGTATTGATGATATGTTAGTGGAAGCTAACTTTATTTTGGCC 862
RAD9B-009      GGGAAACCTCTGGCTTTGAGTATTGATGATATGTTAGTGGAAGCTAACTTTATTTTGGCC 639
               ************************************************************

RAD9B-001      ACATTAGCTGATGAACAAAGTAGAGCATCTTCACCACAGTCACTGTGTCTTTCACAGAAA 991
RAD9B-002      ACATTAGCTGATGAACAAAGTAGAGCATCTTCACCACAGTCACTGTGTCTTTCACAGAAA 929
RAD9B-003      ACATTAGCTGATGAACAAAGTAGAGCATCTTCACCACAGTCACTGTGTCTTTCACAGAAA 981
RAD9B-005      ACATTAGCTGATGAACAAAGTAGAGCATCTTCACCACAGTCACTGTGTCTTTCACAGAAA 922
RAD9B-009      ACATTAGCTGATGAACAAAGTAGAGCATCTTCACCACAGTCACTGTGTCTTTCACAGAAA 699
               ************************************************************

RAD9B-001      CGAAAAAGGTCAGATCTGATTGAAAAAAAGGCTGGCAAAAATGTAACTGGCCAGGCCCTG 1051
RAD9B-002      CGAAAAAGGTCAGATCTGATTGAAAAAAAGGCTGGCAAAAATGTAACTGGCCAGGCCCTG 989
RAD9B-003      CGAAAAAGGTCAGATCTGATTGAAAAAAAGGCTGGCAAAAATGTAACTGGCCAGGCCCTG 1041
RAD9B-005      CGAAAAAGGTCAGATCTGATTGAAAAAAAGGCTGGCAAAAATGTAACTGGCCAGGCCCTG 982
RAD9B-009      CGAAAAAGGTCAGATCTGATTGAAAAAAAGGCTGGCAAAAATGTAACTGGCCAGGCCCTG 759
               ************************************************************

RAD9B-001      GAATGTATTTCAAAAAAAGCAGCACCAAGAAGGCTTTATCCTAAGGAGACTCTCACAAAC 1111
RAD9B-002      GAATGTATTTCAAAAAAAGCAGCACCAAGAAGGCTTTATCCTAAGGAGACTCTCACAAAC 1049
```

```
RAD9B-003      GAATGTATTTCAAAAAAAGCAGCACCAAGAAGGCTTTATCCTAAGGAGACTCTCACAAAC 1101
RAD9B-005      GAATGTATTTCAAAAAAAGCAGCACCAAGAAGGCTTTATCCTAAGGAGACTCTCACAAAC 1042
RAD9B-009      GAATGTATTTCAAAAAAAGCAGCACCAAGAAGGCTTTATCCTAAGGAGACTCTCACAAAC 819
               ************************************************************

RAD9B-001      ATATCTGCATTGGAAAACTGTGGCAGCCCTGCAATGAAAAGAGTGGATGGAGATGTCAGT 1171
RAD9B-002      ATATCTGCATTGGAAAACTGTGGCAGCCCTGCAATGAAAAGAGTGGATGGAGATGTCAGT 1109
RAD9B-003      ATATCTGCATTGGAAAACTGTGGCAGCCCTGCAATGAAAAGAGTGGATGGAGATGTCAGT 1161
RAD9B-005      ATATCTGCATTGGAAAACTGTGGCAGCCCTGCAATGAAAAGAGTGGATGGAGATGTCAGT 1102
RAD9B-009      ATATCTGCATTGGAAAACTGTGGCAGCCCTGCAATGAAAAGAGTGGATGGAGATGTCAGT 879
               ************************************************************

RAD9B-001      GAAGTATCAGAAAGCAGTGTCAGCAACACAGAGGAAGTGCCAGGGTCTCTGTGTCTCAGA 1231
RAD9B-002      GAAGTATCAGAAAGCAGTGTCAGCAACACAGAGGAAGTGCCAGGGTCTCTGTGTCTCAGA 1169
RAD9B-003      GAAGTATCAGAAAGCAGTGTCAGCAACACAGAGGAAGTGCCAGGGTCTCTGTGTCTCAGA 1221
RAD9B-005      GAAGTATCAGAAAGCAGTGTCAGCAACACAGAGGAAGTGCCAGGGTCTCTGTGTCTCAGA 1162
RAD9B-009      GAAGTATCAGAAAGCAGTGTCAGCAACACAGAGGAAGTGCCAGGGTCTCTGTGTCTCAGA 939
               ************************************************************

RAD9B-001      AAGTTTTCTTGCATGTTCTTTGGAGCAGTTTCTTCTGACCAGCAAGAACACTTCAACCAC 1291
RAD9B-002      AAGTTTTCTTGCATGTTCTTTGGAGCAGTTTCTTCTGACCAGCAAGAACACTTCAACCAC 1229
RAD9B-003      AAGTTTTCTTGCATGTTCTTTGGAGCAGTTTCTTCTGACCAGCAAGAACACTTCAACCAC 1281
RAD9B-005      AAGTTTTCTTGCATGTTCTTTGGAGCAGTTTCTTCTGACCAGCAAGAACACTTCAACCAC 1222
RAD9B-009      AAG---------------------------------------------------------- 942
               ***

RAD9B-001      CCTTTCGACAGTCTGGCAAGAGCAAGTGACAGTGAAGAGGACATGAATAATGGCAGTTTC 1351
RAD9B-002      CCTTTCGACAGTCTGGCAAGAGCAAGTGACAGTGAAGAGGACATGAATAATGGCAGTTTC 1289
RAD9B-003      CCTTTCGACAGTCTGGCAAGAGCAAGTGACAGTGAAGAGGACATGAATAATGTGTGCTGC 1341
RAD9B-005      CCTTTCGACAGTCTGGCAAGAGCAAGTGACAGTGAAGAGGACATGAATAATGGCAGTTTC 1282
RAD9B-009      ----------------------------------------------------TGTGCTGC 950
                                                                     * * *

RAD9B-001      TCTATATTCTAATGCTTAATGATGGCTGAGCTGGGCCCCAGC-CCAGTGACTGGCTCATT 1410
RAD9B-002      TCTATATTCTAATGCTTAATGATGGCTGAGCTGGGCCCCAGC-CCAGTGACTGGCTCATT 1348
RAD9B-003      AGGAAAGAATTTAATGGAAGTGATGCCAAATATTTCTGTATTATCTGACATAGAACAGTA 1401
RAD9B-005      TCTATATTCTAATGCTTAATGATGGCTGAGCTGGGCCCCAGC-CCAGTGACTGGCTCATT 1341
RAD9B-009      AGGAAAGAATTTAATGGAAGTGATGCCAAATATTTCTGTATTATCTGACATAGAACAGTA 1010
                  * *   *       **     **  *      *   *    * *  *  *     *

RAD9B-001      TGCCCCTCAAGCACGAG--TTTGCATGTTTAGTGTCTAAAAGAGGTTGTCCAGGACTTCC 1468
RAD9B-002      TGCCCCTCAAGCACGAG--TTTGCATGTTTAGTGTCTAAAAGAGGTTGTCCAGGACTTCC 1406
RAD9B-003      TCCTCCACTGCCAAGACAGCCTGAGTTTGGAGTGGAATAAGGTGGAAGACAAATGTCTCT 1461
RAD9B-005      TGCCCCTCAAGCACGAG--TTTGCATGTTTAGTGTCTAAAAGAGGTTGTCCAGGACTTCC 1399
RAD9B-009      TCCTCCACTGCCAAGACAGCCTGAGTTTGGAGTGGAATAAGGTGGAAGACAAATGTCTCT 1070
               * * ** *   ** **     **  * *  ****    ** * **  * * *     **

RAD9B-001      TTTTAATGG-------AGGATGGGCTTTTAAACCACATCATCTTGTACAACAACCATATC 1521
RAD9B-002      TTTTAATGG-------AGGATGGGCTTTTAAACCACATCATCTTGTACAACAACCATATC 1459
RAD9B-003      GTTCTTTGGCCCTTTAAGAGTTAGCTTTTTACCTGC-ACAAATGGACTAAAAAATCTGGC 1520
RAD9B-005      TTTTAATGG-------AGGATGGGCTTTTAAACCACATCATCTTGTACAACAACCATATC 1452
RAD9B-009      GTTCTTTGGCCCTTTAAGAGTTAGCTTTTTACCTGC-ACAAATGGACTAAAAAATCTGGC 1129
                **   ***       **  *  ****** * *  *  **  * *   ** **   *  *

RAD9B-001      TAGAAATAGCTGTTTGTCAAGTGTATGTAACTTGCTTTAAATCCATTATGCTACTTGTGA 1581
RAD9B-002      TAGAAATAGCTGTTTGTCAAGTGTATGTAACTTGCTTTAAATCCATTATGCTACTTGTGA 1519
RAD9B-003      ACAAAACA--TTGTTATGTAATGTCTTATG----------ATGTGTGC--CTCTCCCTCC 1566
RAD9B-005      TAGAAATAGCTGTTTGTCAAGTGTATGTAACTTGCTTTAAATCCATTATGCTACTTGTGA 1512
RAD9B-009      ACAAAACA--TTGTTATGTAATGTCTTATG----------ATGTGTGC--CTCTCCCTCC 1175
                  *** *  *  ** *  * *** *            **   *    **     *

RAD9B-001      GGCAGAAGAGTTTTCTGTGAAGGAAAAAAGCCCATTAGAGTTCTTCAATTCAATGCACGT 1641
RAD9B-002      GGCAGAAGAGTTTTCTGTGAAGGAAAAAAGCCCATTAGAGTTCTTCAATTCAATGCACGT 1579
RAD9B-003      CCCAAACCTGTTTACAGTCAATTATAACCTGACAAACGAGACTTT--------------T 1612
RAD9B-005      GGCAGAAGAGTTTTCTGTGAAGGAAAAAAGCCCATTAGAGTTCTTCAATTCAATGCACGT 1572
RAD9B-009      CCCAAACCTGTTTACAGTCAATTATAACCTGACAAACGAGACTTT--------------T 1221
                 ** *   **** * ** **  * **     **   ***   **             *
```

```
RAD9B-001      TCACCCTAGAGCTTTTAACATCTTTGCTA-GTTTTATAAAGGTATTTAAACTTTATTCAA 1700
RAD9B-002      TCACCCTAGAGCTTTTAACATCTTTGCTA-GTTTTATAAAGGTATTTAAACTTTATTCAA 1638
RAD9B-003      GTAACATAT-TATTGTTACATCTTTCTGAAACCTTCAAACCGTAAGGAAGTGTTAA---- 1667
RAD9B-005      TCACCCTAGAGCTTTTAACATCTTTGCTA-GTTTTATAAAGGTATTTAAACTTTATTCAA 1631
RAD9B-009      GTAACATAT-TATTGTTACATCTTTCTGAAACCTTCAAACCGTAAGGAAGTGTTAA---- 1276
                 * * **    ** * ********   *    **  **  ***   **   ***

RAD9B-001      CAGCCATTTAGAGTGCCATCAAGATGGCTTGAAATGGAATTTTGTGATTTGTAGTCAGGT 1760
RAD9B-002      CAGCCATTTAGAGTGCCATCAAGATGGCTTGAAATGGAATTTTGTGATTTGTAGTCAGGT 1698
RAD9B-003      ------------C-----------TGGCAAGCAGTTGTACTTTAGACTTTGTGAGAAATT 1704
RAD9B-005      CAGCCATTTAGAGTGCCATCAAGATGGCTTGAAATGGAATTTTGTGATTTGTAGTCAGGT 1691
RAD9B-009      ------------C-----------TGGCAAGCAGTTGTACTTTAGACTTTGTGAGAAATT 1313
                                       ****  * * * * * ***    *****    *  *

RAD9B-001      ATCTTTTGTA-----TTTGATTGCAAACATTTGGATTT-----TAGTTTTCTCATGTAAT 1810
RAD9B-002      ATCTTTTGTA-----TTTGATTGCAAACATTTGGATTT-----TAGTTTTCTCATGTAAT 1748
RAD9B-003      CATAAAGGTGGCTGAGTGGATTTGCATGCTTTAGAACTGTGAATAGAGTTCTAACTGAAA 1764
RAD9B-005      ATCTTTTGTA-----TTTGATTGCAAACATTTGGATTT-----TAGTTTTCTCATGTAAT 1741
RAD9B-009      CATAAAGGTGGCTGAGTGGATTTGCATGCTTTAGAACTGTGAATAGAGTTCTAACTGAAA 1373
                      **       * ****   *   *** **  *     ***  **** *   **

RAD9B-001      ACCATGGCCTTTTTTGTGCATTGTTTTTTATATTTTAAGACTTTAAGTAGAATAAACCCT 1870
RAD9B-002      ACCATGGCCTTTTTTGTGCATTGTTTTTTATATTTTAAGACTTTAAGTAGAATAAACCCT 1808
RAD9B-003      C-CA-GAATTAATTTGGCTCTTGTAGCTTAGTA-ATGAGTCATAGCTACCCACAATAACC 1821
RAD9B-005      ACCATGGCCTTTTTTGTGCATTGTTTTTTATATTTTAAGACTTTAAGTAGAATAAACCCT 1801
RAD9B-009      ------------------------------------------------------------ 1373

RAD9B-001      GGAAAAAAGATCAAGAGTAAAAATATATAGTCACTTTCACTTGGCTTTTTTAGACGGAGT 1930
RAD9B-002      GGAAAAAAGATCAAGAGTAAAAATATATAGTCACTTTCACTTGGCTTTTTTAGACGGAGT 1868
RAD9B-003      TAATAAAAACTCAAGTTC---------------ATCCCAA---------------------- 1846
RAD9B-005      GGAAAAAAGATCAAGAGTAAAAATATATAGTCACTTTCACTTGGCTTTTTTAGACGGAGT 1861
RAD9B-009      ------------------------------------------------------------ 1373

RAD9B-001      CTCACTTTGTCACTCAGGCTCAAGTGCAGTGGTGCAATCTCTGCTCACTGCAACATCTGC 1990
RAD9B-002      CTCACTTTGTCACTCAGGCTCAAGTGCAGTGGTGCAATCTCTGCTCACTGCAACATCTGC 1928
RAD9B-003      ------------------------------------------------------------ 1846
RAD9B-005      CTCACTTTGTCACTCAGGCTCAAGTGCAGTGGTGCAATCTCTGCTCACTGCAACATCTGC 1921
RAD9B-009      ------------------------------------------------------------ 1373

RAD9B-001      CTCCCAGGTCCAAGCGATTCTCCTGCCTCAGCCTCCCGTGCAGCTGGGATTGCAGGTGCG 2050
RAD9B-002      CTCCCAGGTCCAAGCGATTCTCCTGCCTCAGCCTCCCGTGCAGCTGGGATTGCAGGTGCG 1988
RAD9B-003      ------------------------------------------------------------ 1846
RAD9B-005      CTCCCAGGTCCAAGCGATTCTCCTGCCTCAGCCTCCCGTGCAGCTGGGATTGCAGGTGCG 1981
RAD9B-009      ------------------------------------------------------------ 1373

RAD9B-001      TGCCACCATGCCTGGCTAATTTCTGGTATTTTGTAGAGACAGGGTTTCGCCATGTTGGCC 2110
RAD9B-002      TGCCACCATGCCTGGCTAATTTCTGGTATTTTGTAGAGACAGGGTTTCGCCATGTTGGCC 2048
RAD9B-003      ------------------------------------------------------------ 1846
RAD9B-005      TGCCACCATGCCTGGCTAATTTCTGGTATTTTGTAGAGACAGGGTTTCGCCATGTTGGCC 2041
RAD9B-009      ------------------------------------------------------------ 1373

RAD9B-001      AGGGTGGTCTTGAACTCCTGGCCTCAAGTGATCTGCCCACCTCGGCCTCCCAAAGTGCTG 2170
RAD9B-002      AGGGTGGTCTTGAACTCCTGGCCTCAAGTGATCTGCCCACCTCGGCCTCCCAAAGTGCTG 2108
RAD9B-003      ------------------------------------------------------------ 1846
RAD9B-005      AGGGTGGTCTTGAACTCCTGGCCTCAAGTGATCTGCCCACCTCGGCCTCCCAAAGTGCTG 2101
RAD9B-009      ------------------------------------------------------------ 1373

RAD9B-001      GGATTACAGACTTGAGCCACTGCGCCCAACCTGGAGTGTTTTTACATATTGTAAAATTTT 2230
RAD9B-002      GGATTACAGACTTGAGCCACTGCGCCCAACCTGGAGTGTTTTTACATATTGTAAAATTTT 2168
RAD9B-003      ------------------------------------------------------------ 1846
RAD9B-005      GGATTACAGACTTGAGCCACTGCGCCCAACCTGGAGTGTTTTTACATATTGTAAAATTTT 2161
RAD9B-009      ------------------------------------------------------------ 1373
```

```
RAD9B-001      ATTTCCTAACCTCAAATTGTTCTGATTTTCAGATGTGATTTTTTATTTTGCAGTGTGCTG 2290
RAD9B-002      ATTTCCTAACCTCAAATTGTTCTGATTTTCAGATGTGATTTTTTATTTTGCAGTGTGCTG 2228
RAD9B-003      ------------------------------------------------------------ 1846
RAD9B-005      ATTTCCTAACCTCAAATTGTTCTGATTTTCAGATGTGATTTTTTATTTTGCAGTGTGCTG 2221
RAD9B-009      ------------------------------------------------------------ 1373

RAD9B-001      CAGGAAAGAATTTAATGGAAGTGATGCCAAATATTTCTGTATTATCTGACATAGAACAGT 2350
RAD9B-002      CAGGAAAGAATTTAATGGAAGTGATGCCAAATATTTCTGTATTATCTGACATAGAACAGT 2288
RAD9B-003      ------------------------------------------------------------ 1846
RAD9B-005      CAGGAAAGAATTTAATGGAAGTGATGCCAAATATTTCTGTATTATCTGACATAGAACAGT 2281
RAD9B-009      ------------------------------------------------------------ 1373

RAD9B-001      ATCCTCCACTGCCAAGACAGCCTGAGTTTGGAGTGGAATAAGGTGGAAGACAAATGTCTC 2410
RAD9B-002      ATCCTCCACTGCCAAGACAGCCTGAGTTTGGAGTGGAATAAGGTGGAAGACAAATGTCTC 2348
RAD9B-003      ------------------------------------------------------------ 1846
RAD9B-005      ATCCTCCACTGCCAAGACAGCCTGAGTTTGGAGTGGAATAAGGTGGAAGACAAATGTCTC 2341
RAD9B-009      ------------------------------------------------------------ 1373

RAD9B-001      TGTTCTTTGGCCCTTTAAGAGTTAGCTTTTTACCTGCACAAATGGACTAAAAAATCTGGC 2470
RAD9B-002      TGTTCTTTGGCCCTTTAAGAGTTAGCTTTTTACCTGCACAAATGGACTAAAAAATCTGGC 2408
RAD9B-003      ------------------------------------------------------------ 1846
RAD9B-005      TGTTCTTTGGCCCTTTAAGAGTTAGCTTTTTACCTGCACAAATGGACTAAAAAATCTGGC 2401
RAD9B-009      ------------------------------------------------------------ 1373

RAD9B-001      ACAAAACATTGTTATGTAATGTCTTATGATGTGTGCCTCTCCCTCCCCCAAACCTGTTTA 2530
RAD9B-002      ACAAAACATTGTTATGTAATGTCTTATGATGTGTGCCTCTCCCTCCCCCAAACCTGTTTA 2468
RAD9B-003      ------------------------------------------------------------ 1846
RAD9B-005      ACAAAACATTGTTATGTAATGTCTTATGATGTGTGCCTCTCCCTCCCCCAAACCTGTTTA 2461
RAD9B-009      ------------------------------------------------------------ 1373

RAD9B-001      CAGTCAATTATAACCTGACAAACGAGACTTTTGTAACATATTATTGTTACATCTTTCTGA 2590
RAD9B-002      CAGTCAATTATAACCTGACAAACGAGACTTTTGTAACATATTATTGTTACATCTTTCTGA 2528
RAD9B-003      ------------------------------------------------------------ 1846
RAD9B-005      CAGTCAATTATAACCTGACAAACGAGACTTTTGTAACATATTATTGTTACATCTTTCTGA 2521
RAD9B-009      ------------------------------------------------------------ 1373

RAD9B-001      AACCTTCAAACCGTAAGGAAGTGTTAACTGGCAAGCAGTTGTACTTTAGACTTTGTGAGA 2650
RAD9B-002      AACCTTCAAACCGTAAGGAAGTGTTAACTGGCAAGCAGTTGTACTTTAGACTTTGTGAGA 2588
RAD9B-003      ------------------------------------------------------------ 1846
RAD9B-005      AACCTTCAAACCGTAAGGAAGTGTTAACTGGCAAGCAGTTGTACTTTAGACTTTGTGAGA 2581
RAD9B-009      ------------------------------------------------------------ 1373

RAD9B-001      AATTCATAAAGGTGGCTGAGTGGATTTGCATGCTTTAGAACTGTGAATAGAGTTCTAACT 2710
RAD9B-002      AATTCATAAAGGTGGCTGAGTGGATTTGCATGCTTTAGAACTGTGAATAGAGTTCTAACT 2648
RAD9B-003      ------------------------------------------------------------ 1846
RAD9B-005      AATTCATAAAGGTGGCTGAGTGGATTTGCATGCTTTAGAACTGTGAATAGAGTTCTAACT 2641
RAD9B-009      ------------------------------------------------------------ 1373

RAD9B-001      GAAACCAGAATTAATTTGGCTCTTGTAGCTTAGTAATGAGTCATAGCTACCCACAATAAC 2770
RAD9B-002      GAAACCAGAATTAATTTGGCTCTTGTAGCTTAGTAATGAGTCATAGCTACCCACAATAAC 2708
RAD9B-003      ------------------------------------------------------------ 1846
RAD9B-005      GAAACCAGAATTAATTTGGCTCTTGTAGCTTAGTAATGAGTCATAGCTACCCACAATAAC 2701
RAD9B-009      ------------------------------------------------------------ 1373

RAD9B-001      CTAATAAAAACTCAAGTTCATCCC-- 2794
RAD9B-002      CTAATAAAAACTCAAGTTCATCCC-- 2732
RAD9B-003      ------------------------- 1846
```

```
RAD9B-005      CTAATAAAAACTCAAGTTCATCCCAA 2727
RAD9B-009      -------------------------- 1373
```

Appendix 3

Alignment of RAD9B-001,002, 003, 005 and 009 proteins

```
RAD9B-001      ------------------------------------------------------------ 0
RAD9B-002      MAAMLKCVMSGSQVKVFGKAVQALSRISDEFWLDPSKKGLALRCVNSSRSAYGCVLFSPV 60
RAD9B-003      MAAMLKCVMSGSQVKVFGKAVQALSRISDEFWLDPSKKGLALRCVNSSRSAYGCVLFSPV 60
RAD9B-005      ------------------------------------------------------------ 0
RAD9B-009      MAAMLKCVMSGSQVKVFGKAVQALSRISDEFWLDPSKKGLALRCVNSSRSAYGCVLFSPV 60


RAD9B-001      ------------MSENELDTTLHLKCKLGMKSILPIFRCLNSLERNIEKCRIFTRSDKCK 48
RAD9B-002      FFQHYQWSALVKMSENELDTTLHLKCKLGMKSILPIFRCLNSLERNIEKCRIFTRSDKCK 120
RAD9B-003      FFQHYQWSALVKMSENELDTTLHLKCKLGMKSILPIFRCLNSLERNIEKCRIFTRSDKCK 120
RAD9B-005      ------------MSENELDTTLHLKCKLGMKSILPIFRCLNSLERNIEKCRIFTRSDKCK 48
RAD9B-009      FFQHYQWSALVKMSENELDTTLHLKCKLGMKSILPIFRCLNSLERNIEKCRIFTRSDKCK 120
                          ********************************************


RAD9B-001      VVIQFFYRHGIKRTHNICFQESQPLQVIFDKNVCTNTLMIQPRLLADAIVLFTSSQEEVT 108
RAD9B-002      VVIQFFYRHGIKRTHNICFQESQPLQVIFDKNVCTNTLMIQPRLLADAIVLFTSSQEEVT 180
RAD9B-003      VVIQFFYRHGIKRTHNICFQESQPLQVIFDKNVCTNTLMIQPRLLADAIVLFTSSQEEVT 180
RAD9B-005      VVIQFFYRHGIKRTHNICFQESQPLQVIFDKNVCTNTLMIQPRLLADAIVLFTSSQEEVT 108
RAD9B-009      VVIQFFYRHD---------------------------------------------------- 130
               *********.

RAD9B-001      LAVTPLNFCLKSSNEESMDLSNAVHSEMFVGSDEFDFFQIGMDTEITFCFKELKGILTFS 168
RAD9B-002      LAVTPLNFCLKSSNEESMDLSNAVHSEMFVGSDEFDFFQIGMDTEITFCFKELKGILTFS 240
RAD9B-003      LAVTPLNFCLKSSNEESMDLSNAVHSEMFVGSDEFDFFQIGMDTEITFCFKELKGILTFS 240
RAD9B-005      LAVTPLNFCLKSSNEESMDLSNAVHSEMFVGSDEFDFFQIGMDTEITFCFKELKGILTFS 168
RAD9B-009      ------------------LSNAVHSEMFVGSDEFDFFQIGMDTEITFCFKELKGILTFS 171
                                 ************************************

RAD9B-001      EATHAPISIYFDFPGKPLALSIDDMLVEANFILATLADEQSRASSPQSLCLSQKRKRSDL 228
RAD9B-002      EATHAPISIYFDFPGKPLALSIDDMLVEANFILATLADEQSRASSPQSLCLSQKRKRSDL 300
RAD9B-003      EATHAPISIYFDFPGKPLALSIDDMLVEANFILATLADEQSRASSPQSLCLSQKRKRSDL 300
RAD9B-005      EATHAPISIYFDFPGKPLALSIDDMLVEANFILATLADEQSRASSPQSLCLSQKRKRSDL 228
RAD9B-009      EATHAPISIYFDFPGKPLALSIDDMLVEANFILATLADEQSRASSPQSLCLSQKRKRSDL 231
               ************************************************************

RAD9B-001      IEKKAGKNVTGQALECISKKAAPRRLYPKETLTNISALENCGSPAMKRVDGDVSEVSESS 288
RAD9B-002      IEKKAGKNVTGQALECISKKAAPRRLYPKETLTNISALENCGSPAMKRVDGDVSEVSESS 360
RAD9B-003      IEKKAGKNVTGQALECISKKAAPRRLYPKETLTNISALENCGSPAMKRVDGDVSEVSESS 360
RAD9B-005      IEKKAGKNVTGQALECISKKAAPRRLYPKETLTNISALENCGSPAMKRVDGDVSEVSESS 288
RAD9B-009      IEKKAGKNVTGQALECISKKAAPRRLYPKETLTNISALENCGSPAMKRVDGDVSEVSESS 291
               ************************************************************

RAD9B-001      VSNTEEVPGSLCLRKFSCMFFGA--VSSDQQEHFNHPFDSLARASDSEEDMNNGSFSIF- 345
RAD9B-002      VSNTEEVPGSLCLRKFSCMFFGA--VSSDQQEHFNHPFDSLARASDSEEDMNNGSFSIF- 417
RAD9B-003      VSNTEEVPGSLCLRKFSCMFFGA--VSSDQQEHFNHPFDSLARASDSEEDMNNVCCRKEF 418
RAD9B-005      VSNTEEVPGSLCLRKFSCMFFGA--VSSDQQEHFNHPFDSLARASDSEEDMNNGSFSIF- 345
RAD9B-009      VSNTEEVPGSLCLRKCAAGKNLMEVMPNISVLSDIEQYPPLPRQPEFGVE---------- 341
               ************** :.      : . .    . :  * *  :   :

RAD9B-001      -----------      345
RAD9B-002      -----------      417
RAD9B-003      NGSDAKYFCII      429
RAD9B-005      -----------      345
RAD9B-009      -----------      341
```

Appendix 4

Alignment of RAD9B-001 with RAD9A

```
RAD9A-001      MKCLVTGGNVKVLGKAVHSLSRIGDELYLEPLEDGLSLRTVNSSRSAYACFLFAPLFFQQ 60
RAD9B-001      ------------------------------------------------------------M 1


RAD9A-001      YQAATPGQDLLRCKILMKSFLSVFRSLAMLEKTVEKCCISLNGRSSRLVVQLHCKFGVRK 120
RAD9B-001      SENELDTTLHLKCKLGMKSILPIFRCLNSLERNIEKCRIFTRSDKCKVVIQFFYRHGIKR 61
                :        *:**: ***:* :**.*  **:.:*** *  .. ..::*:*:. :.*:::

RAD9A-001      THNLSFQDCESLQAVFDPASCPHMLRAPARVLGEAVLPFSPALAEVTLGIGRGRRVILRS 180
RAD9B-001      THNICFQESQPLQVIFDKNVCTNTLMIQPRLLADAIVLFTSSQEEVTLAVTPLNFC-LKS 120
               ***:.**:.: **.:**   * : *    *:*.:*:: *: :  ****.:   .   *:*

RAD9A-001      YHEEEADSTAKAMVTEMCLGEEDFQQLQAQEGVAITFCLKEFRGLLSFAESANLNLSIHF 240
RAD9B-001      S-NEESMDLSNAVHSEMFVGSDEFDFFQIGMDTEITFCFKELKGILTFSEATHAPISIYF 179
                 :**: . ::*: :** :*.::*: :*   .. ****:**::*:*:*:*:::  :**:*

RAD9A-001      DAPGRPAIFTIKDSLLDGHFVLATLSDTDSHSQDLGSPERHQPVPQLQAHSTPHPDDFAN 300
RAD9B-001      DFPGKPLALSIDDMLVEANFILATLADEQSRASSPQSLCLSQKRK----RSDL-IEKKAG 234
               * **:*  ::*.* *::.:*:****:* :*::..  *    *       :*    :. *.

RAD9A-001      DDIDSYMIAMETTIG-NEGSRVLPSISL--------SPGPQPPKSPGPHS--EEEDEAEP 349
RAD9B-001      KNVTGQA--LECISKKAAPRRLYPKETLTNISALENCGSPAMKRVDGDVSEVSESSVSNT 292
               .:: .    :*         *: *. :*        . .*   :  *  *  .*.. ::

RAD9A-001      STVPGTPPPKKFRSLFFGSILAPVRSPQ-GPSPVLAEDSEGEG---------- 391
RAD9B-001      EEVPGSLCLRKFSCMFFGAVSSDQQEHFNHPFDSLARASDSEEDMNNGSFSIF 345
```

Appendix 5

Alignment of RAD9B-002 with RAD9A

```
RAD9A-001      ----MKCLVTGGNVKVLGKAVHSLSRIGDELYLEPLEDGLSLRTVNSSRSAYACFLFAPL 56
RAD9B-002      MAAMLKCVMSGSQVKVFGKAVQALSRISDEFWLDPSKKGLALRCVNSSRSAYGCVLFSPV 60
                   :**:::*.:***:****::****.**::*:* :.**:** ********.*.**:*:

RAD9A-001      FFQQYQAATP---------GQDLLRCKILMKSFLSVFRSLAMLEKTVEKCCISLNGRSSR 107
RAD9B-002      FFQHYQWSALVKMSENELDTTLHLKCKLGMKSILPIFRCLNSLERNIEKCRIFTRSDKCK 120
               ***:** ::              *:**: ***:* :**.*  **:.:*** *  .. ..:

RAD9A-001      LVVQLHCKFGVRKTHNLSFQDCESLQAVFDPASCPHMLRAPARVLGEAVLPFSPALAEVT 167
RAD9B-002      VVIQFFYRHGIKRTHNICFQESQPLQVIFDKNVCTNTLMIQPRLLADAIVLFTSSQEEVT 180
               :*:*:. :.*:::***:.**:.: **.:**   * : *    *:*.:*:: *: :  ***

RAD9A-001      LGIGRGRRVILRSYHEEEADSTAKAMVTEMCLGEEDFQQLQAQEGVAITFCLKEFRGLLS 227
RAD9B-002      LAVTPLNFC-LKSS-NEESMDLSNAVHSEMFVGSDEFDFFQIGMDTEITFCFKELKGILT 238
               *.:   .   *:*  :**: . ::*: :** :*.::*: :*   .. ****:**::*:*:

RAD9A-001      FAESANLNLSIHFDAPGRPAIFTIKDSLLDGHFVLATLSDTDSHSQDLGSPERHQPVPQL 287
RAD9B-002      FSEATHAPISIYFDFPGKPLALSIDDMLVEANFILATLADEQSRASSPQSLCLSQKRK-- 296
               *:*:::  :**:** **:*  ::*.* *::.:*:****:* :*::..  *    *

RAD9A-001      QAHSTPHPDDFANDDIDSYMIAMETTIG-NEGSRVLPSISL--------SPGPQPPKSPG 338
RAD9B-002      --RSDL-IEKKAGKNVTGQA--LECISKKAAPRRLYPKETLTNISALENCGSPAMKRVDG 351
                 :*    :. *.::: .    :*         *: *. :*        . .*   :  *

RAD9A-001      PHS--EEEDEAEPSTVPGTPPPKKFRSLFFGSILAPVRSPQ-GPSPVLAEDSEGEG---- 391
RAD9B-002      DVSEVSESSVSNTEEVPGSLCLRKFSCMFFGAVSSDQQEHFNHPFDSLARASDSEEDMNN 411
                 *  .*.. :: . ***:   :** .:***:: :  :.    *   **. *:.*

RAD9A-001      ------ 391
RAD9B-002      GSFSIF 417
```

Appendix 6

Alignment of RAD9B-001 and RAD9B-002 with RAD9A

```
RAD9A-001      ----MKCLVTGGNVKVLGKAVHSLSRIGDELYLEPLEDGLSLRTVNSSRSAYACFLFAPL 56
RAD9B-001      ------------------------------------------------------------ 0
RAD9B-002      MAAMLKCVMSGSQVKVFGKAVQALSRISDEFWLDPSKKGLALRCVNSSRSAYGCVLFSPV 60


RAD9A-001      FFQQYQAATP---------GQDLLRCKILMKSFLSVFRSLAMLEKTVEKCCISLNGRSSR 107
RAD9B-001      ------------MSENELDTTLHLKCKLGMKSILPIFRCLNSLERNIEKCRIFTRSDKCK 48
RAD9B-002      FFQHYQWSALVKMSENELDTTLHLKCKLGMKSILPIFRCLNSLERNIEKCRIFTRSDKCK 120
                                *:**: ***:* :**.*  **:.:*** *  .. ..:

RAD9A-001      LVVQLHCKFGVRKTHNLSFQDCESLQAVFDPASCPHMLRAPARVLGEAVLPFSPALAEVT 167
RAD9B-001      VVIQFFYRHGIKRTHNICFQESQPLQVIFDKNVCTNTLMIQPRLLADAIVLFTSSQEEVT 108
RAD9B-002      VVIQFFYRHGIKRTHNICFQESQPLQVIFDKNVCTNTLMIQPRLLADAIVLFTSSQEEVT 180
               :*:*:. :.*:::***:.**:.: **.:**   * : *    *:*.:*:: *: :  ***

RAD9A-001      LGIGRGRRVILRSYHEEEADSTAKAMVTEMCLGEEDFQQLQAQEGVAITFCLKEFRGLLS 227
RAD9B-001      LAVTPLNFC-LKSS-NEESMDLSNAVHSEMFVGSDEFDFFQIGMDTEITFCFKELKGILT 166
RAD9B-002      LAVTPLNFC-LKSS-NEESMDLSNAVHSEMFVGSDEFDFFQIGMDTEITFCFKELKGILT 238
               *.:   .   *:*  :**: . ::*: :** :*.::*: :*   .. ****:**::*:*:

RAD9A-001      FAESANLNLSIHFDAPGRPAIFTIKDSLLDGHFVLATLSDTDSHSQDLGSPERHQPVPQL 287
RAD9B-001      FSEATHAPISIYFDFPGKPLALSIDDMLVEANFILATLADEQSRASSPQSLCLSQKRK-- 224
RAD9B-002      FSEATHAPISIYFDFPGKPLALSIDDMLVEANFILATLADEQSRASSPQSLCLSQKRK-- 296
               *:*:::  :**:** **:*  ::*.* *::.:*:****:* :*::..  *    *

RAD9A-001      QAHSTPHPDDFANDDIDSYMIAMETTIG-NEGSRVLPSISL--------SPGPQPPKSPG 338
RAD9B-001      --RSDL-IEKKAGKNVTGQA--LECISKKAAPRRLYPKETLTNISALENCGSPAMKRVDG 279
RAD9B-002      --RSDL-IEKKAGKNVTGQA--LECISKKAAPRRLYPKETLTNISALENCGSPAMKRVDG 351
                 :*    :. *..:: .    :*         *: *. :*        . .*   :  *

RAD9A-001      PHS--EEEDEAEPSTVPGTPPPKKFRSLFFGSILAPVRSPQ-GPSPVLAEDSEGEG---- 391
RAD9B-001      DVSEVSESSVSNTEEVPGSLCLRKFSCMFFGAVSSDQQEHFNHPFDSLARASDSEEDMNN 339
RAD9B-002      DVSEVSESSVSNTEEVPGSLCLRKFSCMFFGAVSSDQQEHFNHPFDSLARASDSEEDMNN 411
                 *  .*.. :: . ***:   :** .:***:: :  :.    *   **. *:.*

RAD9A-001      ------ 391
RAD9B-001      GSFSIF 345
RAD9B-002      GSFSIF 417
```

Appendix 7

Alignment of RAD9B-001 with SpRad9-M50

```
RAD9B-001       -------------------MSENELDTTLHLKCKLGMKSILPIFRCL-----------NS 30
Rad9-M50        MVTLKKAFFDKYIFQPDSVLLTGLMTPT--IRIRTQVKPILSVFRNKIFDFIPTVVTTNS 58
                                    :  . :  *  :: :  :* ** :**            **

RAD9B-001       L-----------ERNIEK-CRIFTRSDKCKVVIQFFYRHGIKRTHNICFQESQPLQVIFD 78
Rad9-M50        KNGYGSESASRKDVIVENVQISISTGSECRIIFKFLCKHGVIKTYKISYEQTQTLHAVFD 118
                           :  :*:    :: ..:*:::::*: :**: :*::*.::::* *:.:**

RAD9B-001       KNVCTNTLMIQPRLLADAIVLFTSSQEEVTLAVTPLNFCLKSSNEESMD----LSNAVHS 134
Rad9-M50        KSLSHNNFQINSKILKDLTEHFGQRTEELTIQPLQERVLLTSFTEEVVHNRDILKQPTQT 178
                *.:. *.: *: ::* *    * .  **:*:     .. *.* .** :.    *.: .::

RAD9B-001       EMFVGSDEFDFFQIGMDTEITFCFKELKGILTFSEATHAPISIYFDFPGKPLALSIDD-- 192
Rad9-M50        TVSIDGKEFERVALNEGVSVTLSLREFRAAVILAEALGSSICAYYGVPGKPILLTFAKGK 238
                 : :...**: . :. ...:*:.::*::. : ::**  : *. *:..****: *:: .

RAD9B-001       -MLVEANFILATLADEQSRA------------SSPQSLCLSQKRKRSDLIEKKAGKNVTG 239
Rad9-M50        NSEIEAQFILATVVGSDEQEVSSMMGNRWQHSSTPASLFNSVERNNSLTA--V-AHNPPG 295
                   :**:*****:...:.:             *:* **  * :*:.*       .:*  *

RAD9B-001       QALECISKKAAPRRLYPKETLTNISALENCGSPAMKRVDGDVSEVSESSVSNTEEVPGSL 299
Rad9-M50        S-IGWQTDQSDSSRMFNS---------------ALDRSDE-TNGIKEPST--TNDAGQS- 335
                . :   :.::   *:: .               *:.* *  .. :.* *.  *::.  *

RAD9B-001       CLRKFSCMFFGAVS-SDQQEHFNHPFDSLARA-SDSEEDMNNGSFSIF-  345
Rad9-M50        -------LFLDGIPNESELAAFNNDVNDDAEFGPTQAEQSYHGIFSQED  377
                     :*:..:  ..:   **: .:. *.    . *:  :* **
```

Appendix 8

Alignment of RAD9B-002 with SpRad9-M50

```
RAD9B-002      MAAMLKCVMSGSQVKVFGKAVQALSRISDEFWLDPSKKGLALRCVNSSRSAYGCVLFSPV 60
Rad9-M50       ------------------------------------------------------MVTLKKA 7
                                                                      * :. .

RAD9B-002      FFQHYQWSALVKMSENELDTTLHLKCKLGMKSILPIFRCL-----------NSL------ 103
Rad9-M50       FFDKYIFQPDSVLLTGLMTPTIRI--RTQVKPILSVFRNKIFDFIPTVVTTNSKNGYGSE 65
               **::* :.    :  . :  *:::  :  :* ** :**            **

RAD9B-002      -----ERNIEK-CRIFTRSDKCKVVIQFFYRHGIKRTHNICFQESQPLQVIFDKNVCTNT 157
Rad9-M50       SASRKDVIVENVQISISTGSECRIIFKFLCKHGVIKTYKISYEQTQTLHAVFDKSLSHNN 125
                    :  :*:    :: ..:*:::::*: :**: :*::*.::::* *:.:***.:. *.

RAD9B-002      LMIQPRLLADAIVLFTSSQEEVTLAVTPLNFCLKSSNEESMD----LSNAVHSEMFVGSD 213
Rad9-M50       FQINSKILKDLTEHFGQRTEELTIQPLQERVLLTSFTEEVVHNRDILKQPTQTTVSIDGK 185
               : *: ::* *    * .  **:*:     .. *.* .** :.    *.: .:: : :...

RAD9B-002      EFDFFQIGMDTEITFCFKELKGILTFSEATHAPISIYFDFPGKPLALSIDD---MLVEAN 270
Rad9-M50       EFERVALNEGVSVTLSLREFRAAVILAEALGSSICAYYGVPGKPILLTFAKGKNSEIEAQ 245
               **: . :. ...:*:.::*::. : ::**  : *. *:..****: *:: .     :**:

RAD9B-002      FILATLADEQSRA-----------SSPQSLCLSQKRKRSDLIEKKAGKNVTGQALECIS 318
Rad9-M50       FILATVVGSDEQEVSSMMGNRWQHSSTPASLFNSVERNNSLTA--V-AHNPPGS-IGWQT 301
               *****:...:.:             *:* **  * :*:.*       .:*  *. :   :

RAD9B-002      KKAAPRRLYPKETLTNISALENCGSPAMKRVDGDVSEVSESSVSNTEEVPGSLCLRKFSC 378
Rad9-M50       DQSDSSRMFNS--------------ALDRSDE-TNGIKEPST--TNDAGQS-------- 335
               .::   *:: .               *:.* *  .. :.* *.  *::.  *

RAD9B-002      MFFGAVS-SDQQEHFNHPFDSLARA-SDSEEDMNNGSFSIF- 417
Rad9-M50       LFLDGIPNESELAAFNNDVNDDAEFGPTQAEQSYHGIFSQED 377
```

Appendix 9

Alignment of RAD9B-001 and RAD9B-002 with SpRad9-M50

```
RAD9B-001      ------------------------------------------------------------ 0
RAD9B-002      MAAMLKCVMSGSQVKVFGKAVQALSRISDEFWLDPSKKGLALRCVNSSRSAYGCVLFSPV 60
Rad9-M50       ------------------------------------------------------MVTLKKA 7


RAD9B-001      ------------MSENELDTTLHLKCKLGMKSILPIFRCL-----------NSL------ 31
RAD9B-002      FFQHYQWSALVKMSENELDTTLHLKCKLGMKSILPIFRCL-----------NSL------ 103
Rad9-M50       FFDKYIFQPDSVLLTGLMTPTIRI--RTQVKPILSVFRNKIFDFIPTVVTTNSKNGYGSE 65
                           :  . :  *:::  :  :* ** :**            **

RAD9B-001      -----ERNIEK-CRIFTRSDKCKVVIQFFYRHGIKRTHNICFQESQPLQVIFDKNVCTNT 85
RAD9B-002      -----ERNIEK-CRIFTRSDKCKVVIQFFYRHGIKRTHNICFQESQPLQVIFDKNVCTNT 157
Rad9-M50       SASRKDVIVENVQISISTGSECRIIFKFLCKHGVIKTYKISYEQTQTLHAVFDKSLSHNN 125
                    :  :*:    :: ..:*:::::*: :**: :*::*.::::* *:.:***.:. *.

RAD9B-001      LMIQPRLLADAIVLFTSSQEEVTLAVTPLNFCLKSSNEESMD----LSNAVHSEMFVGSD 141
RAD9B-002      LMIQPRLLADAIVLFTSSQEEVTLAVTPLNFCLKSSNEESMD----LSNAVHSEMFVGSD 213
Rad9-M50       FQINSKILKDLTEHFGQRTEELTIQPLQERVLLTSFTEEVVHNRDILKQPTQTTVSIDGK 185
               : *: ::* *    * .  **:*:     .. *.* .** :.    *.: .:: : :...

RAD9B-001      EFDFFQIGMDTEITFCFKELKGILTFSEATHAPISIYFDFPGKPLALSIDD---MLVEAN 198
RAD9B-002      EFDFFQIGMDTEITFCFKELKGILTFSEATHAPISIYFDFPGKPLALSIDD---MLVEAN 270
Rad9-M50       EFERVALNEGVSVTLSLREFRAAVILAEALGSSICAYYGVPGKPILLTFAKGKNSEIEAQ 245
               **: . :. ...:*:.::*::. : ::**  : *. *:..****: *:: .     :**:

RAD9B-001      FILATLADEQSRA------------SSPQSLCLSQKRKRSDLIEKKAGKNVTGQALECIS 246
RAD9B-002      FILATLADEQSRA------------SSPQSLCLSQKRKRSDLIEKKAGKNVTGQALECIS 318
Rad9-M50       FILATVVGSDEQEVSSMMGNRWQHSSTPASLFNSVERNNSLTA--V-AHNPPGS-IGWQT 301
               *****:...:.:             *:* **  * :*:.*       .:*  *. :   :

RAD9B-001      KKAAPRRLYPKETLTNISALENCGSPAMKRVDGDVSEVSESSVSNTEEVPGSLCLRKFSC 306
RAD9B-002      KKAAPRRLYPKETLTNISALENCGSPAMKRVDGDVSEVSESSVSNTEEVPGSLCLRKFSC 378
Rad9-M50       DQSDSSRMFNS---------------ALDRSDE-TNGIKEPST--TNDAGQS-------- 335
               .::   *:: .               *:.* *  .. :.* *.  *::.  *

RAD9B-001      MFFGAVS-SDQQEHFNHPFDSLARA-SDSEEDMNNGSFSIF- 345
RAD9B-002      MFFGAVS-SDQQEHFNHPFDSLARA-SDSEEDMNNGSFSIF- 417
Rad9-M50       LFLDGIPNESELAAFNNDVNDDAEFGPTQAEQSYHGIFSQED 377
```

Appendix 10

Alignment of SpRad9-M50 with C12orf32

```
Rad9-M50      MVTLKKAFFDKYIFQPDSVLLTGLMTPTIRIRTQVKPILSVFRNKIFDFIPTVVTTNSKN 60
C12ORF32      ------------------------MPPRKKRRQPSQKAPLLFHQQ-----P-------LE 24
                                     * *  : *   :    :*:::     *        :

Rad9-M50      GYGSESASRKDVIVENVQISISTGSECRIIFKFLCKHGVIKTYKISYEQTQTLHAVFDKS 120
C12ORF32      GPKHSCASTQLPITHTRQVP-----------SKPIDHSTITSW----------------- 56
              *   ..** :  *... *:            .   .*..*.::

Rad9-M50      LSHNNFQINSKILKDLTEHFGQRTEELTIQPLQERVLLTSFTEEVVHNRDILKQPTQTTV 180
C12ORF32      -----------VSPDFDTAAG--------------SLFPAYQKHQNRARHSSRKPTTSK- 90
                         :  *:    *               *: :: :.  : *.  ::** :.

Rad9-M50      SIDGKEFERVALNEGVSVTLSLREFRA----------AVILAEALGSSICAYYGVPGK-- 228
C12ORF32      -FPHLTFESPQSS--SSETLGIPLIRECPSESEKDVSRRPLVPVLSPQSCGNMSVQALQS 147
               :    **    .   * **.:  :*             *. .*. . *.  .* .

Rad9-M50      -PILL---TFAKGKNSEIEAQFILATVVGSDEQEVSSMMGNRWQHSSTPASLFNSVERNN 284
C12ORF32      LPYVFIPPDIQTPESSSVKEE-----LIPQDQKE-NSLLSCTL-HTGTPNS----PEPG- 195
               * ::    : . :.*.:: :     :: .*::* .*::.    *:.** *     * .

Rad9-M50      SLTAVAHNPPG----SIGWQTDQSDSSRMFNSALDRSDETNGIKEPSTTNDAGQSLFLDG 340
C12ORF32      -PVLVKDTPEDKYGIKVTWRRRQHLLAYL----RERG-------------KLSRSQFLVK 237
                . * ..* .    .: *:  *   : :     :*.             . .:* **

Rad9-M50      IPNESELAAFNNDVNDDAEFGPTQAEQSYHGIFSQED       377
C12ORF32      S-----------------------------------       238
```

Appendix 11

Alignment of the amplified RAD9B-S003 with the full length RAD9B-003

```
RAD9B-003       GCAGAGACGAGATCGCGAAGCTTTGAAAAGCGCGGGCAACATCCGGGCACCTGGGCCGTC 60
RAD9B-S003      ------------------------------------------------------------ 0

RAD9B-003       GAGCTGAGGCGCGCCTTCCGAGCCTGCTTTTTAGGGCGGATGGCAGCCATGCTGAAGTGC 120
RAD9B-S003      -------------------------------------ATGGCAGCCATGCTGAAGTGC 21
                                                      **********************

RAD9B-003       GTGATGAGCGGCAGTCAGGTGAAAGTATTTGGGAAAGCAGTTCAAGCTCTATCACGAATT 180
RAD9B-S003      GTGATGAGCGGCAGTCAGGTGAAAGTATTTGG-GAAGCAGTTCAAGCTCTATCACGAATT 80
                ********************************  ************************

RAD9B-003       AGTGACGAGTTCTGGCTAGACCCATCTAAAAAAGGTCTTGCTCTAAGATGTGTGAATTCT 240
RAD9B-S003      AGTGACGAGTTCTGGCTAGACCCATCTAAAAAAGGTCTTGCTCTAAGATGTGTGAATTCT 140
                ************************************************************

RAD9B-003       TCTCGGTCAGCATATGGATGTGTCCTGTTCTCTCCTGTGTTTTTTCAGCATTATCAATGG 300
RAD9B-S003      TCTCGGTCAGCATATGGATGTGTCCTGTTCTCTCCTGTGTTTTTTCAGCATTATCAATGG 200
                ************************************************************

RAD9B-003       TCAGCTTTAGTGAAAATGAGTGAAAATGAACTTGACACAACACTGCATTTAAAATGCAAA 360
RAD9B-S003      TCAGCTTTAGTGAAAATGAGTGAAAATGAACTTGACACAACACTGCATTTAAAATGCAAA 260
                ************************************************************

RAD9B-003       TTGGGAATGAAGTCAATTTTGCCCATCTTTAGATGTCTGAATTCCCTTGAAAGAAATATA 420
RAD9B-S003      TTGGGAATGAAGTCAATTTTGCCCATCTTTAGATGTCTGAATTCCCTTGAAAGAAATATA 320
                ************************************************************

RAD9B-003       GAGAAGTGCAGAATATTCACCAGATCTGATAAATGCAAAGTAGTTATTCAATTCTTCTAC 480
RAD9B-S003      GAGAAGTGCAGAATATTCACCAGATCTGATAAATGCAAAGTAGTTATTCAATTCTTCTAC 380
                ************************************************************

RAD9B-003       AGACATGGTATTAAAAGAACTCATAATATATGTTTTCAAGAAAGTCAGCCTTTGCAAGTT 540
RAD9B-S003      AGACATGGTATTAAAAGAACTCATAATATATGTTTTCAAGAAAGTCAGCCTTTGCAAGTT 440
                ************************************************************

RAD9B-003       ATTTTTGACAAGAATGTTTGTACTAATACGCTAATGATTCAACCAAGATTGCTTGCTGAT 600
RAD9B-S003      ATTTTTGACAAGAATGTTTGTACTAATACGCTAATGATTCAACCAAGATTGCTTGCTGAT 500
                ************************************************************

RAD9B-003       GCCATTGTTCTTTTTACATCAAGTCAAGAGGAAGTTACTCTTGCTGTTACTCCACTGAAT 660
RAD9B-S003      GCCAAATATTTCTGTATTATCTGACTCGAGATCCTAAAGT-------------------- 540
                ****    * * * **      * *  ***    * *

RAD9B-003       TTTTGCCTCAAGAGTTCTAATGAGGAATCAATGGATTTGAGCAATGCTGTACACAGTGAG 720
RAD9B-S003      ------------------------------------------------------------ 540

RAD9B-003       ATGTTTGTTGGCTCAGATGAGTTTGACTTCTTTCAAATTGGAATGGACACTGAGATAACA 780
RAD9B-S003      ------------------------------------------------------------ 540

RAD9B-003       TTTTGTTTCAAAGAATTGAAGGGAATACTGACATTTTCAGAAGCTACACATGCTCCTATA 840
RAD9B-S003      ------------------------------------------------------------ 540

RAD9B-003       TCCATTTATTTTGATTTCCCTGGGAAACCTCTGGCTTTGAGTATTGATGATATGTTAGTG 900
RAD9B-S003      ------------------------------------------------------------ 540

RAD9B-003       GAAGCTAACTTTATTTTGGCCACATTAGCTGATGAACAAAGTAGAGCATCTTCACCACAG 960
```

```
RAD9B-S003     ------------------------------------------------------------ 540

RAD9B-003      TCACTGTGTCTTTCACAGAAACGAAAAAGGTCAGATCTGATTGAAAAAAAGGCTGGCAAA 1020
RAD9B-S003     ------------------------------------------------------------ 540

RAD9B-003      AATGTAACTGGCCAGGCCCTGGAATGTATTTCAAAAAAAGCAGCACCAAGAAGGCTTTAT 1080
RAD9B-S003     ------------------------------------------------------------ 540

RAD9B-003      CCTAAGGAGACTCTCACAAACATATCTGCATTGGAAAACTGTGGCAGCCCTGCAATGAAA 1140
RAD9B-S003     ------------------------------------------------------------ 540

RAD9B-003      AGAGTGGATGGAGATGTCAGTGAAGTATCAGAAAGCAGTGTCAGCAACACAGAGGAAGTG 1200
RAD9B-S003     ------------------------------------------------------------ 540

RAD9B-003      CCAGGGTCTCTGTGTCTCAGAAAGTTTTCTTGCATGTTCTTTGGAGCAGTTTCTTCTGAC 1260
RAD9B-S003     ------------------------------------------------------------ 540

RAD9B-003      CAGCAAGAACACTTCAACCACCCTTTCGACAGTCTGGCAAGAGCAAGTGACAGTGAAGAG 1320
RAD9B-S003     ------------------------------------------------------------ 540

RAD9B-003      GACATGAATAATGTGTGCTGCAGGAAAGAATTTAATGGAAGTGATGCCAAATATTTCTGT 1380
RAD9B-S003     ------------------------------------------------------------ 540

RAD9B-003      ATTATCTGACATAGAACAGTATCCTCCACTGCCAAGACAGCCTGAGTTTGGAGTGGAATA 1440
RAD9B-S003     ------------------------------------------------------------ 540

RAD9B-003      AGGTGGAAGACAAATGTCTCTGTTCTTTGGCCCTTTAAGAGTTAGCTTTTTACCTGCACA 1500
RAD9B-S003     ------------------------------------------------------------ 540

RAD9B-003      AATGGACTAAAAAATCTGGCACAAAACATTGTTATGTAATGTCTTATGATGTGTGCCTCT 1560
RAD9B-S003     ------------------------------------------------------------ 540

RAD9B-003      CCCTCCCCCAAACCTGTTTACAGTCAATTATAACCTGACAAACGAGACTTTTGTAACATA 1620
RAD9B-S003     ------------------------------------------------------------ 540

RAD9B-003      TTATTGTTACATCTTTCTGAAACCTTCAAACCGTAAGGAAGTGTTAACTGGCAAGCAGTT 1680
RAD9B-S003     ------------------------------------------------------------ 540

RAD9B-003      GTACTTTAGACTTTGTGAGAAATTCATAAAGGTGGCTGAGTGGATTTGCATGCTTTAGAA 1740
RAD9B-S003     ------------------------------------------------------------ 540

RAD9B-003      CTGTGAATAGAGTTCTAACTGAAACCAGAATTAATTTGGCTCTTGTAGCTTAGTAATGAG 1800
RAD9B-S003     ------------------------------------------------------------ 540

RAD9B-003      TCATAGCTACCCACAATAACCTAATAAAAACTCAAGTTCATCCCAA 1846
RAD9B-S003     ---------------------------------------------- 540
```